Targeting BRAF mutant pre-mRNA alternative splicing in melanoma

Francisco Aya Moreno

DOCTORAL THESIS UPF / 2023

Thesis Supervisors:

Dr. Juan Valcárcel

Genome Biology Program, Centre for Genomic Regulation (CRG)

Dr. Ana Arance

Translational Genomics and targeted therapies in solid tumors, Institut d'Investigacions Biomèdiques August Pi i Sunyer (IDIBAPS)

DEPARTMENT OF MEDICINE AND LIFE SCIENCES

upf. Universitat Pompeu Fabra Barcelona

A las personas que creyeron en mí

Abstract

Alternative splicing of BRAF mRNA can provide a resistance mechanism to BRAF and MEK inhibitors that has been described mostly in *BRAF*-mutant melanoma. The mechanisms underlying the production of a variety of BRAF mRNA isoforms, e.g., the BRAF3-9 (which lacks exons 4 to 8), remain poorly understood.

Analysis of RNA-seq from melanoma samples identified for the first time BRAF mRNA isoforms associated with resistance in wild type BRAF and in treatment-naïve melanoma samples. Using minigene assays and whole-genome sequencing, we have reasonably rule out a contribution of single-nucleotide sequence variants (such as intronic mutations) in the generation of these isoforms. Using a CRISPR-Cas9 knockout screen, we have identified genetic vulnerabilities related to splicing and chromosome dynamics in melanoma cells, but not splicing factors particularly involved in the generation of BRAF3-9.

Importantly, we have identified large intragenic deletions as the underlying mechanism for the production of BRAF3-9 and BRAF1-9 isoforms, suggesting that this can be a general mechanism for the production of resistance-associated mRNA variants in melanoma.

Keywords

Alternative splicing, Melanoma, BRAF, Drug resistance, MAPK, Targeted therapy

Resumen

El *splicing* alternativo del ARNm de BRAF es un mecanismo de resistencia a los inhibidores de BRAF y MEK descrito principalmente en melanomas que presentan mutaciones en *BRAF*. Los mecanismos moleculares responsables de la producción de las distintas isoformas de ARNm de BRAF descritas no se conocen profundidad.

Gracias al análisis de RNA-*seq* de muestras de melanoma hemos identificado por primera vez isoformas de BRAF que han sido asociadas con la adquisición de resistencia en muestras con BRAF no mutado y que no habían recibido tratamiento. Utilizando minigenes y secuenciación genómica, hemos podido descartar razonablemente la contribución de sustituciones de nucleótido en la secuencia genómica de *BRAF* como responsables de la generación de estas isoformas. Un screening masivo de *knockout* génico mediante CRISPR-Cas9 nos ha permitido identificar vulnerabilidades génicas en células de melanoma relacionadas con *splicing* y dinámica de cromatina, pero no factores de *splicing* implicados específicamente en la generación de BRAF3-9.

De especial relevancia, hemos identificado deleciones intragénicas de gran tamaño como el mecanismo responsable de la producción de las isoformas BRAF3-9 y BRAF1-9, lo que sugiere que éste puede ser un mecanismo general para la producción de isoformas de mRNA asociadas con la adquisición de resistencia en melanoma.

Preface

Although BRAF and MEK inhibitors demonstrated unprecedented response rates in *BRAF*-mutant melanoma, treatment failure occurs in approximately 50% of patients within the first year, due to the development of different mechanisms of resistance. Understanding the mechanisms underlying the acquisition of resistance is thus an urgent unmet clinical need.

In this Thesis we focused on the alternative splicing of BRAF mRNA as a mechanism for acquisition of resistance, which has been associated with the production of a variety of BRAF mRNA isoforms (e.g., BRAF3-9, BRAF1-11, BRAF1-9). These isoforms produced an aberrant BRAF protein lacking the RAS-binding domain and gaining an increased tendency to dimerization, thus reactivating the MAPK pathway. Previous publications pointed to an intronic mutation as the responsible for the generation of one of these alternative spliced BRAF isoforms.

Inspired by these findings, this Thesis aimed at further elucidating the underlying mechanisms behind the production of alternatively spliced isoforms of BRAF mRNA, in the hope to identify potential therapeutic approaches overcome this mechanism of resistance to BRAF and MEK inhibitors.

Taking advantage of a collection of cellular models displaying different BRAF isoforms together with the application of cutting-edge technologies, we have made important progress to understand the molecular basis of this mechanism of resistance, ruling out

classical models of splicing regulation and establishing genomic intergenic deletions as the cause of the generation of resistance-associated mRNA isoforms.

Abbreviations

A3'SS – alternative 3' splice site
A5'SS – alternative 5' splice site
AS – alternative splicing
ASO – antisense oligonucleotide
BPS – branch point sequence
BRAF – v-raf murine sarcoma viral oncogene homolog B1
BRAFi – BRAF inhibitor/s
BRAFi+MEKi – BRAFi in combination with MEKi
BRAFi±MEKi – BRAFi monotherapy or in combination with MEKi
CRD – cysteine-rich domain
CRISPR – clustered regularly interspaced short palindromic repeats
CTLA-4 – cytotoxic T-lymphocyte antigen 4
DNA – deoxyribonucleic acid
EEJ – exon-exon junction
ERK – extracellular signal-regulated kinase ½
ES – exon skipping
ESE – exonic splicing enhancers
ESS – exonic splicing silencers
FACS – Fluorescence-activated cell sorting
FDR – false discovery rate
gDNA – genomic DNA
hnRNP – heterogeneous nuclear ribonucleoprotein
ICI – immune-checkpoint inhibitors
IR – intron retention
ISE – intronic splicing enhancers
ISS – intronic splicing silencers
MAPK – mitogen-activated protein kinase
MAPKi – MAP kinase pathway inhibitors
MEK – MAPK kinase
RRA – robust ranking aggregation method
MLE – maximum-likelihood estimation
BF – Bayesian factor
siRNA – small interfering RNA
MEKi – MEK inhibitor/s
MOI – multiplicity of infection
mRNA – messenger RNA
NR – not reported
NSCLC – non-small-cell lung cancer
ORF – open reading frame
ORR – objective response rates
OS – overall survival
PCR – polymerase chain reaction
PD-1 – programmed death 1
PFS – progression-free survival
PPT – polypyrimidine tract
RAF – rapidly accelerated fibrosarcoma
RAS – rat sarcoma virus
RBD – RAS-GTP binding domain
RBM – RNA-binding motif
RBP – RNA binding protein
RNA – ribonucleic acid
RNAP II – RNA polymerase II
RNP – ribonucleoprotein
RRM – RNA recognition motif
RT-PCR – reverse transcriptase PCR
RTK – receptor tyrosine kinase
SF3B – splicing factor 3b
sgRNA – single-guide RNA
snRNA – small nuclear RNA
snRNP – small nuclear RNP complexes
SNV – single nucleotide variant
SR – arginine-serine-rich protein
SS – splice site
SSO – splice-switching oligonucleotide
TCGA – The Cancer Genome Atlas
TKOv3 – Toronto KnockOut sgRNA library, version 3
UTR – untranslated region
WGS – whole genome sequencing

Table of contents

Table of contents

List of figures

INTRODUCTION

RESULTS

PART I

PART II

PART III

DISCUSSION

MATERIALS AND METHODS

List of tables

INTRODUCTION

RESULTS

PART I

PART II

PART III

PART V

MATERIALS AND METHODS

1 INTRODUCTION

1.1 Pre-mRNA splicing

The "central dogma of molecular biology" involves the transcription of the genomic information stored in DNA into RNA molecules, that will be eventually translated into proteins[1]. The units of this flow of genetic information in cells are genes. Although RNA acts as an intermediate between DNA and proteins, the primary transcript (pre-mature RNA or pre-mRNA) requires several modifications to generate a mature or messenger RNA (mRNA) in eukaryotes. For most mammalian genes, the maturation of this mRNA precursors after their synthesis by RNA polymerase II (RNAP II) includes three main steps linked to transcription[2], namely 5' capping (addition of an untemplated guanosine triphosphate to the 5' end followed by its methylation at N7 position; this cap structure protects RNA from nucleases, facilitates its nucleo-cytoplasmic transport and enhances mRNA translation)[3], 3' polyadenylation (addition of a polyadenosine tail at the 3' end after cleavage that confers mRNA stability and is required for nuclear export and translation)[4] and pre-mRNA splicing.

Pre-mRNA splicing is the process by which introns are removed from primary RNA transcripts and exons are joined covalently together. This major processing step of RNA generates a mature and translatable mRNA consisting of exons —the coding segments and the 5' and 3' untranslated regions (UTRs)—, and requires the excision of the noncoding internal sequences (introns) of pre-mRNA[5–7]. Splicing can be *constitutive*, when the exon is invariably included in the mRNA, or *alternative*, if the exon is present only in a proportion of mRNA transcripts. Given that 90-95% of human

multiexon genes (both coding as well as long non-coding) undergo alternative splicing[8,9] and, that human coding genes contain an average of eight introns per gene (in some cases longer than one megabase)[10,11], RNA splicing plays a central role in the generation of mRNA (and subsequently protein) diversity as well as in gene expression and its regulation, and therefore in phenotypic complexity[2].

The splicing reaction takes place in the nucleus and can occur after (*post-transcriptional*) or during (*co-transcriptional*) the synthesis of the pre-mRNA by the RNAP II[12,13]. The main orchestrator of pre-mRNA splicing is the spliceosome, and it requires the recognition and direct interaction with pre-mRNA sequence elements (*cis*-elements) that define the intron-exon boundaries. Moreover, this is a highly and exquisitely regulated process by other *cis*- and *trans*-factors.

1.1.1 The *cis*-elements: defining intron-exon boundaries in the pre-mRNA sequence

The first step in pre-mRNA splicing is the recognition by the spliceosome of sequence (*cis*) elements located at the intron-exon boundaries. There are 4 key *cis* elements necessary for splicing: the splice sites (SS), the branch point sequence (BPS) and the polypyrimidine tract (PPT)[14]. In mammals, the 5' SS or donor site is defined by a 9-nucleotide consensus sequence, YAG/GURAGU, whereas the consensus sequence for the 3' SS or acceptor site consists of NYAG/G (where Y is a pyrimidine, R is adenosine or guanine, and

N is any nucleotide)[15–17]. Although these sequences degenerated during evolution and across species, the dinucleotides GU in the 5'SS (GC in a small fraction of introns) and AG in the 3'SS are highly conserved and have proved to be essential for splicing in most pre-mRNAs of higher eukaryotes[18–21]. Nearby upstream the 3'SS, a sequence stretch characterized by a high percentage of pyrimidines (PPT) is preceded by the BPS, which contains the branch point adenosine located approximately 20-40 nucleotides upstream from the AG of the 3'SS[16,22,17] (Figure 1A).

The importance of these sequences in the pre-mRNA relies on their recognition by U-rich small nuclear RNAs (snRNAs) through base-pairing interactions[23,24]. Thus, the level of base pairing complementarity determines the strength or weakness of a particular SS, giving rise to a fine-tuned regulation of splicing by many other splicing regulatory elements (both *cis*- and *trans*-acting factors)[19,25].

1.1.2 The spliceosome and the splicing reaction

Pre-mRNA splicing is carried out, stepwise and —typically— in a highly precise and accurate manner, by the spliceosome. This splicing machinery or spliceosome is a highly dynamic and macromolecular ribonucleoprotein (RNP) complex that, upon recognition of the above mentioned sequences, assembles and undergoes massive conformational transitions in order to catalyze splicing of nuclear pre-mRNA[12]. There are two different spliceosomes: the major (or U2-dependent) spliceosome, which processes >95% of all introns, and the minor (or U12-dependent)

spliceosome[26,27]. U12-type introns are characterized by different sequence elements at the splice sites. Each spliceosome consists of 5 small nuclear RNP complexes (snRNPs): U1, U2, U4, U5 and U6 in the major spliceosome whereas the minor spliceosome is composed by its functional analogues, known as U5 (the only one common between the two spliceosomes), U11, U12, U4atac and U6atac[26].

Intron removal implies 2 consecutive S_N2-type transesterification reactions, which are facilitated by the spliceosome (Figure 1B). First, an intron lariat-3' exon is generated by the nucleophilic attack of the phosphodiester bond at the boundary between the first exon and the intron by the 2'-hydroxyl of the adenosine of the BPS. This lariat intron is thus linked by a 2'-5' phosphodiester bond between the BPS and the 5'-terminal nucleotide of the intron. Then, the 3'-hydroxyl of the free 5' exon carries out a nucleophilic attack on the phosphodiester bond at the boundary between the intron and the second exon, leading to the ligation between the 5' and 3' exons and the release of the intron[12,28–30]. Although seemingly straightforward from a biochemical point of view (two phosphodiester bonds are broken and two are formed), the spliceosome is necessary to orchestrate the entire process, from the recognition of the SS until the close positioning of the reactive groups, allowing these transesterifications to happen.

The assembly of the spliceosome occurs stepwise and dynamically in terms of composition and conformation[12,31–33] (Figure 1C). First, U1 snRNP binds to the 5' SS through base-pairing between sequences at the 5' end of the U1 snRNA while the Py-tract/3' SS AG and BPS are recognized by the two subunits of the splicing factor U2AF and

by BBP/SF1 (branch point binding protein/splicing factor SF1), leading to formation of complex E. This step is followed by the binding of U2 snRNP to the BPS (complex A), involving base pairing interactions between U2 snRNA and nucleotides flanking the BPS adenosine. Then, the preformed U4/U6.U5 tri-snRNP is recruited and complex B (also known as pre-catalytic spliceosome) is generated. The release of U1 and U4 yields a rearrangement and the formation of complex B^{act}, which can be activated for catalysis (B*). The first catalytic step of splicing is carried out within complex B* and the result is the formation of complex C, in which, after repositioning of the catalytic center, step 2 occurs[34]. Finally, the mature mRNA is released, the lariat intron bound to U2, U5 and U6, and the spliceosome dissociates, and its components recycled for another round of spliceosome assembly and splicing reactions.

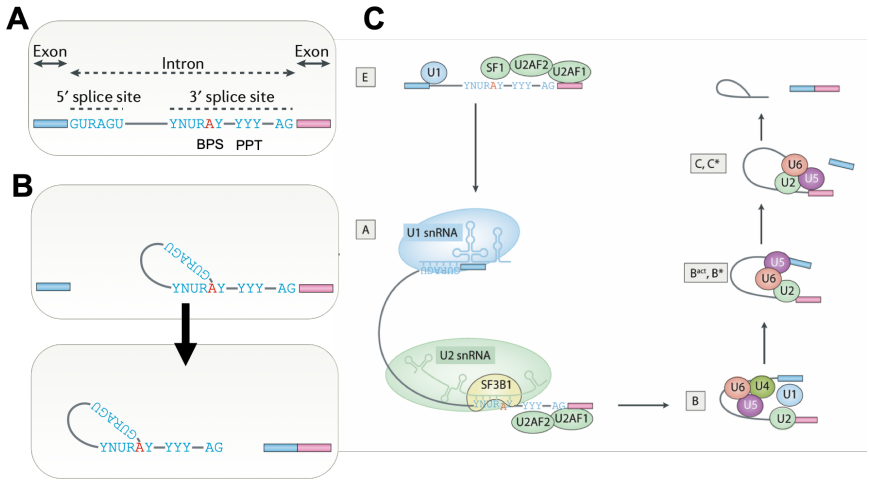

Figure 1. Pre-mRNA splicing. A | A pre-mRNA molecule and the exon-intron consensus sequences at the 5' and 3' splice sites. The branch point adenosine is represented in red. **B |** The splicing reaction involves 2 catalytic steps to remove an intron. **C |** Splice site recognition and the spliceosome assembly dynamics. BPS, branch point sequence; PPT, polypyrimidine tract. (Adapted from[35])

1.1.3 Alternative splicing

The selection of different and competing 5'SS and/or 3'SS within the same pre-mRNA alters the exonic and/or intronic sequences included in the final mRNA transcript. This highly regulated process known as alternative splicing (AS) is a crucial post-transcriptional regulator of gene expression and contributor to the proteome complexity within and between cells[36], as it allows the generation of more than one unique mRNA transcript from a single gene. Given that 90-95% of human genes undergo some level of alternative splicing according to genome-wide analyses, the biological relevance of this process seems highly likely[8,9], , although proteome analyses suggest that one main isoform is produced[37–39].

The different possibilities of alternatively spliced isoforms are depicted in Figure 2 and are defined by the choice between competing SS. Namely, these events are cassette exon skipping (ES), intron retention (IR), alternative 5'SS (A5'SS) and alternative 3'SS (A3'SS) (Figure 2A).

1.1.4 Other splicing regulatory elements: enhancers, silencers, and regulatory proteins

The recognition and usage of different SS depend on 3 key factors: the splice site strength (usually defined as similarity to consensus sequences and, thus proportionally related to spliceosome affinity), *cis*-regulatory sequences and *trans*-acting factors.

The *cis*-acting RNA sequence elements[40–42] assist splicing decisions either by recruiting RNA binding proteins (RBP) or by generating

secondary RNA structures[43]. They can be considered enhancers or silencers, depending on the outcome of splicing (increase or decrease of exon inclusion in the final transcript, respectively). These additional RNA motifs can be located within exons (exonic splicing enhancers [ESE] or exonic splicing silencers [ESS]) or introns (intronic splicing enhancers [ISE] or intronic splicing silencers [ISS]). Therefore, recognition of neighboring SS is facilitated or inhibited by the binding of auxiliary splicing factors to these *cis*-elements in the precursor RNA, in a context-dependent manner[44] (Figure 2B).

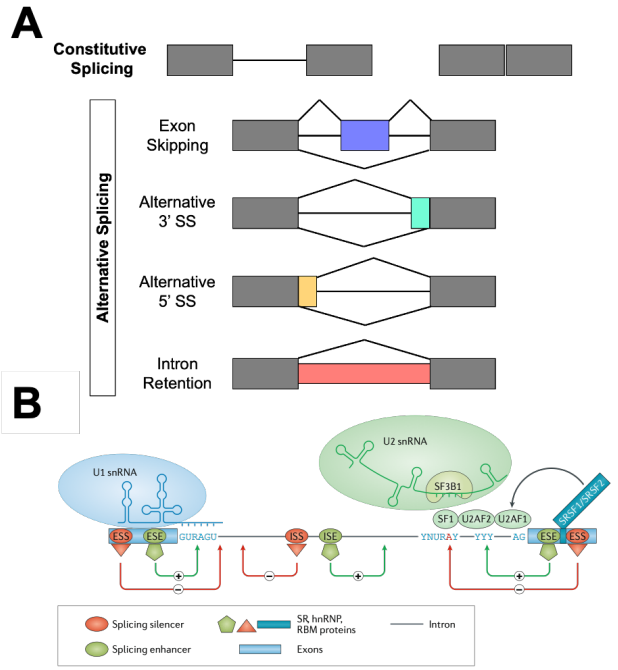

Figure 2. Alternative splicing. A | Patterns of alternative splicing. **B** | Regulation of alternative splicing by protein binding to different exonic and intronic regulatory elements. SS, splice site; snRNA, small nuclear RNA; ESS, exonic splicing silencer; ESE, exonic splicing enhancer; ISS, intronic splicing silencer; ISE, intronic splicing enhancer; SR, arginine-serine-rich; hnRNP, heterogeneous nuclear ribonucleoprotein; RBM, RNA-binding motif. (Adapted from[35])

ESEs regions are paradigmatically bound by serine/arginine-rich (SR) proteins[45,46], which have a binding preference for purine-rich exonic motifs[47,48], and promote the recruitment of spliceosomal components[49]. In general, these *trans*-acting factors bound to ESEs exert a positive splicing effect on both constitutive and alternative exons, resulting in an increased exon definition and consequently inclusion of the nearby exon[49,50].

Conversely, classic examples of splicing silencers (ISSs and ESSs) recruit the PPT- binding protein (PTB)[51–54] or heterogeneous nuclear ribonucleoproteins (hnRNPs)[42]. The inhibition of splicing (or decrease of exon inclusion) led by these *trans*-acting factors can be generated by different mechanisms, such as blocking the recruitment of spliceosome elements, competing with SR proteins or even by looping out exons, among others[55–58].

However, the interplay of *cis*- and *trans*-acting factor and the outcome of alternative splicing for a specific transcript is more complex and depends on additional circumstances[59]. For instance, the *trans*-factor NOVA has opposite effects depending on the position of its binding site in the pre-mRNA, promoting skipping if bound upstream of an alternative exon and promoting inclusion if bound downstream[60]. Additionally the cell-context is determinant[44,61–64], not only due to the existence of tissue-specific *trans*-acting factors such as NOVA[60] or RBFOX[65], but also because of differences in the levels or activity of the different spliceosome components and the positive or negative interaction of splicing factors[66,67]. Lastly, the coupling of splicing and both transcription and chromatin machineries adds another layer of complexity in splicing regulation[68].

A deeper knowledge of *cis*-regulatory features, due to genome-wide maps of splicing factors and transcriptome-wide analyses carried out in the last decade, has allowed the assembly of a highly complex "splicing code" which has the potential of predicting splicing outcomes[48,69–72]. The incorporation of different layers of regulation and their combinatorial effects, such as those previously mentioned, will definitely complement the accuracy of these predictions at different and specific cell conditions[42,73].

1.2 Alternative splicing in cancer

Recent genomic and RNA sequencing studies have demonstrated a significant mis-regulation of splicing in cancer[35,74–77]. These alterations can be either splicing disruptions of individual genes involved in cancer progression, as well as disruptions (mutations or changes in expression) of RNA splicing factors. Thus, recent studies have also identified widespread changes in alternatively spliced isoforms of tumor samples compared to healthy tissues[8,9,76,78–80]. These findings reveal a common dysregulation of splicing in cancer and point towards possible options for potential therapeutic development[35,74,81,82].

1.1.5 Splicing alterations in cancer

There are different types of mechanisms that can lead to mis-splicing in cancer. The most common alterations include mutations of *cis*-elements and splicing factors perturbations (either mutations or altered expression).

Integrated data that included genome-wide patterns of RNA splicing across different tumor types and their normal tissue counterparts has revealed that one third of single nucleotide variants (SNV) and about 20% of somatic missense mutations can lead to alterations in the spliceosome performance through the disruption of 5´or 3´SS, branch site or splicing regulatory elements[76,80,83]. Of note, the most common event associated to SNV affecting splice sites was intron retention, and these events occurred more frequently in tumor suppressor genes

(i.e. *TP53*, *ARID1A* and *PTEN*), resulting in premature termination codons[78,79,83–85]. Conversely, splicing disruptions of oncogenes are mostly driven by synonymous exonic mutations that affect ESE or ESS sequences[79].

On the other hand, splicing factors are frequently mutated in cancer[77]. Although somatic mutations in genes encoding core spliceosome elements were identified initially in hematological malignancies[86,87], splicing factor mutations are present across multiple tumor types[76,77,88–90]. These mutations usually occur usually in a mutually exclusive manner and as heterozygous point mutations at restricted residues, suggesting a potential synthetic lethal interaction that prevents accumulation of mutations and more than one hit in the splicing machinery. Overall, splicing factor 3b subunit 1 (SF3B1)[86–89,91–94], U2 snRNA auxiliary factor 1 (U2AF1)[95–99], serine/arginine-rich splicing factor 2 (SRSF2)[99–101] and zinc-finger, RBM and serine/arginine-rich 2 (ZRSR2)[86,99,102] are the splicing factors more recurrently affected.

In addition to mutations affecting genes encoding splicing factors, non-coding snRNA mutations, mainly in the U1, U2 and U11, have been also identified in several cancers[90,103,104]. Beyond mutations of spliceosome elements, up- or downregulation of splicing factors through expression changes or post-translational modifications can also lead cancer-associated mis-splicing[75].

1.1.6 Splicing events contribute to tumor progression

Given the widespread alterations of splicing in cancer, that these perturbations affect every hallmark of cancer[105] is not surprising. Mis-regulation of splicing provides cancer cells with the opportunity to promote growth and survival thanks to the generation of altered spliced isoforms[106–111]. Some of these genes that undergo to isoform switches affect key processes in cancer biology such as apoptosis (i.e., *Bcl-x*[112–114], *Fas*[115–118]), metabolism (*PKM*[119–125]), angiogenesis (*VEGF-A*[126–129]), cell cycle (*Cyclin D1*[130–134]), metastasis and invasion (*CD44*[135–137]) or epithelial-mesenchymal transition (*FGFR*[138–143]), among others[74,35].

In addition, the presence or generation of alternatively spliced isoforms of some oncogenes, such as *BRAF*, which will be further discussed throughout this thesis, have been related to therapy resistance[144]. Examples of such genes that undergo alternative splicing conferring resistance include the androgen receptor (AR and its AR-v7 transcript, lacking the ligand-binding domain to testosterone) in castration-resistant prostate cancer patients[145–147], the breast cancer gene 1 (*BRCA1*) that can have an impact in platinum sensitivity in ovarian and breast cancer patients[148,149] or the aberrant splicing of CD19 in patients relapsing following CART-19 (chimeric antigen receptor-armed autologous T-cells against CD19) therapy due to loss of the cognate CD19 epitope[150,151].

1.1.7 Targeting splicing in cancer

Mis-splicing of cancer provides an appealing opportunity for treatment, either by modulating or reversing the production of a specific isoform or by regulating specific components of the splicing

machinery. The therapeutic rationale for this latter approach is based on the dependency on the wild-type spliceosome function of splicing-mutant cancer cells, making these cells particularly vulnerable to global perturbations in splicing, leading to synthetic lethality effects[152–156].

Briefly, current views of therapeutic targeting of splicing can be divided into two strategies: antisense oligonucleotides (ASOs) and small-molecule splicing modulators[35,74,81,82,157].

Oligonucleotide-based therapeutics consists of short synthetic single-stranded nucleic acids that base-pair with specific complementary[158] regions in RNA. These interactions can promote i) mRNA degradation by enzymatic cleavage by RNase H which degrades RNA in RNA/DNA hybrids (i.e. mipomersen[159] or inclisaran[160] for the treatment of hypercholesterolemia), ii) repression of regulatory RNAs or, iii) the modification of alternative splicing patterns. The latter, also known as splice-switching oligonucleotides (SSOs), compete with the binding of splicing factors to *cis*-acting elements on pre-mRNAs and thus modulate SS competition. Eteplirsen and nusinersen are the first SSOs approved by the U.S. Food and Drug Administration (FDA) for the treatment of Duchenne muscular dystrophy and spinal muscular atrophy, respectively. While eteplirsen hybridizes to *DMD* (the gene encoding dystrophyin) and promotes skipping of exon 51, which harbors frameshift mutations[161], nusinersen was designed to bind the 5' region of intron 7 of *SMN2* to promote exon 7 inclusion and thus increase SMN protein levels[162]. Finding a specific splicing event with a meaningful impact in cancer cell survival and a delivery method that minimize

systemic toxicities are the major challenges of ASOs in cancer therapeutics. After promising results *in vitro* and *in vivo* (and also some disappointing initial results in patients), there are currently several clinical trials for ASOs targeting different pre-mRNAs (e.g., *bcl-2*[163–166], *H-ras*[167,168], *STAT3*[169,170] or *Grb2*[171] among others) assessing safety and efficacy in different clinical situations

Small molecules that are able to modulate splicing can be divided into SF3B inhibitors and splicing inhibitor sulfonamides, namely RBM39 degraders. SF3B inhibitors are the earliest class of splicing modulators and include spliceostatin A[172], sudemycins[173,174], pladienolide[95,175], E7107[176–178] (analog of pladienolide), H3B-8800[179,180] (oral analog of E7107) and herboxidiene[181,182]. Through the binding to the branch site binding pocket of the SF3B complex, these drugs prevent the interaction with the U2 snRNP and consequently lead to increased intron retention or, by exploiting differences in sensitivity between alternative SS, lead to cassette exon skipping. While phase I clinical trials with E7107 were discontinued due to unacceptable toxicity[177,178], H3B-8800 —proven to be more selective for spliceosome-mutant cells[179]— is currently under clinical investigation in SF3B1-mutant hematological malignancies (NCT02841540)[180].

Apart from SF3B1 binding agents, other spliceosome inhibitors agents under investigation are compounds that disrupt U2AF homology motifs preventing early spliceosome assembly (e.g., NSC 194308)[183,184] and protein arginine methyltransferase inhibitors (e.g., PRMT5 inhibitors)[185,186]. Finally, aryl sulfonamide molecules such as indisulam promote proteasomal degradation of accessory splicing

factors such as RBM39 and RBM23 and dose-dependent splicing alterations with good safety profiles[187–189], probably due to keeping intact core spliceosome components.

In addition, dysregulation of splicing (either intrinsically related to cancer or pharmacologically induced) brings another promising therapeutic opportunity in combination with immunotherapies[190,191]. Splicing-derived neoepitopes[192–194]—e.g. those induced by the generation of novel transcript isoforms upon treatment with splicing inhibitors— might increase the likelihood of response, similarly to the effects of increased mutational burden[195–197] or of deficient mismatch repair[198–200].

1.3 Cutaneous Melanoma

Cutaneous melanoma is the most common form of melanoma —a malignancy of melanocytes— and responsible of most deaths related to skin cancer[201]. Ultraviolet exposure is the main risk factor of cutaneous melanoma[202,203], especially leisure-time sun habits which have impacted on the increase of melanoma incidence rates in fair-skinned population from Western world countries over the past decades[204]. In 2020, the International Agency for Research on Cancer (IARC) predicted a sustained increase in the estimated global burden from melanoma[205].

1.3.1 Clinical and genomic classification

Clinical and histopathological classification based on tumor thickness and ulceration (T stage), lymph node involvement (N stage) and presence of distant metastases (M stage), and serum lactate dehydrogenase (LDH) levels, according to the American Joint Committee on Cancer (AJCC), are essential for risk calculation and treatment decisions[206,207]. However, the histological subtypes of cutaneous melanoma (namely superficial spreading, nodular or acral lentiginous) are less relevant for prognosis or subsequent treatments.

From the genetic point of view, several studies demonstrated the acquisition of gene alterations through the malignant transformation of benign naevi and disease progression[208,209]. Of note, $BRAF^{V600E}$ is one of the earliest acquired activating mutations[210–216]. However, other molecular events also affected the mitogen-activated protein kinase (MAPK) pathway such as *N-RAS*, but also different cellular

pathways like the PTEN-AKT-PI3K (phosphatase and tensin homolog – protein kinase B - phosphatidylinositol-3 kinase) pathway[216–219]. Other relevant events that have been described in melanoma over the past decades occurred in cell-cycle control genes (e.g., cyclin-dependent kinase -inhibitor 2 A [*CDKN2A*], cyclin-dependent kinase 4 [*CDK4*] or cyclin D1 [*CCND1*][220–222]) or mutations in the telomerase reverse-transcriptase promoter (*TERT*)[223,224], among others.

The Cancer Genome Atlas Network described the genomic alterations landscape of cutaneous melanoma and established four different subtypes based on the pattern of the most prevalent mutated genes: mutant *BRAF*, mutant *RAS*, mutant *NF1* and triple-wild type[225,226]. The *BRAF*-mutant is the most frequent subtype and accounts for approximately 50% of melanomas, followed by the mutated *RAS* (28%), *NF1* (14%) and triple-wild type. Although this genomic classification provided a novel framework for exploring druggable targets and potential predictive biomarkers, currently only the *BRAF* mutation status has a relevant clinical value and is crucial in the clinical setting[227–229].

1.3.2 The therapeutic landscape of melanoma

Until 2011, no systemic therapies for melanoma had demonstrated an improvement of overall survival (OS). However, the therapeutic landscape of advanced melanoma drastically changed over the past decade with the incorporation of two major therapy strategies: immune-checkpoint inhibitors (ICI) and MAP kinase pathway

inhibitors (MAPKi). As a result, a paradigm shift in terms of survival of advanced metastatic melanoma patients occurred: while median OS with monochemotherapy was 6-10 months[230], current median OS for first-line treatment drastically have drastically increased up to 32-60+ months[231,232] (Figure 3).

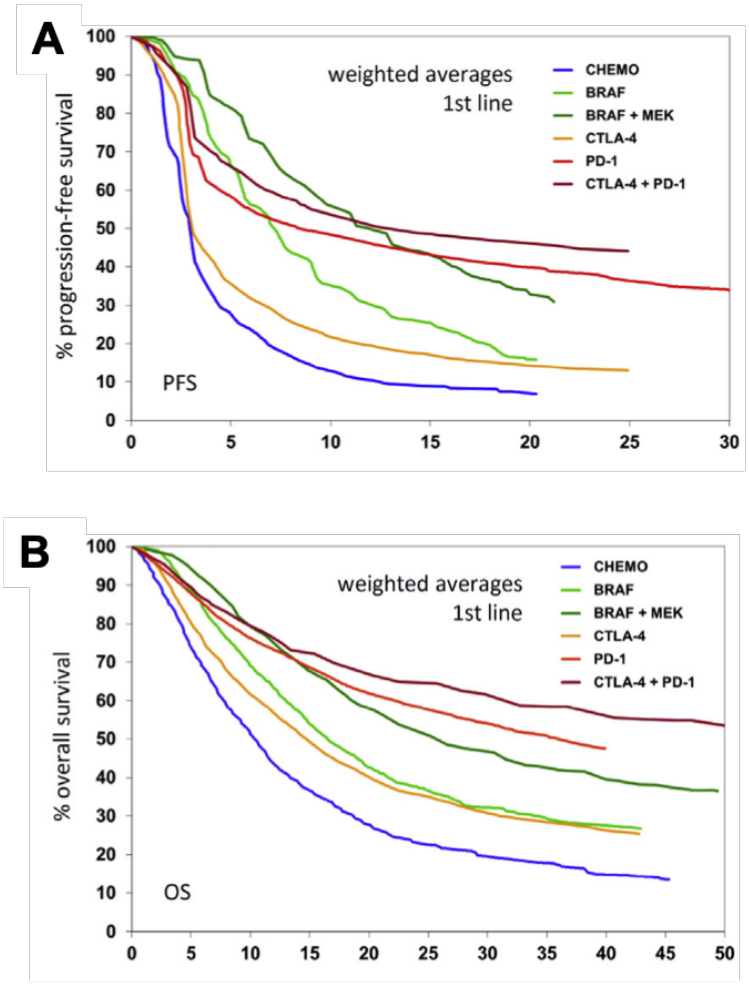

Figure 3. Survival curves created by weighted averaging of selected clinical trials in metastatic melanoma. A | Progression-free survival (PFS) and, **B |** overall survival (OS) in first-line therapy. (Adapted from[232]). Time in x axis is measured in months. CHEMO (blue line), chemotherapy; BRAF (light green), BRAF inhibitors; BRAF + MEK (dark green), BRAF and MEK inhibitor combination;

CTLA-4 (yellow), anti-cytotoxic T-lymphocyte antigen 4; PD-1 (light red), anti-programmed death 1; CTLA-4 + PD-1 (dark red), anti-PD-1 and anti-CTLA-4 combination

Ipilimumab, an anti-cytotoxic T-lymphocyte antigen 4 (CTLA-4) antibody, was the first ICI approved for a solid tumor and the first treatment that demonstrated an improvement in OS in a randomized clinical trial for advanced melanoma[233,234]. This breakthrough served as a major catalyst for the development and clinical research in checkpoint immunotherapy, particularly programmed death 1 (PD-1) blockade, which rapidly became the backbone of most immunotherapeutic approaches and improved clinical outcomes across several tumor types[235–238]. Nivolumab[239–241] and pembrolizumab[242–244] proved to be superior to dacarbazine and ipilimumab, respectively, and subsequently, PD-1-based therapy became standard of care for advanced melanoma. Nowadays, improvement of the ICI therapy is mostly being further driven by combinations, either with other ICIs or with other therapeutic agents[245,246]. Regarding ICIs combinations, ipilimumab plus nivolumab[247,248] and relatlimab (lymphocyte-activation gene 3 [LAG-3] antibody) plus nivolumab[249] have already shown to improve efficacy compared to ipilimumab and nivolumab, respectively, in patients with metastatic melanoma. Other combinations currently being explored in melanoma include MAPKi[250–253] or antiangiogenic agents[254] with anti-PD-1 antibodies.

Vemurafenib and dabrafenib were the first oral BRAF inhibitors (BRAFi) to be approved for the treatment of advanced *BRAF*-mutant melanoma[255]. Both BRAFi showed unprecedented objective

response rates (ORR) of approximately 50% of patients in two randomized phase 3 clinical trials[255,256]. Soon after, it was demonstrated that the addition of MAPK kinase (MEK) inhibitors (MEKi) improved clinical outcomes in this population (Table 1), and currently 3 different BRAFi+MEKi combinations are available for the treatment of unresectable *BRAF*-mutant melanoma patients: vemurafenib plus cobimetinib[257,258], dabrafenib plus trametinib[259,260] and encorafenib plus binimetinib[261,262]. Unfortunately, despite impressive ORR and meaningful improvements in progression-free survival (PFS) and OS with BRAFi+MEKi, disease progression almost invariably occurs, due to the acquisition of resistance to MAPK targeted therapy.

The milestones of the two therapeutic strategies (ICI and BRAF-MEK targeted therapy) in metastatic melanoma have been translated into clinical benefit for patients with earlier stages of melanoma. Thus, adjuvant dabrafenib plus trametinib or anti-PD-1 therapy (either nivolumab or pembrolizumab) have recently demonstrated to improve relapse-free survival and have become standard of care for high-risk melanoma patients after complete surgical resection[263–266]. Likewise, neoadjuvant treatment—that is, systemic therapy administered before surgery with the dual aim of determining therapy efficacy and prognosis— are also being investigated in resectable high-risk melanoma patients[267–271].

Study	n	Tx	ORR (%)	mPFS, months (95%CI)	PFS rate (%)				HR (95%CI)	mOS, months (95%CI)	OS rate (%)				HR (95%CI)
					12 mo	24 mo	36 mo	60 mo			12 mo	24 mo	36 mo	60 mo	
BRIM-3 ref [272,273]	337	Vem	57	6.9 (6.1-7.0)	NR	NR	NR	NR	0.38 (0.32-0.46)	13.6 (12.0–15.4)	56	30	21	NR	0.81 (0.7-1)
	338	DTIC	9	1.6 (1.6-2.1)	NR	NR	NR	NR		9.7 (7.9-12.8)	46	24	19	NR	
coBRIM ref [258,274,275]	247	V + C	70	12.6 (9.5-14.8)	NR	32	23	14	0.58 (0.46-0.72)	22.5 (20.3-28.8)	74.5	49	38.5	31	0.70 (0.55-0.9)
	248	Vem	50	7.2 (5.6-7.5)	NR	16	13	10		17.4 (15.0-19.8)	63.8	39	31.1	26	
BREAK-3 ref [256,276,277]	187	Dab	50	5.1	NR	NR	16	12	0.30 (0.18-0.51)	NR	NR	NR	31	24	NR
	63	DTIC	6	2.7	NR	NR	3	3		NR	NR	NR	28	22	
METRIC ref [278]	214	Tram	29	4.9	NR	NR	NR	NR	0.54 (0.41-0.73)	15.6	60.9	32	NR	13.3	0.84 (0.63-1.11)
	108	DTIC or paclitaxel	9	1.5	NR	NR	NR	NR		11.3	49.6	29.4	NR	17	
COMBI-v ref [279,280]	352	D + T	67	11.4	NR	30	25	NR	0.56 (0.46-0.69)	26.1	72	53	45	NR	0.69 (0.53-0.89)
	352	Vem	53	7.3	NR	16	11	NR		17.8	65	39	32	NR	
COMBI-d ref [259,281]	211	D + T	68	11.0	NR	30	22	NR	0.71 (0.57-0.88)	25.1	74	52	44	NR	0.75 (0.58-0.96)
	212	Dab	55	8.8	NR	16	12	NR		18.7	68	43	32	NR	

Study	n	Tx	ORR (%)	mPFS, months (95%CI)	PFS rate (%)				HR (95%CI)	mOS, months (95%CI)	OS rate (%)				HR (95%CI)
					12 mo	24 mo	36 mo	60 mo			12 mo	24 mo	36 mo	60 mo	
COLUMBUS part 1 ref [261,282,283]	192	E (450) + B	64.5	14.9 (11.0-18.5)	56	37	29	23	EB vs V: 0.54 (0.41-0.71) EB vs E: 0.68 (0.52-0.9)	33.6 (24.4-39.2)	76	58	47	34.7	EB vs V: 0.61 (0.48-0.79)
	194	Enc	51.5	9.6 (7.5-14.8)	NR	NR	25	19		23.5 (19.6-33.6)	NR	NR	41	34.9	
	191	Vem	40.8	7.3 (5.6-8.2)	32	20	14	10		16.9 (14.0-24.5)	63	43	31	21.4	
COMBI-I* ref [284]	267	Sparta + D + T	69	16.2 (12.7-23.9)	58	44	NR	NR	0.82 (0.66-1.03)	NR	NR	68	NR	NR	0.79 (0.59-1.05)
	265	D + T	64	12.0 (10.2-15.4)	50	36	NR	NR		NR	NR	62	NR	NR	
IMspire150 ref [252,285]	256	Atezo + V + C	66.7	15.1	54	NR	NR	NR	0.79 (0.64-097)	39.0	76.1	61.5	NR	NR	0.84 (0.66-1.06)
	258	V + C	65	10.6	45	NR	NR	NR		25.8	76.5	53.3	NR	NR	
KEYNOTE-022* Phase 2 ref [286,287]	60	Pembro + D + T	63	16.9 (11.3-27.9)	62	41	NR	NR	0.53 (0.34-0.83)	Not reached	80	63	NR	NR	0.64 (0.38-1.06)
	60	D + T	72	10.7 (7.2-16.8)	47	16	NR	NR		26.3	73	52	NR	NR	

Table 1. Key clinical outcomes of randomized clinical trials with MAPK inhibitors. All clinical trials in the table are phase III randomized clinical trials, except for KEYNOTE-022 which is a phase II randomized clinical trial. Abbreviations: n, number; ORR, objective response rate; mPFS, median progression-free survival; mo, months; CI, confidence interval; HR, hazard ratio; mOS, median overall survival; NR, not

reported; Vem, vemurafenib; DTIC, dacarbazine; V + C, vemurafenib + cobimetinib; Dab, dabrafenib, Tram, trametinib; D + T, dabrafenib + trametinib; E + B, encorafenib + binimetinib; Enc, encorafenib; Sparta, spartalizumab; Atezo, atezolizumab; Pembro, pembrolizumab. *COMBI-I and KEYNOTE-022 failed to meet primary endpoint of investigator-assessed PFS.

1.4 BRAF in melanoma

First identified as an oncogene decades ago[288], sequencing efforts in 2002 determined a high frequency of oncogenic somatic mutations in *BRAF* (v-raf murine sarcoma viral oncogene homolog B1) particularly within the kinase domain, in a wide range of human cancer cell lines (including melanoma, colorectal cancer, and non-small-cell lung cancer [NSCLC])[289,290]. Notably, missense mutations were identified in more than 60% of melanoma samples and the most common mutation was a single substitution at the V600 position (c.1799 T > A, p.V600E)[211]. This mutation encodes the constitutively active $BRAF^{V600}$-mutant oncoprotein, which constitutively activates the MAPK pathway leading to uncontrolled cell proliferation and melanoma cells survival.

1.4.1 The *BRAF* gene and the oncogenic mutation

Located in chromosome 7 (7q34), the *BRAF* gene encodes a protein belonging to the RAF family of serine/threonine protein kinases, part of the MAPK/extracellular signal-regulated kinase 1/2 (ERK) signaling pathway. This gene (RefSeq accession number NM_004333, Ensembl ID ENSG00000157764) has a genomic size of 190,752 nucleotides (Figure 4A). The transcript (NM_004333.6, ENST00000646891) consists of 18 coding exons, with a transcript length of 6,459 base pairs and an ORF (open reading frame) of 766 amino acids (Figure 4B).

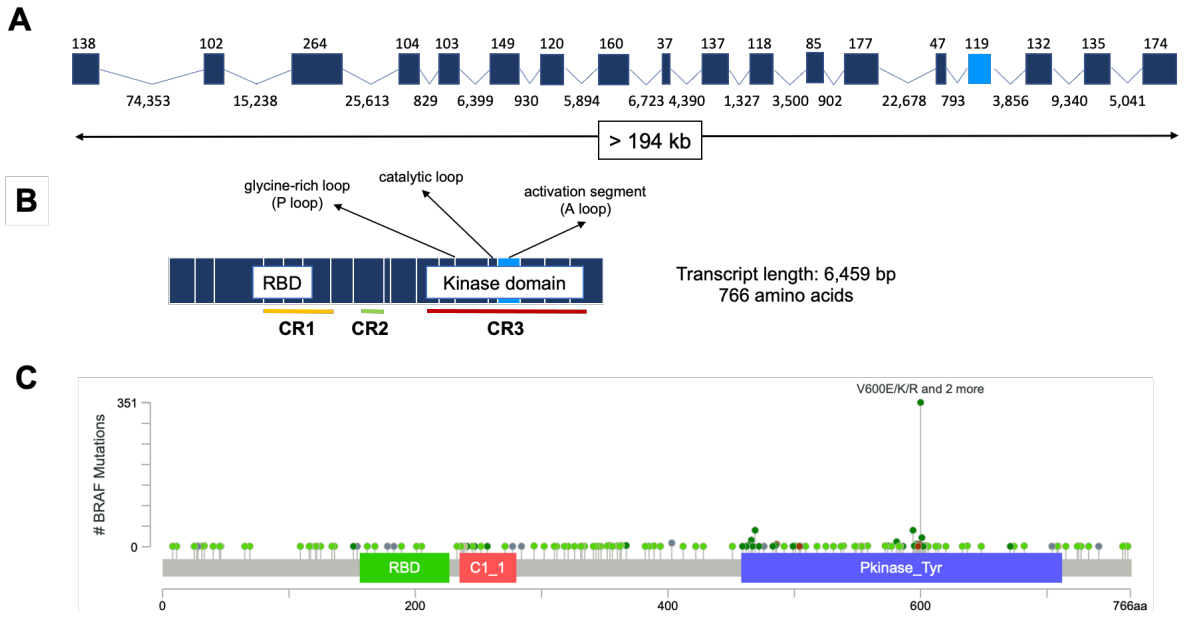

Figure 4. Representation of the *BRAF* gene, its transcript and protein domains. A | *BRAF* gene and its genomic length, including exons and introns sizes. Exon 15, where the hotspot mutation T1799A is located, is represented in light blue**. B** | BRAF transcript exons and the functional protein representation. RAS-GTP binding domain (RBD) is encompassed within the conserved region 1 (CR1, yellow) and the kinase domain within CR3 (red). Exon 15 (light blue) encodes for the activation segment. **C** | Spectrum of BRAF mutations from cBioportal[291,292]. MSK-IMPACT Clinical Sequencing Cohort[290] and Pan-cancer analysis of whole genomes (ICGC/TCGA)[293] cohorts were included. Missense mutations are represented in green, truncating mutations in gray and in-frame mutations in red. Dark colors correspond to putative driver mutations and light colors to mutations of unknown significance.

BRAF shares with the other RAF paralogs (ARAF and CRAF) three highly conserved regions (CR): CR1 and CR2, both regulatory regions in the N-terminus, and CR3 or the C-terminus catalytic domain (Figure 4B). CR1 contains the RAS-GTP binding domain (RBD) and the cysteine-rich domain (CRD), which can also interact with RAS proteins, both required for membrane recruitment. CR2, that encompasses the serine- and threonine-rich region, acts as a flexible hinge between CR1 and CR3. CR3 encodes the serine/threonine kinase domain in the C-terminus. The BRAF kinase domain contains the N region, the glycine-rich ATP-phosphatase-binding loop (also known as P-loop), the catalytic loop and the activation segment or A-loop (which is preceded by a DFG motif). Two regulatory 14-3-3 biding sites flanks the BRAF kinase domain[294–299]. The binding of these 2 sites through a 14-3-3 dimer keeps BRAF in an autoinhibited conformation that blocks the kinase domain dimerization[300].

BRAF mutations can be divided into 3 groups[301,302]: a) class I, which constitutively activates BRAF as monomer (V600E/K/D/R/M); b) class II mutations, which generate RAS-independent BRAF constitutive dimers (e.g., K601E/N/T, L597Q/V, BRAF fusion proteins); and c) class III mutations, which impair (or even inactivate) the BRAF kinase activity (such as the kinase-dead D594N/G mutations, or the kinase-impaired G466V/E mutants, among others). Class III mutations promote MAPK co-activation with RAS, and are therefore not independent drivers, which are often associated with other mutations (e.g., *RAS* or *NF1* mutations) (Figure 5). It is noteworthy that both kinase-activating class I and class II mutations,

which are by far the most frequent, achieve ERK signaling in a RAS-independent manner. However, while class I mutant proteins function as monomers, class II mutant proteins require dimerization. Some of the most common mechanisms of resistance (that are explained below) reactivate the MAPK pathway due to dimerization of BRAF (class II), such as BRAF amplification, NRAS mutation or "alternative splicing" of BRAF. About 80% of activating mutations occurred in the P-loop or activation segment (within or adjacent to the DFG motif) and lead to destabilization of the inactive conformation of the DFG motif/activation segment, thus mimicking the active conformation which in physiological state is induced by phosphorylation of the activation segment. This BRAF mutation classification is of clinical relevance, because currently available BRAFi are BRAF "monomer" inhibitors, and for this reason, only class I BRAF mutants are sensitive.

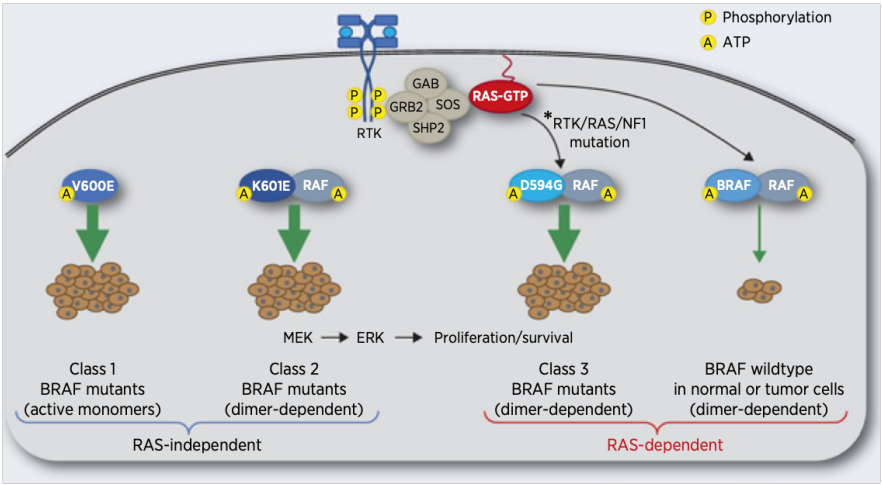

Figure 5. MAPK activation and classes of BRAF mutants. Class I and II mutations (left, blue) activate the MAPK pathway in a RAS-independent manner, while class III mutations and BRAF wild type (right, red) require the upstream RAS signal. Only class I mutation (e.g., V600E) act as a monomer, while the rest of BRAF mutants and wild type require dimerization to activate downstream MEK. Class III mutation impairs the kinase activation and requires co-occurrent

alterations (e.g., *RAS* or *NF1* mutations) that drive to co-operative MAPK activation (Adapted from[303])

As mentioned before, *BRAF*^{V600E} is by far the most common RAF mutation detected in cancer, and belongs to the class I BRAF mutations, together with the V600M/K/R/D mutations. Tumor molecular profiling of different tumor types showed that oncogenic *BRAF* mutations were particularly frequent in hairy cell leukemia (nearly 100%), papillary thyroid cancer (70%), cutaneous melanoma (42%), Langerhans cell histiocytosis (39%)[304,305,290]. Moreover, although not as frequent, *BRAF* mutations in colorectal cancer (10%) and NSCLC (4%) are clinically relevant since MAPKi have been included as part of the standard of care for these patients.

1.4.2 The MAPK pathway

The MAPK (RAS-RAF-MEK-ERK) pathway is an essential signaling pathway from cell surface to the nucleus for cell growth, proliferation and survival[306]. In short, growth factors binding to receptors of tyrosine kinase (RTK) at the cell surface lead to phosphorylation of RAS[307]. GTP-loaded RAS then recruits RAF proteins (such as BRAF) to the membrane by binding their RBD. A number of phosphorylation events take place to release 14-3-3 protein, allow oligomerization and activate the BRAF kinase domain[308–310]. Upon activation, RAF kinases phosphorylate MEK1/2 which in turn activate ERK1/2. Lastly, multiple ERK-phosphorylated substrates induce transcriptional changes promoting cell proliferation and survival.

Cryogenic electron microscopy studies have recently shown that, in the quiescent state, wild-type BRAF proteins form complexes with MEK1 and 14-3-3 proteins, a configuration that is also stabilized by the cysteine-rich domain (CRD)[300,311,312]. The CRD is an auto-inhibited structure that prevents dimerization of the BRAF kinase domain due to the blockade of the BRAF dimer interface and the occlusion of the membrane-binding region of the CRD by binding of 14-3-3. Relief of the auto-inhibition state promoted by RAS interaction releases the inhibitory effect of 14-3-3. Phosphorylation of different sites at the activation segment, as well as RAS clustering that increases RAF concentration in the membrane allow the formation of active, back-to-back BRAF dimers[300]. Lastly, dimerization induces RAF catalytic activity, leading to phosphorylation of MEK.

In contrast to wild-type BRAF proteins that require RAS-induced (oligo)dimerization, the constitutive activation of the MAPK pathway driven by $BRAF^{V600}$ mutants occurs by means of RAS-independent catalytically active monomers[313,314]. Activating mutations occur predominantly in the activation segment. These mutations destabilize the nonproductive off-state conformation of the activation segment and the surrounding catalytic cleft (αC helix OUT). Displacement of helix αC towards an OUT conformation prevents phosphorylation of the activation segment, thus precluding the formation of a salt bridge (between residues K483 and E501) required for coordination of ATP phosphate groups[313]. Specifically, the V600E mutation forms a salt-bridge with residue K507, which constitutes the core of the dimerization interface[297,300]. This salt

interaction has a key structural impact on BRAF, resembling the productive on-state conformation (αC helix IN) adopted only upon dimerization in the wild-type BRAF, and leading to increased kinase activity compared to the wild-type enzyme[315].

1.4.3 The MAPK inhibitors

Initial studies showed that RNA interference targeting $BRAF^{V600E}$ induced growth arrest and promoted apoptosis[316–318]. Later on, class II non-selective RAF inhibitors, such as the multikinase inhibitor sorafenib, failed to prove clinical benefit in *BRAF*-mutant melanoma patients[319]. Therefore, a second-generation of ATP-competitive, selective BRAFi —vemurafenib and dabrafenib—, also known as class I RAF inhibitors (mostly active against the activated conformation of RAF kinases), that bind to the active DFG motif-IN conformation / αC helix OUT position, were developed to specifically target $BRAF^{V600E}$ and demonstrated remarkable antitumor activity in early phase clinical trials[320,321]. Intriguingly, these BRAFi were potent inhibitors of $BRAF^{V600E}$ but at the same time were also inducing activation of the MAPK pathway in wild-type BRAF cells[322–325]. Further biochemical studies revealed the link between the selectivity of $BRAF^{V600E}$ and the paradoxical activation of wild-type BRAF: vemurafenib successfully inhibits active $BRAF^{V600E}$ monomers, stabilizing the αC helix in the OUT (inactive) conformation, and at the same time induces negative allostery when binding to a protomer within RAF dimers, leading to dimer partner transactivation and preventing vemurafenib binding of this protomer[314,323,324,313]. This property is a double-edged sword: the

exquisite preference for $BRAF^{V600}$ monomers that provides a broad therapeutic index, however limits the antitumor efficacy in class II or III BRAF mutations[301,326] and explains why any mechanism that promotes BRAF dimerization confers resistance to this type of inhibitors.

RAF monomer-selective inhibitors (vemurafenib, dabrafenib and encorafenib) in combination with MEKi (cobimetinib, trametinib and binimetinib, respectively) are currently the standard of care in advanced BRAF-mutant melanoma[258,261,260]. Nevertheless, dabrafenib plus trametinib is also approved for the treatment of advanced $BRAF^{V600E}$ NSCLC[327] and for locally advanced or metastatic $BRAF^{V600E}$ anaplastic thyroid cancer[328]; and encorafenib in combination with cetuximab (anti-epidermal growth factor receptor [EGFR] antibody) for the treatment of metastatic $BRAF^{V600E}$ colorectal cancer[329].

Drug development efforts are currently directed to overcome the limitations of RAF inhibitors with next generation compounds that a) avoid paradoxical activation (paradox breakers), b) equally target both monomers and dimers or, c) selectively inhibit RAF dimers[330].

1.4.4 Mechanisms of resistance

Despite the impressive ORR and the improvement of PFS and OS, the median duration of response to BRAFi+MEKi is around 12 months, and most patients experience treatment failure due to acquisition of resistance. Although resistance to MAPK inhibitors can be classified according to the time of treatment (intrinsic or primary, secondary or acquired, and adaptive resistance), the

underlying mechanisms are common and most of them lead to the reactivation of the MAPK pathway[331,332]. Genetic mechanisms of resistance have been widely described, but non-genomic (including transcriptomic and methylomic) and immune mechanisms can also play an important role[333].

Some examples of the mechanisms that can reactivate the MAPK pathway are RTK upregulation and overexpression (i.e., platelet-derived growth factor receptor β [PDGFRβ], insulin-like growth factor 1 receptor [IGF1R] or hepatocyte growth factor [HGF])[334,335] or mutations in *RAS*[334] and *MEK*[336–338]. On the other hand, MAPK signaling restoration due to an increased dimerization of RAF has been observed through *BRAF* amplification or copy-number gain[338,339], alternative splicing of BRAF[340] and elevated CRAF levels[341], among others. In addition, the MAPK signaling can be restored and bypassed by means of the PI3K-AKT-mTOR (mammalian target of rapamycin) pathway[342,343] or dysregulation of cell-cycle related proteins[344,345]. Moreover, several studies demonstrated that different mechanisms of resistance can arise from a single melanoma cell line[334,340,346], and this heterogeneity was also observed in patients developing resistance[333,347].

1.4.5 Alternative splicing of BRAF

In 2001, a novel mechanism of resistance to vemurafenib was identified: aberrantly spliced $BRAF^{V600E}$ isoforms enhanced dimerization and therefore reactivated the MAPK pathway. This finding was first observed in the BRAF-mutant melanoma cell line SKMEL-293 after exposure to vemurafenib (2 μM). In three of the 5

resistant clones, analysis of BRAF protein expression and cDNA revealed the presence of a smaller protein (p61BRAF^{V600E} with a molecular weight of 61 kDa instead of 90 kDa) that corresponded to a novel transcript lacking exons 4-8. Inspection of the *BRAF* locus on chromosome 7q34 by array CGH data suggested no evidence of an intragenic somatic deletion within the *BRAF* gene. In addition, six tumor samples of nineteen patients that developed vemurafenib resistance also harbored different shortened BRAF^{V600E} transcripts lacking exons 4-10, exons 4-8, exons 2-8 and exons 2-10. Interestingly, these BRAF splicing variants were not detected in melanoma cell lines or tumors that had not been exposed to BRAFi and, these events were confined to the mutant *BRAF* allele[340]. Later on, other studies also proved evidence for the emergence of different alternative transcripts after BRAFi monotherapy or BRAFi+MEKi exposure, allegedly generated through alternative splicing, both in *in vitro* and *in vivo* experiments[339,348–350] (Table 2) (Figure 6).

BRAF AS variant	Treatment of resistant tumors with BRAF AS (clinical studies)	Cell lines with BRAF AS	How was resistance acquired?
BRAF1-9	BRAFi[340,347,351]	1205Lu PRT#4[348]	*in vivo* (xenografts)
		SMU027[349]	*in vivo* (patient)
BRAF1-11	BRAFi[340,347,351,352] BRAFi+MEKi[353]	M397AR[339]	*in vitro*[339]
		WMD009[349]	*in vivo* (patient)
BRAF2-11	*Not detected in patient's tumors*	1205Lu PRT#3[348]	*in vivo*[348] (xenografts)
BRAF3-9	BRAFi[340,347,351]	SKMEL293-C3[340]	*in vitro*[340]
BRAF3-11	BRAFi[340]	BR4[349]	*in vitro*[349]

Table 2. Summary of the different alternative spliced isoforms of BRAF detected across different studies. All BRAF AS, but BRAF2-11, variants were detected in resistant tumor from patients after BRAFi (BRAF inhibitor monotherapy). BRAF1-11 was also detected in patient's tumor progressing on BRAFi + MEKi combination. All BRAF AS variants were detected in different cellular models. These cell lines were established from *in vitro* exposure of a given cell line (e.g., M397AR), from *in vivo* exposure of 1205Lu-xenografts (e.g., 1205Lu PRT#4) or from short term-derived culture from resistant tumors biopsied from patients (e.g., SMU027). BRAF AS, alternatively spliced isoforms of BRAF.

Likewise, several studies reported that samples from patients that developed resistance to BRAFi also displayed the presence of $BRAF^{V600E}$ isoforms[340,339,352,354,351,355]. A multicenter study[355] that included 3 different patient cohorts[347,351,354] with a total of 100 patients and 132 tumor samples at BRAFi progression, showed that up to 27% (21 of 77 samples with an identified mechanism of resistance) of resistant patients developed BRAF splice variants. However, less is known regarding BRAF alternative splicing (AS) as a resistance mechanism to combined BRAFi+MEKi: only 2 different studies that included 11 and 5 patients who received dabrafenib-trametinib evaluated the presence of AS of BRAF, and BRAF1-11 was detected in 1 patient[353,356]. In all studies, the detection of BRAF splice variants was based on RT-PCR or RNA-seq. In addition, recently it has been shown that these BRAF variants can also be detected in plasma cell-free RNA[357].

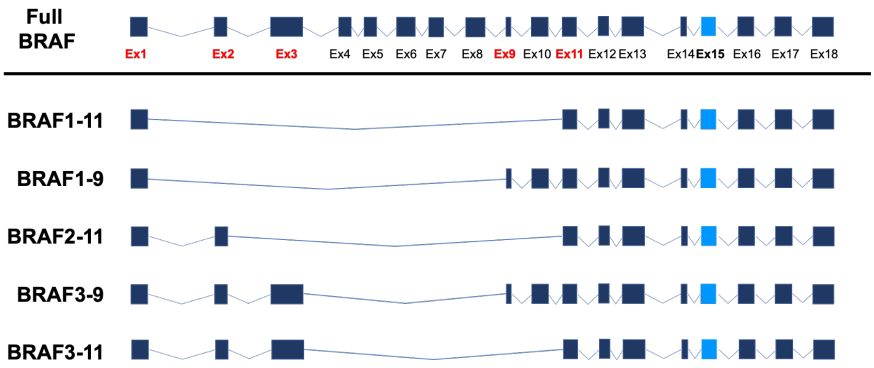

Figure 6. Alternative spliced isoforms of BRAF associated with acquisition of resistance to MAPK inhibitors. Exons involved, either as acceptor or as donors, in alternative spliced isoforms are marked in red bold. Exon 15, where the hotspot mutation T1799A is located, is represented in light blue. Ex, exon.

The mechanisms underlying the generation of AS of BRAF were only studied in the parental SKMEL-293 cell line and its resistant counterpart subline C3, which harbors the BRAF3-9 isoform (lacking exons 4-8). A mutation in the -51 nucleotide (a C-to-G conversion) upstream of the 3'SS of intron 8 in the *BRAF*^{V600E} allele was deemed to be responsible of the AS isoform. This mutation was *in silico* predicted to be a branch point. In addition, pre-mRNA splicing modulators spliceostatin A and meayamycin B counteracted the production of BRAF3-9 (and BRAF1-11 in the case of M397AR cell line), thus overcoming vemurafenib resistance[358]. In contrast, another study did not support the presence of any -51 nucleotide mutation upstream of the 3'SS of intron 8, as important for the generation of the BRAF3-9 in three patients samples[359].

MAPKi resistance mechanisms have been explored in other *BRAF*-mutant cancer types and the spectrum of alterations is similar to those reported in melanoma[360–362]. In particular, AS of BRAF has also been

detected after vemurafenib exposure in the $BRAF^{V600E}$ NSCLC cell line HCC364[363].

1.4.6 BRAF genomic aberrations

Apart from copy number alterations, amplifications and alternative spliced isoforms, other genomic rearrangements of BRAF such as fusions, duplications and deletions have been also described and, in some cases, related to BRAFi±MEKi resistance.

Fusion genes affecting oncogenes are a common class of cancer driver genomic aberrations, and among all kinases BRAF is by far one of the most prevailing fusion partners across tumor types[290]. Classically described in pilocytic astrocytoma[364], but also found in other tumor types[365], more than 50 BRAF fusions have been described. Most of them produce a N-terminal partner gene protein (i.e., *SND1* or *KIAA1549*) and a C-terminal upstream portion of the BRAF protein, usually encompassing the kinase domain[366,365,290,367,368]. Breakpoints within *BRAF* are located in introns 7, 8, 9 or 10. Sensitivity to BRAFi, evaluated *in vitro* in cell lines with different BRAF fusions, depended on the presence of a dimerization domain in the N-terminal partner of the fusion protein[369,368]. Furthermore, a case report of a BRAF-mutant melanoma patient that experienced disease progression under vemurafenib showed the presence of a BRAF fusion as the responsible of the BRAFi resistance[370]. Similarly, BRAF kinase domain duplications have also been detected in resistant melanoma xenografts and in clinical patient tumors[371,350]. Interestingly, breakpoints also occurred within the same region.

Moreover, large intragenic deletions of *BRAF* have been also identified in diverse tumor types (including bladder cancer, colorectal cancer, prostate cancer, NSCLC and melanoma), mostly affecting exons that encode the RBD[290]. Particularly, a clinical case of a *BRAF*-mutant melanoma patient who progressed on dabrafenib plus trametinib due to an internal deletion involving exons 2-8 in *BRAF* was reported[372]. Similarly, an internal deletion including exons 2-10 and exon 2-8 were identified in BRAFV600E colorectal cancer patients who progressed on vemurafenib plus anti-EGFR therapy[373,374]. In NSCLC patients, deletions in *BRAF* have been also reported, although a BRAF rearrangement was detected in 1 of 7 matched samples of vemurafenib-treated patients at progression[375]. Although these deletions could mimic aberrantly spliced isoforms, AS and intragenic deletion of BRAF have been considered independent mechanisms of resistance. Short in-frame deletions within the αC loop of *BRAF* were also identified in pancreatic and thyroid tumor samples from TCGA. This shortened truncated loop force the αC in a IN conformation, thus providing vemurafenib (that binds the αC OUT) resistance due to this conformational change[376,377].

2 OBJECTIVES

Given the clinical relevance of the generation of alternatively spliced (AS) isoforms of BRAF, due to their links with the acquisition of resistance to MAPK inhibitors resistance, we aimed to improve our understanding of the molecular mechanisms involved and their potential clinical implications.

To shed light on this relevant mechanism of resistance, we set up the following objectives:

1. Asses the nature and frequency of BRAF AS across different melanoma samples using RNA-sequencing datasets

2. Unravel the mechanisms underlying the generation of BRAF AS isoforms, with a special focus on finding a common mechanism that might explain the generation of the different BRAF AS isoforms associated with the acquisition of resistance

3 RESULTS

3.1 PART I. The spectrum of BRAF mRNA isoforms in melanoma: RNA-seq data

Given the limited size of cohorts in previous studies of BRAF mRNA isoforms[351,347,355,333], we aimed to explore the spectrum of BRAF alternative splicing events in a higher number of melanoma samples. For this purpose, we first collected publicly available melanoma RNA-seq samples, from both patient tumor samples of patients and from cell lines (see below) to generate our own custom dataset. This was complemented by an analysis of BRAF mRNA isoforms in the cutaneous melanoma dataset of the TCGA project (https://www.cancer.gov/tcga)[225].

To address this, we performed alternative splicing analysis using VAST-TOOLS (Vertebrate Alternative Splicing and Transcription Tools)[64,378], a toolset for profiling and comparing AS events in RNA-seq data. In short, we performed the reads alignment with VAST-TOOLS and then quantified the read counts for all possible exon-exon junction (EEJ) combinations in the *BRAF* gene across all the samples (Figure 7). To avoid spurious detection of extremely rare mRNA variants or misalignment due to sequencing errors, we only took into consideration EEJ events with a minimum coverage of 5 supporting reads in at least one of the samples.

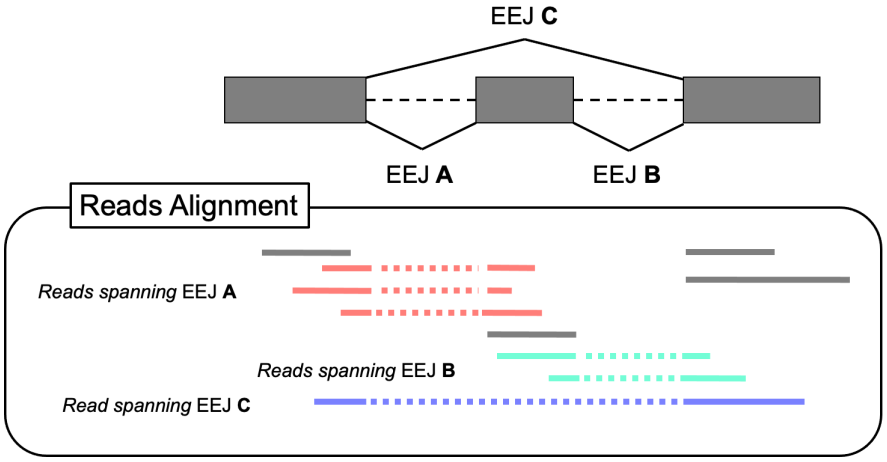

Figure 7. Exon-exon junction detection in RNA-seq. Schematic diagram representing the quantification of read counts for each EEJ (exon-exon junction)

3.1.1 Custom Melanoma dataset

First, we built our custom melanoma datasets collecting RNA-seq datasets from public repositories comprising both melanoma cell lines and melanoma patients, predominantly *BRAF*-mutant (74%, 200 of 270). Information regarding the sample origin (primary tumor or metastasis) and exposure/resistance to BRAFi±MEKi were also gathered when available.

A total of 270 samples (119 from patients and 151 from cell lines) were included from 9 different datasets available in the Sequence Read Archive (SRA), Gene Expression Omnibus (GEO) or BioProject repository (see Materials and Methods). Eighty-three samples were considered resistant (44 from patients and 39 from cell lines) and 87 samples were considered sensitive to BRAFi±MEKi. No specific information was found for the remaining 100 samples. Among the 119 samples derived from patient tumors, 57 were from primary melanoma and 62 from metastatic lesions. Phenotypic and

clinical data are summarized in Table 3 (detailed information of the patient and cell lines samples is provided in Materials and Methods).

	Patient samples	Cell line samples	Total
	119	151	270
BRAFi sensitivity			
Sensitive	18	69	87
Resistant	44	39	83
NR	57	43	100
Origin			
Primary tumor	57	-	
Metastasis	62	-	
Mutational status			
BRAF mutant	85[#]	115*	
NRAS mutant	15	16	
Non-*BRAF*/Non-*NRAS* mutation	19	1	

Table 3. Phenotypic and clinical features of samples included in the custom melanoma dataset. NR, not reported. [#]*BRAF* mutation status was as follows: V600E in 50 cases, V600K in 10 cases, V600R in 2 cases, and not specified in 23 (4 of which were also *NRAS* mutant). ***BRAF* mutation status was: V600E in 112 cases, not specified in 3 cases.

In our custom dataset, we included samples that were single-end (3 cohorts[350,379,380]) and paired-end sequenced, and the read length ranged from 48 to 200 nucleotides. Considering exclusively the BRAF locus, the mean number of reads was 261.5 and the median number of reads was 169.5. The coverage of BRAF EEJs among the 270 samples ranged from 7 up to 4,070 reads (Figure 8).

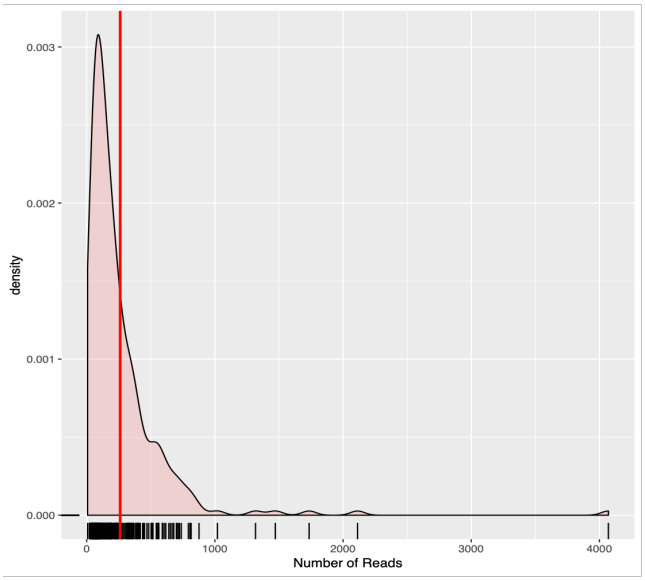

Figure 8. Density plot of number of exon-exon junction reads across BRAF. Red line represents the mean number of reads

The analysis of the EEJ reads distribution demonstrated that all canonical EEJ could be detected; however, the mean coverage or number of reads were not homogeneous across the different EEJ (Figure 9A). We also detected several alternative, non-canonical EEJ. Among the alternative EEJ identified, we were able to detect the EEJ 1-11 and 3-9, which were previously related to resistance to MAPKi[339,340]. Besides, we observed an exceptional number of alternative EEJ, whose biological significance remains unknown (Figure 9).

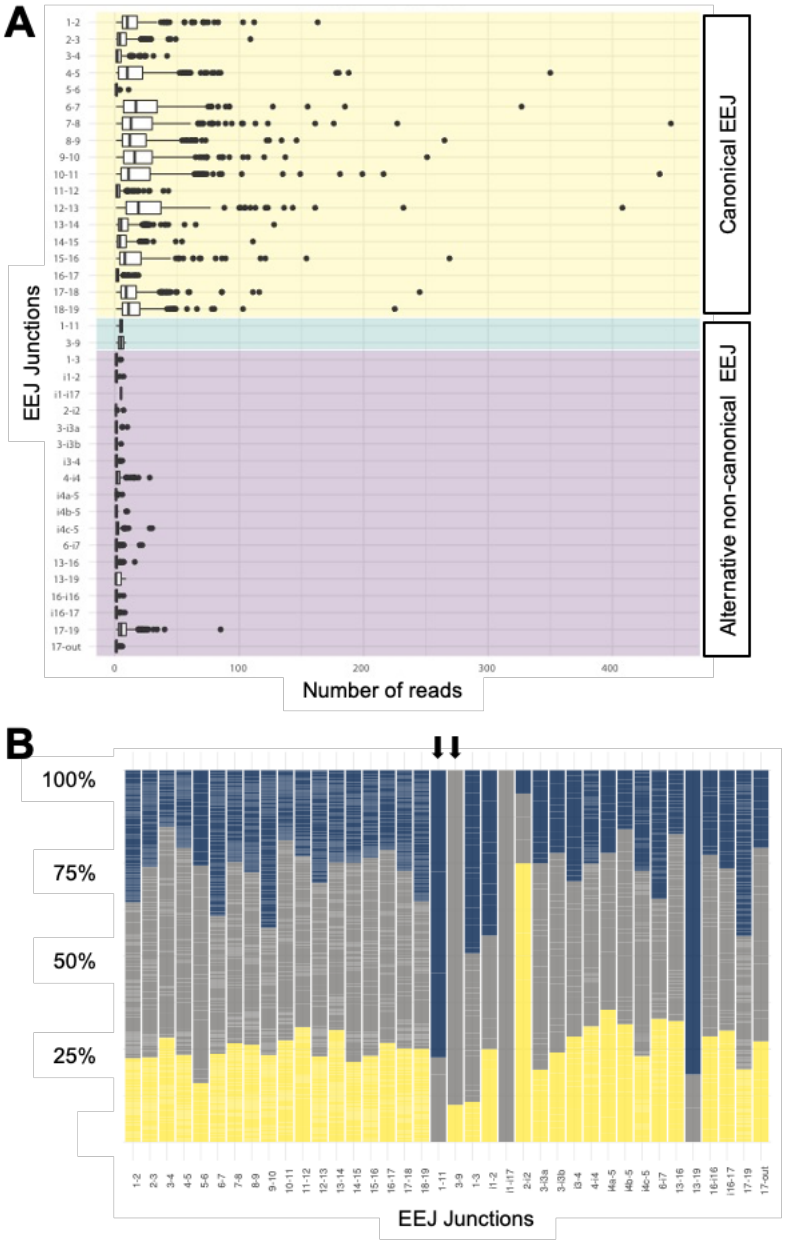

Figure 9. Exon-exon junction reads distribution across BRAF in the custom melanoma dataset. A | Boxplots showing mean number of EEJ reads in the custom dataset. Green background indicates EEJ previously related to MAPKi resistance, such as BRAF1-11 and BRAF3-9. **B |** Distribution of EEJ reads according to MAPKi sensitivity (% of resistant in grey, % of sensitive in yellow, % of not-reported in dark blue). Seven samples harbored 1-11 and 3-9 EEJ reads (indicated with black arrows), three of which in BRAF wild-type primary melanomas whose MAPKi sensitivity was not reported (dark blue).

Next, we explored possible associations between EEJ reads distribution and specific features of the samples. Thus, we observed that 3 samples out of the 7 samples in which BRAF1-11 or BRAF3-9 were detected, were *BRAF* wild type and primary melanomas; therefore, these patients must have not been previously exposed to MAPKi and yet they displayed a selection of BRAF isoforms associated with resistance to these inhibitors. The remaining 4 samples harboring resistance-associated isoforms were *BRAF*-mutant and 3 of them were categorized in this dataset as resistant (Figure 9). The *BRAF*-mutant sample that was not categorized as resistant corresponded to an "on-treatment" sample from a melanoma cell line (M229) that was tested across different time points during BRAFi treatment[381], and therefore whether the cell line was sensitive or resistant could not be inferred. Given the heterogeneity and diversity of the cohorts related to both samples and methods, we acknowledge that the results drawn from our custom dataset (e.g., a lower frequency of AS) must be interpreted with caution and avoid generalizations.

Sashimi plots generated using the BAM files of the aforementioned samples also identified these alternative EEJ reads, thus confirming the presence of these BRAF isoforms (Figure 10).

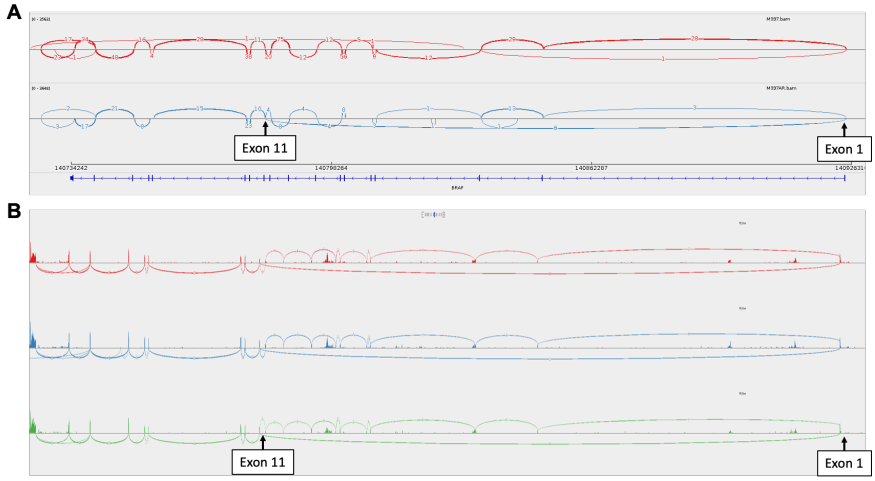

Figure 10. Sashimi plots of BRAF from samples with AS BRAF isoforms. A | Sashimi plots obtained from RNA-seq data from the *BRAF*-mutant melanoma cell line M397 (red), parental, and M397AR (blue), resistant due to the presence of BRAF1-11. **B |** Sashimi plots obtained from RNA-seq data from 3 different *BRAF*-wild type primary melanomas, which display EEJ reads that correspond to BRAF1-11.

To our knowledge, this is the first evidence to date of the presence of alternative isoforms of BRAF, such as BRAF1-11, in a) *BRAF*-wild type melanoma and in b) melanoma samples from patients not exposed patients to MAPKi.

3.1.2 Cutaneous Melanoma TCGA dataset

To extend the analysis of alternative isoforms of BRAF, we next accessed the Skin Cutaneous Melanoma dataset from the TCGA project (Firehose Legacy) (https://www.cancer.gov/tcga)[225]. The TCGA dataset was expected to be homogeneous and useful for comparing molecular subtypes. As the average read length was only 50 nucleotides (despite all samples being paired-ended), this could

lead to a suboptimal performance of VAST-TOOLS, and therefore we reduced the trimming parameter from 50 to 49 nucleotides.

The dataset comprised 472 samples from 469 melanoma patients. The mutational status of the samples was collected from cBioportal[291,292] according to the sample identification from the manifest file. As expected, the most common subgroup was *BRAF*-mutant samples (45.7%), followed by *RAS*-mutant samples (29%) (Figure 11A). The most common *BRAF* mutation was V600E (78.7%), and the most common *RAS* gene affected was *NRAS* (Figures 11B and 11C).

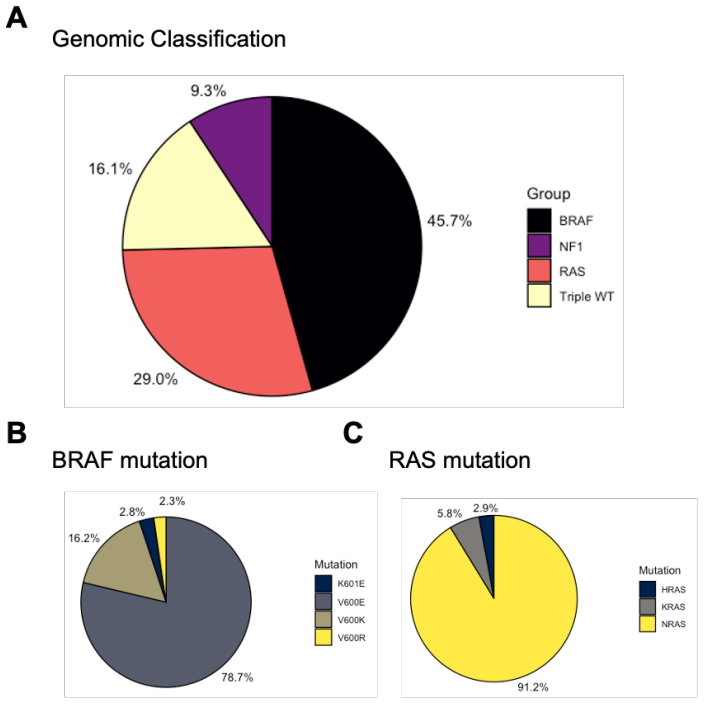

Figure 11. Genomic landscape of Skin Cutaneous Melanoma TCGA dataset. **A |** Genomic classification, **B |** *BRAF* mutations distribution and **C |** *RAS* mutations distribution of the SKCM-TCGA dataset

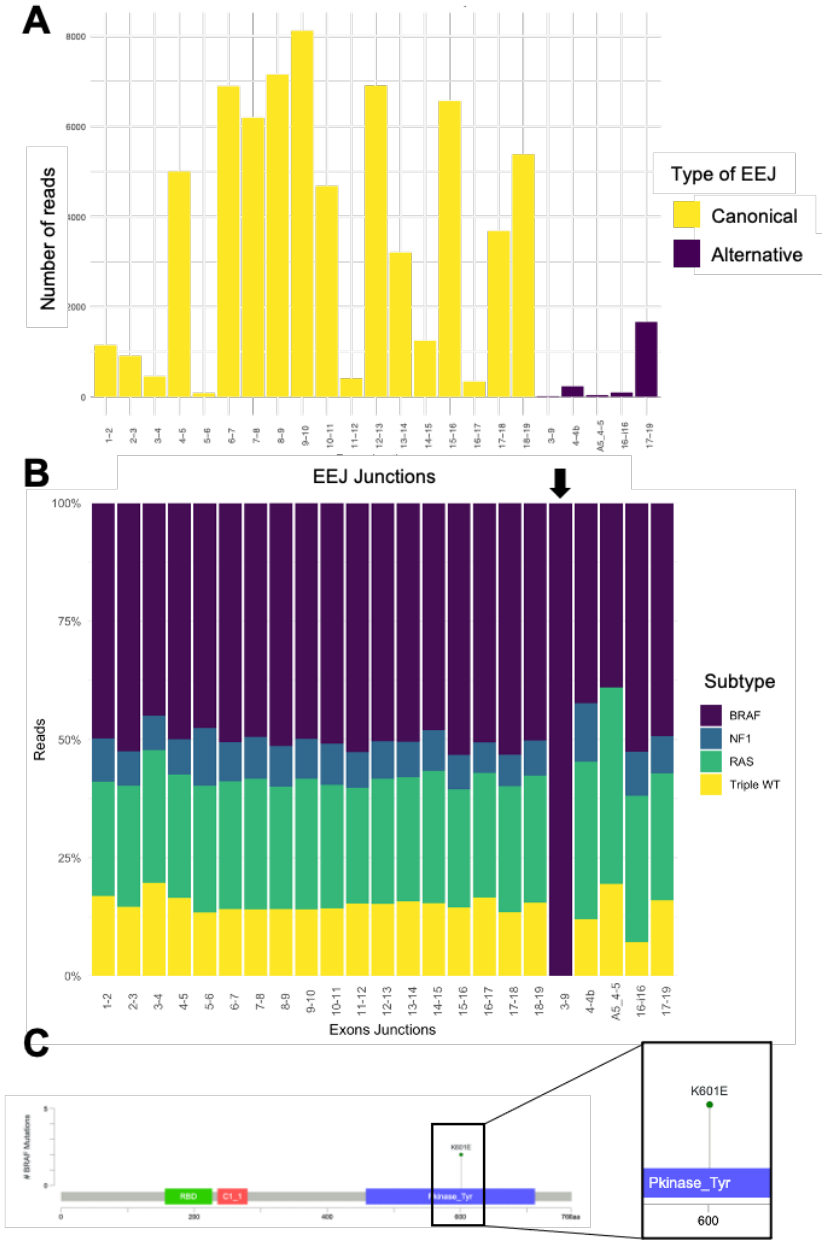

Figure 12. Exon-exon junction analysis across BRAF in the TCGA melanoma dataset. A | Total number of reads of each EEJ in the *BRAF* gene. Yellow bars indicate canonical EEJ and purple bars alternative non-canonical EEJ. **B |** Distribution of EEJ reads according to the TCGA genomic subtype (*BRAF*, *RAS*, *NF1*-mutant and triple wild type). Two *BRAF*-mutant samples harbored 3-9 EEJ reads (indicated with a black arrow). **C |** Both of the samples displaying BRAF3-9 isoform samples harbored the $BRAF^{K601E}$ mutation (Adapted from cBioportal[291,292]).

The distribution of EEJ reads in the *BRAF* gene showed again that all canonical EEJs could be identified and, similarly to the previous dataset, the coverage of the different EEJs was not evenly distributed across the length of the gene *BRAF* (Figure 12A). We found alternative EEJs, including BRAF3-9 (related to resistance), and also other alternative EEJs of unknown biological significance. In this dataset, however, the diversity of alternative EEJ was lower, probably due to the shorter average length of reads. We identified the EEJ corresponding to the alternative isoform BRAF3-9 in 2 melanoma metastatic samples, and both belonged to the *BRAF*-mutant subtype (Figures 12B and 12C), specifically $BRAF^{K601E}$. Unfortunately, clinical information on further treatments received, if any, for these two cases was not available.

To date, resistance-associated BRAF isoforms have been exclusively detected in *BRAF*-mutant melanomas after treatment with BRAFi±MEKi. In this Part I, we have detected, for the first time, BRAF isoforms (i.e., BRAF1-11 and BRAF3-9) in non-V600 BRAF-mutant melanomas ($BRAF^{K601E}$) and in wild-type *BRAF* melanoma tumors, which therefore were not exposed to BRAFi±MEKi. On the other hand, although the datasets were either heterogeneous (our custom dataset) or treatment-naïve (the SKCM-TCGA dataset) —and thus limiting to draw robust conclusions—, we found a lower frequency of AS of BRAF than previously reported.

3.2 PART II. Cellular models to study BRAF mRNA isoforms in melanoma

We collected a number of paired melanoma cell lines (pairs of parental line and its resistant counterpart) and performed RT-PCR to detect the different isoforms. We also studied the emergence of these isoforms as a consequence of BRAFi exposure, as previously reported[334,340,339].

We used the melanoma cell lines described in Table 4. Mutation information was retrieved from publicly available databases such as Cellosaurus[382] (https://www.cellosaurus.org) and Cosmic[383] (https://cancer.sanger.ac.uk/cosmic).

Cell line	BRAF status	Other mutations	Phenotype	BRAF isoform	Provider
UACC62	V600E	PTEN c.741dup (p.Pro248fs)	Sensitive	-	Gebauer lab (CRG, Spain)
SKMEL94	V600E	NR	Sensitive	-	
SKMEL147	Wild type	$NRAS^{Q61R}$, CDKN2A c.341C>T (p.Pro114Leu)		-	
SKMEL293	V600E	NR	Sensitive	-	Solit and Rosen labs (MSKCC, USA)
C3	V600E	NR	Resistant	3-9	
M397	V600E	NR	Sensitive		Ribas lab (UCLA, USA)
M397AR	V600E	NR	Resistant	1-11	
1205Lu	V600E	CDK4 c.64A>C p.Lys22Gln	Sensitive	-	Hartsough lab (Drexel, USA)
PRT#3	V600E	NR	Resistant	2-11	

Cell line	BRAF status	Other mutations	Phenotype	BRAF isoform	Provider
PRT#4	V600E	NR	Resistant	1-9	

Table 4. Summary of the different melanoma cell lines used in this study.
NR, not reported.

3.2.1 BRAF mRNA isoform profile of melanoma cell lines

We analyzed the transcript isoform profiles of BRAF of the different cell lines, guided by their described BRAF isoforms (Table 4). After RNA extraction, RT-PCR was performed using different combinations of primers, designed for specific isoform detection.

The different alternative BRAF isoforms were successfully detected in the expected cell lines (Figure 13), the parental cell lines not expressing the alternative BRAF mRNA isoform associated with resistance in their resistant counterparts. Interestingly, each resistant cell line harbored the described alternative resistance-associated BRAF isoform, but we were not able to detect other alternative (also resistance-associated) BRAF transcript isoforms in the same cell line. We conclude that each resistant cell line exclusively expresses only one specific alternative BRAF isoform. This finding was not in line with the concept that a general alteration of splicing would lead to the generation of multiple aberrant BRAF transcripts in resistant cell lines.

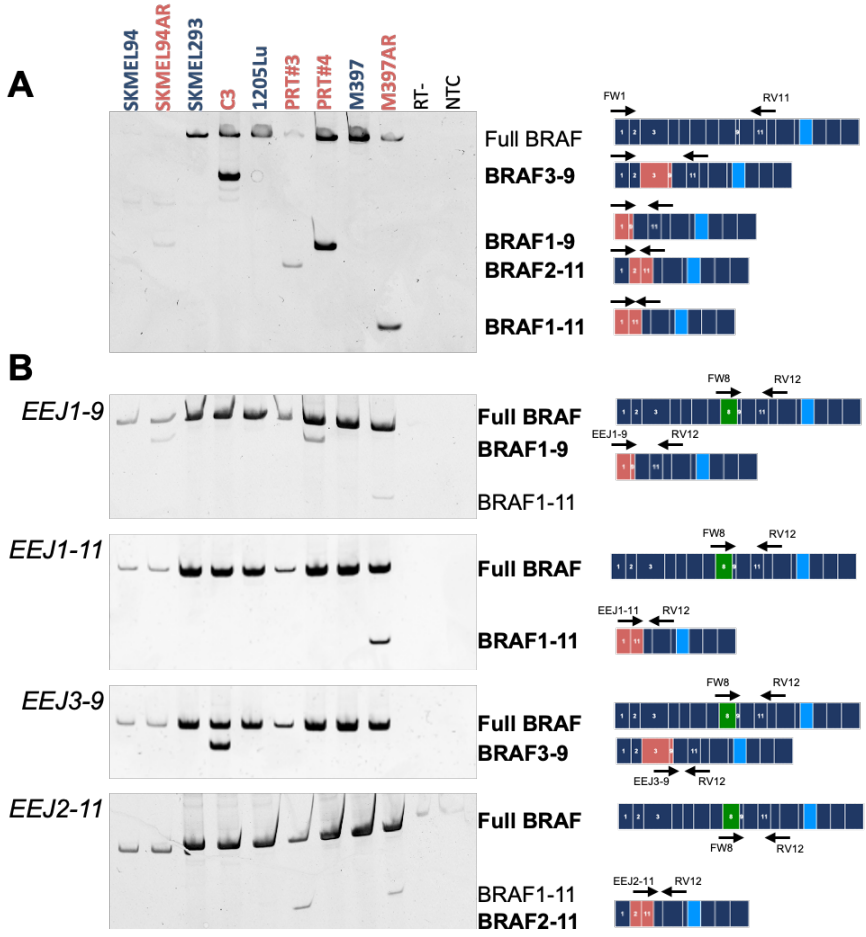

Figure 13. RT-PCRs for detection of different BRAF mRNA isoforms. A | RT-PCR for the detection of any transcript isoform encompassing exons 1 to 11 in RNA isolated from the indicated melanoma cell lines (parental cell lines in dark blue, resistant cell lines in red). The position of forward and reverse primers is indicated, as well as the electrophoretic mobility of the different spliced isoforms**. B |** RT-PCR with primers designed for detection of the full BRAF isoform (FW8) and primers to specifically detect alternative exon-exon junctions (EEJ). Parental cell lines are in dark blue, resistant cell lines in red. SKMEL94AR corresponds to a cell line generated during the work of this Thesis as explained below. On the right side, schematic diagrams of the expected transcript isoforms and position of primers are indicated: light blue exon indicates exon 15, red exons indicate exons involved in alternative EEJ, green exon indicates exon 8 (which is only present in full BRAF isoform and never included in any of the alternative mRNA isoform depicted in the figure). RT-, negative control without reverse transcriptase; NTC, non-template control of the PCR.

3.2.2 Generation of resistant cell lines harboring alternative mRNA isoforms of BRAF

In order to validate that the alternative isoforms of BRAF emerge upon BRAFi exposure, we treated different parental melanoma cell lines and performed RT-PCR at different time points during the treatment, to assess the presence of alternative isoforms.

For this purpose, we continuously exposed SKMEL94, UACC62, M397 and SKMEL293 cell lines to vemurafenib 1 μM and analyzed the presence of BRAF mRNA isoforms from total RNA. Previous studies exposed parental cells to increasing concentrations of BRAFi up to 6 months or treated cells with high concentrations of BRAFi (2 μM) for at least 2 months[340,384]. Unlike those studies, we limited exposure 3-6 weeks and we isolated RNA at a different range of time points, that included 10 3-week replicates, 3 4-week replicates and 3 6-week replicates of each treated cell line. In these short-term experiments, we found a low frequency of alternative BRAF isoforms (6% in SKMEL94 [1 of 16], and 12% in M397 [2 of 16] cell lines) (Table 5), although we cannot rule out that a longer exposure to BRAFi could have increased the frequency, either by facilitating the underlying mechanism or by clonal selection of resistant cells (given that we did not select single-cell derived clones).

Cell line	Sublines, n	Alternative BRAF
SKMEL94	16	1 (BRAF1-9)
UACC62	16	0
M397	16	2 (BRAF1-11)
SKMEL293	16	0

Table 5. Identification of alternative mRNA isoforms of BRAF after short-term (3-6 weeks) exposure to vemurafenib.

Two of the melanoma cell lines that we treated with vemurafenib, M397 and SKMEL293, were previously reported to generate alternative isoforms of BRAF (BRAF1-11 and BRAF3-9, respectively) (Figure 14A). We were able to recapitulate the emergence of BRAF1-11 after BRAFi treatment of M397, but not of BRAF3-9, nor any other non-canonical isoform, after treatment of SKMEL293 cells. Interestingly, BRAF1-11 was once again observed in resistant M397 cells (M397AR), as previously observed[339], suggesting some form of predisposition of this parental cell line to generate a specific alternative BRAF isoform.

At the same time, not all the emerging sublines showed the presence of alternative BRAF isoforms (not even those sublines derived from parental cell lines that had previously demonstrated emergence of BRAF AS, i.e., SKMEL293 and M397), probably due to the development of different resistance mechanism/s. This finding is in line with the variety of mechanisms of resistance observed in different relapsed metastatic samples even from a single patient[347].

On the other hand, exposure to vemurafenib of SKMEL94 cell line revealed the emergence of the BRAF1-9 isoform. No alternative BRAF isoform was previously described to emerge during the process of acquisition of resistance in this cell line. The SKMEL94 subline at week 4 (hereafter SKMEL94AR), which displayed the BRAF1-9 isoform, was then expanded, and the presence of BRAF1-9 was confirmed in 2 different biological replicates (W4_1 and W4_2) (Figure 14B). Sanger sequencing of the PCR product also confirmed the EEJ 1-9 (Figure 14C). Besides, cell viability assay at

72 hours after vemurafenib treatment demonstrated that the subline was indeed resistant (IC50 24 µM *vs* 0.02 µM for the parental cell line) (Figure 14D).

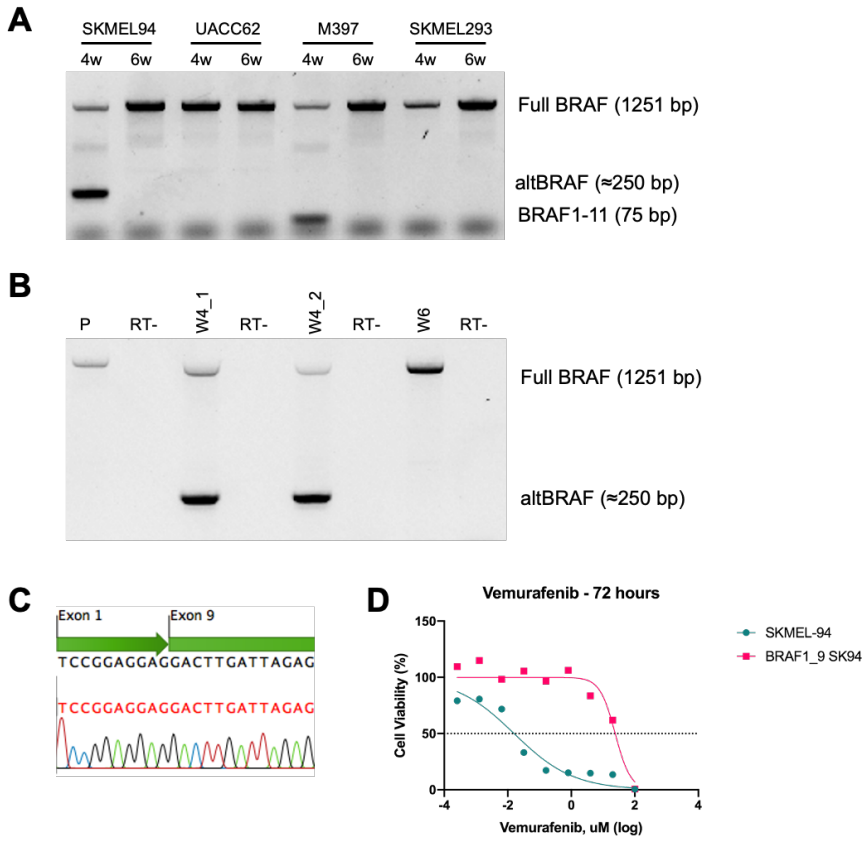

Figure 14. *De novo* generation of BRAF1-9 in a resistant subline from SKMEL94. A | Alternative BRAF mRNA isoforms screening by RT-PCR using primers complementary to exon 1 and exon 11 of four parental *BRAF*-mutant melanoma cell lines (SKMEL94, UACC62, M397 and SKMEL293) after 4 and 6 weeks of continuous exposure to 1 µM vemurafenib. **B |** Confirmation of emergence of an alternative BRAF isoform upon vemurafenib treatment in 2 biological replicates of SKMEL94 subline at week 4 (W4_1 and W4_2). BRAF1-9 which was absent in the parental SKMEL94 (P) and in SKMEL94 subline at week 6 (W6). **C |** Sanger sequencing confirming the exon-exon junction of BRAF1-9. **D |** Cell viability assay in the presence of vemurafenib (72 h) for parental SKMEL94 and the resistant subline SKMEL94AR (BRAF1_9 SK94). w, weeks; P, parental; RT-, negative control of reverse transcription.

In this Part II, we used 4 melanoma models (pairs of cell lines consisting of a parental cell line and its resistant counterpart harboring alternative BRAF mRNA isoforms) to investigate the presence and emergence of BRAF mRNA isoforms. We observed that each resistant cell line exclusively expressed only one specific alternative BRAF isoform, a finding that goes against a general mis-regulation of splicing —which would more likely generate several BRAF mRNA isoforms within the same resistant cell line. Furthermore, apart from successfully establish our own resistant cell line SKMEL94AR —which displayed BRAF1-9 after 4-week exposure to 1 μM vemurafenib—, our attempts to recapitulate the acquisition of alternative mRNA isoforms as a resistance mechanism —in melanoma cell lines that previously developed specific alternative mRNA isoforms— suggested some form of predisposition of each cell line to consistently develop only one specific isoform, and not any other.

3.3 PART III. Contribution of pre-mRNA sequences to the generation of the BRAF3-9 isoform

A previous publication[358] argued that a C-to-G mutation located -51 nucleotides upstream of the 3'SS of intron 8 contributes to the generation of the BRAF3-9 isoform This conclusion was based on results obtained using a reporter BRAF minigene that included genomic sequences spanning 3, 4, 8, 9 and parts of introns 3 and 8. Introduction of the C-to-G substitution at position -51 resulted in increased accumulation of the BRAF3-9 transcript, regardless of whether the reporters were introduced into parental or resistant melanoma cell lines, arguing for an autonomous effect of this nucleotide change.

Based on this publication, we tried to further dissect potential *cis* elements involved in the generation of alternatively spliced BRAF isoforms linked to the acquisition of resistance to BRAFi.

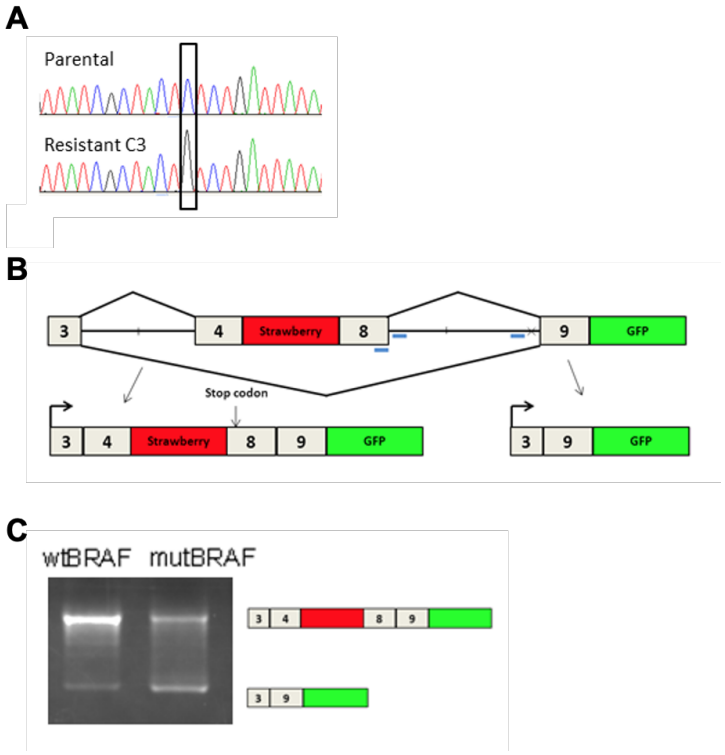

Figure 15. An intronic mutation responsible for alternative splicing BRAF3-9 (reprinted from[358]). **A |** Sanger sequencing of $BRAF^{V600E}$ alleles from parental SKMEL293 (above) and the resistant C3 (below), which displayed the C-to-G mutation at nucleotide -51 of 3' SS of intron 8. **B |** Design of the reporter minigene and the expected spliced transcripts. **C |** Splicing pattern of the reporter minigene transcripts in U2OS cell line. The position of expected RNA isoforms is indicated. wtBRAF and mutBRAF refers to whether a C or a G is present at position -51 from the 3'SS of intron 8.

3.3.1 A BRAF minigene spanning exons 3, 4 and 9 did not recapitulate the reported effect of intron 8 -51 C-to-G nucleotide substitution

We decided to first test the simplest minigene possible to easily address how the selection of the 3'SS of exon 3 (intron 3 *vs* intron 8) is made. To do this, we constructed a minigene that contained exons 3, 4 and 9 with shortened/chimeric introns. The shortened intron

between exons 3 and 4 consisted of the 5'-most 250 nucleotides and the 3'-terminal 296 nucleotides of intron 3. The chimeric intron flanked by exons 4 and 9 consisted of the 5' 302 nucleotides of intron 4 and the 3' terminal 250 nucleotides of intron 8. We generated versions of this minigene with the wild type C (WT) or with the variant G (-51MT) at position -51 upstream the 3'SS of intron 8 (Figure 16A).

First, we transiently transfected the HEK293 cell line with our minigene MG349 using different amount of the plasmid (100 and 200 ng). The results showed a small level of exon 4 skipping, leading to BRAF3-9 isoform, but no difference in the splicing pattern of the wild-type and the -51 nt-mutant minigene (-51MT), particularly in the amount of the skipping isoform that would mimic the production of the BRAF3-9 isoform (Figure 16B). Second, we used different *BRAF*-mutant melanoma cell lines, including the vemurafenib-resistant C3 which was derived from SKMEL293 and produces the BRAF3-9 isoform, to explore a possible cell-dependent effect (such as the presence or regulated expression of a trans-acting splicing factor) (Figure 16C). Again, we observed no differences in the splicing profiles in the presence of the C-to-G -51 nucleotide mutation using our minigene. We conclude that the effect of the C to G -51 substitution in enhancing splicing between exons 3 and 9 of BRAF reported in a previous study[358] was not recapitulated in our minigene system (see also below).

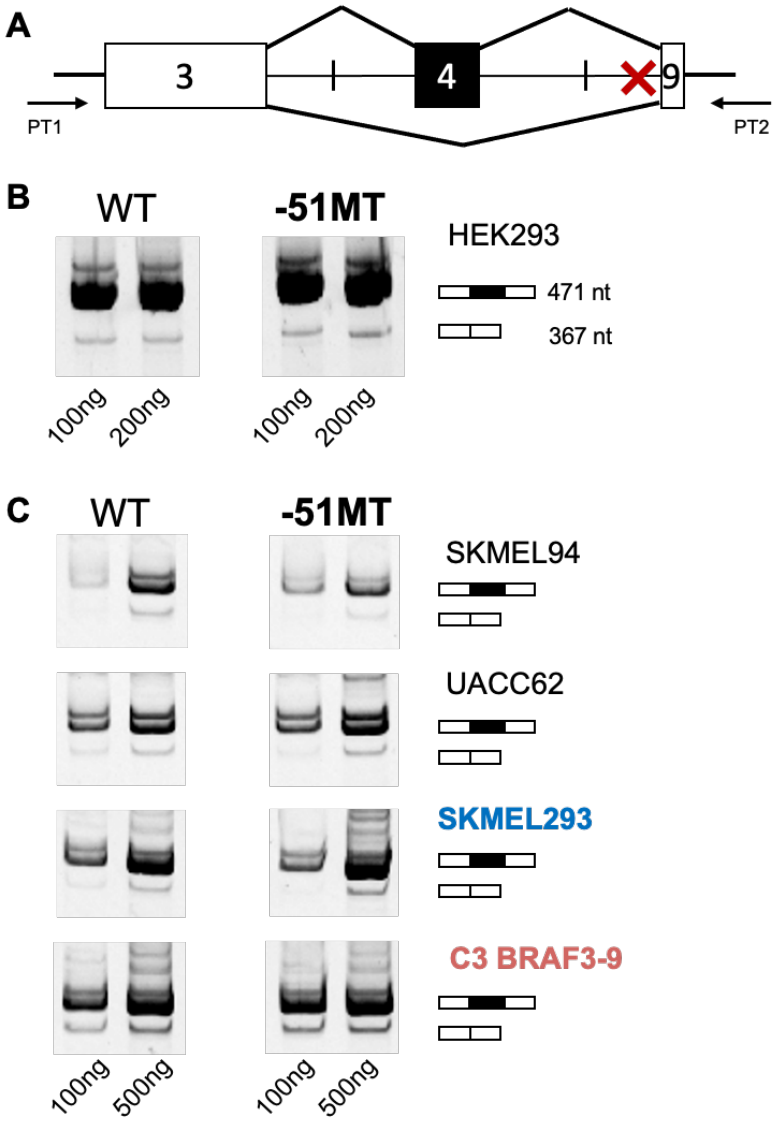

Figure 16. Splicing assays using a simple minigene to assess the production of BRAF3-9 isoform. **A |** Design of MG349 minigene, which contains exons 3, 4 and 9 and two shortened/chimeric introns: a shortened intron 3 with 250 and 296 nucleotides from the 5' and 3' ends of the intron, and a downstream chimeric intron harboring the 5' 302 nucleotides of intron 4 and 250 nucleotides of the 3'end of intron 8. The latter harbored (or not) the -51 nt position C-to-G substitution (indicated with the red cross). PT1 and PT2 primers (arrows) were used. **B |** Splicing pattern analysis of the wild-type (WT) and the -51 nt mutant (-51MT) MG349 minigenes when transfected in HEK293 cells. **C |** Splicing pattern analyses of WT and -51MT MG349 when transfected in the indicated *BRAF*-mutant melanoma cell lines. The position of the expected splicing products is indicated.

3.3.2 A putative re-splicing event involving a 5'SS regenerated upon splicing of exons 3-4 does not play a role in the generation of BRAF 3-9

Given the large genomic distance between the 5'SS of intron 3 and the 3'SS of intron 8 (47 Kb), we hypothesized that BRAF3-9 might emerge due to a re-splicing event. In this hypothetic scheme, after regular removal of introns 1 to 7 (in the case of BRAF3-9), regeneration of a 5' SS in the junction between exons 3 and 4 (which reconstitutes a sequence TG/GTAC, which resembles a 5'SS) might lead to splicing between this newly-formed 5' SS and the 3'SS of intron 8, thus generating the BRAF3-9 isoform by competing with the canonical 5'SS located in intron 8.

To test this hypothesis, we carried out mutagenesis of the 5' nucleotides of exon 4 in our simple minigene system described above. We mutated the dinucleotide GT (GTAC > G<u>A</u>AC) (Figure 17A), thus disrupting the hypothetical 5'SS. We also tested additional mutations (GTA>G<u>AA</u>A; GTA>G<u>G</u>A and GTA>GT<u>A</u>A). We tested these minigenes (in the two versions of intron 8 position -51, C or G) by transfection in SKMEL293 as well as in the C3 resistant melanoma cell lines (Figure 17B).

Our results showed no decrease in the generation of the skipping (3-9) isoform in any of the putative 5'SS mutants, regardless of the presence of the -51-nucleotide mutation and the cell line (parental SKMEL293 and its resistant counterpart C3 BRAF3-9) (Figure 17B). We conclude that a re-splicing event involving the junction between

exons 3 and 4 is unlikely to be responsible for the production of the BRAF3-9 isoform.

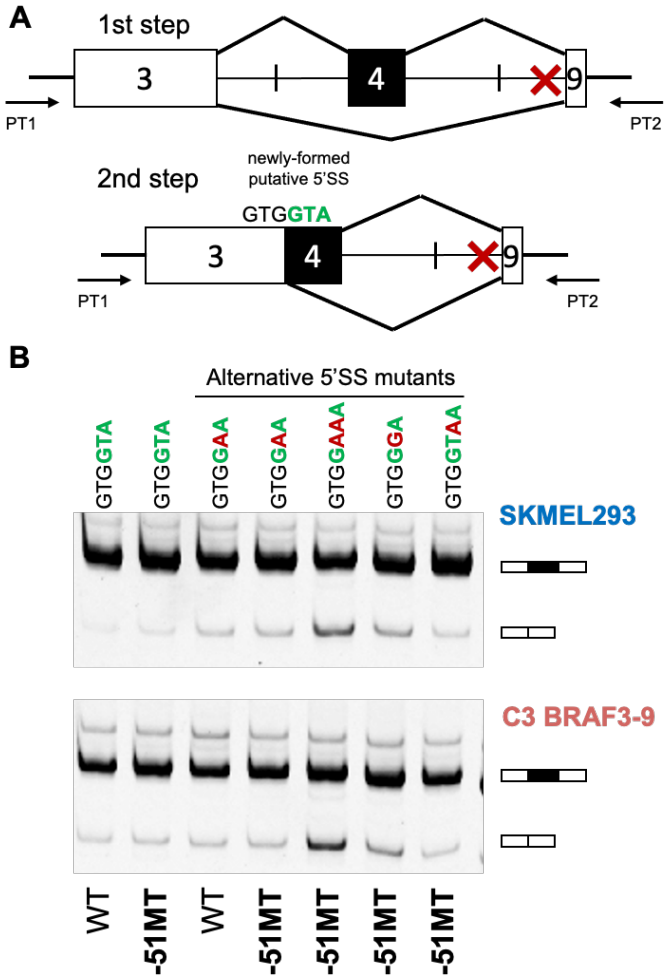

Figure 17. Minigene assays exploring the possible use of a 5' splice site generated upon splicing between BRAF exons 3 and 4 in the generation of the BRAF3-9 isoform. A | Scheme of the hypothetical two-step process for the generation of the BRAF3-9 isoform: splicing between exons 3 and 4 regenerates a newly-formed putative 5'SS which is then in competition with the 5'SS of intron 8 to generate the 3-9 isoform. The 5' first nucleotides of exon 4 are represented in green and the -51-nucleotide mutation in red. PT1 and PT2 primers were used for RT-PCR. **B |** Splicing pattern analysis of the indicated minigenes transfected in SKMEL293 and C3 BRAF3-9 melanoma cell lines was analyzed by RT-PCR as in Figure 16. The status of the -51-nucleotide position (WT and -51MT) is also indicated. The position of the expected splicing products is indicated.

3.3.3 A variety of minigene designs did not recapitulate the reported effect of BRAF intron 8 -51-nucleotide mutation

Given the unsuccessful attempts to recapitulate the effects of the intronic mutation located nearby the 3'SS of intron 8, we decided to introduce the following modifications in the minigene design, summarized in Figure 18.

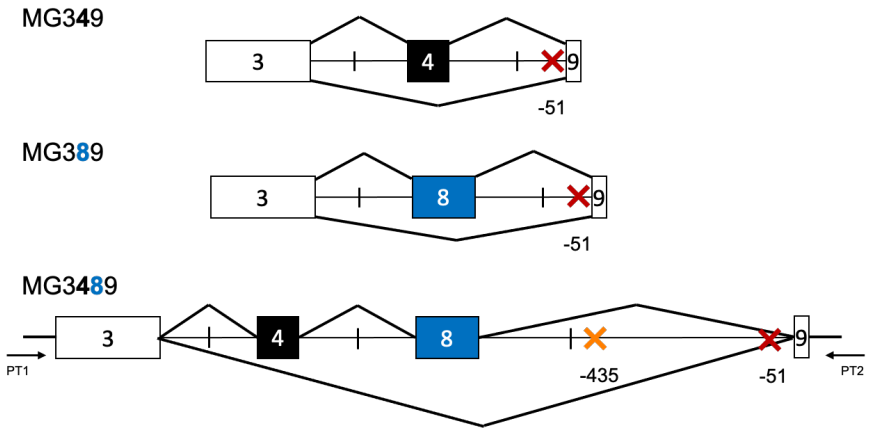

Figure 18. Diverse minigene architectures, including the designs of MG349, MG389 and MG3489. The -51 and -435 position in intron 8 are indicated in red and orange, respectively.

First, we replaced exon 4 and its flanking intronic sequences present in our MG349 minigene by exon 8 and its flanking intronic sequences, to generate the MG389 minigene. In this minigene, exon 8 is flanked by the 3' 300 nucleotides of the preceding intron 7 and the 5' 300 nucleotides of the downstream intron 8. In this design, competition for 5'SS usage involves the 5'SS of intron 3 and the 5'SS of intron 8, which would be the 5'SS in competition in the endogenous pre-mRNA for production of BRAF3-9 isoform. Transfection of this minigene in HEK293 (not shown), parental

SKMEL293 and resistant C3 BRAF3-9 melanoma cell lines showed a small level of exon 8 skipping, but no difference in the splicing pattern was observed depending on the presence or not of the C-to-G mutation at the -51 position, nor depending on the cell line phenotype (parental or resistant) in which the MG389 minigene was transfected (Figure 19B).

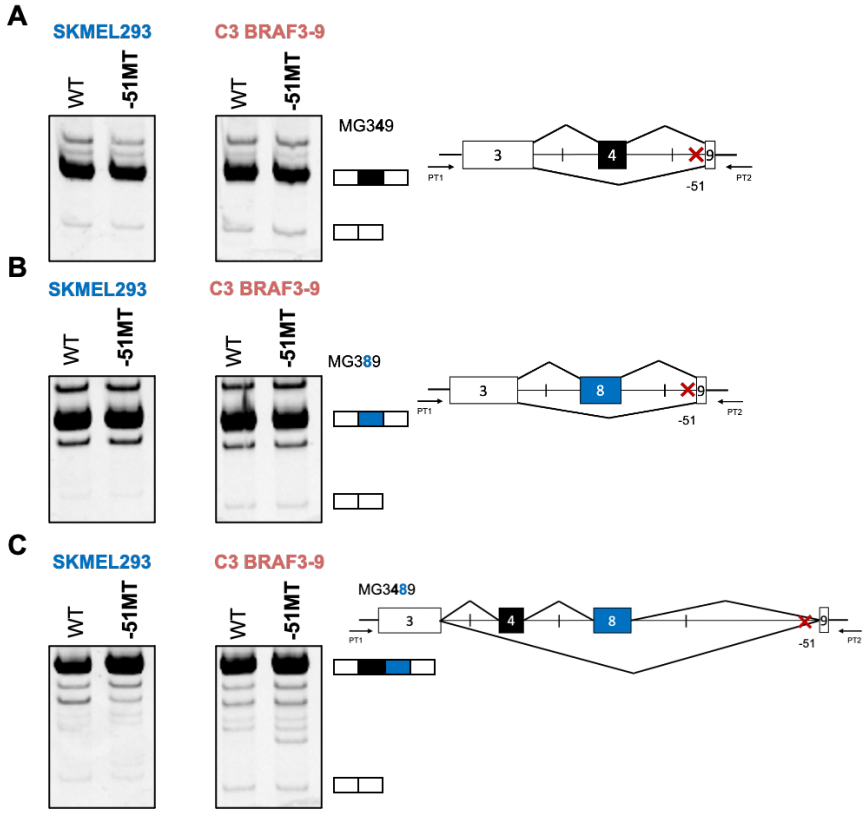

Figure 19. Splicing assays using a variety of minigene designs to explore the reported effect of the -51 mutation in intron 8 on the production of the BRAF3-9 isoform. Wild-type (WT) and -51 nucleotide mutant in intron 8 (-51MT, position in the minigenes indicated in red) versions of the MG349 (A), MG389 (B) and MG3489 (C). Parental SKMEL293 (blue) and resistant C3 BRAF3-9 (red) cell lines were transfected. PT1 and PT2 primers were used. The position of the expected splicing products is indicated.

Next, we designed a minigene that incorporated both exons 4 and 8 between exons 3 and 9 (MG3489), thus further mimicking the competition between native splice sites involved in the generation of BRAF3-9 in the endogenous pre-mRNAs. In this minigene, a longer piece of the 3' end of intron 8 (500 nucleotides) was included to encompass yet another mutation located at the -435-nucleotide position (C>A), which according to the aforementioned study[358] has no impact on the alternative splicing of BRAF3-9. In this design, shortened intron 3 contains 250 and 296 nucleotides of the 5' and 3' ends of intron 3, respectively. Chimeric intron 4-8 contains 302 nucleotides of the 5' end of intron 4 and 300 nucleotides of the 3' end of intron 7. And shortened intron 8 contains 300 and 500 nucleotides of the 5' and 3' ends of intron 8, respectively. Transfection of this minigene in HEK293 (not shown) and in the SKMEL293 and C3 melanoma cell lines resulted in the production of a small proportion of transcripts skipping exons 4 and 8, but no differences in the splicing pattern were observed regardless of the status of the -51-nucleotide mutation (Figure 19C), the -435-nucleotide mutation or the phenotype of the cell line used for the transfection (Figure 20).

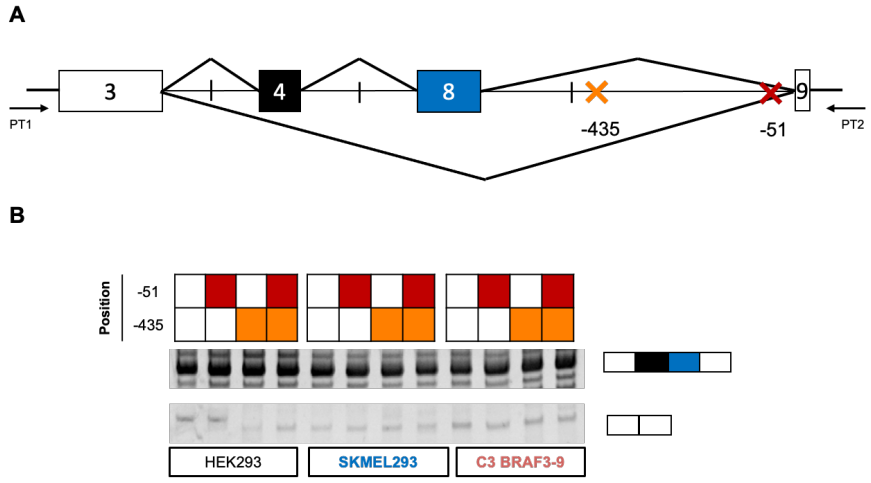

Figure 20. Splicing assays using the MG3489 minigene to assess the production of BRAF3-9 and the effect of -435 and -51 nucleotide mutations. A | Design of the MG3489 minigene, which contains exons 3, 4, 8 and 9, a shortened intron 3 and intron 8, and a chimeric intron 4-8. Intron 8 harbors the -435 nucleotide (indicated in orange) and the -51 nucleotide mutations. PT1 and PT2 primers were used for detection of the transcripts. **B |** Splicing patter analysis of the different combinations of MG3489 mutants (51WT/435WT, 51MT/435WT, 51WT/435MT and 51MT/435MT) when transfected in HEK293, parental SKMEL293 and resistant C3 BRAF3-9. Mutations of MG3489 are indicated with colored squares (orange when -435 nucleotide was mutated; red when -51 nucleotide was mutated). The position of the expected splicing products is indicated.

3.3.4 Intron 8 -51-nucleotide mutation does not impact BRAF3-9 splicing using published minigenes

Considering our failure to recapitulate the reported effects of the C-to-G substitution at position -51 of BRAF intron 8 using various minigenes, we requested the reporter minigene created and described in the previously cited article[358]. This reporter minigene consisted of the entire exons 3, 4, 8 and 9, 300 nucleotides of the 5' and 3' ends of intron 3, and 300 nucleotides and 500 nucleotides of 5' and 3' ends of intron 8, respectively (Figure 21A). The intermediate exon was a chimeric sequence containing exons 4 and 8, and the ORF of the

fluorochrome mStrawberry inserted between these exonic sequences. We prepared versions of this minigene containing wild type or mutant versions at positions -51 and -435 in intron 8, in all possible combinations, and carried out transfections in HEK293 as well as the melanoma cell lines SKMEL293 and its resistant subline C3 BRAF3-9. Splicing patterns of minigene-derived transcripts were detected using different set of primers for the RT-PCR: first, primers encompassing the entire minigene (Figure 21B), and secondly, using primers located in exon 8 and spanning the EEJ3-9 (Figure 21C).

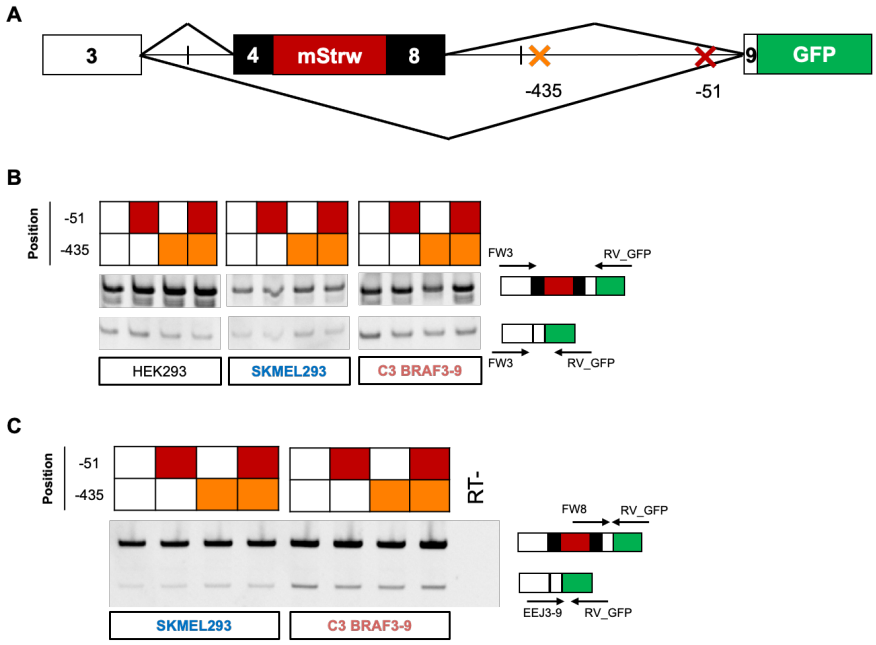

Figure 21. Analysis of splicing profiles of transcripts derived from the minigene reporter originally used to describe the effect of the BRAF intron 8 -51 nucleotide mutation on splicing of BRAF3-9 isoform. A | Schematic representation of the reporter minigene design. The -435 (orange) and -51 (red) nucleotides in intron 8 are indicated. **B** | RT-PCR analysis of splicing isoforms derived from transfection of the minigene shown in A in cell lines HEK293, SKMEL293 and C3 BRAF3-9 using complementary primers to exon 3 and the ORF sequence of GFP. **C** | Same analysis using different set of primers for RT-PCR: FW8, complementary to exon 8 (skipped in the BRAF3-9 isoform); EEJ3-9, complementary to the junction 3-9; and one located in the ORF sequence of GFP

(RV_GFP). Mutations at position -435 is indicated with an orange square and the -51, with a red square. Native sequences are represented with a white square. mStrw, mStrawberry; GFP, green fluorescent protein. FW3, primer complementary to exon 3; FW8, complementary to exon 3; EEJ3-9, primer complementary to exon-exon junction 3-9; RV-GFP, primer complementary to the ORF of GFP.

Once again, we did not observe any changes in the splicing patterns, regardless the -435 or the -51-nucleotide mutation status or the cell type transfected. Therefore, we were not able to recapitulate the previously described effect of the -51-nucleotide mutation, which was presented by the authors as the "molecular basis for a RNA splicing-mediated RAF inhibitor resistance mechanism".

3.3.5 Whole genome sequencing of SKMEL293 and C3 BRAF3-9 does not reveal additional nucleotide differences in the BRAF gene

In view of the negative results of the minigene assays testing the effect of the -51-nucleotide mutation, we decided to sequence the whole genome of SKMEL293 and C3 BRAF3-9 cells to explore possible intronic mutations differing between the two cell lines and that could potentially explain the generation of the alternative BRAF3-9 isoform in the C3 melanoma cell line.

For this purpose, we obtained whole genome sequencing (WGS) results with a 30x coverage, using paired-end short reads of 150 nucleotides. Quality control data after the alignment to reference bwa.hsapiens.hs37d5 is summarized in the Table 6.

Sample	Mill. read-pairs	Yield (Gb)	Avg %			Coverage	
			uniq.	unmap.	dupl.	Mean	Median
SKMEL 293	283.837	85.719	90.51	2.70	11.67	26.46	25.00
C3 BRAF3-9	182.485	55.110	95.45	0.07	11.42	18.05	17.00

Table 6. Summary of WGS quality control data. Mill., million; Avg, average; uniq., unique; unmap., unmapped; dupl., duplicate

Briefly, after alignment to genome reference and cleanup, variant calling was performed using *freebayes* (a haplotype-based, Bayesian, variant detector)[385]. Then, we used *SnpEff* for variant annotation[386] and prediction, and *maftools* for visualization[387] (see Materials and Methods) .

Considering exclusively the *BRAF* locus, we carried out variant calling analysis and we were able to identify a total of 46 genomic variants: 34 single-nucleotide variants (SNV), 1 multi-nucleotide variant (MNV), 3 insertions and 8 deletions. Of the 230 events that were observed across *BRAF*, 222 (96.5%) were located in introns, 6 (2,6%) in exons and 2 (0.87%) in the 3' UTR. Four of the six variants observed in exons were missense variants.

The comparative analysis of the variant calling of the 2 melanoma cell lines, the parental SKMEL293 and the resistant C3 BRAF3-9, yielded the following results (Figure 22):

- T>A mutation located in exon 15 (T1799A, p.V600E) was detected in both samples with a similar read frequency (>50%), in agreement with the mutation being present in heterozygosis.

- in SKMEL293, only one of the variants detected was restricted to the parental cell line: an intronic SNV located in intron 16 (A>C).
- in C3 BRAF3-9, we found 2 variants restricted to this resistant cell line: a T>C SNV located in intron 5 and, as expected, the C>G SNV located at in the -51-nucleotide upstream the 3'SS of intron 8, which was previously described[358].

Remarkably, the 2 *de novo* SNVs identified in both the parental and resistant cell lines were located in introns (intron 16 and intron 5, respectively) but at very long distances from the competing splice sites in introns 3 and 8 involved in the generation of BRAF3-9 isoform, making it unlikely that these variants are involved in the alternative pattern of splicing.

Taking together the negative results of the minigene assays and the intronic sequencing described in this Part III, we considered the hypothesis that an intronic mutation is responsible for the generation of alternative isoforms of BRAF unlikely. This results are also consistent a previous publication analyzing intron 8 of *BRAF* in patients harboring the BRAF3-9 mRNA isoform after acquisition of resistance to BRAFi, which did not detect the -51 nucleotide mutation in any of the patients samples[388].

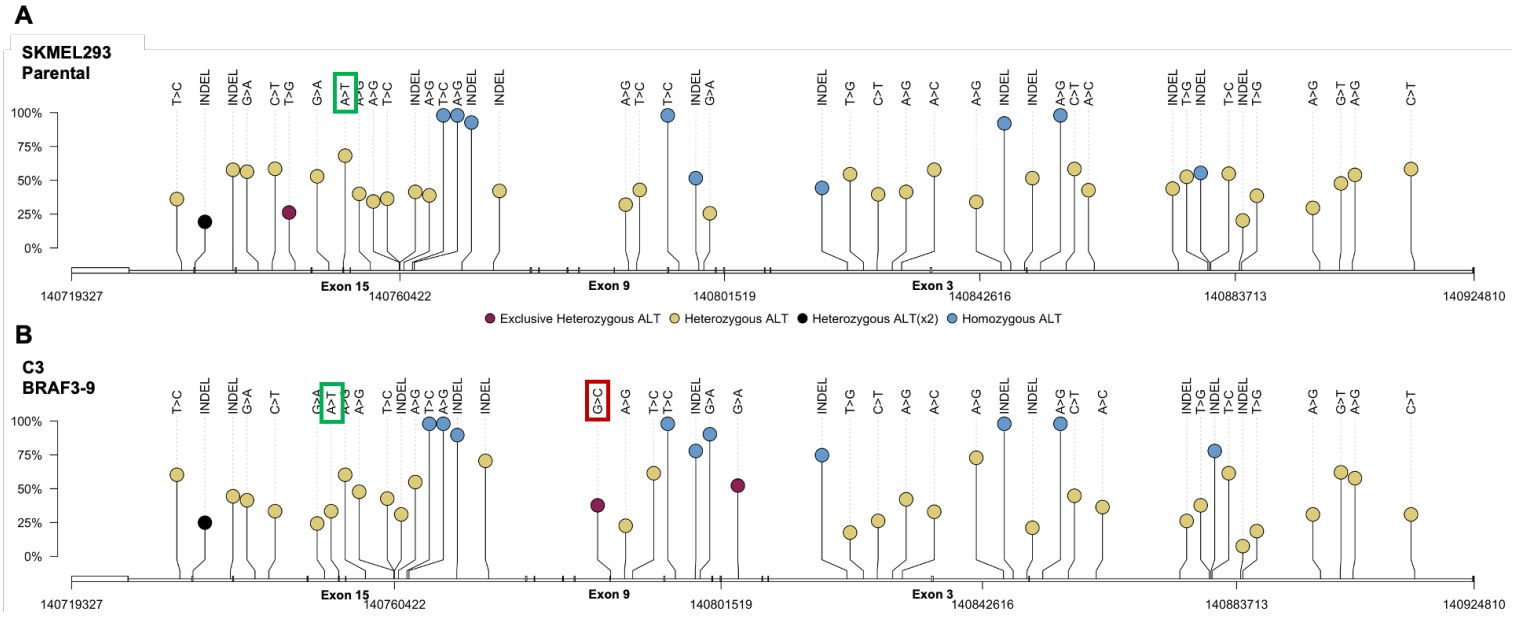

Figure 22. Lollipop plot of *BRAF* gene sequence variants generated from variant calling of SKMEL293 and C3 BRAF3-9 WGS results. BRAF coordinates in the negative strand are represented in the x-axis and the frequency of reads of the alternative variants (number of ALT reads/number of total reads, for a specific locus) in the y-axis. Heterozygous variants —those affecting only one allele (Heterozygous ALT)— were more frequent than variants affecting both alleles (Homozygous ALT, blue dots). Among Heterozygous ALT variants, red dots indicate that the SNV was detected only in one of the two cell lines; yellow dots, SNV detected in both cell lines. Heterozygous ALT (x2), represented with black dot, refers to different variants affecting the same locus (in our case, different INDELs). The T>A (V600E) (A>T in the negative strand) is marked with a green square, and the C>G (G>C in the negative strand) intron 8 -51 mutation with a red square.

3.4 PART IV: Association between BRAF V600E mutation and BRAF alternative splicing

Previous studies linked the V600E mutation (located in exon 15) with the alternative BRAF isoforms in different ways: first, the isoforms were detected solely after treatment with BRAFi±MEKi (and therefore only in BRAF-mutant melanoma samples or patients); second, it was suggested that all the alternative BRAF isoforms retained the V600E mutation[358,389]. However, considering i) the long genomic distances between exon 15 and the 5'SS of intron 3 (81 kilobases) and between exon 15 and the 3'SS of intron 8 (34 kilobases), and 2) the related fact that exon 15 -containing the V600E mutation- is transcribed long after the competing splice sites between exons 3 and 9 have been transcribed, it is intriguing how the mutational status of exon 15 might influence the pattern of splicing between exons 3 and 9 (Figure 23A). Such a "retrograde" remote modulation of an alternative splicing event would be unprecedented.

We therefore decided to further investigate the association between the production of alternative BRAF isoforms and the presence of the V600E mutation. We therefore wondered whether the alternative BRAF transcripts were generated in cells displaying a general mis-regulation of splicing (cell-intrinsic model) —which should affect both mutant and native BRAF alleles—, or if, in contrast, the aberrant transcripts were produced only from one of the alleles (allele V600E-specific) —the V600E mutated one, which would affect somehow the pattern of splicing— (Figure 23B).

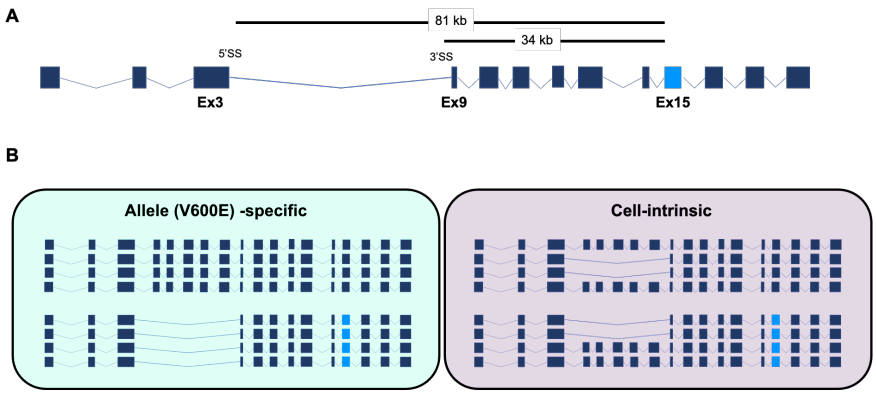

Figure 23. Two models for generation of BRAF3-9 isoform. A | Schematic representation of the splicing pattern leading to BRAF3-9 mRNA, indicating the genomic distances between intron 3 5'SS and intron 8 3'SS and between the T1799A (V600E) mutation located in exon 15. Exon 15 is indicated in light blue. **B |** Hypothetic models for the generation of BRAF3-9. In the allele-specific model, all the transcripts displaying the BRAF3-9 pattern of exon skipping are generated exclusively from the mutant allele. In the cell-intrinsic model, alternative BRAF isoforms are generated from both mutant and native alleles due to a general dysregulation of the splicing machinery in these cells.

3.4.1 Analysis of single cell-derived clones of C3 BRAF3-9

To assess the possible heterogeneity in splicing decisions, we carried out splicing pattern analyses from clonal populations derived from single cells from the melanoma cell lines SKMEL293 and the C3 BRAF3-9. Briefly, DAPI (4′,6-diamidino-2-phenylindole, a blue-fluorescent DNA stain)-negative melanoma cells were single sorted into a 96-well plate containing complete growth medium (including vemurafenib 1 μM for resistant clones). Single cell colonies were visually screened to ensure their clonogenicity and expanded for 3-4 weeks to allow enough number of cells for RNA extraction. Then, RNA was extracted and analyzed by RT-PCR to assess BRAF transcripts splicing.

We sorted and seeded 96 single cells from each cell line. From each 96-well plate, we obtained 36 clones from SKMEL293 and 12 clones from C3 BRAF3-9 (from which only 11 could be screened by RT-PCR) (Figure 24). As expected, all 36 SKMEL293 clones harbored the full BRAF transcript, and no traces of BRAF3-9 transcripts could be detected in any of them (Figure 24A).

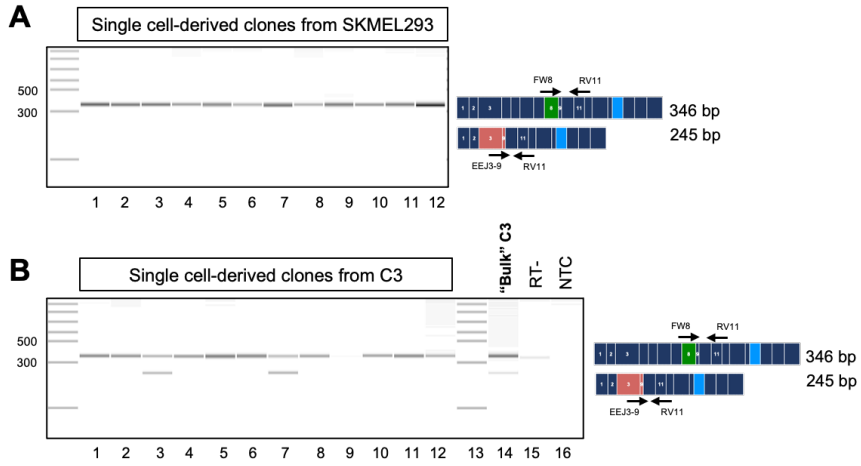

Figure 24. Analysis of the patterns of BRAF splicing in populations derived from single clones of SKMEL293 and C3 BRAF3-9 cell lines. Primers complementary to exon 8 (FW8), to the exon-exon junction 3-9 (EEJ3-9) and to exon 11 (RV11) were used to detect full length (FW8 and RV11) and BRAF3-9 mRNA isoforms (EEJ3-9 and RV11). Position and scheme of expected isoforms are indicated. **A** | RT-PCR results of 12 SKMEL293 clones (from a total of 36 generated clones). All clones expressed exclusively the full BRAF transcript (expected amplification product of 346 bp). **B** | RT-PCR results of 11 C3 BRAF3-9 clones. BRAF3-9 transcript was detected in 2 clones, clone #3 and #7, corresponding to lanes 3 and 7, respectively. Notice that the ratio of BRAF3-9/full length isoform is 50% for these two clones, while the proportion is much lower in the "bulk" cell population (lane 14). RT-, negative control without reverse transcriptase; NTC, non-template PCR control.

Regarding the C3 BRAF3-9 clones, all 11 clones also harbored the full BRAF transcript. Importantly, the BRAF3-9 transcript was only detectable in 2 of the 11 C3 BRAF3-9 single cell-derived clones (clones #3 and #7). In these clones, the relative abundance of the full

length and BRAF3-9 isoform was approximately 50%, far higher than the proportion observed in the "bulk" C3 BRAF3-9 population (Figure 24B). We interpreted these results to mean that only a fraction of the "bulk" C3 BRAF3-9 population expresses the BRAF3-9 isoform, but those cells that do, they do it in amounts similar to the full-length isoform. We then considered the possibility that the transcripts exhibiting the BRAF3-9 pattern of splicing could be generated specifically from one of the alleles in these cells.

3.4.2 Association between V600E mutation and the BRAF3-9 isoform

To investigate the possible association between the *BRAF*^{V600E} mutation (T1799A) and the different BRAF transcript isoforms, PCRs were designed for specific amplification of the full BRAF transcript (using a forward primer annealing to exon 8) and the BRAF3-9 isoform (using a forward primer spanning the exon 3-9 junction —EEJ3-9— that, under the conditions of the PCR, requires annealing to the spliced junction for priming and cannot anneal exons 3 or 9 if they are not spliced together), and using a reverse primer annealing with sequences in exon 15 3' to the 1799 position (mutated from T to A in BRAF V600E). The resulting RT-PCR products from clones #3 and #7, derived from C3 BRAF3-9 cell line, were then sequenced by the Sanger method.

Interestingly, while the full BRAF transcript did not harbor the T>A substitution, the BRAF3-9 transcript of clones #3 and #7 did harbor the T>A mutation (Figure 25A and 25B). The absence of a background trace corresponding to another nucleotide at this locus in

the electropherogram of each amplification product suggested that each PCR product corresponded to a single allele.

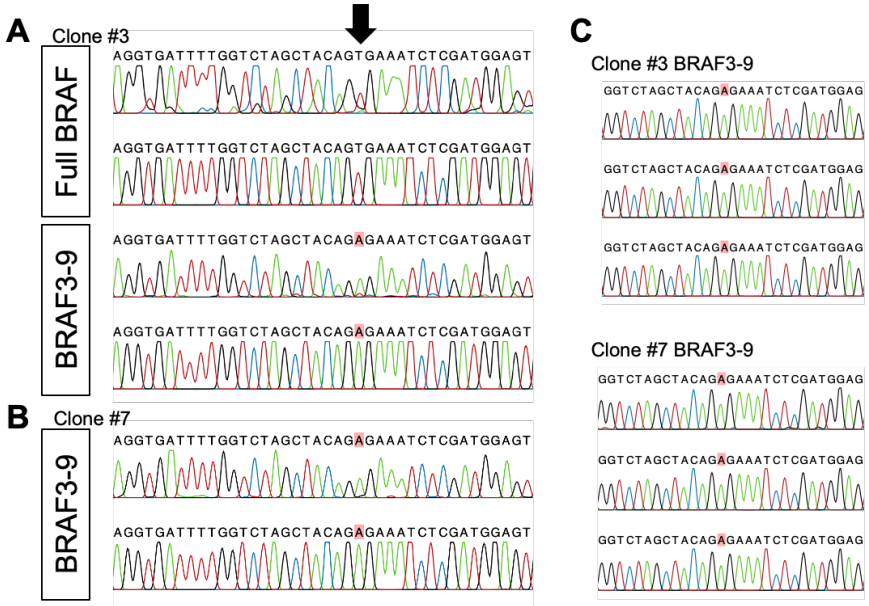

Figure 25. Sanger sequencing of full BRAF and BRAF3-9 mRNA isoforms from RT-PCR products amplified from single cell-derived clones of C3 BRAF3-9 cell line. A | Sequences from full-length BRAF (RT-PCR from exon 8 to exon 15) and BRAF3-9 (RT-PCR from EEJ3-9 to exon 15) amplification products from C3 BRAF3-9 clone #3 and **B |** Same for C3 BRAF3-9 clone #7. Notice that full-length amplification products contain a T at position 1799 (arrow), while BRAF3-9 amplification products contain an A at this position (corresponding to the V600E mutant allele, in red). **C |** Examples of Sanger sequencing of individual clones obtained by ligation and transformation of BRAF3-9 PCR amplification products in bacteria for clones #3 and #7. Adenosines in red correspond to the T1799A mutation in exon 15.

To confirm that each isoform (the full BRAF or BRAF3-9) is always generated from the same specific allele (the native T1799 and mutant T1799A, respectively), we ligated the PCR products from clones #3 and #7 in a pGEM vector, transformed the ligation products in *E. coli*, amplified the plasmids from isolated bacterial colonies and sequenced the plasmid inserts by the Sanger method. As predicted, sequencing of these colonies from single PCR molecules confirmed

that all the BRAF3-9 transcripts were generated from the V600E (T1799A) allele (Figure 25C).

3.4.3 Association between V600E mutation and other BRAF mRNA isoforms

To further explore the association between the V600E mutation and other BRAF mRNA isoforms associated with the acquisition of resistance to vemurafenib, we used a similar approach for additional melanoma cell lines. To do this, we carried out RT-PCR assays using specific primers that spanned the different EEJ of interest: EEJ 1-9, EEJ 1-11, and EEJ 2-11, followed by Sanger sequencing of the PCR products.

Consistent with the concept emerging from the results shown above, all PCR products corresponding to the alternative BRAF isoforms — including BRAF1-9 from 2 different cell lines (PRT#4, SKMEL94AR), BRAF1-11 (M397AR), and BRAF2-11 (PRT#3)— displayed the T1799A mutation. Besides, all the electropherograms (except for PRT#4) were clearly compatible with having only adenosine at position 1799 (Figure 26). This finding indicates again that the alternative BRAF transcripts are generated from the mutant (T1799A) allele, regardless of the alternative BRAF isoform made by each of the cell lines.

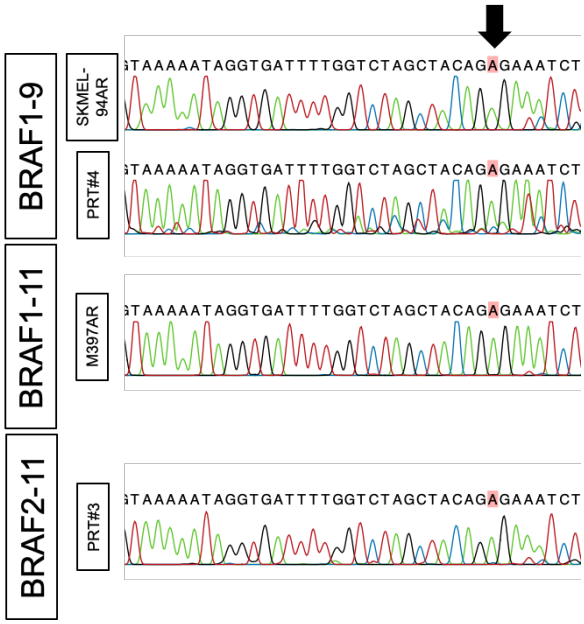

Figure 26. Mutational status at BRAF position 1799 of alternative BRAF mRNA isoforms. Sanger sequencing in the region of exon 15 (position 1799 is indicated with an arrow) of the different amplification products corresponding to alternative BRAF transcripts in the indicated BRAFi-resistent melanoma cell lines. The previously described alternative BRAF isoforms in each cell line are indicated. Adenosines in red correspond to the T1799A mutation in exon 15.

In this Part IV, analysis of single cell-derived clones of the C3 BRAF3-9 cell line indicated, not only that the "bulk" C3 resistant cell line was heterogeneous, but also that the production of BRAF3-9 is T1799A (p.V600E) allele-specific. This finding pointed towards the participation of a *trans*-acting factor in the generation of BRAF3-9 that might be acting as a link between the T1799A mutation and the splicing choices involving the 5' SS of intron 3 and 8 and the 3'SS of intron 8, which are more than 80, 35 and 30 kilobases away from exon 15, respectively.

3.5 PART V: Searching for *trans*-acting factors involved in the generation of alternative BRAF isoforms

After the analysis of potential mutations in the BRAF gene that could eventually explain the activation of alternative splicing isoforms associated with resistance to BRAF inhibitors, using minigenes, WGS and characterization of allele-specific transcripts, we turned our attention to the identification of *trans*-acting factors that could be involved in this event.

To do so, we first used the data generated from WGS of both melanoma cell lines, SKMEL293 and "bulk" C3 BRAF3-9, to identify differential mutations between the two cell lines, with a special focus on RNA Binding Proteins (RBPs). In addition, we performed a genome-wide CRISPR-Cas9 knockout screen to identify genotype-associated vulnerabilities related to the resistant phenotype (which depends on the production of specific alternative BRAF mRNA isoforms) that ultimately might be responsible for the generation of these specific splice site choice decisions, for instance because of alterations in particular splicing factor(s).

3.5.1 Genome-wide variant analysis of SKMEL293 and "bulk" C3 BRAF3-9

WGS data from melanoma cell lines SKMEL293 and its resistant "bulk" counterpart C3 BRAF3-9 was analyzed. As mentioned before, *freebayes*[385] was used for the variant calling and *SnpEff*[386] and *VEP*[390] for variant annotations, then *maftools*[387] were used for data visualization. Overall, a total of 7,412 genes were identified that

contained at least one variant compared to reference genome (hg38), and a total of 27,003 annotated variants (according to VEP) were identified. The most common class of variant was missense mutations (24,186), followed by mutations affecting splice sites (1,559). The resistant C3 BRAF3-9 cell line accumulated a higher number of alterations across all variant classes (Table 7) (Figure 27C).

	SKMEL293 (parental)	**C3 BRAF3-9** (resistant)
Frame Shift Deletion	64	71
Frame Shift Insertion	52	58
In Frame Deletion	175	178
In Frame Insertion	143	151
Missense Mutation	11521	12665
Nonsense Mutation	134	137
Nonstop Mutation	18	19
Splice Site	754	805
Translation Start Site Mutation	28	30
Total	12889	14114

Table 7. Summary of the genomic variants detected in the indicated melanoma cell lines, relative to the reference genome (hg38)

Single-nucleotide variants were the most frequent variant type (Figure 27A); and among them, C>T mutations accounted for the most common class of SNVs (Figure 27B). The high frequency of C-to-T mutations might be related to UV-induced DNA damage, which principally induces C>T transitions. Among the genes that accumulated the higher number of variants in both cell lines, we identified several genes from the Mucin family (such as *MUC3A*, *MUC16*, *MUC4*, *MUC6* and *MUC12*), *AHNAK2* (that encodes a large nucleoprotein), *HLA-DRB1*, *OBSCN* (Obscurin, Cytoskeletal

Calmodulin and Titin-Interacting RhoGEF), *FCGBP* (Fc Gamma Binding Protein) and *FSIP2* (Fibrous Sheath Interacting Protein 2). The complete list of the mutated genes and their variant class can be found in Supplementary Table S1.

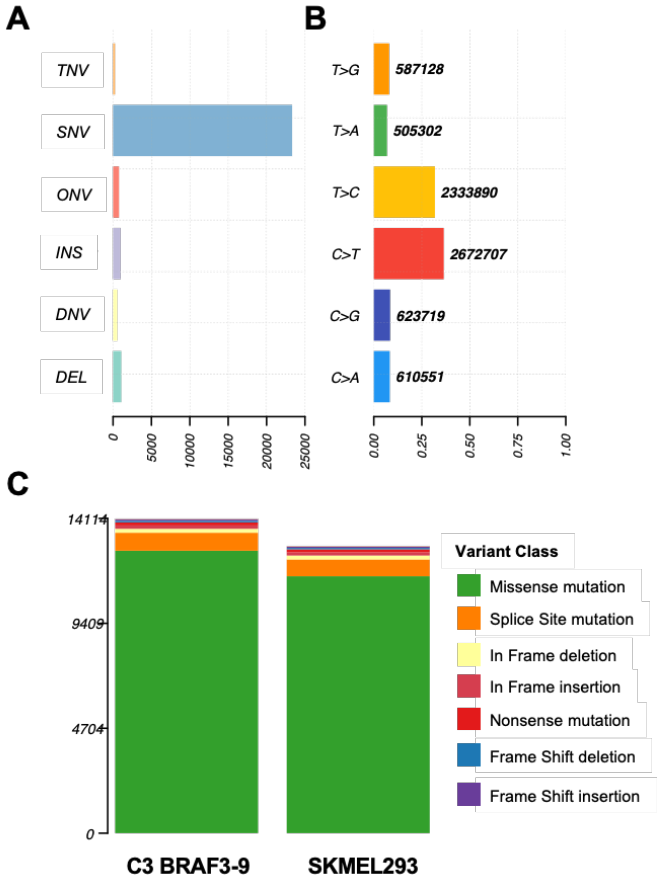

Figure 27. Genome-wide nucleotide variant analysis of SKMEL293 and "bulk" C3 BRAF3-9, compared to reference genome (hg38). **A |** Total number of each variant type detected in both cell lines. Single-nucleotide variants (SNP) were the most frequent type of variant. **B |** Proportion of the different classes of SNV detected, being the C>T mutations the most frequently observed. Total number of SNV detected are indicated. **C |** Distribution of the different classes of variants per sample, in "bulk" C3 BRAF3-9 and in parental SKMEL293. Missense mutations were the most frequent variant class detected in both cell lines. TNV, tri-nucleotide variant; SNV, single-nucleotide variant; ONV, oligo-nucleotide variant; INS, insertion; DNP, di-nucleotide variant; DEL, deletion.

3.5.2 Variant analysis of splicing-related genes in SKMEL293 and "bulk" C3 BRAF3-9 cell lines

We first focused our analysis on 1110 genes encoding spliceosome-associated proteins or encoding RBPs, either identified in purified splicing complexes or reported to interact with spliceosome components, determined by mass spectrometry analyses from a public database[391] (Supplementary Table S2).

Overall, we observed variants in 254 genes (22.8%), the most common variant class being missense mutations (88.2%, 705 events) followed by splice site mutations (5.7%, 46 events). The distribution of the variant classification across the samples is summarized in Table 8 (Figure 28A).

	SKMEL293 (parental)	**C3 BRAF3-9** (resistant)
Frame Shift Deletion	2	1
Frame Shift Insertion	2	2
In Frame Deletion	9	9
In Frame Insertion	7	8
Missense Mutation	333	372
Nonsense Mutation	3	3
Splice Site Mutation	21	25
Translation Start Site Mutation	1	1
Total	378	421

Table 8. Summary of genomic variants detected in the indicated melanoma cell lines relative to the reference genome (hg38) **in 1110 genes encoding spliceosome-related proteins and RBPs involved in splicing**

The distribution of the variant types and classification was similar to the genome-wide analysis, being the SNVs the most commonly

observed variant type, and the C>T mutations the most frequent SNV class. Among the top 20 mutated genes, we found *SLC25A5* (Solute Carrier Family 25 Member 5), *TTN* (Titin), *SYNE1* (Spectrin Repeat Containing Nuclear Envelope Protein 1), *NUP210* (Nucleoporin 210) and *RNF213* (Ring Finger Protein 213) (Figure 28B).

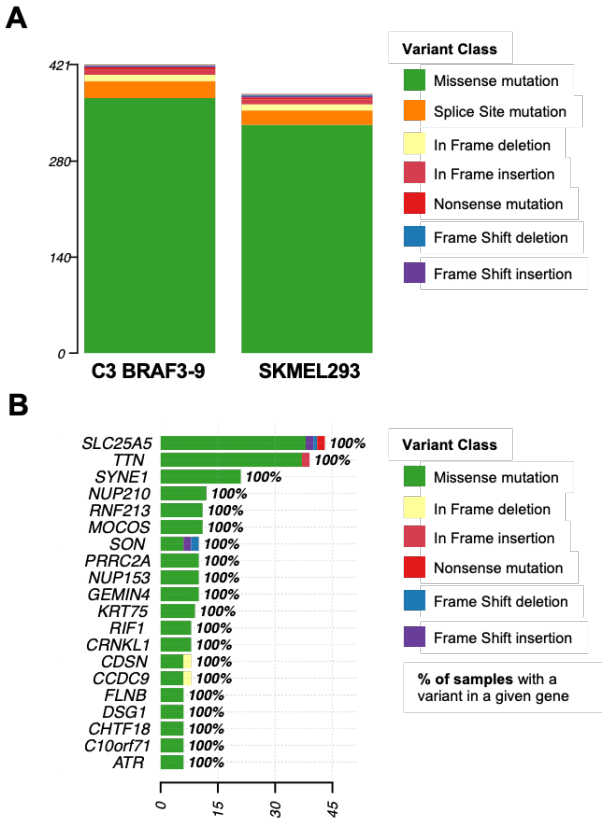

Figure 28. Genome-wide nucleotide variant analysis of SKMEL293 and "bulk" C3 BRAF3-9 compared to reference genome (hg38) **focused on splicing-related genes. A** | Number and class of variants affecting splicing-related genes per sample. The number of variants in the resistant "bulk" C3 BRAF3-9 was higher compared to the parental SKMEL293. Missense mutations were the most common variant class in both cell lines. **B** | Top 20 genes based on the number of variants per gene (x axis). Both cell lines (100% of samples analyzed, as indicated at the right side of each bar) displayed at least one variant in each of these top 20 genes. Color code in the different panels indicate the variant classes.

The resistant "bulk" C3 BRAF3-9 cell line accumulated 43 more variants compared to the parental SKMEL293 (Table 8). Furthermore, we identified 34 genes that were differentially affected between the two cell lines, i.e., in which we detected a mutation in one sample while in its counterpart the same gene showed no variant (Figure 29A). We also identified 27 genes that, being affected in both samples, displayed different variants, for instance *SRSF4* (Serine and Arginine Rich Splicing Factor 4) (Figures 29B and 29C).

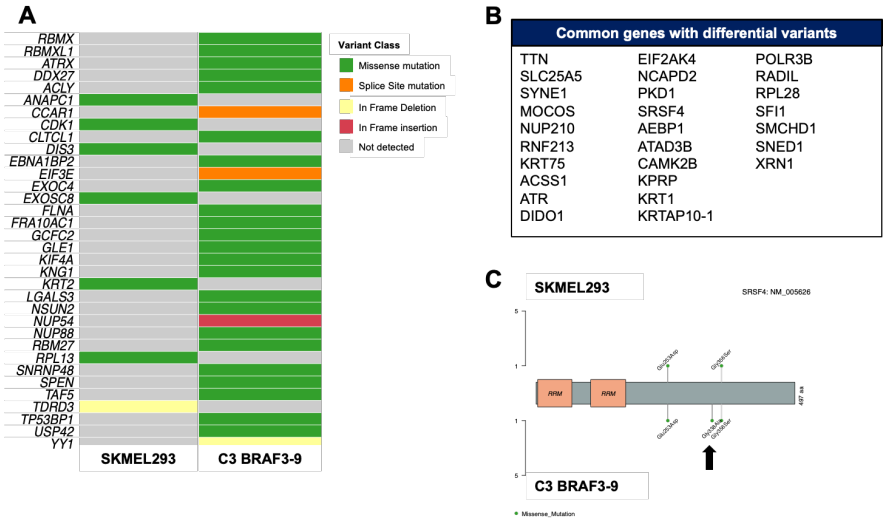

Figure 29. Comparative analysis of splicing-related gene variants in SKMEL293 and "bulk" C3 BRAF3-9 melanoma cell lines compared to the reference genome (hg38). **A |** Genes containing variants exclusive to one of the cell lines and their corresponding variant class. Color code indicate the variant class. Grey color indicates no variant detected in the indicated cell line. **B |** List of genes displaying at least one variant in both cell lines, although harboring at least one different variant among them (either class, location, or a different number of variants). **C |** Variants of *SRSF4* were detected in both cell lines, and one missense mutation (indicated with an arrow) was detected only in the resistant C3 BRAF3-9 cell line (lower part of the lollipop plot).

Next, we further focused our analysis on a selection of 305 genes encoding core spliceosomal components and auxiliary regulatory

factors involved in splicing as well as other RNA-processing steps, including RNA stability, export, or polyadenylation, previously used in our lab for functional network reconstruction of splicing regulation[67] (see Materials and Methods for the gene list).

Of the 305 genes involved in splicing and other RNA processes, 56 genes (18.3%) harbored at least one variant in any of the 2 cell lines analyzed. The most common variant class was again missense mutations, followed by mutations located in splice sites (Table 9).

	SKMEL293 (parental)	**C3 BRAF3-9** (resistant)
In Frame Deletion	2	2
In Frame Insertion	5	5
Missense Mutation	46	51
Splice Site Mutation	9	10
Total	62	68

Table 9. Summary of genomic variants detected in genes related to splicing and other RNA metabolism processes in the indicated melanoma cell lines

The resistant cell line, "bulk" C3 BRAF 3-9, displayed a higher number of variants were identified: specifically, we detected 6 variants that were not present in the parental. These additional variants included 5 missense mutation and 1 splice site mutation (Table 9). The additional variants encompassed 4 differentially affected genes: *CCAR1* (Cell Division Cycle and Apoptosis Regulator 1), *KAT2B* (Lysine Acetyltransferase 2B), *SNRNP48* (Small Nuclear Ribonucleoprotein U11/U12 Subunit 48) and *SPEN* (Spen Family Transcriptional Repressor). These genes harbored missense mutation variants in the resistant C3 BRAF3-9 —except for *CCAR1*, that harbored a splice site mutation— and no variants were detected in the parental cell line (Figure 30). Conversely, we found a

missense mutation in *DIS3* (DIS3 Homolog, Exosome Endoribonuclease and 3'-5' Exoribonuclease) in the parental cell line, that was not present in the resistant C3 BRAF3-9 cell line.

Genes that accumulated > 1 variants included *CRNKL1* (Crooked Neck Pre-MRNA Splicing Factor 1), *TET1* (Tet Methylcytosine Dioxygenase 1), *SRSF4*, *SNW1* (SNW Domain Containing 1), *HFM1* (Helicase for Meiosis 1), *CACTIN* (Cactin, Spliceosome C Complex Subunit) and *ADAR* (Adenosine Deaminase RNA Specific) (Figure 28). *TET1* and *SRSF4* harbored more missense mutations in the resistant "bulk" C3 BRAF3-9 than in the parental SKMEL293 cell line (Figures 30A and 30B).

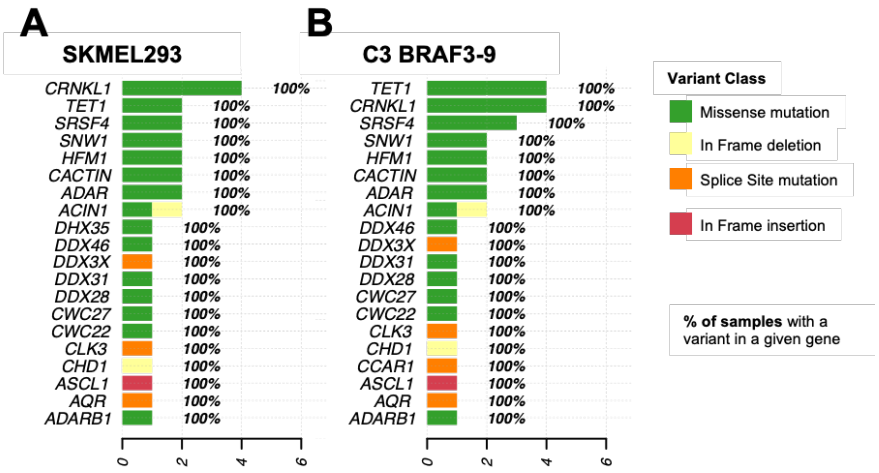

Figure 30. Top 20 mutated genes in the SKMEL293 and "bulk" C3 BRAF3-9 melanoma cell lines focused on splicing-related genes. Top 20 genes based on the number of variants per gene (x axis) in the parental SKMEL293 (A) and in the resistant "bulk" C3 (B) cell lines. The % on the right side of each bar indicates the number of samples affected among the total analyzed (which in our case is only one cell line, either the parental or the resistant). Color code in the different panels indicate the variant classes.

Our genome-wide variant analysis is a highly valuable source of information that merits further exploration. In our search for key players in the production of BRAF3-9 isoform leading to BRAFi-resistance, we focused on a limited number of genes with functions in splicing. We have shown some differences between the parental SKMEL293 and the resistant "bulk" C3 BRAF3-9 melanoma cell lines. First, the resistant cell line displayed a higher number of genome-wide variants, which was also observed in the analysis focused on splicing-related genes. Although this analysis did not take into account other factors such as regulation of expression or post-translational modifications, the comparisons of the variant calling profiles of these genes in the 2 cell lines identified *trans*-acting factors potentially contributing to the generation of splicing variants that warrants further investigation (Figures 29 and 30). Our comparative analyses demonstrated the presence of 34 genes that were differentially affected, 27 of which were only affected in the resistant cell line, while 7 were only affected in the parental (Figure 29A). No frameshift variants, indicating a strong functional impact, were detected. Instead, missense mutations and splice site mutations of unclear functional effect were identified. For instance, the two RNA recognition motifs (RRM) of SRSF4 did not harbor any of the two shared missense mutation nor the one acquired upon resistance. Likewise, the arginine–serine-rich (RS) domain hosted a G356S mutation in both cell lines, and a G338A mutation in the resistant cell line (Figure 29C). Whether these missense mutations in the RS domain, specially the detected exclusively in the resistant cell line,

can influence the activity of the domain requires further investigation.

In an attempt to elucidate whether any of these mutations might be clinically relevant, we also screened the tumor samples harboring the BRAF3-9 isoforms included in the TCGA dataset, for the presence of any mutation in any of the most frequent mutated genes (i.e., *TET1, ADAR, SRSF4, CRNLK1, SNW1, CACTIN, HFM1*) in the cBioportal database[291,292]. None of the two samples displayed a mutation in any of these genes. This finding downplayed the hypothesis of a mutation in a *trans*-acting factor from our selected gene list, being responsible for the production of BRAF3-9.

3.5.3 Genome-wide CRISPR knockout screening reveals vulnerabilities associated to the resistant phenotype

Previous studies have demonstrated the value of high-throughput forward genetic screening approaches to reveal molecular mechanisms associated with specific phenotypes, including drug resistance in human cancers[392–403]. Inspired by these successes, we performed a genome-wide CRISPR (Clustered Regularly Interspaced Short Palindromic Repeats)/Cas9 knockout screening to unravel potential *trans*-acting factors involved in the maintenance of the BRAF3-9 isoform.

Briefly, Cas9 mediates a doble-strand DNA break at a target locus, specified by a single-guide RNA (sgRNA), that would eventually lead to a loss-of-function perturbation of the genome locus. Some sgRNA libraries designed for CRISPR knockouts screening included GeCKO (Genome-Scale CRISPR Knock-Out)[393] or TKO (Toronto KnockOut)[394]. The enrichment/depletion of sgRNAs over time in these knockout screenings reveal lethal or essential genes, genetic dependencies, and drug-mediated cell vulnerabilities.

The experimental design

The experimental design is schematized in Figure 31 (see further details in Materials and Methods). Briefly, after amplification of the sgRNA library, large scale production of lentivirus containing the genome-scale sgRNA TKOv3 library was achieved. The TKOv3

library contains 70,948 sgRNA targeting 18,053 protein coding genes (4 sgRNAs/gene) with 142 control non-targeting guides (EGFP, LacZ and luciferase) for a total library size of 71,090. Then, the lentiviral library was transduced at a low multiplicity of infection (MOI) in inducible Cas9 expressing melanoma cells, that we previously produced (see Materials and Methods). This low MOI is necessary to ensure that most cells received only one sgRNA, thus allowing the independent interrogation of different genes. After 48 hours of selection with puromycin, followed by 48 hours of Cas9 induction with doxycycline, the screening was conducted maintaining an appropriate number of cells to ensure a coverage of at least 200-fold of each sgRNA, and under vemurafenib pressure in the case of the resistant cell lines (see below). Finally, sequencing data of the sgRNAs, amplified by PCR from extracted genomic DNA (gDNA) at different time points of the procedure, was analyzed to identify changes in sgRNAs distribution, for instance enrichment/depletion of particular sgRNAs, pointing to potential non-essential/essential genes, respectively, given the knockout nature of the screen.

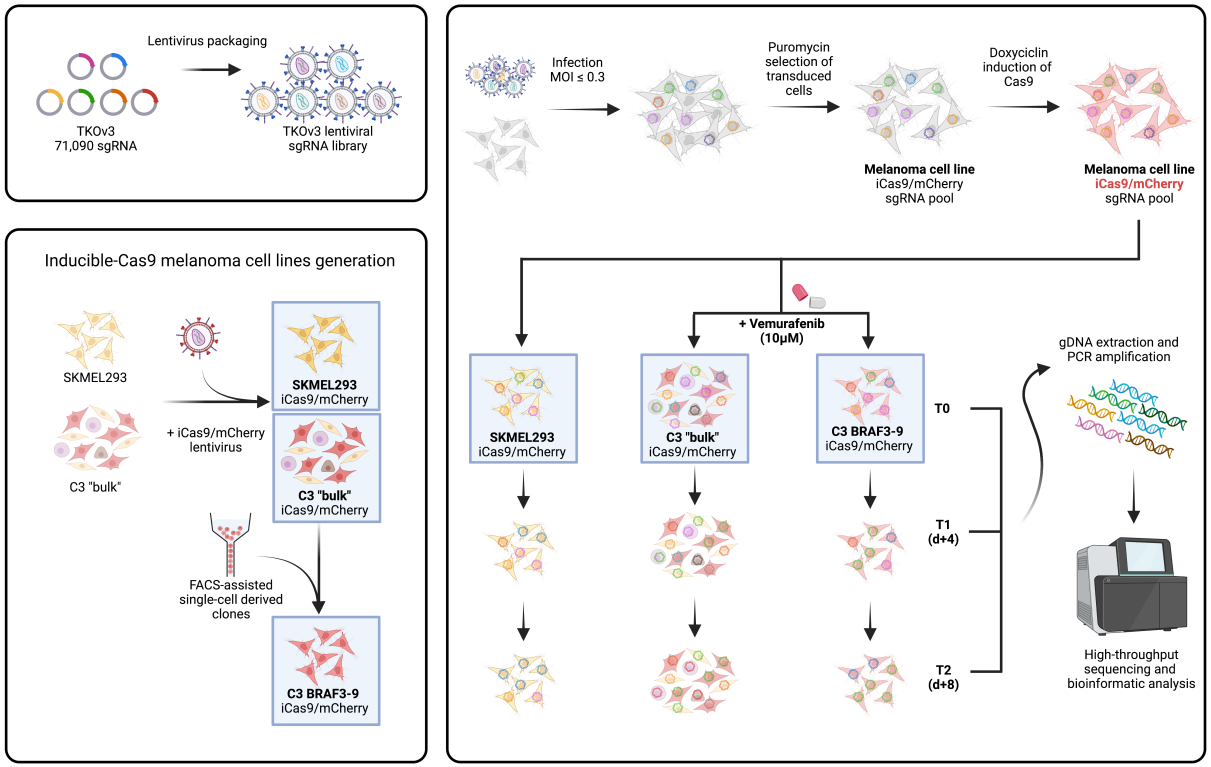
Lentivirus packaging
TKOv3
71,090 sgRNA
TKOv3 lentiviral
sgRNA library
Inducible-Cas9 melanoma cell lines generation
SKMEL293
C3 "bulk"
+ iCas9/mCherry
lentivirus
SKMEL293
iCas9/mCherry
C3 "bulk"
iCas9/mCherry
FACS-assisted
single-cell derived
clones
C3 BRAF3-9
iCas9/mCherry
Infection
MOI ≤ 0.3
Puromycin
selection of
transduced
cells
Doxyciclin
induction of
Cas9
Melanoma cell line
iCas9/mCherry
sgRNA pool
Melanoma cell line
iCas9/mCherry
sgRNA pool
+ Vemurafenib
(10μM)
SKMEL293
iCas9/mCherry
C3 "bulk"
iCas9/mCherry
C3 BRAF3-9
iCas9/mCherry
T0
T1
(d+4)
T2
(d+8)
gDNA extraction and
PCR amplification
High-throughput
sequencing and
bioinformatic analysis

Figure 31. Overview of the experimental design of our genome-scale CRISPR knockout screening. First, inducible-Cas9 melanoma cell lines were established (left bottom figure), from the parental SKMEL293 and resistant "bulk" C3 cell lines. A single cell-derived clone BRAF3-9 from "bulk" C3 was also generated. After large scale production of sgRNA lentivirus (left upper figure), the 3 cell lines were transduced at low MOI, selected with puromycin and the Cas9 was induced for 48 h with doxycycline. Resistant cell lines (C3 "bulk"- and C3 BRAF3-9-iCas9/mCherry) were screened under 10 μM vemurafenib. Cells were harvested at d+4 (T1) and at d+8 (T2) for amplified sgRNA sequencing and analysis. sgRNA, single-guide RNA; TKOv3, Toronto KnockOut version 3; iCas9, inducible Cas9; FACS, Fluorescence-activated cell sorting; MOI, multiplicity of infection; gDNA, genomic DNA. Created with www.BioRender.com.

Regarding the design of our screening (Figure 31), here we highlight some particular aspects that were important to optimize the results:

1. We decided to use previously transduced melanoma cell lines harboring an inducible Cas9-mCherry system, which we established (see Materials and Methods), to avoid off-target effects related to a stable expression of Cas9. For this reason, we used the vector without Cas9 (pLCKO2::TKOv3), instead of the one-component library that also express Cas9. Thus, after the selection of sgRNA-expressing cells, we induced the Cas9 with doxycycline during 48 hours (Figure 31).

2. We screened 3 different cell lines in parallel: the parental SKMEL293, the resistant "bulk" C3 cell population and a single cell-derived C3 clone expressing the BRAF3-9 isoform (approximately 50% of BRAF transcripts were BRAF3-9 in this clonal line). As our objective was to identify essential genes involved specifically in the generation or maintenance of the BRAF3-9 isoform, we hoped to use the SKMEL293 and C3 "bulk" screenings as references for the discrimination

of genes involved in BRAF3-9 production *vs* genes generally required for proliferation (parental cell line) and genes required for growth in the presence of vemurafenib by a variety of mechanisms ("bulk" cell population, as observed in Part IV).

3. Vemurafenib was added to the medium of both of the resistant cell lines: C3 "bulk" and C3 BRAF3-9 clone. However, while usual vemurafenib concentrations are in the 1 μM range, we increased the dose to 10 μM, fitting with the approximately IC50 observed for different C3 BRAF3-9 clones analyzed (Figure 32C). We opted for a higher concentration of vemurafenib also to avoid the emergence of other resistance mechanism due to cell plasticity, and at the same time, to select those genes with greater effects in the BRAF3-9 model.

4. We verified the dependence of the clonal resistant C3 cell line on the BRAF3-9 isoform in a colony formation assay performed using siRNAs targeting exons 5 and 6, and siRNA complementary to the EEJ3-9, which clearly impaired the colony formation capacity in the clonal C3 BRAF3-9 (Figure 32A and 32B).

5. We analyzed sgRNA abundance at earlier time points than usual in this type of screens: at day 4 and at day 8 after Cas9 induction. Given the dependency referred to in point 4) and the expected half-life of both mRNA and translated protein, we reasoned that short-term analyses would preferentially identify genes with immediate effects on cell survival under

vemurafenib selection, e.g. those involved in the generation of the BRAF3-9 isoform, thus hypothetically reducing the chances of the cells developing other mechanisms of resistance over longer periods of time.

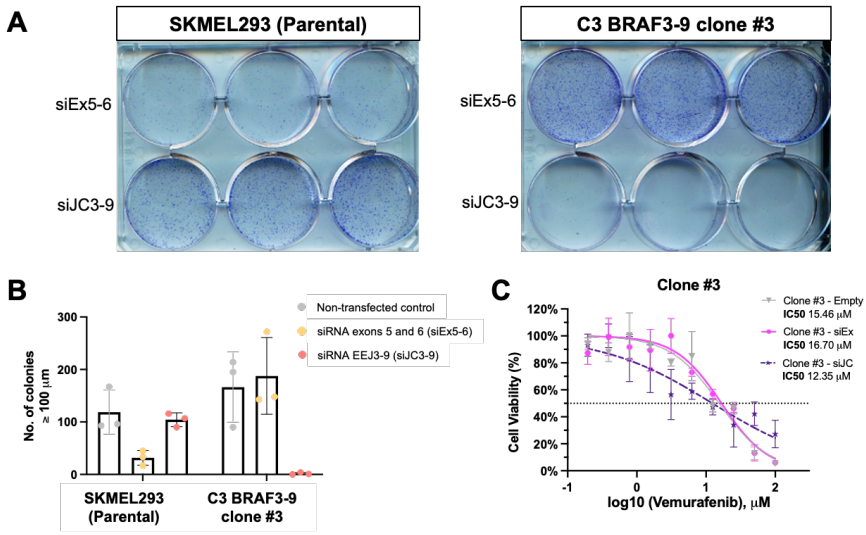

Figure 32. Effect of transfection of siRNAs targeting either full BRAF or BRAF3-9 transcripts on colony formation and vemurafenib sensitivity of the parental SKMEL293 and the clonal resistant cell line C3 BRAF3-9 clone #3. siRNA pools (40 nM) targeting exons 5 and 6 (siEx5-6) or the exon junction 3-9 (siJC3-9) were transfected in SKMEL293 and C3 BRAF3-9 clone #3. **A |** Colony formation assay and **B |** quantification of number of colonies (color codes indicate each experimental group). **C |** Cell viability assay of C3 BRAF3-9 clone #3 at 72 hours after treatment with vemurafenib at the indicated concentrations. The results show that BRAF3-9 knockdown (siJC3-9) led to a decrease in IC50, while full-length BRAF knockdown (siEx5-6) using siRNAs targeting sequences corresponding to the skipped exons 5 and 6 had no effect on vemurafenib sensitivity.

Bioinformatic analyses

For bioinformatic analyses we used both MAGeCK (Model-based Analysis of Genome-wide CRISPR-Cas9 Knockout)[404] and BAGEL (Bayesian Analysis of Gene EssentiaLity)[405] tools. Briefly,

MAGeCK prioritizes and identifies genes as "essential" —negatively selected sgRNAs— using a binomial distribution-based algorithm, either through a modified robust ranking aggregation (RRA) method or through a maximum-likelihood estimation (MLE) method. This basically assumes that if a gene has no effect on selection, their targeting sgRNA should be uniformly distributed through the ranked list of all the sgRNAs. On the other hand, BAGEL evaluates the likelihood that the observed fold changes in sgRNA targeting of a specific gene were drawn from either the essential or from the nonessential calculated distributions of a training set[394].

Quality control analyses were performed using both tools for the 18 samples, which included triplicates of 3 time points (T0, T1 d+4, T2 d+8) for each of the 3 different cell lines (SKMEL293, "bulk" C3, C3 BRAF3-9 single cell-derived clone). The observed Gini index (which measures read depth evenness within samples) was low (Figure 33A), which —reassuringly— suggests low probability of unevenness in the oligonucleotide synthesis, low-quality viral library packaging or poor efficiency during viral transfection. The number of missed sgRNAs was homogeneous across samples (Figure 33B), as were the number of reads and the proportion of mappable reads across samples for each time point (Figure 33C). Reference T0 samples were sequenced at higher read depth of 400-500-fold library coverage, to ensure an optimal library representation that would allow efficient determination of sgRNA fold changes over time. Additionally, we calculated precision-recall (PR) curves of Bayes Factors (BFs) using the provided reference sets (see Materials and Methods). As expected, later time points displayed better recall

(Figure 33D). However, the screen of the "bulk" C3 cell line failed in yielding fitness genes (no genes at 5% false discovery rate [FDR]) (Figure 33D). Hereafter, "bulk" C3 cell line was thus excluded for further analyses, and we focused our analyses on T2 (d+8) due to better performances in PR outcomes.

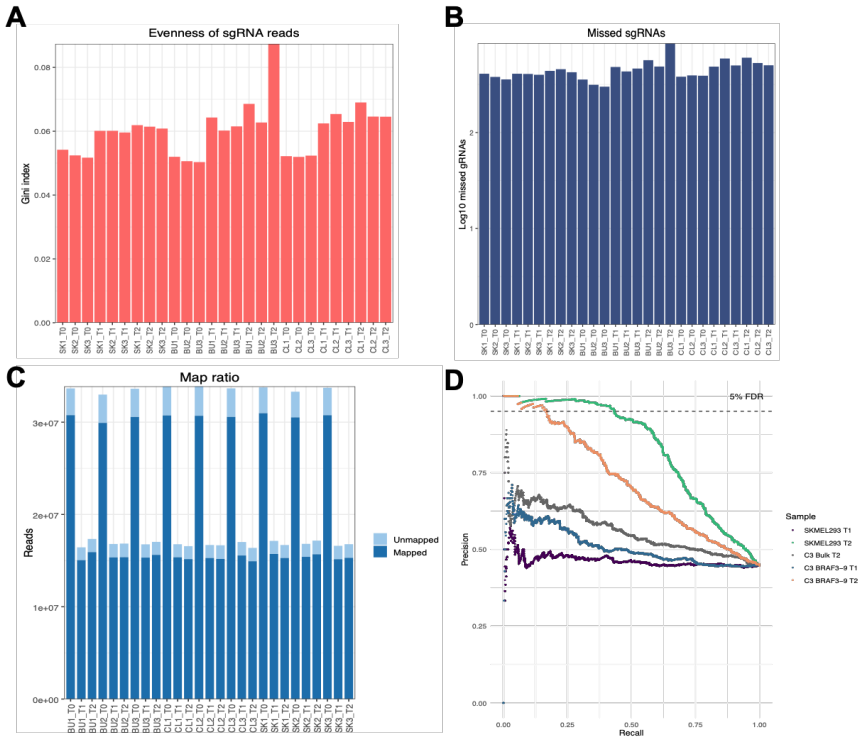

Figure 33. Quality control assessment of CRISPR screen data using MAGeCK and BAGEL. Distribution of **A** | the Gini index, **B** | the number of missed sgRNAs and **C** | read counts and the mapping percentages (calculated with MAGeCK) across samples and time points. The Gini index measures the evenness of the sgRNA read counts, namely the log scaled read count distribution. A Gini index < 0.2 is considered optimal in a negative selection experiment. **D** | Precision-recall plots of fitness genes for each time point and cell line (calculated with BAGEL). Dashed line indicates the 5% FDR threshold.

MAGeCK RRA analysis

Using MAGeCK RRA, the results of the screen at day 8 (T2) revealed a significant number of depleted sgRNAs, but no significant enrichment of any sgRNA or gene (Figure 34A and 34D). A total of 211 genes with a FDR ≤ 10% were identified in SKMEL293 cells and 197 in the C3 BRAF3-9 cell line. Of these, 116 and 136 genes showed a fold change (FC) ≤ 1.5, respectively (Figure 34C and 34F). The top rank genes in both cell lines were plotted in Figure 34B and 34E and the top 20 essential genes listed in Table 10 and Table 11 (full list available in Supplementary Table S3).

Rank	Gene	RRA score	p value	FDR	"Good" sgRNA
1	*RRM1*	$1.84x10^{-6}$	$2.74x10^{-4}$	0.000215	4
2	*SMU1*	$1.90x10^{-6}$	$2.74x10^{-4}$	0.000215	4
3	*HSPA5*	$5.90x10^{-6}$	$2.74x10^{-4}$	0.000215	4
4	*PSMC6*	$3.81x10^{-6}$	$2.74x10^{-4}$	0.000215	4
5	*RPL12*	$1.19x10^{-4}$	$2.74x10^{-4}$	0.000215	4
6	*GGPS1*	$2.92x10^{-4}$	$2.74x10^{-4}$	0.000215	4
7	*SS18L2*	$2.60x10^{-3}$	$2.74x10^{-4}$	0.000215	3
8	*WBP11*	$2.62x10^{-3}$	$2.74x10^{-4}$	0.000215	3
9	*PSMA5*	$2.79x10^{-3}$	$2.74x10^{-4}$	0.000215	4
10	*PLK1*	$2.82x10^{-3}$	$2.74x10^{-4}$	0.000215	4
11	*NXF1*	$3.95x10^{-3}$	$2.74x10^{-4}$	0.000215	4
12	*RPSA*	$7.02x10^{-3}$	$2.74x10^{-4}$	0.000215	4
13	*CCT5*	$9.73x10^{-3}$	$2.74x10^{-4}$	0.000215	4
14	*POLR1B*	$9.98x10^{-3}$	$2.74x10^{-4}$	0.000215	4
15	*INTS8*	$1.18x10^{-2}$	$2.74x10^{-4}$	0.000215	3
16	*TCP1*	$1.28x10^{-2}$	$2.74x10^{-4}$	0.000215	4
17	*BUB3*	$1.42x10^{-2}$	$2.74x10^{-4}$	0.000215	4
18	*RAN*	$1.58x10^{-2}$	$2.74x10^{-4}$	0.000215	3
19	*COPB2*	$1.69x10^{-2}$	$2.74x10^{-4}$	0.000215	3
20	*TPX2*	$1.77x10^{-2}$	$2.74x10^{-4}$	0.000215	4

Table 10. Top 20 essential genes identified by CRISPR knockout screen in SKMEL293 cells (d+8). Robust ranking aggregation (RRA) scores, p value and

False Discovery Rates (FDR) for each gene are shown. “Good” sgRNAs indicates the number of sgRNAs for a given gene hit that fall below a default FDR of 0.25.

Rank	Gene	RRA score	p value	FDR	“Good” sgRNA
1	*RRM1*	2.24×10^{-8}	2.74×10^{-3}	0.00015	4
2	*PLK1*	4.08×10^{-8}	2.74×10^{-3}	0.00015	4
3	*HSPA5*	4.24×10^{-8}	2.74×10^{-3}	0.00015	4
4	*RPL12*	3.00×10^{-7}	2.74×10^{-3}	0.00015	4
5	*INTS6*	2.63×10^{-5}	2.74×10^{-3}	0.00015	4
6	*SOX10*	4.13×10^{-5}	2.74×10^{-3}	0.00015	4
7	*SMU1*	4.49×10^{-6}	2.74×10^{-3}	0.00015	4
8	*NXF1*	1.52×10^{-4}	2.74×10^{-3}	0.00015	4
9	*WEE1*	4.58×10^{-4}	2.74×10^{-3}	0.00015	3
10	*COPA*	5.21×10^{-5}	2.74×10^{-3}	0.00015	4
11	*CKAP5*	8.31×10^{-4}	2.74×10^{-3}	0.00015	3
12	*SF3B3*	1.36×10^{-4}	2.74×10^{-3}	0.00015	4
13	*CCND1*	1.44×10^{-3}	2.74×10^{-3}	0.00015	4
14	*PCF11*	2.26×10^{-3}	2.74×10^{-3}	0.00015	4
15	*SNRNP200*	2.65×10^{-4}	2.74×10^{-3}	0.00015	3
16	*ETF1*	4.81×10^{-3}	2.74×10^{-3}	0.00015	3
17	*FBXO5*	5.11×10^{-3}	2.74×10^{-3}	0.00015	4
18	*MCL1*	5.54×10^{-3}	2.74×10^{-3}	0.00015	3
19	*CCNA2*	6.06×10^{-3}	2.74×10^{-3}	0.00015	4
20	*RNF113A*	6.71×10^{-3}	2.74×10^{-3}	0.00015	3

Table 11. Top 20 essential genes identified by CRISPR knockout screen in C3 BRAF3-9 cells (d+8). Robust ranking aggregation (RRA) scores, p value and False Discovery Rates (FDR) for each gene are shown. “Good” sgRNAs indicates the number of sgRNAs for a given gene hit that fall below a default FDR of 0.25.

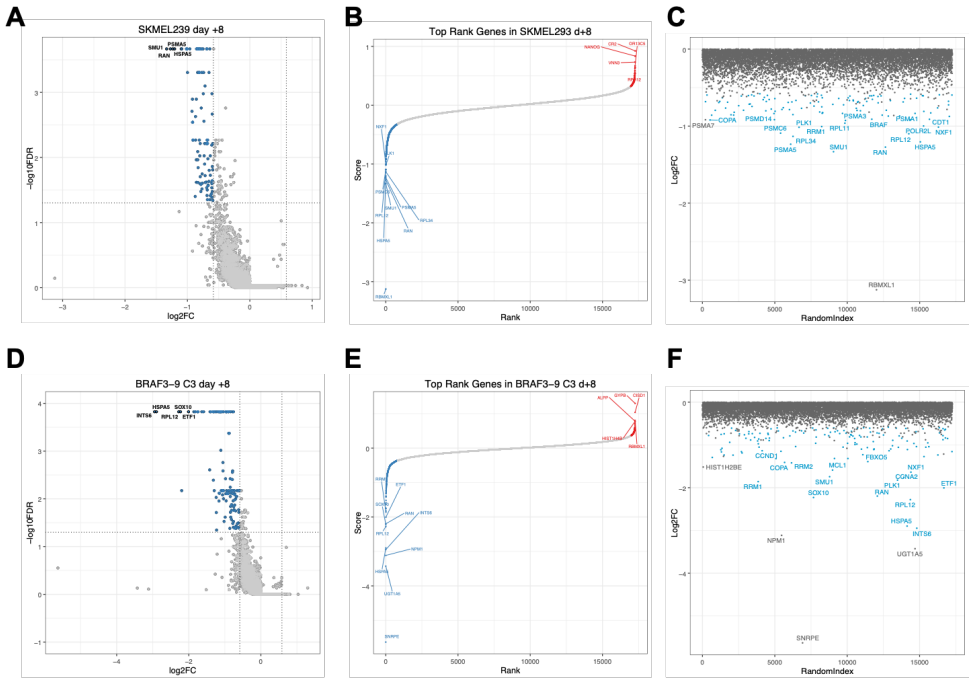

Figure 34. Essential genes in SKMEL293 (top figures) **and C3 BRAF3-9** (bottom figures) **cell lines identified by the CRISPR-Cas9 knockout screen at day +8 using MAGeCK RRA. A | and D |** Volcano plots of sgRNA enrichment revealed no significant positively selected genes. Dashed line denotes 5% FDR. Blue dots indicate negatively selected hits with a FDR ≤ 5% and a fold change ≤ -1.5. **B | and E |** Rank plots showing negatively selected or essential genes (blue dots) and positively selected genes (red dots). **C | and F |** FC enrichment dot plots; blue dots represent gene hits with FDR ≤ 10% and fold change ≤ -1.5. A, B and C correspond to SKMEL293 cell line and D, E and F to C3 BRAF3-9 cell line. FDR, false discovery rate; Score, RRA score; FC, fold-change.

When comparing the essential genes identified in the 2 cell lines (filtered by FDR ≤ 10% and FC ≤ -1.5), we observed 49 common essential genes and 67 essential genes exclusively identified in SKMEL293 cells and 87 exclusive of the C3 BRAF3-9 cell line. Among them, the list of exclusive essential genes of C3 BRAF3-9 with a FDR < 5%, and their protein function according to the PANTHER knowledgebase[406,407] are showed in Table 12.

Gene ID	Gene Name	PANTHER Protein Class
POLA1	DNA polymerase alpha catalytic subunit	DNA metabolism protein
TOP2A	DNA topoisomerase 2-alpha	DNA metabolism protein
AURKA	Aurora kinase A	non-receptor serine/threonine protein kinase
CENPI	Centromere protein I	
CDC45	Cell division control protein 45 homolog	replication origin binding protein
CRTC3	CREB-regulated transcription coactivator 3	transcription cofactor
PRKCA	Protein kinase C alpha type	non-receptor serine/threonine protein kinase
CCNB2	G2/mitotic-specific cyclin-B2	kinase activator
PSMC4	26S proteasome regulatory subunit 6B	protease
PPP1R15B	Protein phosphatase 1 regulatory subunit 15B	
RAD21	Double-strand-break repair protein rad21 homolog	
EIF2S1	Eukaryotic translation initiation factor 2 subunit 1	translation initiation factor
ETF1	Eukaryotic peptide chain release factor subunit 1	translation release factor
ZC3H13	Zinc finger CCCH domain-containing protein 13	
CCT8	T-complex protein 1 subunit theta	chaperonin
PSMD6	26S proteasome non-ATPase regulatory subunit 6	

Gene ID	Gene Name	PANTHER Protein Class
SMC4	Structural maintenance of chromosomes protein 4	
CCNA2	Cyclin-A2	kinase activator
SF3B1	Splicing factor 3B subunit 1	RNA splicing factor
GSPT1	Eukaryotic peptide chain release factor GTP-binding subunit ERF3A	translation factor
SNRNP200	U5 small nuclear ribonucleoprotein 200 kDa helicase	scaffold/adaptor protein
ANAPC1	Anaphase-promoting complex subunit 1	ubiquitin-protein ligase
NUP205	Nuclear pore complex protein Nup205	
MCL1	Induced myeloid leukemia cell differentiation protein Mcl-1	
DYNC1I2	Cytoplasmic dynein 1 intermediate chain 2	microtubule or microtubule-binding cytoskeletal protein
LRR1	Leucine-rich repeat protein 1	scaffold/adaptor protein
RRM2	Ribonucleoside-diphosphate reductase subunit M2	reductase
CCND1	G1/S-specific cyclin-D1	kinase activator
CDC6	Cell division control protein 6 homolog	replication origin binding protein
MAD2L1BP	MAD2L1-binding protein	
CENPT	Centromere protein T	
RPS3	40S ribosomal protein S3	ribosomal protein
ABCC6	ATP-binding cassette sub-family C member 6	ATP-binding cassette (ABC) transporter
LIMS1	LIM and senescent cell antigen-like-containing domain protein 1	cell junction protein
CENPN	Centromere protein N	
CDK1	Cyclin-dependent kinase 1	non-receptor serine/threonine protein kinase
MITF	Microphthalmia-associated transcription factor	
POLR3E	DNA-directed RNA polymerase III subunit RPC5	DNA-directed RNA polymerase
SMG1	Serine/threonine-protein kinase SMG1	non-receptor serine/threonine protein kinase

Gene ID	Gene Name	PANTHER Protein Class
POLR2E	DNA-directed RNA polymerases I, II, and III subunit RPABC1	DNA-directed RNA polymerase
VARS1	Valine--tRNA ligase	aminoacyl-tRNA synthetase
XPO1	Exportin-1	transporter
USPL1	SUMO-specific isopeptidase USPL1	cysteine protease
TFAP2A	Transcription factor AP-2-alpha	general transcription factor
RBM48	RNA-binding protein 48	
PRKACA	cAMP-dependent protein kinase catalytic subunit alpha	non-receptor serine/threonine protein kinase
CENPW	Centromere protein W	
NEDD1	Protein NEDD1	
HNRNPU	Heterogeneous nuclear ribonucleoprotein U	
NAA50	N-alpha-acetyltransferase 50	acetyltransferase
DBF4	Protein DBF4 homolog A	kinase activator
CDC5L	Cell division cycle 5-like protein	
HSPA9	Stress-70 protein, mitochondrial	Hsp70 family chaperone
NDC80	Kinetochore protein NDC80 homolog	transcription cofactor
IL1RN	Interleukin-1 receptor antagonist protein	interleukin superfamily
TEX29	Testis-expressed protein 29	
VDAC2	Voltage-dependent anion-selective channel protein 2	voltage-gated ion channel
NUP98	Nuclear pore complex protein Nup98-Nup96	transporter
ELP5	Elongator complex protein 5	
TUBB	Tubulin beta chain	tubulin
CD300LG	CMRF35-like molecule 9	immunoglobulin receptor superfamily
C3orf38	Uncharacterized protein C3orf38	
SNRPB	Small nuclear ribonucleoprotein-associated proteins B and B'	RNA splicing factor
HMGCS1	Hydroxymethylglutaryl-CoA synthase, cytoplasmic	
NUP153	Nuclear pore complex protein Nup153	transporter
FBXO5	F-box only protein 5	

Gene ID	Gene Name	PANTHER Protein Class
TMEM167A	Protein kish-A	
DHX8	ATP-dependent RNA helicase DHX8	RNA helicase
KPNB1	Importin subunit beta-1	transporter

Table 12. Essential genes identified exclusively in C3 BRAF3-9 cells by the CRISPR knockout screen at day +8, using MAGeCK RRA.

Enrichment analyses, using hypergeometric tests and the biological process and cellular components terms, were performed with the essential genes with a FDR ≤ 10% and a FC ≤ -1.5 in both cell lines (Figure 33). Interestingly, essential genes of SKMEL293 cells were enriched for proteasome-related processes and ribosomal components, whereas essential genes of C3 BRAF3-9 were mostly related to spindle formation and chromosome segregation as well as to splicing components (mainly of the catalytic and pre-catalytic steps). Considering essential genes exclusively in C3 BRAF3-9 cells with a FDR ≤ 5% (Table 12), 6 genes belonged to catalytic step 2 spliceosome functional group (*SF3B1, SNRNP200, HNRNPU, CDC5L, SNRPB* and *DHX8*) and 7 genes to the spindle assembly group, including *AURKA, CCNB2, NDC80, FBXO5, RPS3, TUBB* and *KPNB1*.

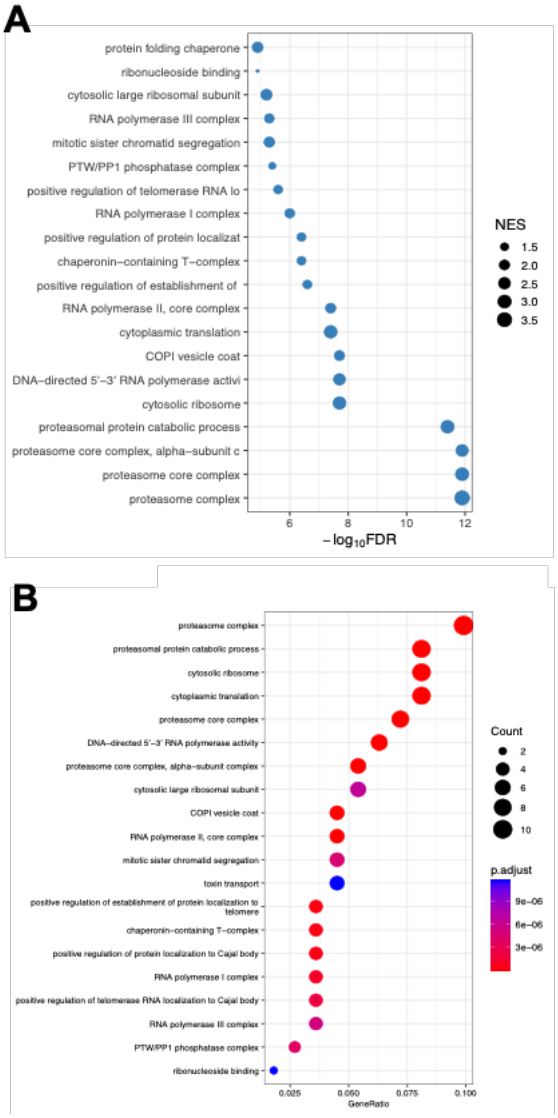

Figure 35. Gene ontology enrichment analysis of essential genes identified by the CRISPR-Cas9 knockout screen in SKMEL293 cell line. Top 20 gene ontology biological process terms (A) and cellular component terms were used. Essential genes were identified with MAGeCK and then filtered by FDR ≥ 10% and a fold-change ≤ -1.5. NES, normalized enrichment scores.

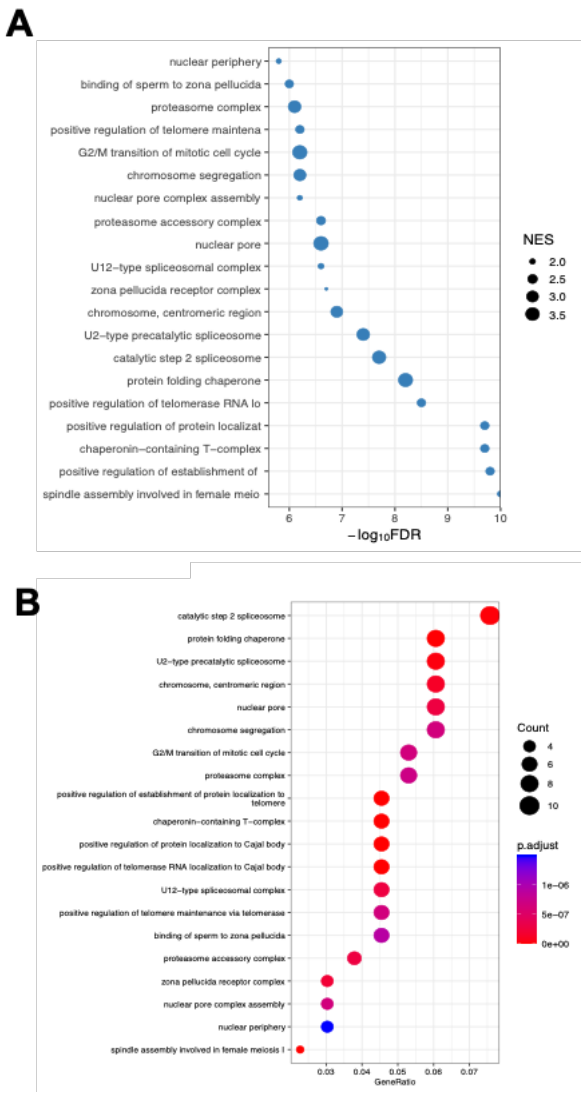

Figure 36. Gene ontology enrichment analysis of essential genes identified by the CRISPR-Cas9 knockout screen in C3 BRAF3-9 cell line. Top 20 gene ontology biological process terms (A) and cellular component terms were used. Essential genes were identified with MAGeCK and then filtered by FDR ≥ 10% and a fold-change ≤ -1.5. NES, normalized enrichment scores.

How essential is BRAF?

Not surprisingly, *BRAF* was identified as a significant essential gene in the SKMEL293 screen with a FDR ≤ 10% and FC ≤ -1.5 (Figure

34C). Surprisingly, however, this appeared not to be the case in the C3 BRAF3-9 screen, despite the survival of this cell line being dependent on the production of the BRAF3-9 isoform, as shown above (Figure 32). A deeper analysis of the effect of each sgRNA targeting *BRAF* and their distribution on the BRAF locus showed that, while all 4 sgRNAs were depleted at d+8 in the SKMEL293 cell line, 2 sgRNAs did not change over time in C3 BRAF3-9 cells, leading to BRAF not being scored as a reliable hit in the screen. While the sgRNA with the greater depletion in the resistant cell line targets *BRAF* exon 1, the remaining sgRNAs target exons 5, 6 and 7 —which are sequences not present in the mature mRNA of the BRAF3-9 isoform—, thus explaining their lack of depletion despite the essentiality of the *BRAF* gene in this cell line as well (Figure 34). Therefore, the absence of *BRAF* among the essential gene hits of our screen in C3 BRAF3-9 cells can be explained by the distribution of the sgRNAs used in the screen across the *BRAF* exons.

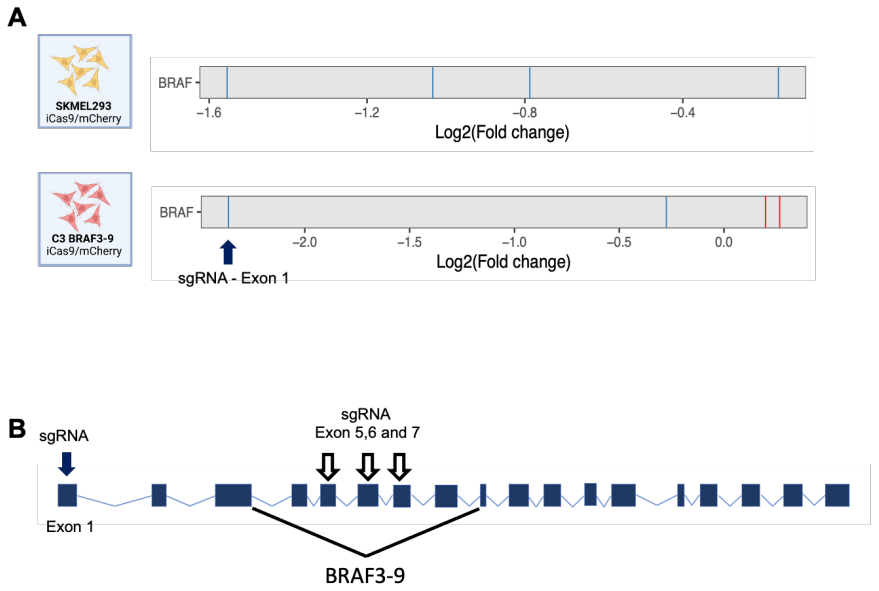

Figure 37. Depletion of *BRAF*-targeting sgRNAs in the CRISPR-Cas9 knockout screen of SKMEL293 and C3 BRAF3-9 cell lines and their distribution in the *BRAF* locus. A | Fold change of *BRAF*-targeting sgRNAs in the CRISPR-Cas9 knockout screen for the indicated cell lines. Blue lines represent negative fold changes and red lines, positive fold changes. **B** | Schematic representation of *BRAF* exon-intron architecture, the splicing pattern of the BRAF3-9 isoform and location of the sgRNAs target sequences. Blue arrow indicates sgRNA targeting exon 1, white arrows the position of sgRNA against exon 5, 6 and 7.

MAGeCK MLE analysis

MAGeCK MLE can be used to analyze data from more complex experimental designs —for instance, screens with multiple conditions—, as opposed to MAGeCK RRA, which only allows comparison between two experimental conditions —for instance our previously described analysis of T0 *versus* T2 (d+8)— (see Materials and Methods). Similarly, MAGeCK MLE also provides a "beta score" for each targeted gene, which basically measures a degree of

selection upon gene perturbation but, unlike MAGeCK RRA, is calculated with a maximum-likelihood estimation (MLE) method.

Using MAGeCK MLE, we compared SKMEL293 and C3 BRAF3-9 at day +8 and recapitulated some of the hits identified with MAGeCK RRA (Supplementary Table S4). To focus our selection, we filtered hits with a beta score ≥ |0.5|. Genes related to the proteasome (e.g., *PSMC6*, *PSMA3*), transcription (e.g., *POLR1B*) or ribosomal activity (e.g., *RPL34*) were again identified as essential for the SKMEL293 cell line. Similarly, genes encoding splicing or transcription factors (such as *SF3B1* or *SOX10*) and genes encoding cell cycle regulators (such as *CCNA2*) were identified as essential for the C3 BRAF3-9 cell line. Other genes consistently identified as essential for the resistant cell line using both methods were *PLK1* (Polo Like Kinase 1), *FBXO5* (F-Box Protein 5) and *INTS6* (Integrator Complex Subunit 6) (Figure 38A).

Functional enrichment analyses of these negatively selected genes in the C3 BRAF3-9 cell line revealed an enrichment of similar biological process and molecular function terms as those described with MAGeCK RRA. Some of these biological processes included terms related to chromosome dynamics (i.e., anaphase-promoting complex binding, regulation of DNA replication, spindle assembly and chromosome segregation involved in female meiosis), splicing factor binding and cell cycle (e.g.., regulation of mitotic cell cycle or cyclin A2-CDK2 complex).

We then selected hits whose β score range between T2 (d+8) of SKMEL293 and C3 BRAF3-9 was > 0.5 —that is, genes with the

most changing or divergent effects between the two cell lines—(Figure 38B). While some of these hits (*HIST1H3G*, *ANP32D*, *C4B*, *SNRPE*, *NPM1*, *RBMXL1*) were identified as essential despite relying on the effect of only 1 of the 4 sgRNAs, several genes are repeatedly identified as essential mainly for the resistant C3 BRAF3-9, such as *CCNA2*, *XPO1* or *FBXO5* (Figure 38B). Other genes such as *NXF1*, *PLK1* and *INTS6* are consistently found among the genes negatively selected in both cell lines.

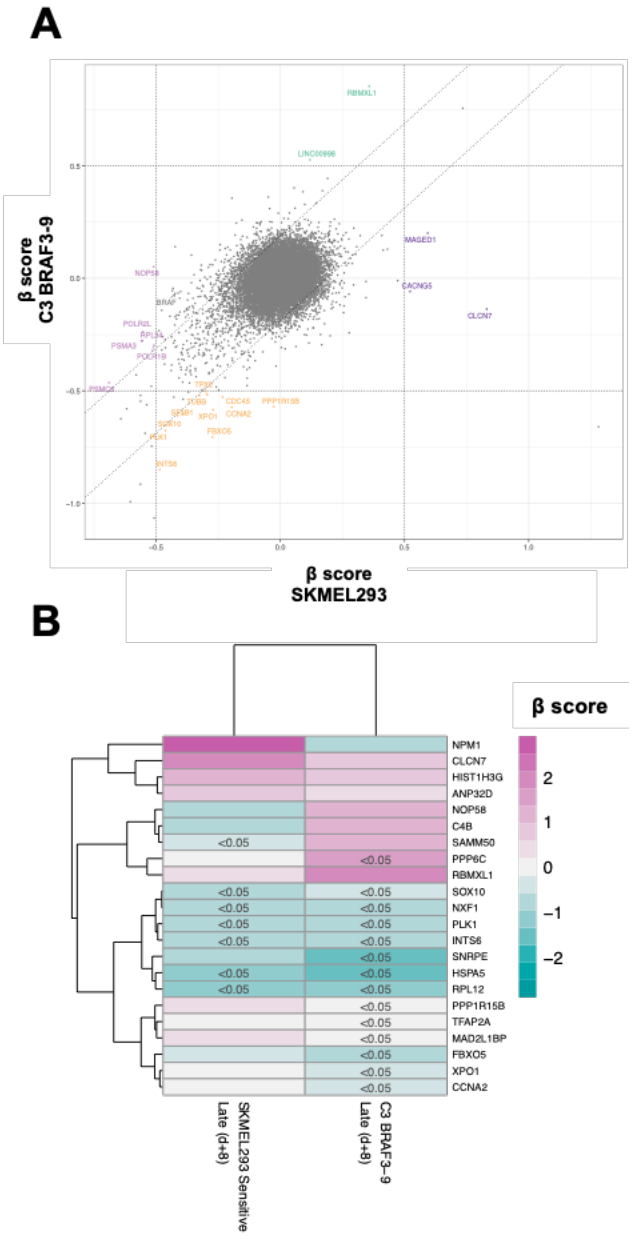

Figure 38. Comparative analysis of essential hits in SKMEL293 and C3 BRAF3-9 cell lines identified by CRISPR knockout screen at day +8 using MAGeCK MLE. A | Nine-square plot showing calculated β scores of genes from SKMEL293 and C3 BRAF3-9 cell lines at day +8. β scores for the parental condition (SKMEL293) are represented in x-axis and for resistance due to BRAF3-9 (C3 BRAF3-9) in the y-axis. Purple dots indicate hits that are unchanged in the

C3 BRAF3-9 but show changes in the parental SKMEL293: light purple dots correspond to hits that are depleted ("essential") and dark purple dots to hits that are enriched ("non-essential"). Orange and green dots indicate hits that changed only in the resistant C3 BRAF3-9: green dots correspond to hits enriched ("non-essential"), and orange dots correspond to hits depleted ("essential"). **B |** Heatmap of hits with the most divergent β scores between SKMEL293 and C3 BRAF3-9. Genes selected showed a β score range > 0.5 (that is for a given gene, [βscore in C3 BRAF3-9] – [βscore in SKMEL293] > 0.5). False discovery rate <5% is represented as <0.05 in each cell. SAMM50 showed a different effect on each cell line (depleted in the SKMEL293, as shown in green; and enriched in the C3 BRAF3-9, as shown in pink, according to the βscore color code in the legend), and this was identified as an essential gene in the SKMEL293 cell line with a FDR ≤ 5%. Conversely, PPP6C was identified as having opposing effects, but enriched in the C3 BRAF3-9 cell line.

BAGEL analysis

The BAGEL tool recapitulated most of the essential hits previously identified in the SKMEL293 and C3 BRAF3-9 cell lines screens at day 8. The top 20 essential genes, ordered by BFs —a log Bayes factor where more positive scores indicate higher confidence that a given gene's knockout causes a decrease in cell fitness—, are listed in Table 13 for SKMEL293 cell line and in Table 14 for C3 BRAF3-9 cells. Once again, we observed genes related to proteasome (e.g., *PSMC6*, *PSMA5* or *PSMA3*), transcription (e.g., *POLR1B* or *POLR2L*) and splicing (e.g., *SMU1*, *SF3B3*) among the top fitness gene hits identified in the parental cell line (Table 13). On the other hand, in the resistant cell line we identified again *INTS6*, *PLK1* or *FBXO5*, among other essential genes (Table 14).

Gene	BF	Recall	Precision	FDR
SMU1	27.043	0.002	1.000	0.000
HSPA5	24.409	0.002	1.000	0.000
RAN	24.021	0.003	1.000	0.000
PSMC6	23.490	0.005	1.000	0.000
RPL12	23.196	0.006	1.000	0.000

Gene	BF	Recall	Precision	FDR
RRM1	22.759	0.008	1.000	0.000
PSMA5	21.516	0.009	1.000	0.000
PSMA3	21.174	0.011	1.000	0.000
WEE1	20.502	0.012	1.000	0.000
COPA	20.413	0.014	1.000	0.000
PDE1B	20.178	0.014	1.000	0.000
SF3B3	19.008	0.015	1.000	0.000
PLK1	18.951	0.017	1.000	0.000
POLR1B	18.626	0.019	1.000	0.000
POLR2L	18.350	0.020	1.000	0.000
SNRPD2	17.794	0.022	1.000	0.000
HMGCR	17.734	0.022	1.000	0.000
ETF1	17.322	0.022	1.000	0.000
NXF1	17.202	0.023	1.000	0.000
PSMB7	16.957	0.025	1.000	0.000

Table 13. Top fitness effect genes identified by the CRISPR-Cas9 knockout screen in SKMEL293 cells at day +8, calculated using BAGEL. BF, Bayes factor; FDR, false discovery rate.

Gene	BF	Recall	Precision	FDR
INTS6	38.664	0.000	1.000	0.000
PLK1	35.762	0.002	1.000	0.000
RPL12	34.491	0.003	1.000	0.000
NXF1	33.003	0.005	1.000	0.000
HSPA5	30.305	0.005	1.000	0.000
RAN	27.167	0.006	1.000	0.000
ETF1	25.748	0.006	1.000	0.000
RRM1	23.989	0.008	1.000	0.000
HMGCS1	23.592	0.008	1.000	0.000
FBXO5	23.206	0.008	1.000	0.000
RRM2	23.068	0.008	1.000	0.000
SF3B1	22.856	0.009	1.000	0.000
BORA	22.445	0.009	1.000	0.000
CCNA2	21.749	0.011	1.000	0.000
SF3B3	21.398	0.012	1.000	0.000
SOX10	21.160	0.012	1.000	0.000
MCL1	20.268	0.012	1.000	0.000
TPX2	20.178	0.014	1.000	0.000

Gene	BF	Recall	Precision	FDR
SMU1	19.453	0.015	1.000	0.000
CIB3	18.993	0.015	1.000	0.000

Table 14. Top fitness effect genes identified by the CRISPR-Cas9 knockout screen in C3 BRAF3-9 cells at day +8, calculated using BAGEL. BF, Bayes factor; FDR, false discovery rate.

The BAGEL analysis of the CRISPR-Cas9 knockout screen identified a total of 951 gene hits in the SKMEL293 cell line (BF range: 2.937-27.043) and 304 genes in the C3 BRAF3-9 (BF range: 4.89-38.664) with a FDR < 5% (Supplementary Table S5 contains the complete gene list) (Figure 39).

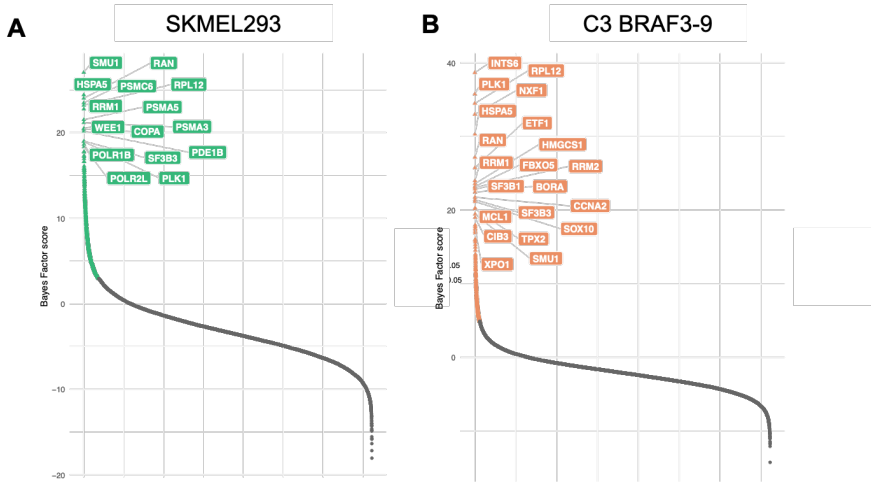

Figure 39. Top rank fitness gene hits of CRISPR-Cas9 knockout screens at day 8 in SKMEL293 (A) **and of C3 BRAF3-9** (B) **cell lines, calculated using BAGEL.** Rank plots represent Bayes Factor scores of gene hits. Genes represented in color —green for SKMEL293 (A) and orange for C3 BRAF3-9 (B) screens— correspond to fitness gene hits with FDR < 5%.

We observed a total of 164 common hits between the screens in the SKMEL293 and C3 BRAF3-9 cell lines at day 8 using BAGEL; and 137 hits that were identified as essential only in the resistant C3 BRAF3-9 cell line. The fitness gene hits list is shown in Table 15.

Gene ID	Gene Name	PANTHER Protein Class
BORA	BORA aurora kinase A activator	
CIB3	Calcium and integrin-binding family member 3	
PP1R15B	Protein phosphatase 1, regulatory subunit 15B	
TFAP2A	Transcription factor AP-2-alpha	general transcription factor
MAD2L1BP	MAD2L1-binding protein	
CRTC3	CREB-regulated transcription coactivator 3	transcription cofactor
AKIP1	A-kinase-interacting protein 1	
SKA1	Spindle and kinetochore-associated protein 1	
KATNB1	Katanin p80 WD40 repeat-containing subunit B1	
FAM124A	Protein FAM124A	
CCT8	T-complex protein 1 subunit theta	chaperonin
HSD17B6	17-beta-hydroxysteroid dehydrogenase type 6	dehydrogenase
CENPW	Centromere protein W	
SCL24A1	Solute carrier family 24	
MARC1	Mitochondrial amidoxime-reducing component 1	

Table 15. Essential genes with a FDR < 1% identified exclusively in C3 BRAF3-9 cells by the CRISPR knockout screen at day +8, using BAGEL. The essential gene hits are shown in decreasing order of BF magnitude.

Validation of hits

From the essential gene hits identified in our screen, we selected 20 hits for independent validation. This selection was made on the basis of the gene hits having a greater (or an exclusive) effect on the resistant C3 BRAF3-9 cell line (i.e., *INTS6* or *BORA*), but also including potential genes hits related to splicing (i.e., *PRPF8* or *SF3B1*) that could be particularly relevant for the generation of the alternative BRAF3-9 isoform.

We carried out knockdown using transfection of small interfering RNA (siRNA) pools (4 siRNAs/gene) at 40 nM in a C3 BRAF3-9 clonal population (clone #3) in triplicates. 72 hours after siRNA transfection, RNA was extracted, reverse transcribed using oligodT and the patterns of *BRAF* splicing analyzed by semi-quantitative PCR (Figure 40A). The target genes included: *SNRPB*, *SMU1*, *PRPF8*, *SF3B1*, *SNRNP200*, *INTS6*, *RRM1*, *RRM2*, *MCL1*, *XPO1*, *CDC5L*, *CLK3*, *SNW1*, *RBM39*, *RBM48*, *BORA*, *SNRPE*, *FBXO5*, *AURKA* and *NFX1*.

Quantification of the proportion of the BRAF transcripts showed that BRAF3-9 accounted for approximately 50% of BRAF transcripts across the different knockdowns and controls. Statistical analysis detected significant, albeit minor differences in the proportion of BRAF3-9 detected between the control non-targeting siRNA and siRNAs targeting the core splicing factor PRPF8 (56% *versus* 51%, p value 0.04), and between the control siRNA and knockdown of the Ribonucleotide Reductase Regulatory Subunit M2 (RRM2) (58% *versus* 51%, p value 0.0067) (Figure 40B). However, we acknowledge that, although statistically significant, these slight differences are unlikely to contribute in major ways to the generation of BRAF3-9 isoforms.

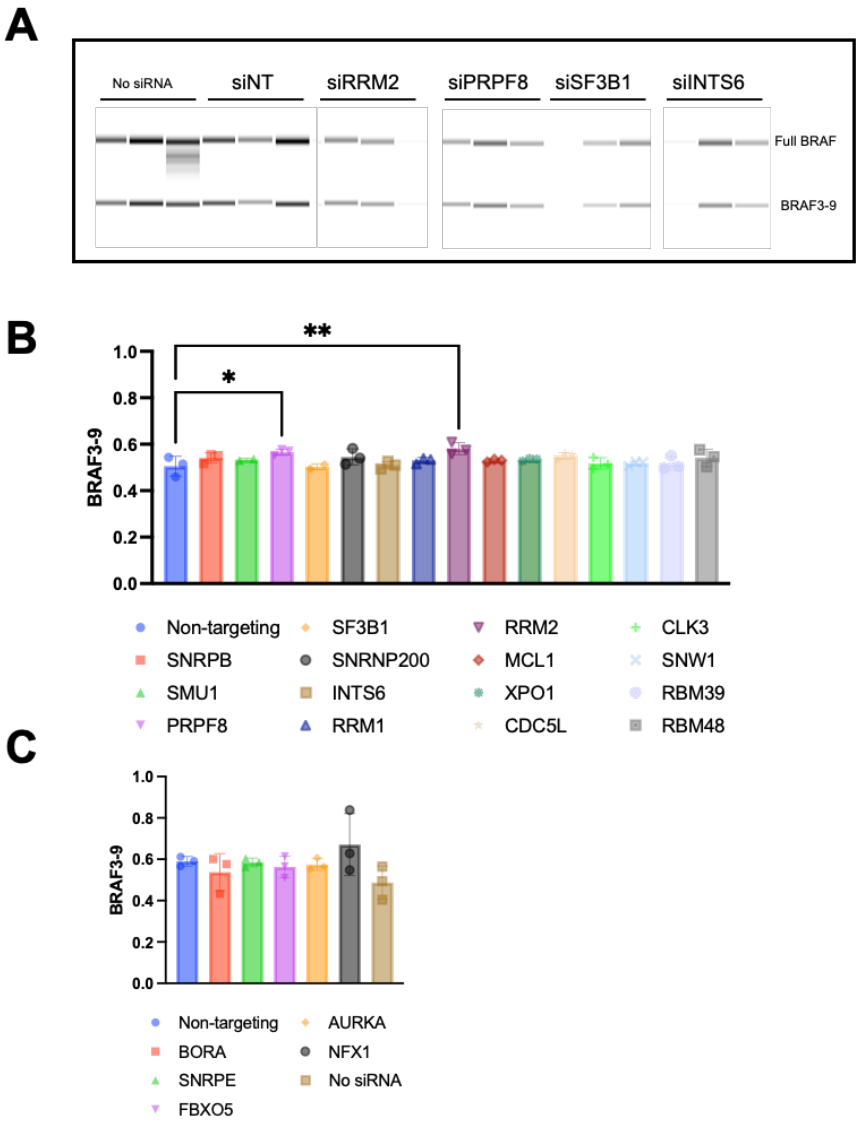

Figure 40. Knockdowns of selected essential gene hits and their effect on the proportion of BRAF 3-9 isoform in C3 BRAF3-9 cells. A| Some examples of RT-PCRs monitoring expression of BRAF full length and BRAF3-9 isoform from in knockdowns experiments using the non-targeting control (siNT), and siRNAs targeting RRM2, PRPF8, SF3B1 and INTS6. Experiments were carried out in biological triplicates. **B | and C |** Bar plots indicating the mean proportion of the BRAF3-9 isoform across the different knockdowns. One-way ANOVA was used for statistical analysis.

Therefore, we conclude that our CRISPR-Cas9 screen in two melanoma cells has identified a number of genes important for the proliferation and viability of these cell lines, including hits of particular relevance for survival of melanoma cells that rely on the production of the BRAF3-9 isoform for proliferation in the presence of vemurafenib at 10uM. However, our screen has not led to the clear identification of genes that are essential to promote the production of the pattern of splicing of the BRAF3-9 isoform.

3.6 PART VI: BRAF isoforms are generated due to allele-specific intragenic deletions

A number of results presented in this Thesis made us reconsider the possibility that genomic alterations could be behind the production of BRAF3-9 mRNA isoforms, and potentially other alternatively spliced isoforms related with the acquisition of resistance. First, we observed that alternative BRAF isoforms were always associated with the presence of the V600E mutation, i.e., various patterns of BRAF alternative splicing involving exons 1 to 11, associated with the acquisition of resistance to vemurafenib, were linked to the presence of a mutation in exon 15 that is necessary for BRAF susceptibility to the drug. This suggests that the decision to make resistance-associated isoforms is likely linked to allele-specific sequences rather than to cell-intrinsic properties of the splicing machinery of resistant cells.

Second, we were unable to recapitulate the postulated alternative splicing event induced by nucleotide differences in intron 8 -51 position, using a variety of minigene designs mimicking BRAF3-9 splicing decisions, nor to modulate the generation of the alternative BRAF3-9 isoform in endogenous transcripts through knockdowns of a variety of splicing factors, including some that were found important for viability of vemurafenib-resistant melanoma cells.

While genomic deletions of *BRAF* genomic sequences were ruled out in previous studies[340], we considered the possibility that cellular heterogeneity in the mechanisms of acquisition of resistance may

have hidden the presence of genomic deletions in a subpopulation of cells. This possibility seemed likely after we observed that, upon expansion of single clones from the "bulk" C3 BRAF3-9 cell line, while the majority of clones did not produce the BRAF3-9 isoform, in those which did the BRAF3-9 isoform represents approximately 50% of all BRAF transcripts, suggesting again production of alternatively spliced transcripts exclusively from one allele.

Therefore, we decided to revisit whether genomic rearrangements in the *BRAF* gene could be behind the generation of BRAF alternative isoforms.

3.6.1 WGS of "bulk" C3 BRAF3-9 cell line was compatible with an intragenic deletion in *BRAF*

First, we examined the coverage reads of the entire *BRAF* locus. We observed a slight but clear decrease in the reads aligned to the region within exons 3 and exon 9, which might be explained by an intragenic deletion affecting a subpopulation of cells (Figure 41).

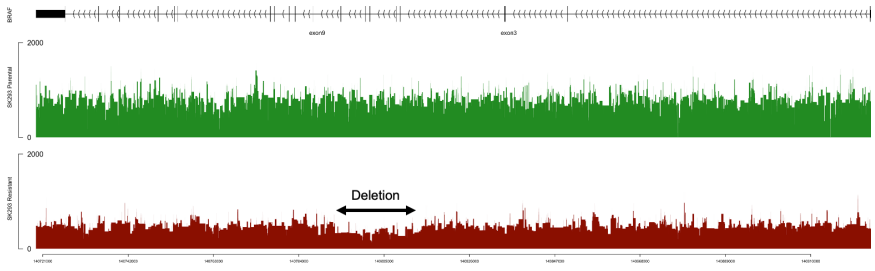

Figure 41. Coverage plot of BRAF genomic reads from WGS analyses of SKMEL293 parental (green) **and SKMEL293-C3 "bulk" resistant** (red) **cell lines.** The double arrow indicates the region displaying a drop in the number of

reads in the C3 resistant cell line, consistent with an intragenic deletion between introns 3 and 8 affecting a subset of the cells in the cell line population.

Then, we made a close-up examination of aligned reads across these regions within the *BRAF* locus (Figures 42 and 43). Intriguingly, we observed a clear drop in the coverage track spanning from a region in intron 3 and a region in intron 8 in the C3 BRAF3-9 sample (Figures 42B and 43B). These drops were not detected in the parental SKMEL293 cell line (Figure 42A and 43A) and were accompanied by reads that aligned partially to the reference sequence, and that were in fact spanning sequences from these two introns, consistent with the possibility of the presence of a genomic deletion occurring between intron 3 and intron 8. The 5' breakpoint was located 20,091 nucleotides downstream of the 5'SS of intron 3 and the 3' breakpoint at 5,219 nucleotides upstream the 3'SS of intron 8 (Figure 44).

We confirmed the presence of an intragenic deletion of 21,714 nucleotides by detecting the amplification of a PCR product from genomic DNA of the C3 BRAF3-9 cell line, which upon Sanger sequencing confirmed the presence of the mentioned intragenic deletion (Figure 44).

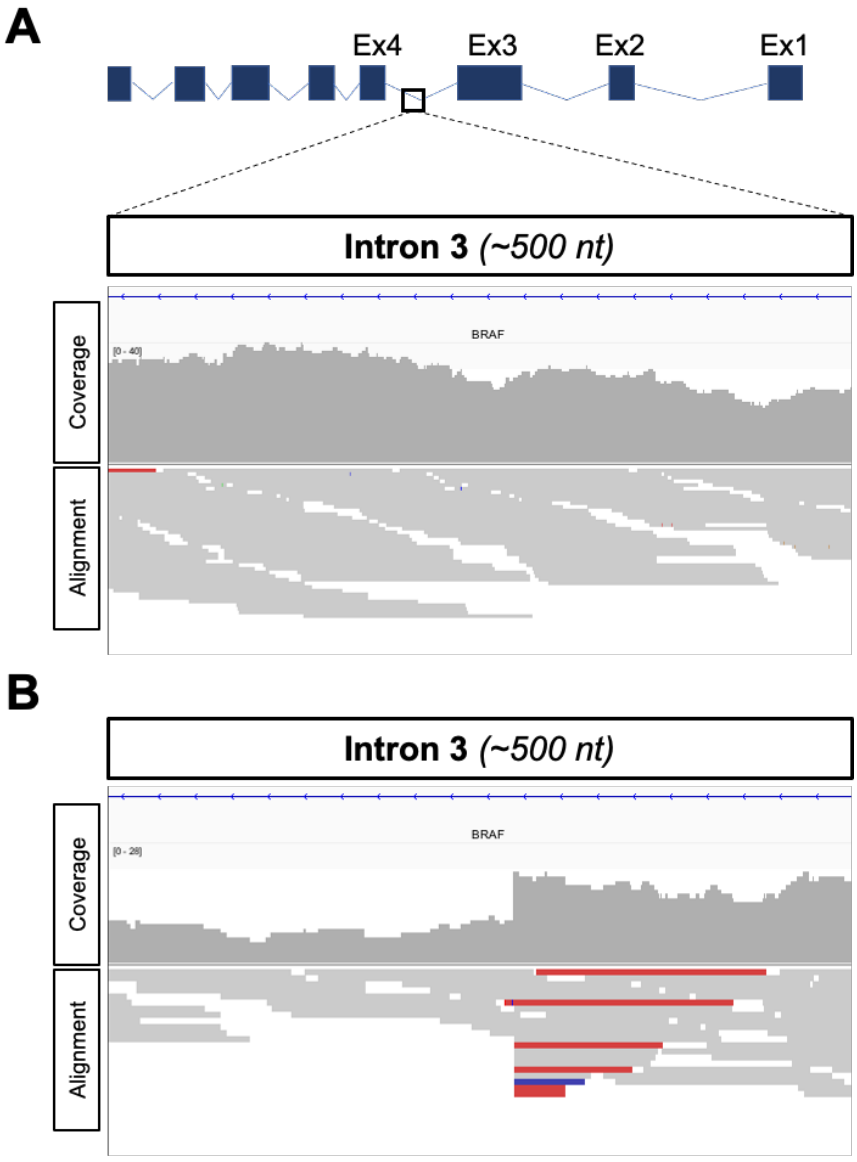

Figure 42. Intragenic deletion of BRAF revealed by WGS of C3 BRAF3-9 cell line (intron 3). Snapshots of IGV (Integrative Genomics Viewer) using sequencing reads from WGS of parental SKMEL293 cell line (A) and the C3 BRAF3-9 cell line (B) in the intron 3 region. Schematic representation of partial *BRAF* gene locus (in the negative strand) indicating the region of intron 3 displayed with IGV. Red alignments indicate reads compatible with the presence of a genomic deletion. Coverage track of C3 BRAF3-9 reads illustrate a sharp decrease in read density after the breakpoint of intron 3.

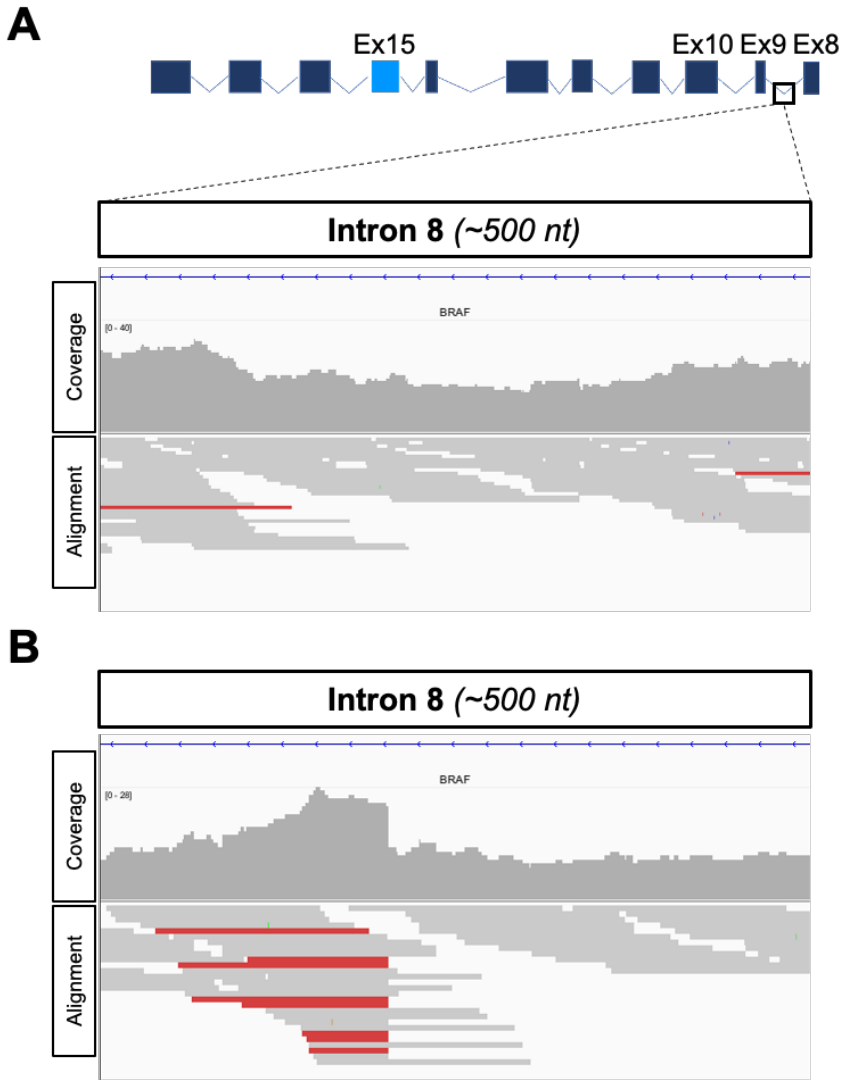

Figure 43. Intragenic deletion of BRAF revealed by WGS of C3 BRAF3-9 cell line (intron 8). Snapshots of IGV (Integrative Genomics Viewer) using sequencing reads from WGS of parental SKMEL293 cell line (A) and the C3 BRAF3-9 cell line (B) in the intron 8 region. Schematic representation of partial *BRAF* gene locus (in the negative strand) indicating the region of intron 8 displayed with IGV. Red alignments indicate reads compatible with the presence of a genomic deletion. Coverage track of C3 BRAF3-9 reads illustrate a sharp decrease in read density before the breakpoint of intron 8.

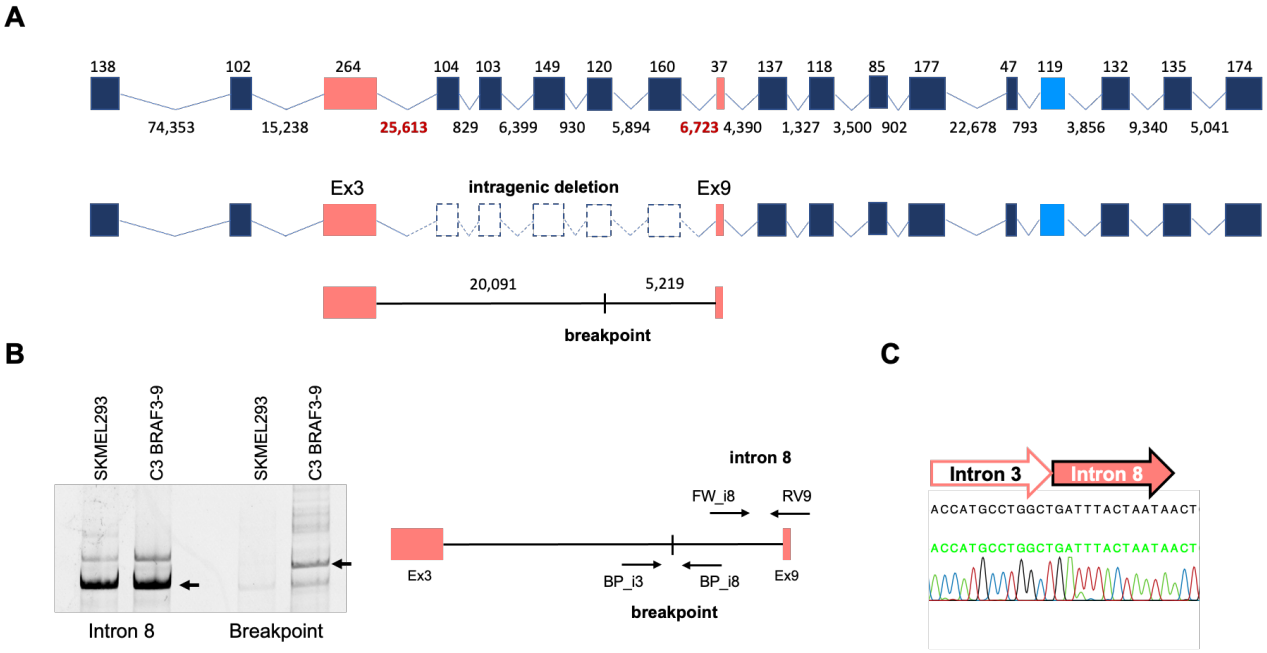

Figure 44. Schematic representation and detection of the BRAF intragenic deletion and breakpoints in introns 3 and 8 determined by PCR from genomic DNA of the C3 BRAF3-9 cell line. A| Schematic representation of the genomic length and structure the *BRAF* gene and representation of the intragenic deletion and the *de novo* generated intron and its breakpoint. **B |** PCR using genomic DNA extracted from SKMEL293 and C3 BRAF3-9 cell lines using primers spanning the breakpoint identified by WGS (BP_i3, BP_i8) and primers for the detection of intron 8 as a control. Arrows indicate the expected position of each amplification product. A schematic representation of primer pairs design is shown. **C |** Sanger sequencing of the PCR amplification product in B (left panel) confirmed the presence of an intragenic deletion between intron 3 and intron 8.

3.6.2 Production of the BRAF1-9 isoform in the SKMEL94AR cell line is also due to an allele-specific genomic deletion

After identifying the mechanism behind the generation of BRAF3-9 in the C3 melanoma cell line, we aimed to test whether a genomic rearrangement within BRAF is also responsible for the production of other transcript isoform and chose BRAF1-9 as another case study. For this purpose, we performed WGS of the SKMEL94AR cell line, a cell line that expresses the BRAF1-9 mRNA isoform and was generated by us from the SKMEL94 cell line after a 4-week treatment with 1 μM vemurafenib. Although the cell line was not clonal, the BRAF1-9 mRNA isoform was expressed at approximately 50% of all BRAF transcripts.

The examination of aligned reads across the *BRAF* locus demonstrated a drop in the coverage track in a region spanning from intron 1 to intron 8, that was accompanied by reads spanning the flanking sequences in these introns and displaying neat breakpoints. These results again suggested the presence of an intragenic deletion as responsible for the production of BRAF1-9 mRNA (Figure 45). The 5' breakpoint was located 56,695 base pairs downstream of the 5'SS of intron 1 and the 3' breakpoint was located 710 base pairs upstream the 3'SS of intron 8 (Figure 46). Interestingly, while BRAF1-9 and BRAF3-9 share deletion of intron 8, the exact location of the breakpoints was different for each of them.

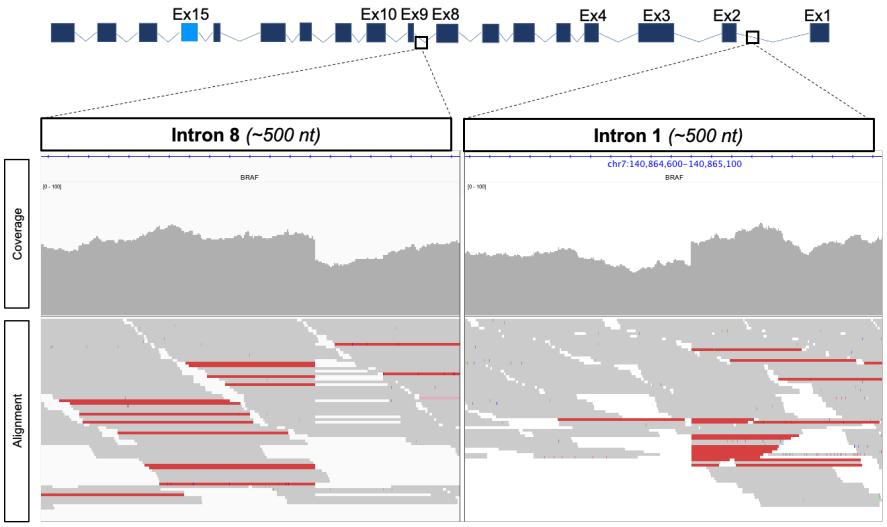

Figure 45. Intragenic deletion of BRAF revealed by WGS of SKMEL94AR cell line (intron 1 and 8). Snapshots of IGV (Integrative Genomics Viewer) using sequencing reads from WGS of parental SKMEL94AR cell line, which displays the BRAF1-9 isoform. Schematic representation of *BRAF* gene locus (in the negative strand) indicating the region of intron 1 and intron 8 displayed with IGV. Red alignments indicate reads compatible with the presence of a genomic deletion. Coverage track of C3 BRAF3-9 reads illustrate a sharp decrease in read density after the breakpoint of intron 3.

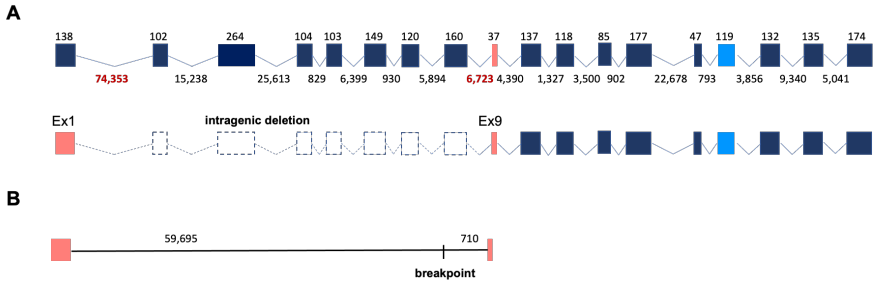

Figure 46. Schematic representation of the *BRAF* intragenic deletion and breakpoints in introns1 and 8 determined by WGS from genomic DNA of the SKMEL94AR cell line. Schematic representation of the genomic length and structure the *BRAF* gene and representation of the intragenic deletion (A) and the *de novo* generated intron and its breakpoint (B).

In this Part VI, we provide conclusive evidence that generation of the BRAF3-9 mRNA isoform in the C3 BRAF3-9 melanoma cell line is due to a genomic deletion of over 21 Kb spanning from intron 3 to

intron 8 and therefore it is not the result of an alternative splice site choice decision involving competing 5' and 3' splice sites in introns 3 and 8. Likewise, WGS of gDNA from the SKMEL94AR cell line, which harbors the BRAF1-9 isoform, also demonstrated the presence of a large intragenic deletion of more than 75 Kb from intron 1 to intron 8. Therefore, genomic rearrangements within *BRAF* are most likely the mechanism underlying the generation of resistance-associated BRAF mRNA isoforms.

4 DISCUSSION

The acquisition of resistance to cancer therapies remains one of the most important hurdles for the long-term success of cancer treatments[408,409]. A better knowledge of the mechanisms of resistance to cancer therapies, together with an understanding of the underlying biological process leading to them, can ultimately materialize in the development of novel drugs or different approaches to cancer treatment. Although this thesis has been focused on melanoma, activating mutations in BRAF —among which the most common is V600E— have also been described across a variety of other tumor types[211]. While for some of them, such as NSCLC, thyroid or colorectal cancer, MAPK inhibitors (MAPKi) —namely BRAF and MEK inhibitors— have been recently included in their therapeutic armamentarium[327–329], melanoma is by far the tumor type in which resistance to these inhibitors has been investigated in greater depth. Nevertheless, recent studies hint that the spectrum of the resistance mechanism to MAPKi overlaps with those described in melanoma[360–362] —including the generation of aberrant BRAF alternatively spliced mRNA isoforms[363]—, and thus the findings of this thesis may be extrapolated in the future to other tumor types.

In 2011, alternative splicing of *BRAF* primary transcripts was described for the first time as a mechanism of resistance to BRAFi[340]. After *in vitro* exposure to vemurafenib, *BRAF*-mutant melanoma cell lines became resistant through the generation of BRAF3-9, an aberrantly spliced isoform of BRAF lacking exons 4 to 8 (and thus, lacking the RAS-binding domain of the protein). These shortened isoforms were more prone to dimerization and, leading to

reactivation of the MAPK pathway. Moreover, not only was alternative splicing of BRAF also observed in human tumors resistant to vemurafenib, but also a variety of alternatively spliced variants of BRAF were identified, such as BRAF3-11, BRAF2-11, BRAF1-9, or BRAF1-11[340,352,351,347,333,355]. In the following years, growing evidence pointed to alternative splicing of BRAF as one of the key mechanisms of resistance to BRAFi ± MEKi. At the same time, alternative splicing of BRAF was thereafter considered a paradigmatic example of how splicing plays an important role at different stages of cancer biology, including the development of resistance to therapies[74,35].

Initial, and apparently successful, efforts were made to mechanistically explain the generation of BRAF3-9 mRNA isoforms (discussed below, together with our results) and even to modulate splicing as a viable therapeutic strategy to re-sensitize cells to BRAFi[358]. However, major questions remained open, in particular regarding the identification of a common molecular mechanism behind the generation of a diverse subset of BRAF mRNA isoforms associated with the acquisition of resistance to vemurafenib, and also how to translate this knowledge into patient care —including, for instance, robust *in vitro* evidence that drugs targeting the splicing process warrant clinical investigation.

Based on these foundations, the objectives of this thesis were to document the frequency with which alternative splicing of BRAF emerges in larger subsets of melanoma samples and, at the same time, to unravel the underlying mechanism behind the generation of these

alternatively spliced variants of BRAF, potentially leading to the development of novel therapeutic strategies.

Our transcriptomic landscape outlines unique features of BRAF alternative splicing

In this thesis, we described in detail the distribution of exon-exon junctions (EEJ) along the BRAF transcripts. VAST-TOOLS[64,378], a toolset for profiling alternative splicing events, was used to analyze RNA-seq data from 2 different datasets: a custom dataset with melanoma samples from tumors and cell lines —some of which had previously received BRAFi±MEKi— and, the SKCM (Skin Cutaneous Melanoma) dataset from the TCGA (The Cancer Genome Atlas) project.

However, we must acknowledge two major limitations in our dataset design: the quality of the RNA-seq data and an insufficiently enriched population. First, there was a considerable heterogeneity across samples in our custom dataset, not only related to the sample origin (tumor or cell line) but also regarding sequencing features such as the wide variety of the read lengths (ranging from 48 to 200 base pairs), the inclusion of both types of reads (paired- and single-end reads) as well as variable coverage of BRAF across the samples. We expected to solve this problem using the SKCM TCGA dataset; but unfortunately, a homogeneous but short read length of 49-nt is likely insufficient for an optimal detection of EEJ reads. Furthermore, although 30.7% of samples from our custom dataset were labelled as MAPKi-resistant, eligible patients participating in the SKCM TCGA

dataset were MAPKi-naïve, as they received no previous systemic therapy, thus, preventing us from assessing the acquisition of resistance in this dataset. It is nevertheless uncertain the extent to which an enriched dataset with a greater number of samples previously exposed to MAPKi, together with more homogenous and high-quality sequencing reads, would have increased the observed frequency of our EEJs of interest.

Nevertheless, with our pipeline, we were able to detect 2 different alternative EEJs that had been previously related to MAPKi-resistance: BRAF3-9 and BRAF1-11 isoforms. We confirmed the presence of these alternative EEJ in samples in which they had been previously reported, both in cell lines such as the M397AR that harbors BRAF1-11, and in patients' tumors such as those included in the analysis published by Hugo *et al*[333]. All these cases, together with another *BRAF*-mutant melanoma cell line treated with MAPKi, belonged to *BRAF*-mutant and MAPKi resistant group.

Previous publications[339,340,347,351,355,353,356] concluded that the BRAF variants generated through alternative splicing were always produced in response to BRAF/MEK targeted therapies, a conclusion supported by matched samples analyses (prior to therapy and at relapse). Likewise, the fact that only patients with (activating) BRAF V600E/K/R received treatment with MAPKi, together with the observation that alternatively spliced variants of BRAF were associated with the presence of the *BRAF*-mutation (usually V600E), led to the general assumption that alternative splicing of BRAF only occurred in the presence of activating *BRAF*-mutations. In contrast, we have been able to also detect alternatively spliced isoforms of

BRAF in 5 treatment-naïve tumor samples from patients: 3 BRAF-wild type melanomas expressing BRAF1-11 and 2 $BRAF^{K601}$ melanomas expressing BRAF3-9. Yet, in line with previous publications, we were not able to detect the alternative EEJ in parental matched sample (when available) of the resistant samples, for instance in the parental cell line M397 or in patients' samples from Hugo *et al*[333].

In view of this striking finding 2 main questions arise. First, what is the effect of expressing an alternatively spliced $BRAF^{V600}$ isoform on the melanoma cell? While it is known that mutant *BRAF* variants can reactivate the MAPK pathway due to an increased tendency to dimerization, the activation state of the MAPK pathway in alternatively spliced, wild-type BRAF melanoma remains unclear. And, on the other hand, another key question is the timing of emergence of these BRAF isoforms in *BRAF*-mutant and wild type *BRAF* melanoma. Our findings suggest that BRAFi±MEKi exposure may not be as indispensable for the generation of BRAF variants as previously thought —BRAF isoforms were only expressed after acquisition of MAPKi resistance—. A possible scenario would be that MAPKi trigger the generation of a BRAF rearrangement by an unknown molecular mechanism. Other possible scenario would be that a BRAF rearrangement occurred early during tumor evolution, and MAPKi *simply* exert a selective pressure that favors the accumulation of BRAF mRNA isoforms, especially if the allele harboring the activating *BRAF*-mutation, which is the protein on which resistance to vemurafenib can confer a survival advantage.

Profiling BRAF mRNA isoforms in in vitro models of BRAF alternative splicing does not support an overall splicing perturbation as the main cause of BRAF alternative splicing

We first built a collection of paired *BRAF*-mutant melanoma cell lines, kindly provided by different labs. This collection consisted of parental cell lines and their resistant sublines isolated after exposure to BRAFi. These resistant cell lines were of particular interest because resistance was associated with the generation of *BRAF* alternatively spliced mRNA isoforms. The cell lines included parental SKMEL293 and resistant SKMEL293-C3 (BRAF3-9), M397 and M397AR (BRAF1-11) and 1205Lu and its 2 resistant sublines, PRT#3 (BRAF2-11) and PRT#4 (BRAF1-9). While the resistant lines in C3 and M397AR were generated *in vitro*, the PRT#3 and #4 cell lines were established after inoculating the 1205Lu cell line in mice, from xenografts tumors relapsing after BRAFi treatment.

As a starting point, we systematically performed RT-PCR analyses with primers designed for the detection of each specific alternative BRAF EEJ, as well as with primers spanning from exon 1 until exon 11 to detect any other possible *BRAF* isoforms. As expected, we unequivocally recognized every predicted specific *BRAF* isoform for each resistant cell line. Besides, whereas each parental cell line exclusively displayed the full *BRAF* isoform, the resistant cell lines harbored both the full *BRAF* and the alternatively spliced variant, in line with previous publications. Our RT-PCR analyses did not detect other alternatively spliced isoforms in each of the samples, arguing against the hypothesis a general mis-regulation of splicing is behind

the generation of *BRAF* alternatively spliced isoforms, but rather that, once settled, each cell line kept generating one specific alternative splicing variant of BRAF in an exclusive and consistent manner.

Furthermore, we also sought to reproduce the *in vitro* acquisition of resistance in the provided cell lines. Among our resistant sublines, 6-12% of them displayed *BRAF* alternative splicing, which is a lower rate compared with to estimated 20-30% of patients relapsing after BRAFi that harbored a BRAF spicing variant[355]. Because we treated parental cell lines for 3, 4 and 6 weeks in our experiments, we cannot rule out that a longer exposure (more alike to the clinical scenario) might have increased the frequency at which we would have detected alternatively spliced BRAF variants. There is however no consensus about the exposure time to a given drug which is required for a cell line to develop resistance (e.g., previous studies about BRAFi resistance in melanoma reported an exposure times of 2 and 6 months[384,340]) nor about the drug dosage and schedule (e.g., increasing concentrations, higher concentrations than estimated *in vivo*). In addition, the relation between the emergence of BRAF isoforms and time to clinical failure to BRAFi±MEKi is not known either.

On the other hand, these results are consistent with the prevailing idea that a variety of mechanisms can contribute to the acquisition of resistance, as well as evidence that different mechanisms of resistance can operate in different metastases from the same patient[347,333,355]. Remarkably, despite the low numbers observed, each parental cell line developed the same *BRAF* mRNA isoform that had been reported previously for that cell line: SKMEL293 originated

BRAF3-9 and M397 originated BRAF1-11. This *predetermination* of the alternatively spliced *BRAF* variant could be due either to distinct properties of the cellular machineries of the different cell lines (allowing only —or preferably— the generation of particular isoforms) or, more likely, due to selection by the drug of pre-existent cells in the culture that expressed the alternatively spliced isoform. However, the fact that *BRAF* isoforms are not identified prior to MAPKi in matched samples argues against the hypothesis of a clonal selection upon drug exposure, unless there is a technical limitation to detect such low levels of alternative BRAF isoform expression (from very few cells in a population prior to BRAFi).

Concurrently, we established a new biological model for the study of BRAF isoforms in vemurafenib-resistant melanoma. The SKMEL94AR subline was derived from the SKMEL94 cell line —a *BRAF*-mutant melanoma cell line, in which resistance mechanisms were not studied previously and expressed no BRAF isoforms— after 4 weeks exposure to 1 μM vemurafenib. This resistant subline harbored the BRAF1-9 mRNA isoform and displayed lower sensitivity to vemurafenib compared to its parental counterpart. While BRAF1-9 isoform was identified as a resistance-associated BRAF isoform in patient samples and other cell lines in previous reports, this was the first report that a SKMEL94 subline can acquire resistance through the expression of the BRAF1-9 isoform.

Contrary to previous reports, intron 8 mutations are not responsible for the generation of BRAF3-9 isoforms

An intronic mutation -51 nucleotides upstream of the 3' splice site (SS) of intron 8 was identified in the resistant cell line C3 BRAF3-9[358]. Through minigene-based experiments, this mutation was shown to promote the accumulation of the BRAF3-9 isoform. Moreover, this study showed that splicing modulators (such as spliceostatin A or meayamycin B) caused not only a significant decrease of the BRAF3-9 isoform relative to full length transcripts but also a re-sensitization to vemurafenib[358].

Inspired on these captivating results, we hypothesized that a common molecular mechanism might underly the generation of the various mRNA isoforms of BRAF. To start addressing this, we aimed to recapitulate the observation of the effects of the -51 mutation using minigenes. In our first approach, we designed a simple minigene, in which the 3 exons involved in the decision (namely, exons 3, 4 and 9) flanked by reduced size / chimeric introns, containing 250 nucleotides from each splice site. In contrast with the design of Salton *et al*[358], we did not include reporter sequences (e.g. fluorochromes such as GFP or Strawberry), to avoid interference of external sequences that might alter splicing regulation. We generated versions of this minigene wild type or mutated at position -51. As transfection of this minigene in different cell lines —including HEK293, and melanoma cell lines SKMEL293 and the resistant subline C3, that endogenously produce BRAF3-9— did not recapitulate the effects of the -51 mutation on the accumulation of BRAF3-9 mRNA isoform, our minigene designs were stepwise modified to generate over 3 additional designs —such as MG349, MG389, MG3489—, but none of them showed any effect of the nature of nucleotide at the -51

position on splicing of the minigene. Moreover, the effects of different nucleotides at the -435 position upstream to the 3'SS in intron 8 were also tested, along with the different versions of position -51, with the same result. Meanwhile, we ruled out another possible hypothesis, i.e., that splicing between exons 3 and 4 regenerates a 5'SS that could then be used for splicing to the 3'SS of intron 9.

Given our inability to reproduce the published results using our minigene designs, we kindly requested the reporter minigene used in the mentioned publication. We were however unable to recapitulate the effects of the intron 8 -51 mutation on the production of the alternatively spliced event mimicking BRAF3-9 mRNA production.

Although our results were clearly disappointing, they were consistent with data published by Pupo *et al*[388] few years after the discovery of the -51 mutation. In this publication, 3 melanoma samples from patients with acquired resistance to BRAFi through the production of BRAF3-9 mRNA isoform were not associated with the presence of the -51nt intronic mutation. Therefore, the hypothesis that mutation of intron 8 position -51 is associated with the production of BRAF3-9 mRNA was restricted to the melanoma cell line SKMEL293 C3.

To investigate the contribution of additional genomic sequences, whole-genome sequencing (WGS) was performed with the parental SKMEL293 cell line as well as with its resistant subline SKMEL293-C3. Aside from the expected single-nucleotide variants (SNV) — namely, the T1799A mutation corresponding to the V600E and the C>G substitution located at the -51-nucleotide upstream the 3'SS of intron 8—, only 2 intronic SNVs were found to differ between the 2

samples. These intronic SNVs —in intron 16 and in intron 5 in the parental and resistant cell line, respectively— are at considerably distances from the competing splice sites, separated from them by other intervening splice sites and therefore do not immediately suggest a mechanism by which they might be involved in the generation of the BRAF3-9 mRNA isoform.

Taking into account our findings using minigene assays and the analysis of WGS, we consider the contribution of intronic mutations to the generation of the alternative isoform BRAF3-9 highly unlikely, despite the exciting previously published results which were unfortunately unable to reproduce.

Single-cell clonal expansion analyses revealed heterogeneity of the resistant SKMEL293-C3 cell line and confirmed co-occurrence of V600E and alternative isoforms in BRAF

To decipher whether cells of the SKMEL293 C3 cell line generate full length and BRAF3-9 isoforms in uniform or variable proportions, we analyzed single-cell derived clones.

Our results clearly showed that the SKMEL293-C3 cell line was composed of approximately 20% of cells that express the BRAF3-9 isoforms, the remaining 80% of the cells were also resistant but did not express BRAF3-9, and therefore resistance arose in these cells through a mechanism unrelated to the generation of BRAF3-9. We cannot exclude, however, that cells harboring BRAF3-9 survived or grew worse than the rest of the cells during the single-cell cloning

process and therefore that the proportion of cells expressing BRAF3-9 in the "bulk" culture is actually higher than 20% (but see below).

Moreover, our results showed that clonal sublines from SKMEL293-C3 expressing the BRAF3-9 isoform produce approximately 50% of each transcript. This finding is in line with our observation that all BRAF3-9 transcripts were $BRAF^{V600E}$ —and, conversely, all full BRAF transcripts were $BRAF^{V600}$—, also consistent with the fact that the V600E mutation is heterozygous. Thereafter, taking advantage of other resistant cell lines harboring different alternative isoforms of BRAF, we verified the co-occurrence of V600E and *BRAF* alternative splicing, suggesting that the production of alternatively spliced transcripts occurs always in transcripts derived from the V600E mutated allele.

However, the presence of the V600E mutation is not always associated with the production of BRAF alternative splicing isoforms, given the fact that $BRAF^{V600E}$ cells with no alternative isoforms exist. In addition, our analysis of RNA-seq data demonstrated that we could also detect reads spanning these alternative EEJ in samples without V600E (or other activating BRAF mutations).

Two main observations pushed us to consider the contribution of other genomic factors: the consistency in the isoform produced by different cell lines, and the stability and coherence between expression of *BRAF* isoforms and the presence of the V600E mutation. An allele-specific splicing event (in the absence of any alteration of nearby *cis*-elements) would be extremely extraordinary

in the absence of other contributing factors such as genomic aberrations or changes in the spatial conformation of the DNA during transcription.

Genome-wide CRISPR knockout screens uncover early vulnerabilities related to splicing and chromosome dynamics, but no evidence of modulation of BRAF3-9 mRNA isoform production

With the aim of identifying *trans*-acting factors contributing to BRAF3-9 isoform production, we performed a genome wide CRISPR knockout screening.

This high throughput, "forward genetics" approach has been widely used to discover genetic vulnerabilities of a specific phenotype. An example of successful application of this methodology is the identification of RBM39 as a crucial RNA binding protein (RBP) for survival and RNA splicing in acute myeloid leukemia[399].

With the intention of optimizing the outcomes of the screening, we decided to sequence data generated after 8 days of induction of CRISPR-Cas9-mediated genome editing and to treat resistant cells with 10x higher concentration of vemurafenib (around the calculated IC50), compared to usual concentration of growth media for resistant sublines. Both measures were applied to avoid the emergence of a different mechanism of resistance as an adaptative response to the induced genetic stress in the presence of vemurafenib, while at the same time to try to capture those genes with an immediate and stronger effect in the cell viability. Having said that, we recognize that the analysis of later time points might have provided more robust information regarding the essentiality of determined genes, not yet

enriched at such earlier time point. This is reflected in the precision-recall curves calculated with BAGEL, where better performances are obtained at later time points.

Also regarding the design, we overestimated the potential value of including in the screen the resistant "bulk" C3 cell line, which we conceived as a way to better compare vulnerabilities induced by dependance on the expression of the BRAF3-9 isoform (clonal C3 line) and dependances caused by other molecular mechanisms present in the "bulk" C3 cell line population. Unfortunately, the resistant "bulk" C3 screening was not informative at all, which may be due to the very same heterogeneity factor that we wanted to take advantage of, i.e., the variety of mechanisms underlying resistance in this cell line made it very difficult to obtain robust results for any particular set of sgRNAs / targets. Whether, also in this case, a longer time point might have helped in elucidating hits, remains unclear.

Despite the design caveats mentioned above, a considerable number of essential hits were identified with the different bioinformatic tools used. Importantly, most of them were recapitulated across the different tools, although their position in the gene rank occasionally varied. Notably, the functional enrichment analysis of the essential genes argued that splicing-related and chromosome dynamics-related processes were particularly important for survival/proliferation of the C3 BRAF3-9 cell line.

Focused on factors that might regulate the production of the BRAF3-9 via splicing, we selected top essential genes with known functions in the regulation of splicing. However, the results of the validation

assays through individual knockdowns of 20 genes did not succeed in modulating the splicing of BRAF, as shown by the rather uniform ratios between the BRAF3-9 and full isoform. We cannot rule out, however, that in none of these instances we achieved enough levels of protein depletion or decreased activity (which we have not independently determined) as to recapitulate the effects of the knockout achieved in the screen by CRISPR-Cas9 genome editing. It is worth mentioning that the measured outcome of the screen (sgRNA depletion or enrichment, secondary to cell viability) and of our validations (proportion of BRAF3-9 mRNA isoform) are distinct. Yet, we expected that the proportion of BRAF3-9 mRNA would be a surrogate marker with an impact on cell viability, in agreement with our results confirming that an siRNA against the EEJ 3-9 decreased colony formation capacity and increased vemurafenib sensitivity.

At least 2 previous publications have reported essential gene hits in BRAF-mutant melanoma. However, differences in the design and objectives make these screens hard to compare between them. Shalem *et al*[393] screened the *BRAF*-mutant melanoma cell line A375 after transducing the GeCKO sgRNA library with the aim to identify genes involved in the acquisition of vemurafenib resistance, without taking into account any resistance mechanism in particular. For this purpose, vehicle-treated *vs* vemurafenib-treated A375 cells were compared at day 7 and 14.On the other hand, Li *et al*[400] screened a resistant *BRAF*-mutant melanoma cell line (M238R1), whose resistance mechanism was unknown, although BRAF alterations such as alternative splicing or mutations were rule out. In that case, a custom-made sgRNA library, containing 6000 cancer-related genes

was transduced, and the cells were treated with DMSO or 1 μM vemurafenib until day 14. Despite the mentioned heterogeneity in methods and design, cell-cycle genes (e.g., *CDK6*, *CCND1*) are identified as essential across experiments, including ours. The different experimental conditions (for instance, Shalem *et al* screened parental cells under vemurafenib) and the different resistant mechanisms (e.g., M238R1 does not harbor BRAF isoforms) can explain the absence of other common essential hits between the screens.

Despite our original focus on identifying genes involved in the generation of BRAF3-9, data from our CRISPR knockout screen can likely be of great value. Remarkably, the identification of splicing-related genes as essential genes in C3 BRAF3-9, albeit not involved in the production of BRAF3-9 splicing, may reveal a general mis-regulation of splicing relevant for tumor progression or aggressiveness. On the other hand, we also identified as essential a subset of essential genes involved in spindle assembly and chromosome segregation, some of which may contribute to BRAF genomic rearrangements as an indirect consequence of chromosome mis-segregation processes (see below).

A large intragenic deletion can explain the mechanism of the generation of alternative BRAF isoforms

The collective results discussed above increasingly forced us to reconsider the potential contribution of genomic alterations in the generation of *BRAF* mRNA isoforms. Previous genomic

characterization of the parental SKMEL293 and SKMEL293-C3 resistant cell lines ruled our genomic alterations, based on results of Comparative Genome Hybridization (CGH) analyses[340]. Given the relatively limited quantitative resolution of this technique, we decided to search for genomic alterations in WGS data from the SKMEL293 and the resistant "bulk" C3 cell lines. Although the tools designed for SNV calling are typically suboptimal to detect large genomic rearrangements, we observed a slight decrease in the number of reads aligned in the coverage track in a large region between introns 3 and 8. While in a clonal C3 BRAF3-9 cell line a drop in the coverage of at least 50% should have been noticeable the heterogeneity of the "bulk" SKMEL293-C3 cell line led to a decrease of only approximately 30% of the total surrounding number of reads.

Our subsequent findings are consistent with a large intragenic deletion, from intron 3 to intron 8, being behind the generation of the BRAF3-9 isoform in this cell line model. This means that the generation of this isoform is not the consequence of a choice between alternative splice sites in competition but rather the natural consequence of the absence of all intervening annotated splice sites between the 5'SS of intron 3 and the 3'SS of intron 8 that consequently undergo "canonical" splicing. Moreover, we extend our findings to the SKMEL94AR cell line, which expresses the BRAF1-9 isoform, and for which WGS revealed a large intragenic deletion, this time from intron 1 to intron 8, as likely responsible for the production of BRAF1-9 mRNA isoform.

After the first publication describing the BRAF alternative splicing did not report an intragenic somatic deletion within the *BRAF* gene

(by array CGH[340]), every article exploring resistance mechanisms that detected any alternative isoform of BRAF used whole-exome sequencing[339,347,355,356], by RT-PCR[347,348,351,355,357,411] and/or RNA sequencing[333,363]. Since these methods ignore intronic regions, the intragenic deletion has been systematically neglected.

Recently, whole-genome sequencing studies have shed light on the genomic alterations of BRAF, consisting mainly of fusions, kinase duplications and deletions. Indeed, among all kinases, BRAF fusions are one of the most common across different tumor types[290]. Fusions containing the BRAF kinase domain have been described in several tumor types[365], such as pilocytic astrocytoma[364], non-small-cell lung cancer (NSCLC)[375] and melanoma[366,368,369,412,413]. BRAF fusions have been also related to resistance to therapies; in particular, Kulkarni *et al*[370] identified an *AGAP3-BRAF* fusion gene in a vemurafenib-resistant tumor.

Somatic deletions in BRAF have been described also in different tumor types, including melanoma, NSCLC, prostate cancer, colorectal cancer and bladder cancer[290,375]. These deletions consisted of multiexonic deletions that encompassed exons 1 to 11 in different combinations (Figure 47). At the transcriptomic level, some of these deletions clearly mimicked what was previously described as alternatively spliced variants of BRAF.

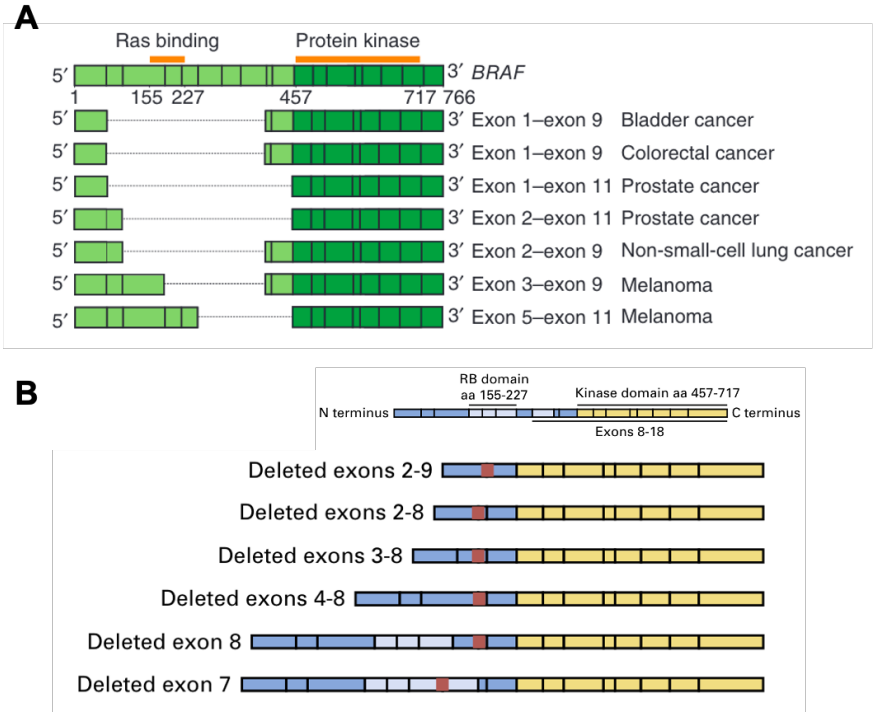

Figure 47. Schematic representations of reported BRAF deletions. A | *BRAF* deletions across different tumor types from the MSK-IMPACT dataset (adapted from Zehir *et al*[290]). **B |** *BRAF* deletions in non-small-cell lung cancer (adapted from Sheikine *et al*[375]).

Moreover, three case reports have associated BRAF deletions to resistance to MAPKi. Tung *et al*[374] identified a BRAF deletion from exon 2 to exon 10 (then, producing the BRAF1-11 isoform) in a patient with *BRAF*-mutant colorectal cancer who underwent irinotecan, cetuximab plus vemurafenib treatment. Similarly, Yaeger *et al*[373] also described a patient with BRAF V600E colorectal cancer that developed acquired resistance to encorafenib, cetuximab plus alpelisib through a deletion spanning from exon 2 to exon 8 of *BRAF* (mimicking the BRAF1-9 isoform). Lastly, Johnson *et al*[372] identified a BRAF deletion involving exons 2 to 8 (BRAF1-9) in a *BRAF*-

mutant melanoma patient that progressed on dabrafenib plus trametinib treatment. Despite the similarities in the exons that are affected, the deletions occurring in BRAF have been always understood as a distinct mechanism from that leading to alternative splicing of BRAF isoforms associated with drug resistance.

We propose that our results can be generally relevant to understand the molecular alterations leading to the generation of *BRAF* mRNA isoforms involved in the acquisition of resistance to BRAF inhibitors. The results of our minigene assays, our examination of intron mutations and their effects on alternative splice site choice, and the limited effects on BRAF3-9 mRNA production of the knockdown of transcripts encoding splicing factors, even those found relevant for the survival/proliferation of a melanoma cell line that strictly depends on the production of the BRAF3-9 isoform cast doubts on the contribution of splicing alterations to the generation of resistance-associated *BRAF* mRNA isoforms, at least in the model of the melanoma cell lines SKMEL293 and C3. On the other hand, WGS and direct PCR analyses, along with the V600E allele-specific expression of BRAF mRNA isoforms all point to the presence of an intragenic deletion of BRAF as the molecular mechanism for expression of the alternative mRNA isoforms. In addition, similar findings affecting BRAF1-9 makes the genomic deletions the likely common mechanism behind the production of different resistance-associated BRAF mRNA isoforms.

We believe that the data generated from the genome-wide CRISPR knockout screening can be enriched with the incorporation of later time points (i.e., at day 14 and at day 28). Moreover, this valuable data might be useful to better understand the mechanism behind the genomic rearrangements in BRAF and, at the same tame to elucidate potential targets to overcome resistance in this scenario. In line with this, regulating those genes identified in our screen that are related to chromosome dynamics, either once resistance is established or during its acquisition, may help to identify the crucial hits involved in these deletions. Obviously, to perform the screening in resistant cell lines harboring other alternative isoforms of BRAF will also be of interest to identify common genes that might be involved in the same mechanism.

By the time we hand in this thesis, genomic experiments are being carried out to identify deletions in other cell lines and their breakpoints.

On the other hand, the fact that alternative isoforms can be detected in wild-type and treatment-naïve melanoma, together with the evidence that BRAF deletions also occur in other tumor types (with or without activating mutations), suggests that there is a clonal selection exerted by BRAFi. Accordingly, $BRAF^{V600E}$ cells are sensitive to MAPKi until they acquire a deletion that make them more prone to dimerization, and consequently resistant to currently approved BRAFi.

The detection of these deletions in patients would be useful in the clinical practice as they could guide some treatment decisions.

Unfortunately, the most widely used molecular tests in clinical practice are focused on target regions and/or whole exome sequencing, but ad hoc tests to detect the most common genomic reorganizations in the introns of the BRAF locus could be envisioned. Furthermore, a detailed description of clinical and tumor features from patients with BRAF deletions will also be of special interest. For instance, the presence of a predisposition to genomic rearrangements (e.g., mismatch repair deficiency) could be interpreted as cancer vulnerabilities and therefore become potential targets of novel therapeutic approaches.

In summary, we believe that our results shed light on the molecular mechanisms by which resistance-associated *BRAF* mRNA isoforms are generated, thus challenging the classical views of a paradigmatic example on how splicing can contribute to the emergence of resistance to cancer therapies. We have identified intragenic deletions in *BRAF* that would be responsible for the generation of these alternative isoforms, similar to deletions previously described that were considered anecdotal and not embodying the molecular events in most cases of acquired resistance through expression of alternative mRNA isoforms. Additionally, our genome scale CRISPR knockout screen undoubtedly represents a rich source of information to generate novel hypotheses related to resistance to therapy in melanoma and/or genomic rearrangements of *BRAF*.

5 CONCLUSIONS

- We provide the first evidence for the presence of alternatively spliced mRNA isoforms of *BRAF*, previously associated with the acquisition of resistance to BRAFi±MEKi, in MAPKi-naïve melanomas and/or without activating *BRAF* mutations.
- Acquisition of resistance to vemurafenib treatment in melanoma is achieved by a variety of mechanisms, even in established cell lines (unless clonally derived); thus, only a fraction of the cells in resistant C3 melanoma cell line generate alternative mRNA isoforms of *BRAF* associated with the acquisition of resistance
- We established a new vemurafenib-resistant subline (SKMEL94AR) derived from SKMEL94 cells that harbors the BRAF1-9 mRNA isoform.
- Minigene studies do not recapitulate the activation of BRAF3-9 mRNA isoform by intron 8 mutations that differ between the parental SKMEL293 melanoma cell line and the vemurafenib-resistant SKMEL293-C3 cell line. WGS of the two cell lines did not identify other candidate mutations.
- Clonal analyses of vemurafenib-resistant cell lines showed that resistance-associated *BRAF* mRNA isoforms are invariably produced from the allele harboring the V600E mutation, while full-length transcripts are generated from the wild type allele.

CONCLUSIONS

- Genome-wide CRISPR knockout screens revealed vulnerabilities of melanoma cell lines associated with splicing and chromosome dynamics, but not specifically with the generation of the BRAF3-9 mRNA isoform. Further investigations and validations are warranted.
- Large intragenic deletions have been detected in resistant melanoma cell lines harboring BRAF3-9 (SKMEL293-C3 cell line) and BRAF1-9 (SKMEL94AR), which explain the mechanism underlying the production of these BRAF mRNA isoforms.

6 MATERIALS AND METHODS

6.1 RNAseq analysis

Samples and datasets

RNA sequencing data of melanoma patients and cell lines was downloaded from the Sequence Read Archive (SRA), Gene Expression Omnibus (GEO) or BioProject repository. The publication reference, accession number and number of samples included in each publication are provided in Table 16. Our custom melanoma dataset consisted of a total 270 RNAseq samples, and the phenotype or clinical characteristics are summarized in Table 17.

GEO or BioProject Accession	Number of samples	Reference
GSE65186	*62*	Hugo *et al.*[333]
GSE112509	*57*	Kunz *et al.*[380]
GSE80829	*62*	Tsoi *et al.*[381]
PRJEB21553	*33*	Caltech (not published)
GSE99867	*12*	Sanlorenzo *et al.*[414]
GSE61544	*14*	Muller *et al.*[415]
GSE122041	*27*	Paudel *et al.*[416]
GSE75313	8	Song *et al.*[379]
GSE73738	*7*	Kemper *et al.*[363]

Table 16. List of RNA-seq datasets collected for our custom melanoma dataset. Caltech, The California Institute of Technology

SAMPLE	Reads	Status	Treatment	Mutation	Origin	Time	Lesion
A875_BRAF	217	S		V600E	CL		
AV1	590	S	BRAFi	V600E	CL	Pre	
AV1_RM	556	R	BRAFi	V600E	CL	Post	
AV4	383	S	BRAFi	V600E	CL	Pre	
AV4_RM	446	R	BRAFi	V600E	CL	Post	
AV5	470	S	BRAFi	V600E	CL	Pre	
AV5_CHREXP	395	S	BRAFi	V600E	CL	On	
B518A2_BRAF	144	S		V600E	CL		
BLM_NRAS	183	S		NRAS	CL		
D04	418	S	MEKi	NRASQ61	CL	Pre	
D04_6H	557	R	MEKi	NRASQ61	CL	On	
D04_RM	724	R	MEKi	NRASQ61	CL	Post	
D10_BRAF	114	S		V600E	CL		
M005	7	S	BRAFi	V600E	CL	Pre	

SAMPLE	Reads	Status	Treatment	Mutation	Origin	Time	Lesion
M005AR	36	S	BRAFi	V600E	CL	On	
M016X1_NRAS	132	S		NRAS	CL		
M019	79	R	BRAFi	V600E	CL	Pre	
M019AR	134	R	BRAFi	V600E	CL	Post	
M026	117	S	BRAFi	V600E	CL	Pre	
M026AR	104	R	BRAFi	V600E	CL	Post	
M029AR	53	R	BRAFi	V600E	CL	Post	
M202_b	29		none	NRASQ61	CL		
M207_b	270		none	NRASQ61	CL		
M229_a	1317	S	none	V600E	CL	Pre	
M229_b	240		none	V600E	CL		
M229_C	95	S	none	V600E	CL	Pre	
M229_d	98	S	none	V600E	CL	Pre	
M229_d_D21	79	S	BRAFi	V600E	CL	On	
M229_d_D3	118	S	BRAFi	V600E	CL	On	
M229_d_D60	103	S	BRAFi	V600E	CL	On	
M229_d_D90	38	R	BRAFi	V600E	CL	Post	
M229_D21	79	S	BRAFi	V600E	CL	On	
M229_D3	115	S	BRAFi	V600E	CL	On	
M229_D90	54	R	BRAFi	V600E	CL	On	
M229_TNF	100	S	none	V600E	CL		
M229AR_a	311	R	BRAFi+MEKi	V600E	CL	Post	
M229AR_b	175	R	BRAFi	V600E	CL	Post	
M229AR_b	175	R	BRAFi	V600E	CL	Post	
M230_b	74		none		CL		
M233_b	31		none	V600E	CL		
M233_C	24	R	none	V600E	CL	Pre	
M233_D21	20	R	BRAFi	V600E	CL	On	
M233_D3	78	R	BRAFi	V600E	CL	On	
M238_a	653	S	none	V600E	CL	Pre	
M238_b	175		none	V600E	CL		
M238AR_a	617	R	BRAFi	V600E	CL	Post	
M238AR_b	58	R	BRAFi	V600E	CL	Post	
M243_b	298		none		CL		
M244_b	48		none		CL		
M245_b	133		none		CL		
M249_b	382		none	V600E	CL		
M249_C	47	S	none	V600E	CL	Pre	
M249_D21	39	S	BRAFi	V600E	CL	On	
M249_D3	59	S	BRAFi	V600E	CL	On	
M249AR_b	66	R	BRAFi	V600E	CL	Post	
M255_b	139		none	V600E	CL		
M255_C	43	R	none	V600E	CL	Pre	
M255_D21	46	R	BRAFi	V600E	CL	On	
M255_D3	77	R	BRAFi	V600E	CL	On	
M257_b	146		none	WT	CL		
M262_b	92		none	V600E	CL		
M262_C	72	S	none	V600E	CL	Pre	
M262_D21	69	S	BRAFi	V600E	CL	On	
M262_D3	79	S	BRAFi	V600E	CL	On	
M263_b	135		none	V600E	CL		
M263_C	55	S	none	V600E	CL	Pre	
M263_D21	46	S	BRAFi	V600E	CL	On	
M263_D3	55	S	BRAFi	V600E	CL	On	
M263_TNF	45	S	none	V600E	CL		
M285_b	106		none		CL		
M296_b	230		none		CL		
M297_b	230		none	V600E	CL		
M308_b	156		none	V600E	CL		
M311_b	41		none		CL		
M318_b	325		none		CL		

SAMPLE	Reads	Status	Treatment	Mutation	Origin	Time	Lesion
M368_b	85		none		CL		
M370_b	62		none	V600E	CL		
M375_b	241		none		CL		
M376_b	265		none		CL		
M381_b	195		none		CL		
M381_C	49	R	none	BRAF	CL	Pre	
M381_D21	47	R	BRAFi	BRAF	CL	On	
M381_D3	65	R	BRAFi	BRAF	CL	On	
M395_b	139	S	none	V600E	CL	Pre	
M395AR_b	135	R	BRAFi	V600E	CL	Post	
M397_b	47	S	none	V600E	CL	Pre	
M397_b_2D	51	S	BRAFi	V600E	CL	On	
M397_b_AR	80	R	BRAFi	V600E	CL	Post	
M397_b_DTP	59	S	BRAFi	V600E	CL	On	
M397_c	250	S	none	V600E	CL	Pre	
M397_C	44	S	none	V600E	CL	Pre	
M397_d	46	S	none	V600E	CL	Pre	
M397_d_D11	48	S	BRAFi	V600E	CL	On	
M397_d_D21	66	S	BRAFi	V600E	CL	On	
M397_d_D3	70	S	BRAFi	V600E	CL	On	
M397_d_D73	80	R	BRAFi	V600E	CL	Post	
M397_D21	65	S	BRAFi	V600E	CL	On	
M397_D3	68	S	BRAFi	V600E	CL	On	
M397_D73	77	R	BRAFi	V600E	CL	On	
M397_TNF	36	S	none	V600E	CL		
M397AR_c	63	R	BRAFi	V600E	CL	Post	
M398_DMOS_b	196		none		CL		
M399_b	165		none	V600E	CL		
M402_b	130		none		CL		
M403_b	394		none	V600E	CL		
M406_b	82		none	V600E	CL		
M407_b	120		none	V600E	CL		
M408_b	244		none		CL		
M409_b	94		none	V600E	CL		
M409_C	80	S	none	V600E	CL	Pre	
M409_D21	75	S	BRAFi	V600E	CL	On	
M409_D3	74	S	BRAFi	V600E	CL	On	
M409AR_b	300	R	BRAFi	V600E	CL	Post	
M410_b	175		none	V600E	CL		
M411_b	99		none	V600E	CL		
M412_b	403		none		CL		
M416_b	70		none	V600E	CL		
M417_b	87		none	V600E	CL		
M418_b	60		none		CL		
M420_b	367		none	V600E	CL		
M421_b	109		none	V600E	CL		
M423_b	333		none		CL		
MEL008_BRAF	141	S		V600E	CL		
MEL112_NRAS	185	S		NRAS	CL		
MEL888_BRAF	163	S		V600E	CL		
MEL9007_NRAS	269	S		NRAS	CL		
MEL9523_BRAF	61	S		V600E	CL		
MEL9908_NRAS	171	S		NRAS	CL		
MM415	407	S	MEKi	NRASQ61	CL	Pre	
MM415_6H	334	S	MEKi	NRASQ61	CL	On	
MM415_RM	395	R	MEKi	NRASQ61	CL	Post	
MZ2MEL_NRAS	229	S		NRAS	CL		
PB_2	560		none		CL		
PM_1	543		none	NRAS	Pt		T
PM_10	32		none	WT	Pt		T
PM_11	324		none	NRAS	Pt		T

SAMPLE	Reads	Status	Treatment	Mutation	Origin	Time	Lesion
PM_12	361		none	NRAS	Pt		T
PM_13	114		none	NRAS	Pt		T
PM_14	806		none	BRAF	Pt		T
PM_15	263		none	NRAS	Pt		T
PM_16	148		none	NRAS	Pt		T
PM_17	738		none	WT	Pt		T
PM_18	352		none	BRAF+NRAS	Pt		T
PM_19	161		none	NRAS	Pt		T
PM_2	145		none	NRAS	Pt		T
PM_20	410		none	BRAF	Pt		T
PM_21	604		none	BRAF	Pt		T
PM_22	234		none	BRAF	Pt		T
PM_23	85		none	WT	Pt		T
PM_24	95		none	WT	Pt		T
PM_25	811		none	BRAF+NRAS	Pt		T
PM_26	72		none	WT	Pt		T
PM_27	61		none	NRAS	Pt		T
PM_28	272		none	BRAF	Pt		T
PM_29	96		none	WT	Pt		T
PM_3	190		none	NRAS	Pt		T
PM_30	111		none	BRAF	Pt		T
PM_31	81		none	NRAS	Pt		T
PM_32	188		none	WT	Pt		T
PM_33	123		none	WT	Pt		T
PM_34	82		none	WT	Pt		T
PM_35	185		none	WT	Pt		T
PM_36	91		none	BRAF	Pt		T
PM_37	209		none	BRAF	Pt		T
PM_38	96		none	BRAF	Pt		T
PM_39	195		none	WT	Pt		T
PM_4	118		none	BRAF+NRAS	Pt		T
PM_40	233		none	BRAF	Pt		T
PM_41	98		none	BRAF	Pt		T
PM_42	187		none	BRAF	Pt		T
PM_43	83		none	BRAF	Pt		T
PM_44	213		none	WT	Pt		T
PM_45	39		none	BRAF	Pt		T
PM_46	80		none	BRAF	Pt		T
PM_47	47		none	BRAF	Pt		T
PM_48	160		none	WT	Pt		T
PM_49	154		none	WT	Pt		T
PM_5	174		none	NRAS	Pt		T
PM_50	179		none	WT	Pt		T
PM_51	204		none	WT	Pt		T
PM_52	169		none	BRAF	Pt		T
PM_53	110		none	WT	Pt		T
PM_54	91		none	BRAF	Pt		T
PM_55	367		none	BRAF	Pt		T
PM_56	226		none	NRAS	Pt		T
PM_57	48		none	WT	Pt		T
PM_6	130		none	NRAS	Pt		T
PM_7	505		none	BRAF+NRAS	Pt		T
PM_8	700		none	WT	Pt		T
PM_9	417		none	NRAS	Pt		T
PT01_a	319	S	none	V600E	Pt	Pre	M
PT01AR_a	4070	R	BRAFi	V600E	Pt	Post	M
PT02_a	484	S	none	V600K	Pt	Pre	M
PT02AR_a	563	R	BRAFi	V600K	Pt	Post	M
PT02AR_b	667	R	BRAFi	V600K	Pt	Post	M
PT03_a	512	S	none	V600E	Pt	Pre	M
PT03AR_a	815	R	BRAFi	V600E	Pt	Post	M

SAMPLE	Reads	Status	Treatment	Mutation	Origin	Time	Lesion
PT03AR_b	706	R	BRAFi	V600E	Pt	Post	M
PT03AR_c	679	R	BRAFi	V600E	Pt	Post	M
PT04_a	560	S	none	V600K	Pt	Pre	M
PT04AR_a	2113	R	BRAFi	V600K	Pt	Post	M
PT05_a	116	S	none	V600E	Pt	Pre	M
PT05AR_a	270	R	BRAFi	V600E	Pt	Post	M
PT05AR_b	189	R	BRAFi	V600E	Pt	Post	M
PT05AR_c	243	R	BRAFi	V600E	Pt	Post	M
PT06_a	503	S	none	V600K	Pt	Pre	M
PT06AR_a	169	R	BRAFi	V600K	Pt	Post	M
PT06AR_b	150	R	BRAFi	V600K	Pt	Post	M
PT08_a	590	S	none	V600E	Pt	Pre	M
PT08AR_a	341	R	BRAFi	V600E	Pt	Post	M
PT08AR_b	280	R	BRAFi	V600E	Pt	Post	M
PT08AR_c	326	R	BRAFi	V600E	Pt	Post	M
PT09_a	369	S	none	V600E	Pt	Pre	M
PT09AR_a	517	R	BRAFi	V600E	Pt	Post	M
PT09AR_b	312	R	BRAFi	V600E	Pt	Post	M
PT10_a	170	S	none	V600E	Pt	Pre	M
PT10AR_a	193	R	BRAFi	V600E	Pt	Post	M
PT10AR_b	590	R	BRAFi	V600E	Pt	Post	M
PT10AR_c	28	R	BRAFi	V600E	Pt	Post	M
PT10AR_d	98	R	BRAFi	V600E	Pt	Post	M
PT10AR_e	83	R	BRAFi	V600E	Pt	Post	M
PT10AR_f	220	R	BRAFi	V600E	Pt	Post	M
PT10AR_g	1735	R	BRAFi	V600E	Pt	Post	M
PT10AR_h	508	R	BRAFi	V600E	Pt	Post	M
PT10AR_i	343	R	BRAFi	V600E	Pt	Post	M
PT15_a	189	S	none	V600E	Pt	Pre	M
PT15AR_a	517	R	BRAFi	V600E	Pt	Post	M
PT15AR_b	333	R	BRAFi	V600E	Pt	Post	M
PT16_a	137	S	none	V600E	Pt	Pre	M
PT16AR_a	286	R	BRAFi	V600E	Pt	Post	M
PT17_a	241	S	none	V600E	Pt	Pre	M
PT17AR_a	641	R	BRAFi	V600E	Pt	Post	M
PT17AR_b	1472	R	BRAFi	V600E	Pt	Post	M
PT18_a	28	S	none	V600E	Pt	Pre	M
PT18AR_a	27	R	BRAFi+MEKi	V600E	Pt	Post	M
PT19_a	211	S	none	V600E	Pt	Pre	M
PT19AR_a	49	R	BRAFi+MEKi	V600E	Pt	Post	M
PT19AR_b	195	R	BRAFi+MEKi	V600E	Pt	Post	M
PT20_a	351	S	none	V600E	Pt	Pre	M
PT20AR_a	392	R	BRAFi	V600E	Pt	Post	M
PT20AR_b	1020	R	BRAFi+MEKi	V600E	Pt	Post	M
PT21AR_a	283	R	BRAFi	V600E	Pt	Post	M
PT21AR_b	319	R	BRAFi+MEKi	V600E	Pt	Post	M
PT21AR_c	331	R	BRAFi+MEKi	V600E	Pt	Post	M
PT22_a	222	S	none	V600E	Pt	Pre	M
PT22AR_a	717	R	BRAFi+MEKi	V600E	Pt	Post	M
PT22AR_b	876	R	BRAFi+MEKi	V600E	Pt	Post	M
PT22AR_c	793	R	BRAFi+MEKi	V600E	Pt	Post	M
PT23_a	185	S	none	V600K	Pt	Pre	M
PT23AR_a	181	R	BRAFi+MEKi	V600K	Pt	Post	M
PT24_a	196	S	none	V600R	Pt	Pre	M
PT24AR_a	180	R	BRAFi+MEKi	V600R	Pt	Post	M
SKMEL147_NRAS	117	S		NRAS	CL		
SKMEL28_a	239	S	none	V600E	CL	Pre	
SKMEL28_c	49	S	none	V600E	CL	Pre	
SKMEL28_c_2D	65	S	BRAFi	V600E	CL	On	
SKMEL28_c_AR	64	R	BRAFi	V600E	CL	Post	
SKMEL28_c_DTP	52	S	BRAFi	V600E	CL	On	

SAMPLE	Reads	Status	Treatment	Mutation	Origin	Time	Lesion
SKMEL28AR_a	222	R	BRAFi+MEKi	V600E	CL	Post	
SKMEL28AR_b	161	R	BRAFi	V600E	CL	Post	
SKMEL5_PROGRESS_a	349	R	BRAFi	V600E	CL	Post	
SKMEL5_PROGRESS_b	436	R	BRAFi	V600E	CL	Post	
SKMEL5_PROGRESS_c	547	R	BRAFi	V600E	CL	Post	
SKMEL5_REGRESS_a	259	S	BRAFi	V600E	CL	On	
SKMEL5_REGRESS_b	225	S	BRAFi	V600E	CL	On	
SKMEL5_REGRESS_c	312	S	BRAFi	V600E	CL	On	
SKMEL5_STAT_a	354	S	BRAFi	V600E	CL	On	
SKMEL5_STAT_b	451	S	BRAFi	V600E	CL	On	
SKMEL5_STAT_c	243	S	BRAFi	V600E	CL	On	
WM1366_NRAS	129	R		NRAS	CL		

Table 17. Phenotypic and clinical characteristics of the samples included in our custom melanoma dataset. Reads: number of reads spanning an exon junction in BRAF; Status: R= resistant to MAPK inhibitors; S=sensitive to MAPK inhibitors (MAPKi); Origin: Pt=patient tumor; CL=cell line; Time: time of sample acquisition relative to initiation of treatment with MAPKi; Pre=prior to MAPKi; Post=at progression after MAPKi; On=during MAPKi treatment; Lesion: M=melanoma metastasis; T=primary melanoma.

We also downloaded RNAseq data from the TCGA project (https://www.cancer.gov/tcga) and analyzed a total of 472 samples from the Skin Cutaneous Melanoma (TCGA, Firehose Legacy).

Splicing analysis – VAST-TOOLS

First, we run FastQC[417] to carry out quality control checks on raw sequence data from the samples included in our datasets. None of the samples had to be discarded due to quality concerns.

We used the toolset VAST-TOOLS v 2.3 (Vertebrate Alternative Splicing and Transcription Tools)[64,378] (https://github.com/vastgroup/vast-tools) for the strand-specific alignment of reads (genome reference hg38, Hs2). In general, default settings were used, except for trimming length (--trimLen 48) in the TCGA dataset. The eej2 output of VAST-TOOLS reported the read counts for all possible exon-exon junction (EEJ) combinations. We then obtained from this file the number of EEJ reads mapping to all the potential donor or acceptor sites from each reference exon of

BRAF. For each EEJ event, a minimum coverage of 5 reads was required in at least one sample.

Plots for data visualization were generated with *ggplot2*[418] package in R (v4).

Sashimi plots

For selected samples and genes, sashimi plots were created to visualize exon-exon junctions from the aligned RNA-seq data.

First, fastq files were mapped using STAR and the reference genome GRCh38/hg38 (Genome Reference Consortium Human Build 38). Indexed and aligned data were then exported to the Integrative Genome Viewer (IGV)[419] to display the sashimi plots.

6.2 *In cellulo* assays and transcriptomic profiling

Cell lines

Melanoma cells, listed in Table 18, were kindly provided by the indicated reasearch groups, and cultured in the specified medium. HEK293 and 293T were grown in GlutaMAX® Dulbecco's modified Eagle's (DMEM, Life Technologies) medium. All growth media were supplemented with 10% fetal bovine serum (FBS) —except for the MCDB-modified medium—, and with penicillin (50 U/ml)/streptomycin (50 µg/ml) (Life Technologies). MCDB modified media consisted of MCDB 153 media containing 20% Leibovitz-L15 media, 2% fetal bovine serum, 0.2% sodium bicarbonate, and 5µg/mL insulin. Resistant cell lines were maintained with 1 µM vemurafenib (PLX4032; Selleck, Cat#S1267).

All cells were maintained at 37ºC and 5% CO_2 atmosphere. Cells were routinely tested for mycoplasma (by PCR detection method).

Cell line	Growth medium	Vemurafenib 1µM	Provider
UACC62	DMEM	No	Gebauer lab (CRG, Spain)
SKMEL94	DMEM	No	
SKMEL94AR#	DMEM	Yes	
SKMEL147	DMEM	No	
SKMEL293	RPMI	No	Solit and Rosen labs (MSKCC, USA)
C3 and derived clones	RPMI	Yes	
M397	DMEM	No	Ribas lab (UCLA, USA)
M397AR	DMEM	Yes	
1205Lu	MCDB mod.	No	Hartsough lab (Drexel, USA)
PRT#3	MCDB mod.	Yes	
PRT#4	MCDB mod.	Yes	

Table 18. Melanoma cell lines, growth medium and providers. DMEM: Glutamax Dulbecco's modified Eagle's medium; RPMI: Roswell Park Memorial Institute 1640, L-glutamine supplemented (Life Technologies); MCDB mod: MCDB 153 modified medium. #SKMEL94AR cell line was generated during this project.

RNA extraction and semi-quantitative RT-PCR

Cells were harvested, pelleted, and washed with PBS (phosphate buffered saline). Lysis, DNase treatment and total RNA extraction was performed using Maxwell simplyRNA kit (Promega), following the manufacturers' instructions. RNA was quantified with SPECTROstar® Nano, a spectrometer-based absorbance microplate reader. Routinely, 100-500 ng of total RNA were reverse-transcribed with 1 µl SuperScript™ III (Invitrogen) or RTmax from the Protein Technologies Unit core facility of the Centre for Genomic Regulation, 2,5 µM oligo-dT (Sigma or IDT) and 12.5 ng/µl of random primers (Life Technologies), in a 20 µl final reaction volume. Reaction buffer (5X) consisted of 250 mM Tris-HCl (pH 8.3 at room temperature), 375 mM KCl and 15 mM $MgCl_2$. After 5 min of denaturation at 65ºC, the buffer and the enzyme were added. Then, reactions were prewarmed at 25ºC, followed by 60 min at 50ºC of reverse-transcription and 15 min at 70ºC for inactivation.

Semi-quantitative PCR reactions were performed using GoTaq enzyme (Promega) and 1 µl of previously synthesized cDNA. Routinely, 0.15 µl of GoTaq polymerase, 1 µM of primers and 1.5 µl of dimethylsulfoxide (DMSO) was used in a 30 µl reaction volume. PCR cycling parameters were as follows (unless otherwise specified): initial incubation at 95°C (3'), 30 cycles of 95°C (15"),

60°C (30”), 72°C (1”) and a final incubation at 72°C (10’). In case of expected amplicons longer that 1 kb, elongation time (72ºC) was increased up to 90’’ or 120’’. Primers used are listed in Table 21.

Routinely, PCR products were separated by vertical electrophoresis in 6% polyacrylamide gels run in Tris-borate-EDTA (TBE) 1X. Gels were stained with GelRed stain (Biotium) and visualized with Gel Doc™ XR+ (BioRad). Alternatively, diluted PCR products were separated by high throughput capillary electrophoresis using a Caliper LabChip® GX workstation with HT DNA 5K (Perkin Elmer). Imaging and isoform quantification were performed with LabChip GX Reviewer software.

Amplicon analysis

PCR amplicons of interest were Sanger sequenced after DNA purification from either the corresponding agarose gel or by silica-membrane-based method of the PCR reaction products. PCR products were separated by electrophoresis in 1-2% agarose gels run in TBE 1X and, once the amplicon was sliced, the DNA was extracted from the gel using the QIAquick® Gel Extraction Kit (Qiagen), following the manufacturer’s recommendation. Alternatively, amplified product was directly purified from the PCR reaction using the QIAquick® PCR Purification Kit (Qiagen), a silica-membrane-based purification kit, following the manufacturer’s recommendation.

DNA concentration was measured using SPECTROstar® Nano and delivered to Eurofins Genomics together with the intended sequencing primer, according to the company specifications.

Cell viability assay

$1x10^5$ cells were plated in 4 replicates in 96-well plates and, after overnight incubation, complete medium with different drug concentrations was added in a final volume of 200 µl/well. A set of wells included cells treated with DMSO as control, and empty wells with just medium only for background subtraction. One plate was prepared for each time point. Plates were incubated for the desired periods of exposure. Resazurin stock was prepared dissolving 5 mg of high purity resazurin in 1 ml of PBS and filter-sterilized. Resazurin stock (5 mg/ml, 20 mM, Sigma-Aldrich) was diluted in fresh complete medium to a final concentration of 0.15 mg/ml. 40 µl of resazurin solution was added to each well (final concentration 100 µM) and plates were incubated for 3 hours at 37ºC. Absorbance at 560 nm excitation / 590 emission was measured using the plate reader Infinite® M200 (Tecan). The background of just medium was subtracted from all measurements. Data was analyzed and visualized with Prism 9 (v 9.3). In short, dose concentration was log-transformed, measured signal was normalized to the control, and IC50 was calculated using nonlinear regression of log(inhibitor) vs. normalized response (variable slope).

Single cell-derived clones

We generated single cell-derived clones from the "bulk" C3 cell line. Low-passaging cells were trypsinized and resuspended in medium. Alive cells, DAPI-negative, were sorted using a flow cytometer in sterile conditions into a 96-well plate containing 100 µl of complete growth medium. The plates were scanned for single-cell colonies and

small aggregates were visible usually at 7-14 days. Single-cell colonies were trypsinized and seeded in larger well formats until enough number of cells (usually a 24-well plate at 70-80% confluency) could be harvested for RNA extraction and RT-PCR analysis.

Single PCR molecule analysis

For single molecule PCR Sanger sequencing, we cloned the PCR product in the TOPO® TA vector (Invitrogen). Blunt-end (without 3' A-overhangs) PCR products generated by RT-PCR as previously detailed, were cloned in the TOPO vector, following manufacturer's recommendations. The constructs were then transformed into electrocompetent cells (as described below in *Minigenes*). Single colonies were grown, and Sanger sequencing was carried out after DNA purification to validate the identity of the amplification products.

Knockdown and mRNA silencing

For siRNA transfection, 2-2.5x10^5 cells/well were plated in 6-well plate. After overnight incubation, we transfected 20 μM siRNA using 3 μl of Lipofectamine RNAiMAX (Invitrogen) in a final volume of 1 ml of Opti-MEM® medium. Medium was replaced 6-8 h later and cells were collected after 72 h of transfection. Unless otherwise specified, ON-TARGETplus™ SMARTpool siRNAs (Dharmacon™), a mixture of 4 siRNA for the specific target gene were used (Table 19).

Single-stranded RNA targeting BRAF (both the exon junction 3-9 and exons 5 and 6) were annealed using an RNA-annealing buffer containing potassium acetate 1M, HEPES-KOH 300mM pH 7.4 and magnesium acetate 20 mM. For siRNA duplex formation, RNAs were incubated 5' at 95ºC followed by 2 h at 37ºC. Each pair of siRNAs duplexes targeting the exon-junction 3-9 (JC1 and JC2) and the exons 5 and 6 (siEX5 and siEX6) were pooled before transfection. RNAs used are listed in Table 20.

Target gene	Reference
Non targeting	D-001810-10-05
INTS6	L-012417-00-0005
RRM1	L-004270-00-0005
RRM2	L-010379-00-0005
SMU1	L-021129-01-0005
XPO1	L-003030-00-0005
MCL1	L-004501-00-0005
SNRNP200	L-014161-00-0005
SF3B1	L-020061-01-0005
RBM48	L-014780-02-0005
CDC5L	L-011237-00-0005
PRPF8	L-012252-00-0005
SNW1	L-012446-00-0005
RBM39	L-011965-00-0005
SNRPB	L-017766-01-0005
CLK3	L-004802-00-0005
BORA	L-014458-00-0005
SNRPE	L-019719-02-0005
FBXO5	L-012434-00-0005
NFX1	L-006541-00-0005
AURKA	L-003545-01-0005

Table 19. List of siRNAs used in this study. Target genes and reference number of ON-TARGETplus™ siRNA pools of Dharmacon™ are specified.

ID	siRNA duplex	Sequence
JC1_FW	siJC1	GGACAGUGGACUUGAUUAG TT
JC1_RV	siJC1	TT CUAAUCAAGUCCACUGUCC
JC2_FW	siJC2	AGGACAGUGGACUUGAUUA TT
JC2_RV	siJC2	TT UAAUCAAGUCCACUGUCCU
siEX5_FW	siEX5	ACUGAUAUUUCCUGGCUUA TT
siEX5_RV	siEX5	TT UAAGCCAGGAAAUAUCAGU
siEX6_FW	siEX6	CUGUCAAACAUGUGGUUAU TT
siEX6_RV	siEX6	TT AUAACCACAUGUUUGACAG

Table 20. List of RNAs for siRNA duplex formation used in this study. Sequences of single-stranded complementary sequences (forward, FW, and reverse, RV) are indicated for the four siRNAs duplexes targeting the exon-junction 3-9 (JC1 and JC2) and exons 5 (siEx5) and 6 (siEx6).

Colony formation assays

After 72 h of siRNA transfection, $1x10^4$ cells were seeded in replicates into 6-well plates with complete growth media. Cells were incubated and media changed, when necessary, until colonies were visible. Then, cells were fixed with 1 ml methanol per well at room temperature for 10 min and stained with 5% Giemsa. After washing, plates were air-dried and scanned for colony counting using ImageJ.

6.3 Minigenes

Cloning

Genomic DNA (gDNA) extracted from cell lines (using GenElute™ Mammalian Genomic DNA Miniprep Kit, Sigma-Aldrich) or human genomic DNA (Roche) was used for PCR-mediated generation of amplicons corresponding to the genomic regions of interest. PCR reactions were carried out with 20 ng of gDNA, using primers listed in Table 21 and GoTaq enzyme (Promega). PCR annealing temperature was adjusted 5 degrees below the melting temperatures of designed primers. Alternatively, high-fidelity polymerase of Advantage 2 PCR Kit (Takara) was used according to manufacturer's recommendations, especially if long genomic PCR products or amplification of the vector was desired. PCR products were purified from agarose gels after electrophoresis as mentioned above.

pCMV 57 Δi was used as vector for gDNA cloning, flanked by PT1 and PT2 sequences, that allow detection of transcripts from the expression vector by RT-PCR[420]. Empty vector was generated either by PCR with high-fidelity polymerase followed by DpnI digestion (New England BioLabs) for methylated DNA template removal, or by restriction digestion using the appropriate buffer and enzymes (New England BioLabs) according to our cloning strategy, followed by purification from agarose gel.

For restriction enzyme cloning, PCR-amplified inserts (with primers containing the desired restriction site) were purified and then digested using the appropriate buffer and enzymes (New England BioLabs). Ligation, usually at insert:vector ratio of 3:1, was carried out using T4 DNA ligase (New England BioLabs).

For Gibson cloning, 20 ng of vector and inserts at a insert:vector ratio of 8:1 was incubated at 50ºC for 1 hour with a mix of reagents from the Protein Technologies Unit core facility of the Centre for Genomic Regulation.

For transformation, $CaCl_2$-treated chemically competent cells were prepared in house, and single colonies from LB Agar supplemented with ampicillin were grown overnight. DNA was purified using QIAprep® Spin Miniprep Kit (Qiagen) and Sanger sequenced as mentioned above.

Mutagenesis

Site-directed mutagenesis of plasmids were carried out using back-to-back 5' phosphorylated primers with one of the primers containing the desired point mutation. The primers used are listed in Table 21. PCR with high-fidelity polymerase was performed using Advantage 2 PCR Kit (Takara), according to manufacturer's instructions. The methylated non-mutated PCR template was removed by DpnI digestion (New England BioLabs). The linear product was ligated using T4 DNA ligase (New England BioLabs). Bacterial transformation, purification and sequencing were performed as explained above.

Transfections

HEK293 and melanoma cells were transfected with 20-500 ng of DNA plasmid (depending on the cell type, due to their different transfection efficiency), using Lipofectamine 2000 (Invitrogen). Routinely, 2.5 x 10^5 cells were seeded in 6-wells plates and incubated overnight for cell attachment. Diluted transfection reagent (1 µl per transfection) in Opti-MEM® medium (Life Technologies) was mixed with diluted DNA plasmid in Opti-MEM® medium to a final volume of 300 µl per transfection. Plasmid and reagent mix were added dropwise to cells plated in wells with Opti-MEM® to a final volume of 1 ml. After 6-8 hours incubation, medium was replaced. Routinely, after 48 hours cells were collected, RNA extracted, and RT-PCR analyses carried out as detailed above.

Primer	Sequence	Aim
FW_1	GACCCTGCCATTCCGGAG	*RT-sqPCR*
RV_11	CTGCCCATCAGGAATCTCCC	*RT-sqPCR*
FW_8	AATTCCACAGCCCTTCCGAC	*RT-sqPCR*
EJ1_9q	GCCATTCCGGAGGAGGACTT	*RT-sqPCR*
EJ1_11	GCCATTCCGGAGGAGAAAAC	*RT-sqPCR*
EJ3-9	ACAAACAGAGGACAGTGgacttga	*RT-sqPCR*
EJ2_11q	CCACCATCAATATATCTGGAGAAAAC	*RT-sqPCR*
RV12	AACTGCTGAGGTGTAGGTGC	*RT-sqPCR*
PT1	GTCGACGACACTTGCTCAAC	*RT-sqPCR*
PT2	AAGCTTGCATCGAATCAGTAG	*RT-sqPCR*
FW_3	TCTCTGGGGAACGGAACTGA	*RT-sqPCR*
RV_GFP	GGACACGCTGAACTTGTGGC	*RT-sqPCR*
RV16	CTGGTCCCTGTTGTTGATGT	*RT-sqPCR*
S_PT1	aaaGGTACCgtcgacgacacttgctcaacGCCTATGAAGAATACACCAGCAA	*Cloning*
AS_PT2	aaaGCGGCCGCaagcttgcatcgaatcagtagAAAAAAACCTGAAATCACTACTTACC	*Cloning*
i3_RV	aaaggatccCATGACTGTGGTTCAAGTTTGGC	*Cloning*

i3_FW	aaaggatccCTGCGTTGGTGGGTATATTGTAG	*Cloning*
i4_RV	aaactgcagGGGAGGGGGGTAAGAGTCTATT	*Cloning*
i8_FW	aaatgcagCTGAAATGGACATCAACATTTGATTAG	*Cloning*
i7_FW	aaactgcagACTTCTTCAGTTGATGGCCAC	*Cloning*
i8_RV	aaactcgagAGGGCTTCTATCAGTCCTTTG	*Cloning*
FW_plusi8	ctgcagAAAActcgagCACAGCGGTTTGCCACACA	*Cloning*
51mut_FW	GTCTGATTATATGCTTGCTTGG	*Mutagenesis*
51mut_RV	AGTAGCGATAACACTGAATTTTCC	*Mutagenesis*
A5SS_FW	AACCTGCAAGGTGTGGAGTTAC	*Mutagenesis*
A5SS_RV	CCTATGGTATCATAAATATATTGA	*Mutagenesis*
pLCKO2_FW	GAGGGCCTATTTCCCATGATTC	*CRISPR PCR1*
pLCKO2_RV	CAAACCCAGGGCTGCCTTGGAA	*CRISPR PCR1*
CRISPR_F1	ACACTCTTTCCCTACACGACGCTCTTCCGATCT NNTTGTGGAAAGGACGAGGTACCG	*CRISPR PCR2*
CRISPR_F2	ACACTCTTTCCCTACACGACGCTCTTCCGATCT NNNTTGTGGAAAGGACGAGGTACCG	*CRISPR PCR2*
CRISPR_F3	ACACTCTTTCCCTACACGACGCTCTTCCGATCT NNNNTTGTGGAAAGGACGAGGTACCG	*CRISPR PCR2*
CRISPR_F4	ACACTCTTTCCCTACACGACGCTCTTCCGATCT NNNNNTTGTGGAAAGGACGAGGTACCG	*CRISPR PCR2*
CRISPR_F5	ACACTCTTTCCCTACACGACGCTCTTCCGATCT NNNNNNTTGTGGAAAGGACGAGGTACCG	*CRISPR PCR2*
CRISPR_RV	GTGACTGGAGTTCAGACGTGTGCTCTTCCGATCTACTTGCTATTTCTAGCTCTAAAAC	*CRISPR PCR2*

Table 21. List of oligonucleotide DNA primers used in this study.

6.4 DNAseq analysis

Sample preparation and sequencing

Genomic DNA extraction was carried out from cell line pellets, using GenElute™ Mammalian Genomic DNA Miniprep Kit (Sigma-Aldrich) according to manufacturer's instructions. DNA sequencing was performed by the CNAG (National Center for Genomic Analysis) Sequencing Unit. Strand-specific libraries were built with the provided aliquots of DNA (2.5 µg, with a concentration 50-200 ng/µl). Whole-genome sequencing was performed using NovaSeq600 (Illumina), following 2x150 bp paired-ended protocol, targeting > 99 Gb of data per sample to achieve 30x genome coverage.

Variant calling

For reads alignment to genome reference (hg38), we used BWA tool (Burrows Wheeler Aligner)[421] and the *bwa-mem* algorithm. We used the SAMtools[422] program to merge the SAM (sequence alignment map) files, transform SAM files into BAM (binary alignment map) files, to sort BAM files by coordinates.

To avoid PCR amplification artifacts, we deduplicated the BAM files using the Picard tool, *MarkDuplicates* (http://broadinstitute.github.io/picard/). Then, the BAM files were indexed using SAMtools.

Variant calling was carried out using *freebayes* (a haplotype-based, Bayesian, variant detector)[385]. The detected variations, contained in the VCF files were next filtered using BCFtools[422]: read depth (DP)

> 10 and a QUAL (Phred-scaled probability that the observed variant exists at this site) > 20. The workflow of the variant calling is represented in Figure 48.

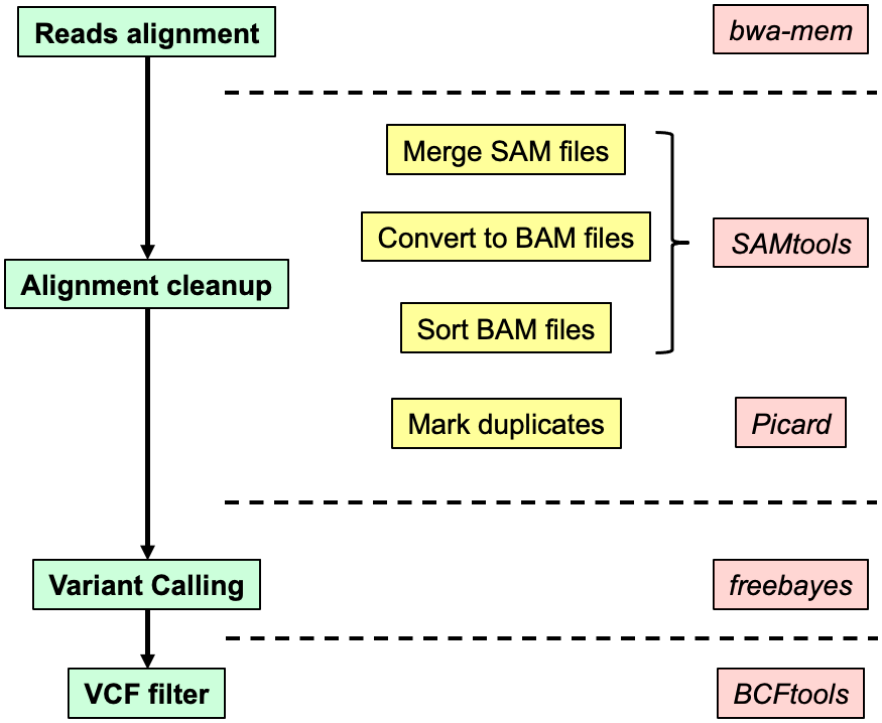

Figure 48. Variant calling workflow. Representation of the steps for the variant calling and the tools used in each step. VCF, variant calling format file; SAM, sequence alignment map format file; BAM, binary alignment map format file

For the *BRAF* gene, the proportion (%) of alternative reads (or variants) for a given locus was calculated as follows: (sample alternative genotype reads (AD) / DP) x 100.

For the genome-wide variant analysis, *SnpEff*[386] and *VEP*[390] were used for variant annotation and functional prediction. We focused our analysis on splicing-related genes, and for that purpose, we used a selection of 1110 genes from a public database[391] (Supplementary

Table S2) and a selection of 305 genes used in our lab for functional network reconstruction of splicing regulation[67] (Table 22).

Plots for visualization data were generated using R (v 4) and the following packages: *maftools*[387], *ggplot2*[418] and *trackViewer*[423].

Gene name	Ensemble ID	Class / Family
SNRNP70	ENSG00000104852	U1 snRNP
SNRPA	ENSG00000077312	U1 snRNP
SNRPC	ENSG00000124562	U1 snRNP
SF3B6	ENSG00000115128	U2 snRNP
SF3A1	ENSG00000099995	U2 snRNP
SF3A2	ENSG00000104897	U2 snRNP
SF3A3	ENSG00000183431	U2 snRNP
SF3B1	ENSG00000115524	U2 snRNP
SF3B2	ENSG00000087365	U2 snRNP
SF3B3	ENSG00000189091	U2 snRNP
SF3B4	ENSG00000143368	U2 snRNP
SNRPA1	ENSG00000131876	SM proteins
SNRPB2	ENSG00000125870	SM proteins
SNRPD1	ENSG00000167088	SM proteins
SNRPD2	ENSG00000125743	SM proteins
SNRPD3	ENSG00000100028	SM proteins
SNRPE	ENSG00000182004	SM proteins
SNRPF	ENSG00000139343	SM proteins
SNRPG	ENSG00000143977	SM proteins
SNRPB	ENSG00000125835	SM proteins
CCAR1	ENSG00000060339	A complex
PRPF40A	ENSG00000196504	A complex
SF1	ENSG00000168066	A complex
THRAP3	ENSG00000054118	A complex
RBM10	ENSG00000182872	A complex
RBM25	ENSG00000119707	A complex
RBM5	ENSG00000003756	A complex
DDX5	ENSG00000108654	A complex
BUB3	ENSG00000154473	A complex
SMNDC1	ENSG00000119953	U2 snRNP related
U2AF1	ENSG00000160201	U2 snRNP related
U2AF2	ENSG00000063244	U2 snRNP related
DDX46	ENSG00000145833	U2 snRNP related
DHX15	ENSG00000109606	U2 snRNP related
CHERP	ENSG00000085872	U2 snRNP related
PUF60	ENSG00000179950	U2 snRNP related
RBM17	ENSG00000134453	U2 snRNP related
U2SURP	ENSG00000163714	U2 snRNP related
HTATSF1	ENSG00000102241	U2 snRNP related
IK	ENSG00000113141	B complex
MFAP1	ENSG00000140259	B complex
PRPF4B	ENSG00000112739	B complex
SMU1	ENSG00000122692	B complex
WBP4	ENSG00000120688	B complex
TFIP11	ENSG00000100109	B complex

Gene name	Ensemble ID	Class / Family
CD2BP2	ENSG00000169217	U5 snRNP
EFTUD2	ENSG00000108883	U5 snRNP
PRPF6	ENSG00000101161	U5 snRNP
PRPF8	ENSG00000174231	U5 snRNP
SNRNP200	ENSG00000144028	U5 snRNP
SNRNP40	ENSG00000060688	U5 snRNP
TXNL4A	ENSG00000141759	U5 snRNP
DDX23	ENSG00000174243	U5 snRNP
SART1	ENSG00000175467	U4/U6.U5 snRNP
SNRNP27	ENSG00000124380	U4/U6.U5 snRNP
USP39	ENSG00000168883	U4/U6.U5 snRNP
SNU13	ENSG00000100138	U4/U6 snRNP
PPIH	ENSG00000171960	U4/U6 snRNP
PRPF3	ENSG00000117360	U4/U6 snRNP
PRPF4	ENSG00000136875	U4/U6 snRNP
PRPF31	ENSG00000105618	U4/U6 snRNP
LSM2	ENSG00000204392	LSm proteins
LSM3	ENSG00000170860	LSm proteins
LSM4	ENSG00000130520	LSm proteins
LSM6	ENSG00000164167	LSm proteins
LSM7	ENSG00000130332	LSm proteins
AQR	ENSG00000021776	PRP19 complex
BCAS2	ENSG00000116752	PRP19 complex
BUD31	ENSG00000106245	PRP19 complex
CDC5L	ENSG00000096401	PRP19 complex
CRNKL1	ENSG00000101343	PRP19 complex
CTNNBL1	ENSG00000132792	PRP19 complex
CWC15	ENSG00000150316	PRP19 complex
HSPA8	ENSG00000109971	PRP19 complex
ISY1	ENSG00000240682	PRP19 complex
PLRG1	ENSG00000171566	PRP19 complex
PPIE	ENSG00000084072	PRP19 complex
PQBP1	ENSG00000102103	PRP19 complex
PRPF19	ENSG00000110107	PRP19 complex
RBM22	ENSG00000086589	PRP19 complex
SNW1	ENSG00000100603	PRP19 complex
WBP11	ENSG00000084463	PRP19 complex
XAB2	ENSG00000076924	PRP19 complex
YBX1	ENSG00000065978	PRP19 complex
HSPA1A	ENSG00000204389	PRP19 complex
BUD13	ENSG00000137656	RES complex
RBMX2	ENSG00000134597	RES complex
SNIP1	ENSG00000163877	RES complex
CCDC12	ENSG00000160799	Bact complex
CDC40	ENSG00000168438	Bact complex
CWC22	ENSG00000163510	Bact complex
CWC27	ENSG00000153015	Bact complex
PPIL3	ENSG00000240344	Bact complex
PPIL2	ENSG00000100023	Bact complex
ZNF830	ENSG00000198783	Bact complex
FUBP3	ENSG00000107164	Bact complex
DHX16	ENSG00000204560	Bact complex
CACTIN	ENSG00000105298	C complex
C9orf78	ENSG00000136819	C complex

Gene name	Ensemble ID	Class / Family
CXorf56	ENSG00000018610	C complex
DGCR14	ENSG00000100056	C complex
FAM32A	ENSG00000105058	C complex
FAM50A	ENSG00000071859	C complex
LENG1	ENSG00000105617	C complex
PPWD1	ENSG00000113593	C complex
PRPF18	ENSG00000165630	C complex
SLU7	ENSG00000164609	C complex
SYF2	ENSG00000117614	C complex
FRG1	ENSG00000109536	C complex
DDX41	ENSG00000183258	C complex
NOSIP	ENSG00000142546	C complex
PPIG	ENSG00000138398	C complex
DHX35	ENSG00000101452	C complex
DHX38	ENSG00000140829	C complex
DHX8	ENSG00000067596	C complex
CDK10	ENSG00000185324	C complex
FAM50B	ENSG00000145945	C complex
ACIN1	ENSG00000100813	EJC / mRNP
EIF4A3	ENSG00000141543	EJC / mRNP
MAGOH	ENSG00000162385	EJC / mRNP
RBM8A	ENSG00000265241	EJC / mRNP
RNPS1	ENSG00000205937	EJC / mRNP
ALYREF	ENSG00000183684	EJC / mRNP
DDX39B	ENSG00000198563	EJC / mRNP
THOC1	ENSG00000079134	TREX
THOC2	ENSG00000125676	TREX
THOC3	ENSG00000051596	TREX
THOC5	ENSG00000100296	TREX
THOC6	ENSG00000131652	TREX
THOC7	ENSG00000163634	TREX
DDX10	ENSG00000178105	helicase
DDX11	ENSG00000013573	helicase
DDX12P	ENSG00000214826	helicase
DDX17	ENSG00000100201	helicase
DDX24	ENSG00000089737	helicase
DDX28	ENSG00000182810	helicase
DDX31	ENSG00000125485	helicase
DDX3X	ENSG00000215301	helicase
DDX52	ENSG00000278053	helicase
DHX30	ENSG00000132153	helicase
DHX32	ENSG00000089876	helicase
DHX33	ENSG00000005100	helicase
DHX57	ENSG00000163214	helicase
DHX9	ENSG00000135829	helicase
HFM1	ENSG00000162669	helicase
MOV10	ENSG00000155363	helicase
SKIV2L2	ENSG00000039123	helicase
TDRD9	ENSG00000156414	helicase
HNRNPA1	ENSG00000135486	hnRNP
HNRNPAB	ENSG00000197451	hnRNP
HNRNPC	ENSG00000092199	hnRNP
FUS	ENSG00000089280	hnRNP
HNRNPA0	ENSG00000177733	hnRNP

Gene name	Ensemble ID	Class / Family
HNRNPA2B1	ENSG00000122566	hnRNP
HNRNPA3	ENSG00000170144	hnRNP
HNRNPCL1	ENSG00000179172	hnRNP
HNRNPD	ENSG00000138668	hnRNP
HNRNPF	ENSG00000169813	hnRNP
HNRNPH1	ENSG00000169045	hnRNP
HNRNPH2	ENSG00000126945	hnRNP
HNRNPH3	ENSG00000096746	hnRNP
HNRNPK	ENSG00000165119	hnRNP
HNRNPL	ENSG00000104824	hnRNP
HNRNPM	ENSG00000099783	hnRNP
HNRNPR	ENSG00000125944	hnRNP
HNRNPU	ENSG00000153187	hnRNP
HNRNPUL1	ENSG00000105323	hnRNP
HNRNPUL2	ENSG00000214753	hnRNP
HNRNPDL	ENSG00000152795	hnRNP
HNRNPLL	ENSG00000143889	hnRNP
ILF2	ENSG00000143621	hnRNP
MATR3	ENSG00000015479	hnRNP
PTBP1	ENSG00000011304	hnRNP
RALY	ENSG00000125970	hnRNP
SYNCRIP	ENSG00000135316	hnRNP
ILF3	ENSG00000129351	hnRNP
SRSF11	ENSG00000116754	SR proteins
SRSF3	ENSG00000112081	SR proteins
SRSF4	ENSG00000116350	SR proteins
SRSF6	ENSG00000124193	SR proteins
SRSF7	ENSG00000115875	SR proteins
SRSF9	ENSG00000111786	SR proteins
SRSF1	ENSG00000136450	SR proteins
SRSF2	ENSG00000161547	SR proteins
SRSF5	ENSG00000100650	SR proteins
TRA2B	ENSG00000136527	SR proteins
SRRM2	ENSG00000167978	SR related
SRRM1	ENSG00000133226	SR related
SRRM3	ENSG00000177679	SR related
RBM6	ENSG00000004534	RNA binding proteins
NSRP1	ENSG00000126653	RNA binding proteins
CIRBP	ENSG00000099622	RNA binding proteins
YBX3	ENSG00000060138	RNA binding proteins
ELAVL1	ENSG00000066044	RNA binding proteins
ESRP1	ENSG00000104413	RNA binding proteins
ESRP2	ENSG00000103067	RNA binding proteins
EWSR1	ENSG00000182944	RNA binding proteins
PAXBP1	ENSG00000159086	RNA binding proteins
IGF2BP3	ENSG00000136231	RNA binding proteins
KIN	ENSG00000151657	RNA binding proteins
LUC7L3	ENSG00000108848	RNA binding proteins
NONO	ENSG00000147140	RNA binding proteins
PRPF39	ENSG00000185246	RNA binding proteins
RBM15	ENSG00000162775	RNA binding proteins
RBM39	ENSG00000131051	RNA binding proteins
RBFOX2	ENSG00000100320	RNA binding proteins
SFPQ	ENSG00000116560	RNA binding proteins

Gene name	Ensemble ID	Class / Family
TIA1	ENSG00000116001	RNA binding proteins
TIAL1	ENSG00000151923	RNA binding proteins
ZNF207	ENSG00000010244	RNA binding proteins
ADAR	ENSG00000160710	RNA editing
ADARB1	ENSG00000197381	RNA editing
ALKBH5	ENSG00000091542	RNA metylation
C19orf43	ENSG00000123144	RNA modifying
PABPC1	ENSG00000070756	RNA modifying
PABPN1	ENSG00000100836	RNA modifying
DBR1	ENSG00000138231	RNA modifying
DIS3	ENSG00000083520	RNA degradation
DIS3L	ENSG00000166938	RNA degradation
EXOSC4	ENSG00000178896	RNA modifying
FTO	ENSG00000140718	RNA metylation
KIAA1429	ENSG00000164944	RNA metylation
METTL14	ENSG00000145388	RNA metylation
METTL3	ENSG00000165819	RNA metylation
WTAP	ENSG00000146457	RNA metylation
WDR83	ENSG00000123154	RNA metylation
YTHDC1	ENSG00000083896	RNA metylation
NCBP1	ENSG00000136937	CBC
NCBP2	ENSG00000114503	CBC
CPSF2	ENSG00000165934	CPSF
CPSF6	ENSG00000111605	CPSF
NUDT21	ENSG00000167005	CPSF
DNAJC8	ENSG00000126698	Other SAPs
CFAP20	ENSG00000070761	Other SAPs
BRINP1	ENSG00000078725	Other SAPs
HSPA5	ENSG00000044574	Other SAPs
CARM1	ENSG00000142453	Other SAPs
PRMT1	ENSG00000126457	Other SAPs
PRMT5	ENSG00000100462	Other SAPs
CLK1	ENSG00000013441	Other SAPs
CLK2	ENSG00000176444	Other SAPs
CLK3	ENSG00000179335	Other SAPs
CLK4	ENSG00000113240	Other SAPs
CDK12	ENSG00000167258	Other SAPs
PPM1G	ENSG00000115241	Other SAPs
SRPK1	ENSG00000096063	Other SAPs
SRPK2	ENSG00000135250	Other SAPs
ZNF326	ENSG00000162664	Other SAPs
LPAR1	ENSG00000198121	Minor
PDCD7	ENSG00000090470	Minor
RECQL5	ENSG00000108469	Minor
RNPC3	ENSG00000185946	Minor
SNRNP25	ENSG00000161981	Minor
SNRNP35	ENSG00000184209	Minor
SNRNP48	ENSG00000168566	Minor
ZCRB1	ENSG00000139168	Minor
ZMAT5	ENSG00000100319	Minor
ZRSR1	ENSG00000212643	Minor
ZRSR2	ENSG00000169249	Minor
ASCL1	ENSG00000139352	chromatin-related
ASH2L	ENSG00000129691	chromatin-related

Gene name	Ensemble ID	Class / Family
BAZ1B	ENSG00000009954	chromatin-related
BRD4	ENSG00000141867	chromatin-related
CBX3	ENSG00000122565	chromatin-related
CHD1	ENSG00000153922	chromatin-related
CTCF	ENSG00000102974	chromatin-related
DEK	ENSG00000124795	chromatin-related
DICER1	ENSG00000100697	chromatin-related
DNMT1	ENSG00000130816	chromatin-related
EHMT2	ENSG00000204371	chromatin-related
AGO2	ENSG00000123908	chromatin-related
EP300	ENSG00000100393	chromatin-related
HDAC1	ENSG00000116478	chromatin-related
HDAC2	ENSG00000196591	chromatin-related
HDAC3	ENSG00000171720	chromatin-related
HDAC4	ENSG00000068024	chromatin-related
HDAC6	ENSG00000094631	chromatin-related
HMGA1	ENSG00000137309	chromatin-related
KAT2A	ENSG00000108773	chromatin-related
KAT2B	ENSG00000114166	chromatin-related
KAT5	ENSG00000172977	chromatin-related
KDM1A	ENSG00000004487	chromatin-related
KHDRBS1	ENSG00000121774	chromatin-related
MBD2	ENSG00000134046	chromatin-related
MECP2	ENSG00000169057	chromatin-related
MORF4L1	ENSG00000185787	chromatin-related
NAB2	ENSG00000166886	chromatin-related
RPS6KA5	ENSG00000100784	chromatin-related
SETD1A	ENSG00000099381	chromatin-related
SETD2	ENSG00000181555	chromatin-related
SIRT1	ENSG00000096717	chromatin-related
SMARCA2	ENSG00000080503	chromatin-related
SMARCA4	ENSG00000127616	chromatin-related
SPEN	ENSG00000065526	chromatin-related
SUV39H1	ENSG00000101945	chromatin-related
TAF15	ENSG00000270647	chromatin-related
TCERG1	ENSG00000113649	chromatin-related
TCERG1L	ENSG00000176769	chromatin-related
TET1	ENSG00000138336	chromatin-related
KDM4B	ENSG00000127663	chromatin-related
BMI1	ENSG00000168283	Polycomb Group Genes
EED	ENSG00000074266	Polycomb Group Genes
EZH2	ENSG00000106462	Polycomb Group Genes
PHC1	ENSG00000111752	Polycomb Group Genes
PHC2	ENSG00000134686	Polycomb Group Genes

Table 22. Selected genes used for functional network reconstruction of splicing regulation.

Large deletions visualization

Sorted BAM files (as explained above) were indexed using SAMtools[422]. Then, indexed BAM files were loaded in IGV[422] for

mapping and coverage track visualization, using hg38 as reference genome. For easier handling of data, BAM files were cut for the *BRAF* gene using SAMtools *view* and *BRAF* coordinates.

6.5 Genome-wide CRISPR knockout screen

For the genome-wide CRISPR knockout screen, we used the TKOv3 library (Toronto Knock-Out), a sgRNA library containing 71,090 guides targeting 18,053 protein-coding genes, following the published protocol[424,425]. We screened the melanoma cell lines, SKMEL293 and C3.

Generation of inducible Cas9/mCherry cell lines

First, $2.5x10^5$ SKMEL293 and "bulk" C3 cells seeded in 6-well plates were infected with lentivirus at 5 different dilutions ranging from 1:5 to 1:500. Lentivirus product was a kind gift from Sergi Aranda (Di Croce Lab, CRG) and was produced by transfection of HEK293T cells with lentiviral envelope and packaging plasmids and the Lenti-iCas9-neo plasmid (Addgene ID# 85400), that contains an inducible reporter downstream of FLAG-tagged spCas9, separated by a P2A self-cleavage sequence. The plasmid was previously modified by inserting the ORF of mCherry as the doxycycline inducible reported instead of EGFP.

Selection media with 1500 µg/ml of Geneticin™ (Life Technologies) was added 24 h after lentivirus infection and replaced every 48-72 h until control wells (not infected) were devoid of live cells. Wells harboring cells with better morphology at the lowest dilution of infection were selected for cell expansion.

Doxycycline tests for iCas9 induction

$3x10^5$ SKMEL293- and C3-, both iCas9/mCherry, cells were seeded in 6-well plates and incubated overnight. Doxycycline at 100, 500, 1000 and 2000 ng/ml was added, and induced cells (DAPI-negative, mCherry positive [yellow-green laser at 561 nm]) were quantified at 24 h and 48 h by flow cytometry in the CRG/UPF Flow Cytometry Unit. For doxycycline induction we chose 500 ng/ml during 48 h, because under these conditions >70% of cells displayes iCas9/mCherry induction (Figure 49).

Single-cell derived BRAF3-9 C3-iCas9/mCherry clone

We performed single-cell derived clones, assisted with FACS (fluorescence activated cell sorting) after 48-hour of doxycycline induction. Alive (DAPI negative) and induced (mCherry positive) cells were single-cell sorted and seeded in 96-well plates. We analyzed by RT-PCR BRAF mRNAs and detected 15 of 27 clones (55.6%) expressing the BRAF3-9 transcript (Figure 50). We then selected clones expressing both the full BRAF and BRAF3-9 for cell expansion.

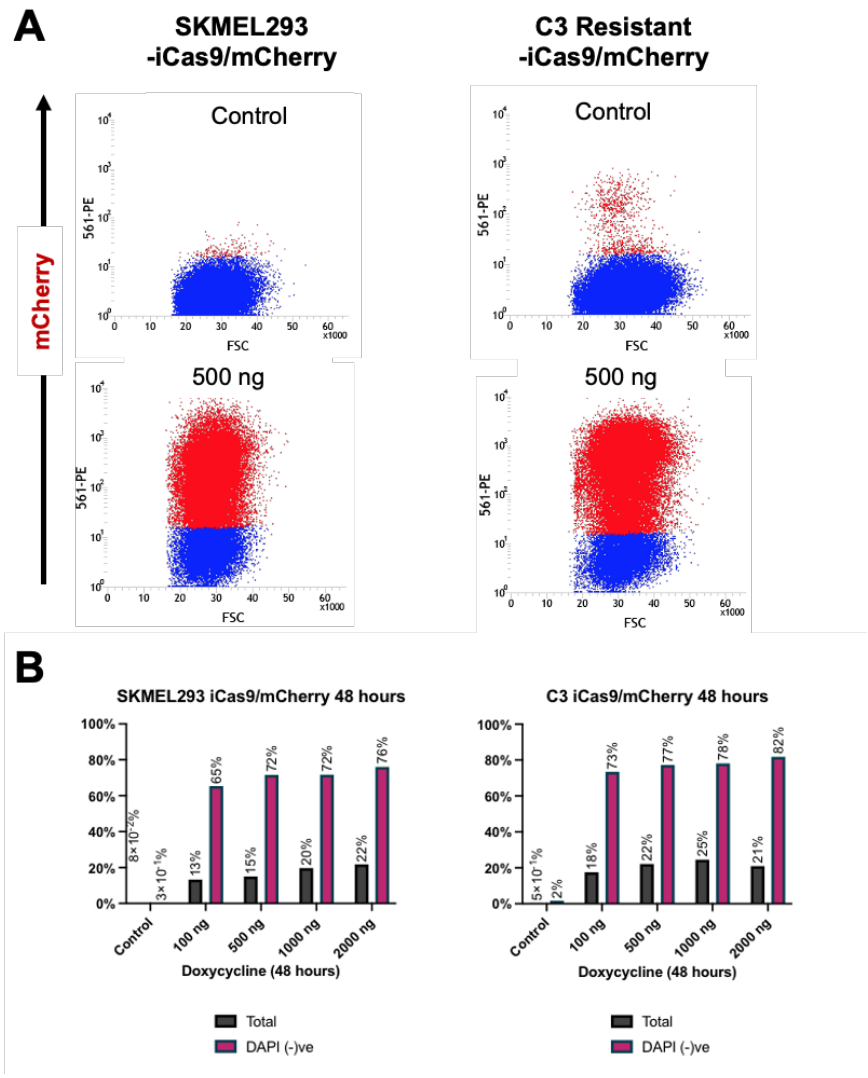

Figure 49. Tests of doxycycline-mediated induction of iCas9/mCherry in SKMEL293-iCas9/mCherry and C3-iCas9/mCherry at 48 hours. A | Schematic representation of flow cytometry analysis of mCherry for both cell lines without doxycycicline (Control) and with 500 ng/ml of doxycycline**. B** | Proportions of the corresponding populations shown in panel A are shown for total number of cells (grey) and for alive cells (DAPI negative, in dark pink).

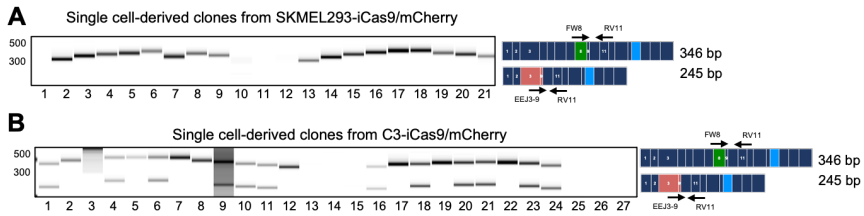

Figure 50. Analysis of the pattern of BRAF splicing in single cell-derived clones from SKMEL293-iCas9/mCherry (A) **and C3-iCas9/mCherry** (B)**.** RT-PCR analyses of the individual clones indicated clones were carried out by RT-PCR using forward primers in exon 8 (full BRAF) / exon-junction 3-9 and a reverse primer in exon 11. The position expected for the amplification products corresponding to the full-length transcript (upper 346 bp product) and the 3-9 mRNA isoform (lower 245 bp product) are indicated.

Cell line characterization for screening

Before screening our cell lines, we characterized the doubling time of cells and tested the cell lines for hexadimethrine bromide (Polybrene, Sigma-Aldrich) sensitivity and puromycin sensitivity for selection of TKOv3 library.

Doubling time

We measured the doubling time of $1x10^5$ cells of the 3 cell lines (SKMEL293-iCas9/mCherry, "bulk" C3-iCas9/mCherry and BRAF3-9 C3-iCas9/mCherry) after seeding them in triplicates in a 6-well plate. After 76 h of incubation, we counted the number of cells with Countess™ Automated Cell Counter (Invitrogen) after adding 10 µl of trypan blue to 10 µl of cells. Doubling time was calculated as follows: duration (hours) x log (2) / [log(final concentration) – log(initial concentration)]. Doubling times of 27 h, 25 h and 25 h were calculated for SKMEL293-iCas9/mCherry, "bulk" C3-iCas9/mCherry and BRAF3-9 C3-iCas9/mCherry, respectively.

Puromycin and hexadimethrine bromide sensitivity

To determine puromycin concentration for selection and sensitivity to hexadimethrine bromide, we seeded $1x10^5$ cells in 12-well plates and, after overnight incubation, we added puromycin and hexadimethrine bromide at different concentrations. 72 hours later, cell viability was measured using the resazurin assay (as detailed above). According to our results (Figure 51), we decided to avoid the use of hexadimethrine bromide and to select TKOv3-infected cells with 2 µg/ml puromycin.

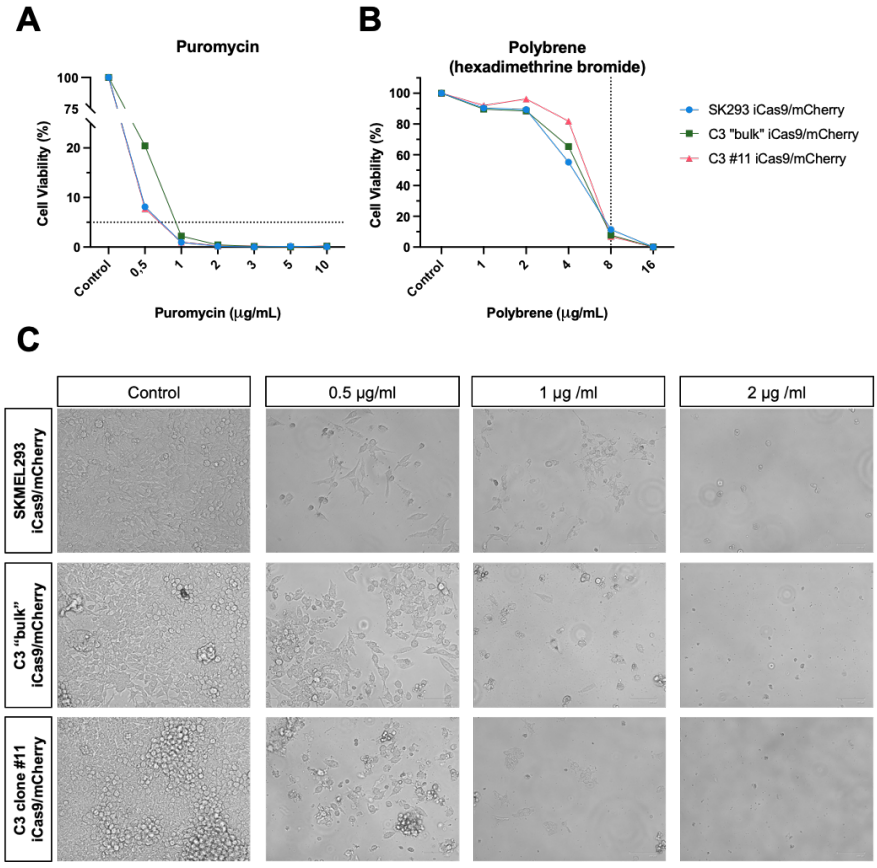

Figure 51. Puromycin and hexadimethrine bromide sensitivity tests. A | Cell viability, measured using resazurin assays, at 72 hours after puromycin addition for

the 3 cell lines. **B |** Cell viability, measured using resazurin assays, at 72 hours after hexadimethrine bromide addition for the 3 cell lines. **C |** Representative images of the 3 iCas9/mCherry-positive cell lines (rows) after 72 hours of puromycin selection at different concentrations of the drug (with 0, 0.5, 1 and 2 μg/ml) (columns).

sgRNA library amplification

pLCKO2::TKOv3 (Addgene ID# 125517) was electroporated in Endura electrocompetent cells. 100 ng of TKOv3 library was electroporated in 25 μl of electrocompetent cells at 10 uF, 600 Ohms, 1800 V using Gene Pulser Xcell™ Electroporation system (BioRad). Recovered cells were incubated at 37ºC for 1 h and then were pooled.

A 40,000-fold dilution of this pool of recovery medium was seeded in a 10-cm LB carbenicillin supplemented plate and incubated for 16 h at 30ºC. As approximately 2,000 colonies were identified, corresponding to 500-1000 colonies per sgRNA, we proceeded with library amplification. Recovered cells were plated in 20 15-cm LB carbenicillin supplemented plates. After incubation as mentioned above, colonies from 20 plates were harvested in LB supplemented with carbenicillin, pelleted and DNA plasmid purified using QIAprep® Spin Maxiprep Kit (Qiagen).

Large-scale CRISPR sgRNA library lentivirus production

6,5-8x10^6 cells HEK293-T were seeded in 15-cm plates and incubated overnight. Transfection plasmids mixtures, at 1:1:1 molar ratio, were prepared: lentiviral packaging plasmid psPAX (Addgene ID# 12260) (7 μg/plate), the VSV-G (Vesicular Stomatitis Virus Glucoprotein) envelope expressing plasmid pMD2.G (Addgene ID# 12259) (4 μg/plate), and the sgRNA library pLCKO2::TKOv3 (5

μg/plate). Transfections were performed using 48 μl/plate of lipid-based reagent Lipofectamine 2000 (Invitrogen) at a 3:1 ratio of transfection reagent: μg of DNA complex. After 18 h of incubation at 37ºC and 5% CO_2, media was replaced by viral harvest media (500 ml DMEM supplemented with 6.4g of filter-sterilized BSA [bovine serum albumin] and 1% penicillin / streptomycin). After 24 h of incubation, lentivirus-containing supernatant was collected and aliquoted.

Determination of MOI

The MOI (multiplicity of infection) calculation is a critical step in a genome-scale CRISPR screen. To achieve a single transduction event (1 sgRNA per cell), the lentivirus library product must be infected at lower MOI, usually around 0.3. Higher MOIs can result in transduction of multiple sgRNAs per cell, potentially leading to misleading outcomes due to the coincidence of multiple genetic perturbations in the same cell.

For functional titration of the pooled CRISPR sgRNA lentiviral library, we tested each cell line in triplicate with different volumes of the virus preparation (0, 0.25, 0.5, 1 and 2 ml) in 15-cm plates with 0.8-1x106 cells. After 24 h of infection, virus media was replaced and selection media containing puromycin 2 μg/ml was added (calculated as described above) for 72 h. Cells from each cell line and triplicate corresponding to infection with different virus volumes were counted using the Countess™ Automated Cell Counter (Invitrogen), as previously described, and then the volume of the virus preparation that led to 30-40% cell survival was considered optimal to achieve

our desired MOI. These volumes were 0.5 ml, 1 ml, and 1 ml for SKMEL293-iCas9/mCherry, "bulk" C3-iCas9/mCherry and BRAF3-9 C3-iCas9/mCherry, respectively (Figure 52).

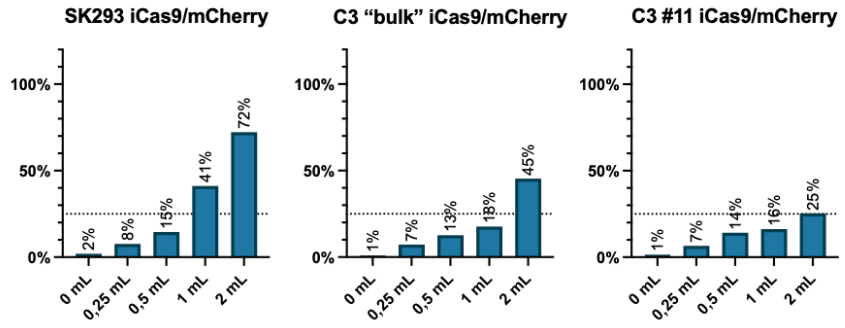

Figure 52. Cell survival (%) after 72 hours of puromycin selection. The percentage of alive cells was related to the volume of virus preparation that was transduced to cells with no subsequent puromycin selection. The dashed line represents a 25% of survival. For an approximate MOI ≤0.3, 0.5 ml, 1 ml and 1 ml were selected for SKMEL293-, "bulk" C3- and BRAF3-9 C3 (clone #11)-iCas9/mCherry, respectively.

Primary screen infection, selection, and cell passaging

Taking into account the MOI calculated using the volume of the virus preparation and the doubling time of each cell line, together with a minimum library coverage of 200-fold for each sgRNA and a recommended 400-fold coverage at time point T0 to ensure optimal sgRNA representation, we seeded 30-35 15-cm plates with $7.5x10^6$ cells per plate. After 24 h incubation, puromycin selection media was added for 48 h (after which the control uninfected cell culture showed no live cells). All the cells from the same cell line were trypsinized and pooled together. Three replicates of approximately $40x10^6$ cell were harvested for gDNA extraction at T0. From the pool of each cell

line, we plated cells into 3 replicates with a total of 15-20x10^6 cells (each replicate of each cell line seeded in 3-5 15-cm plates). This high number of cells ensure a 200-fold representation of each sgRNA, and that this representation is maintained through different passages. Then, 500 ng/ml of doxycycline was added at d+1 for an additional 48 h to induce expression of iCas9/mCherry (Figure 53). Cells were grown in complete media supplemented with vemurafenib 10 μM (in case of the 2 resistant cell lines). At every passage, cells from all wells of in the same replicate were pooled together, mixed and plated again for continuing with the screen. Cells were harvested at d+4 (T1), d+8 (T2), d+14 (T3) and d+28 (T4). A minimum of 20x10^6 cells were collected by centrifugation for gDNA extraction.

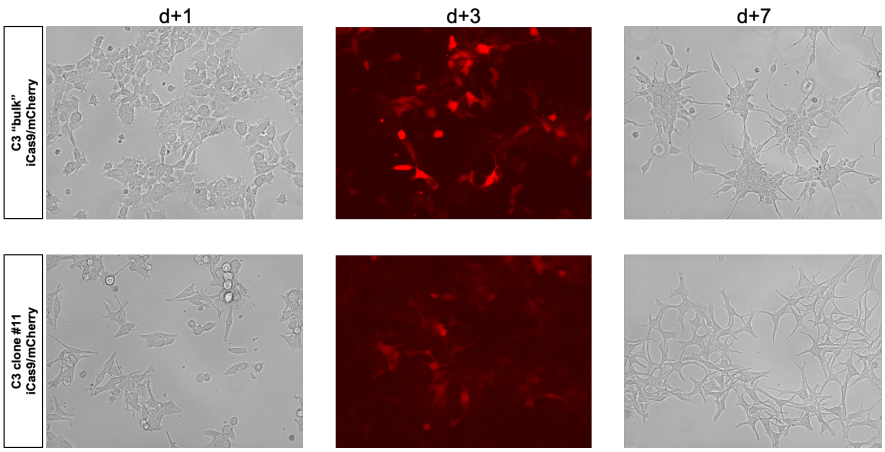

Figure 53. Representative images of "bulk" C3 iCas9/mCherry (upper row) **and BRAF3-9 C3 clone #11 iCas9-mCherry** (bottom row). Images shown correspond to d+1, d+3 after 48 h of doxycycline induction (mCherry visualized with specific fluorescence channel) and d+7.

Sample preparation and sequencing

Genomic DNA extraction

Genomic DNA (gDNA) was purified from thawed pellets of each replicate at all time points, from the three different cell lines, using phenol/chloroform/isoamyl alcohol (PCI) solution (25:24:1), pH 7.8-8.2 (Sigma-Aldrich). First, we washed the pellets with PBS and resuspended them in a digestion buffer containing 100 mM NaCl, 10 mM Tris pH 8.9, 25 mM EDTA, 0.5% SDS (Sodium Dodecyl Sulphate) and 0.1 mg/ml proteinase K. Resuspended cells were incubated overnight in a shaking dry bath at 50ºC, 500 rpm. Next, an equal volume of PCI was added, vortexed vigorously and spined at 15,000 rpm for 5 min. The aqueous solution was removed, and another PCI extraction was carried out. Prior to precipitation, an extra wash with chloroform was carried out and then 5M NaCl was added to a final concentration of 0.1 M, followed by addition of 2.5 volumes of 100% ethanol for nucleic acid precipitation. After incubation at -20ºC for 4 h, the samples were centrifuged for 20 min at 15,000 rpm and the DNA pellet resuspended in 720 µl nuclease-free water (Invitrogen). RNase treatment was carried out with 8 µl of RNase ONE™ ribonuclease (Promega) and 80 µl of the corresponding buffer. To remove buffer and enzymes, a PCI extraction was carried out, followed by a chloroform extraction and ethanol precipitation.

CRISPR sequencing library preparation

First, multiple PCRs using 3.5 µg gDNA in 50 µl volume reaction, reaching a total of 100 µg of gDNA to be amplified (to achieve a representative coverage) were set up. For each 50 µl reaction, 25 µl of Q5® High-Fidelity Master Mix (New England Biolabs) and 2.5 µl of each 10 mM primers (listed in Table 21) were used. PCR cycles consisted of an initial incubation at 98°C (30’’), 25 cycles of 98°C

(10”), 66°C (30”), 72°C (15”) and a final incubation at 72°C (2’). All individual 50 µl reactions were pooled and mixed thoroughly.

5 µl of previously pooled PCR were used as template to set up a second 50 µl PCR with 2.5 µl 10 mM of primers (listed in Table 21) and 25 µl of Q5® High-Fidelity Master Mix (New England Biolabs). For this second PCR, a mix of forward primers were used. These forward primers were designed to anneal with an Illumina Adapter sequence (ACACTCTTTCCCTACACGACGCTCTTCCGATCT), a frameshift ranging from 2-Ns to 6-Ns was inserted to increase sequencing diversity followed by the vector-specific sequence (TTGTGGAAAGGACGAGGTACCG). PCR cycling consisted of initial incubation at 98°C (30’’), 10 cycles of 98°C (10”), 55°C (30”), 65°C (15”) and a final incubation at 65°C (5’). The resulting products were run in 2% agarose gels and the expected 200-bp amplification band was excised and DNA was purified from a gel (as previously detailed). An additional PCR to add unique barcodes combinations was included. Amplicon sequencing was performed using NextSeq 2000 (Illumina), following 1x50 bp single red protocol, at the CRG Genomics Facility. $30x10^6$ for T0 samples and $15x10^6$ reads for the remaining samples were requested for optimal sgRNA coverage and representation.

Data analysis: MAGeCK and BAGEL

Raw sequence data in fastq files were first trimmed with *cutadapt*[426] tool, to remove the vector-specific sequence and the 2-6(Ns).

First, we performed a computational analysis of the CRISPR screen using MAGeCK[427]. We run the *mageck count* command for all

trimmed fastq files, and reads were mapped against the TKOv3 library. With the read count table, we run the *mageck test* subcommand, which uses robust rank aggregation (RRA) method, to calculate scores by comparing T0 versus T2 of each cell line. We removed sgRNAs whose mean value was zero in control, therefore corresponding to a non-transduced sgRNA; and normalized the read counts by counts of sgRNA of non-essential genes. Non-essential genes were defined as those genes which are rarely expressed across a panel of cell lines, a set that was established in previous reports for the application of TKOv3 library for CRISPR screens[405,428].

We also used the *mageck mle* subcommand for multiple condition screening. This subcommand utilizes a maximum-likelihood estimation for robust identification of hits. A binary matrix must be provided, indicating which sample (first column) is affected by which condition (subsequent columns) (Table 23).

For data visualization (including quality control and functional analyses), *MAGeCKFlute*[427] package was used in R (v4). Beta scores from mageck mle calculations were normalized with "loess" method, based on negative control genes.

Additionally, we also performed computational analysis with BAGEL (Bayesian Analysis of Gene EssentiaLity)[405,428]. Before using BAGEL, sequences were mapped using *Bowtie*[429] using the TKOv3 library as reference and the following parameters: -v2 (allowing 2 mismatches) and -m1 (discarding any read that mapped to more than one sequence in the library). Fold changes and Bayes

factors were calculated then with the BAGEL algorithm (https://github.com/hart-lab/bagel).

sample	baseline	as_braf_early	sensitive_early	resistant_early	as_braf_late	sensitive_late	resistant_late
SK1_T0	1	0	0	0	0	0	0
SK2_T0	1	0	0	0	0	0	0
SK3_T0	1	0	0	0	0	0	0
SK1_T1	1	0	1	0	0	0	0
SK2_T1	1	0	1	0	0	0	0
SK3_T1	1	0	1	0	0	0	0
SK1_T2	1	0	0	0	0	1	0
SK2_T2	1	0	0	0	0	1	0
SK3_T2	1	0	0	0	0	1	0
BU1_T0	1	0	0	0	0	0	0
BU2_T0	1	0	0	0	0	0	0
BU3_T0	1	0	0	0	0	0	0
BU1_T1	1	0	0	1	0	0	0
BU2_T1	1	0	0	1	0	0	0
BU3_T1	1	0	0	1	0	0	0
BU1_T2	1	0	0	0	0	0	1
BU2_T2	1	0	0	0	0	0	1
BU3_T2	1	0	0	0	0	0	1
CL1_T0	1	0	0	0	0	0	0
CL2_T0	1	0	0	0	0	0	0
CL3_T0	1	0	0	0	0	0	0
CL1_T1	1	1	0	0	0	0	0
CL2_T1	1	1	0	0	0	0	0
CL3_T1	1	1	0	0	0	0	0
CL1_T2	1	0	0	0	1	0	0
CL2_T2	1	0	0	0	1	0	0
CL3_T2	1	0	0	0	1	0	0

Table 23. The design matrix file for mageck mle. Each sample replicate (e.g., SK1, SK2, SK3 for SKMEL293, BU1, BU2, BU3 for "bulk" C3; and CL1, CL2 and CL3, for BRAF3-9 C3 clone) of each time point (T0, T1 and T2) are distributed across the rows. Each column represents a condition: baseline for T0; as_braf for BRAF3-9 resistant; sensitive for parental SKMEL293; resistant for "bulk" C3 resistant; early, for T1; late for T2.

Plots for data visualization from BAGEL analysis were generated with the *ggplot2*[418] package in R (v4).

Bibliography

1. Crick F. Central Dogma of Molecular Biology. *Nature*. 1970;227(5258):561-563. doi:10.1038/227561a0
2. Manning KS, Cooper TA. The roles of RNA processing in translating genotype to phenotype. *Nat Rev Mol Cell Biol*. 2017;18(2):102-114. doi:10.1038/nrm.2016.139
3. Galloway A, Cowling VH. mRNA cap regulation in mammalian cell function and fate. *Biochimica et Biophysica Acta (BBA) - Gene Regulatory Mechanisms*. 2019;1862(3):270-279. doi:10.1016/j.bbagrm.2018.09.011
4. Elkon R, Ugalde AP, Agami R. Alternative cleavage and polyadenylation: extent, regulation and function. *Nat Rev Genet*. 2013;14(7):496-506. doi:10.1038/nrg3482
5. Berget SM, Moore C, Sharp PA. Spliced segments at the 5' terminus of adenovirus 2 late mRNA. *Proc Natl Acad Sci U S A*. 1977;74(8):3171-3175.
6. Chow LT, Gelinas RE, Broker TR, Roberts RJ. An amazing sequence arrangement at the 5' ends of adenovirus 2 messenger RNA. *Cell*. 1977;12(1):1-8. doi:10.1016/0092-8674(77)90180-5
7. Crick F. Split genes and RNA splicing. *Science*. 1979;204(4390):264-271. doi:10.1126/science.373120
8. Pan Q, Shai O, Lee LJ, Frey BJ, Blencowe BJ. Deep surveying of alternative splicing complexity in the human transcriptome by high-throughput sequencing. *Nat Genet*. 2008;40(12):1413-1415. doi:10.1038/ng.259
9. Wang ET, Sandberg R, Luo S, et al. Alternative isoform regulation in human tissue transcriptomes. *Nature*. 2008;456(7221):470-476. doi:10.1038/nature07509
10. Lander ES, Linton LM, Birren B, et al. Initial sequencing and analysis of the human genome. *Nature*. 2001;409(6822):860-921. doi:10.1038/35057062
11. Venter JC, Adams MD, Myers EW, et al. The Sequence of the Human Genome. *Science*. 2001;291(5507):1304-1351. doi:10.1126/science.1058040
12. Wahl MC, Will CL, Lührmann R. The Spliceosome: Design Principles of a Dynamic RNP Machine. *Cell*. 2009;136(4):701-718. doi:10.1016/j.cell.2009.02.009
13. Carrillo Oesterreich F, Herzel L, Straube K, Hujer K, Howard J, Neugebauer KM. Splicing of Nascent RNA Coincides

with Intron Exit from RNA Polymerase II. *Cell*. 2016;165(2):372-381. doi:10.1016/j.cell.2016.02.045
14. Kennedy CF, Berget SM. Pyrimidine tracts between the 5' splice site and branch point facilitate splicing and recognition of a small Drosophila intron. *Mol Cell Biol*. 1997;17(5):2774-2780. doi:10.1128/MCB.17.5.2774
15. Robberson BL, Cote GJ, Berget SM. Exon definition may facilitate splice site selection in RNAs with multiple exons. *Mol Cell Biol*. 1990;10(1):84-94. doi:10.1128/mcb.10.1.84-94.1990
16. Zhang MQ. Statistical Features of Human Exons and Their Flanking Regions. *Human Molecular Genetics*. 1998;7(5):919-932. doi:10.1093/hmg/7.5.919
17. Sun H, Chasin LA. Multiple Splicing Defects in an Intronic False Exon. *Molecular and Cellular Biology*. 2000;20(17):6414-6425. doi:10.1128/MCB.20.17.6414-6425.2000
18. Schwartz S, Silva J, Burstein D, Pupko T, Eyras E, Ast G. Large-scale comparative analysis of splicing signals and their corresponding splicing factors in eukaryotes. *Genome Res*. 2008;18(1):88-103. doi:10.1101/gr.6818908
19. Izquierdo JM, Valcárcel J. A simple principle to explain the evolution of pre-mRNA splicing. *Genes Dev*. 2006;20(13):1679-1684. doi:10.1101/gad.1449106
20. Irimia M, Penny D, Roy SW. Coevolution of genomic intron number and splice sites. *Trends in Genetics*. 2007;23(7):321-325. doi:10.1016/j.tig.2007.04.001
21. Irimia M, Roy SW, Neafsey DE, Abril JF, Garcia-Fernandez J, Koonin EV. Complex selection on 5′ splice sites in intron-rich organisms. *Genome Res*. 2009;19(11):2021-2027. doi:10.1101/gr.089276.108
22. Query CC, Moore MJ, Sharp PA. Branch nucleophile selection in pre-mRNA splicing: evidence for the bulged duplex model. *Genes Dev*. 1994;8(5):587-597. doi:10.1101/gad.8.5.587
23. Reed R. Initial splice-site recognition and pairing during pre-mRNA splicing. *Current Opinion in Genetics & Development*. 1996;6(2):215-220. doi:10.1016/S0959-437X(96)80053-0
24. Hertel KJ. Combinatorial Control of Exon Recognition *. *Journal of Biological Chemistry*. 2008;283(3):1211-1215. doi:10.1074/jbc.R700035200
25. Roca X, Sachidanandam R, Krainer AR. Determinants of the inherent strength of human 5' splice sites. *RNA*. 2005;11(5):683-698. doi:10.1261/rna.2040605

26. Turunen JJ, Niemelä EH, Verma B, Frilander MJ. The significant other: splicing by the minor spliceosome. *Wiley Interdiscip Rev RNA*. 2013;4(1):61-76. doi:10.1002/wrna.1141
27. Will CL, Lührmann R. Splicing of a rare class of introns by the U12-dependent spliceosome. *Biol Chem*. 2005;386(8):713-724. doi:10.1515/BC.2005.084
28. Padgett RA, Konarska MM, Grabowski PJ, Hardy SF, Sharp PA. Lariat RNA's as intermediates and products in the splicing of messenger RNA precursors. *Science*. 1984;225(4665):898-903. doi:10.1126/science.6206566
29. Ruskin B, Krainer AR, Maniatis T, Green MR. Excision of an intact intron as a novel lariat structure during pre-mRNA splicing in vitro. *Cell*. 1984;38(1):317-331. doi:10.1016/0092-8674(84)90553-1
30. Grabowski PJ, Padgett RA, Sharp PA. Messenger RNA splicing in vitro: an excised intervening sequence and a potential intermediate. *Cell*. 1984;37(2):415-427. doi:10.1016/0092-8674(84)90372-6
31. Papasaikas P, Valcárcel J. The Spliceosome: The Ultimate RNA Chaperone and Sculptor. *Trends in Biochemical Sciences*. 2016;41(1):33-45. doi:10.1016/j.tibs.2015.11.003
32. Will CL, Lührmann R. Spliceosome Structure and Function. *Cold Spring Harb Perspect Biol*. 2011;3(7):a003707. doi:10.1101/cshperspect.a003707
33. Shi Y. Mechanistic insights into precursor messenger RNA splicing by the spliceosome. *Nat Rev Mol Cell Biol*. 2017;18(11):655-670. doi:10.1038/nrm.2017.86
34. Konarska MM, Vilardell J, Query CC. Repositioning of the Reaction Intermediate within the Catalytic Center of the Spliceosome. *Molecular Cell*. 2006;21(4):543-553. doi:10.1016/j.molcel.2006.01.017
35. Bonnal SC, López-Oreja I, Valcárcel J. Roles and mechanisms of alternative splicing in cancer — implications for care. *Nat Rev Clin Oncol*. 2020;17(8):457-474. doi:10.1038/s41571-020-0350-x
36. Kim MS, Pinto SM, Getnet D, et al. A draft map of the human proteome. *Nature*. 2014;509(7502):575-581. doi:10.1038/nature13302
37. Tress ML, Abascal F, Valencia A. Alternative Splicing May Not Be the Key to Proteome Complexity. *Trends Biochem Sci*. 2017;42(2):98-110. doi:10.1016/j.tibs.2016.08.008

38. Tress ML, Abascal F, Valencia A. Most Alternative Isoforms Are Not Functionally Important. *Trends Biochem Sci*. 2017;42(6):408-410. doi:10.1016/j.tibs.2017.04.002
39. Blencowe BJ. The Relationship between Alternative Splicing and Proteomic Complexity. *Trends Biochem Sci*. 2017;42(6):407-408. doi:10.1016/j.tibs.2017.04.001
40. Goren A, Ram O, Amit M, et al. Comparative Analysis Identifies Exonic Splicing Regulatory Sequences—The Complex Definition of Enhancers and Silencers. *Molecular Cell*. 2006;22(6):769-781. doi:10.1016/j.molcel.2006.05.008
41. Fairbrother WG, Yeh RF, Sharp PA, Burge CB. Predictive identification of exonic splicing enhancers in human genes. *Science*. 2002;297(5583):1007-1013. doi:10.1126/science.1073774
42. Wang Z, Burge CB. Splicing regulation: From a parts list of regulatory elements to an integrated splicing code. *RNA*. 2008;14(5):802-813. doi:10.1261/rna.876308
43. Buratti E, Baralle FE. Influence of RNA secondary structure on the pre-mRNA splicing process. *Mol Cell Biol*. 2004;24(24):10505-10514. doi:10.1128/MCB.24.24.10505-10514.2004
44. Fu XD, Ares M. Context-dependent control of alternative splicing by RNA-binding proteins. *Nat Rev Genet*. 2014;15(10):689-701. doi:10.1038/nrg3778
45. Graveley BR. Sorting out the complexity of SR protein functions. *RNA*. 2000;6(9):1197-1211.
46. Jeong S. SR Proteins: Binders, Regulators, and Connectors of RNA. *Mol Cells*. 2017;40(1):1-9. doi:10.14348/molcells.2017.2319
47. Änkö ML, Müller-McNicoll M, Brandl H, et al. The RNA-binding landscapes of two SR proteins reveal unique functions and binding to diverse RNA classes. *Genome Biology*. 2012;13(3):R17. doi:10.1186/gb-2012-13-3-r17
48. Pandit S, Zhou Y, Shiue L, et al. Genome-wide analysis reveals SR protein cooperation and competition in regulated splicing. *Mol Cell*. 2013;50(2):223-235. doi:10.1016/j.molcel.2013.03.001
49. Lam BJ, Hertel KJ. A general role for splicing enhancers in exon definition. *RNA*. 2002;8(10):1233-1241.
50. Schaal TD, Maniatis T. Multiple Distinct Splicing Enhancers in the Protein-Coding Sequences of a Constitutively Spliced Pre-mRNA. *Molecular and Cellular Biology*.

1999;19(1):261-273. doi:10.1128/MCB.19.1.261
51. Valcárcel J, Gebauer F. Post-transcriptional regulation: The dawn of PTB. *Current Biology*. 1997;7(11):R705-R708. doi:10.1016/S0960-9822(06)00361-7
52. Wagner EJ, Garcia-Blanco MA. Polypyrimidine tract binding protein antagonizes exon definition. *Mol Cell Biol*. 2001;21(10):3281-3288. doi:10.1128/MCB.21.10.3281-3288.2001
53. García-Blanco MA, Jamison SF, Sharp PA. Identification and purification of a 62,000-dalton protein that binds specifically to the polypyrimidine tract of introns. *Genes Dev*. 1989;3(12A):1874-1886. doi:10.1101/gad.3.12a.1874
54. Bothwell AL, Ballard DW, Philbrick WM, et al. Murine polypyrimidine tract binding protein. Purification, cloning, and mapping of the RNA binding domain. *J Biol Chem*. 1991;266(36):24657-24663.
55. Zhu J, Mayeda A, Krainer AR. Exon identity established through differential antagonism between exonic splicing silencer-bound hnRNP A1 and enhancer-bound SR proteins. *Mol Cell*. 2001;8(6):1351-1361. doi:10.1016/s1097-2765(01)00409-9
56. Tange TØ, Damgaard CK, Guth S, Valcárcel J, Kjems J. The hnRNP A1 protein regulates HIV-1 tat splicing via a novel intron silencer element. *EMBO J*. 2001;20(20):5748-5758. doi:10.1093/emboj/20.20.5748
57. House AE, Lynch KW. An exonic splicing silencer represses spliceosome assembly after ATP-dependent exon recognition. *Nat Struct Mol Biol*. 2006;13(10):937-944. doi:10.1038/nsmb1149
58. Martinez-Contreras R, Fisette JF, Nasim F ul H, Madden R, Cordeau M, Chabot B. Intronic Binding Sites for hnRNP A/B and hnRNP F/H Proteins Stimulate Pre-mRNA Splicing. *PLoS Biol*. 2006;4(2):e21. doi:10.1371/journal.pbio.0040021
59. Gehring NH, Roignant JY. Anything but Ordinary – Emerging Splicing Mechanisms in Eukaryotic Gene Regulation. *Trends in Genetics*. 2021;37(4):355-372. doi:10.1016/j.tig.2020.10.008
60. Ule J, Stefani G, Mele A, et al. An RNA map predicting Nova-dependent splicing regulation. *Nature*. 2006;444(7119):580-586. doi:10.1038/nature05304
61. Chen M, Manley JL. Mechanisms of alternative splicing regulation: insights from molecular and genomics approaches. *Nat Rev Mol Cell Biol*. 2009;10(11):741-754. doi:10.1038/nrm2777
62. Gallego-Paez LM, Bordone MC, Leote AC, Saraiva-

Agostinho N, Ascensão-Ferreira M, Barbosa-Morais NL. Alternative splicing: the pledge, the turn, and the prestige. *Hum Genet*. 2017;136(9):1015-1042. doi:10.1007/s00439-017-1790-y
63. Baralle FE, Giudice J. Alternative splicing as a regulator of development and tissue identity. *Nat Rev Mol Cell Biol*. 2017;18(7):437-451. doi:10.1038/nrm.2017.27
64. Irimia M, Weatheritt RJ, Ellis JD, et al. A Highly Conserved Program of Neuronal Microexons Is Misregulated in Autistic Brains. *Cell*. 2014;159(7):1511-1523. doi:10.1016/j.cell.2014.11.035
65. Underwood JG, Boutz PL, Dougherty JD, Stoilov P, Black DL. Homologues of the Caenorhabditis elegans Fox-1 protein are neuronal splicing regulators in mammals. *Mol Cell Biol*. 2005;25(22):10005-10016. doi:10.1128/MCB.25.22.10005-10016.2005
66. Saltzman AL, Pan Q, Blencowe BJ. Regulation of alternative splicing by the core spliceosomal machinery. *Genes Dev*. 2011;25(4):373-384. doi:10.1101/gad.2004811
67. Papasaikas P, Tejedor JR, Vigevani L, Valcárcel J. Functional Splicing Network Reveals Extensive Regulatory Potential of the Core Spliceosomal Machinery. *Molecular Cell*. 2015;57(1):7-22. doi:10.1016/j.molcel.2014.10.030
68. Kornblihtt AR, Schor IE, Alló M, Dujardin G, Petrillo E, Muñoz MJ. Alternative splicing: a pivotal step between eukaryotic transcription and translation. *Nat Rev Mol Cell Biol*. 2013;14(3):153-165. doi:10.1038/nrm3525
69. Barash Y, Calarco JA, Gao W, et al. Deciphering the splicing code. *Nature*. 2010;465(7294):53-59. doi:10.1038/nature09000
70. Ben-Dov C, Hartmann B, Lundgren J, Valcárcel J. Genome-wide Analysis of Alternative Pre-mRNA Splicing*. *Journal of Biological Chemistry*. 2008;283(3):1229-1233. doi:10.1074/jbc.R700033200
71. Blencowe BJ. Alternative Splicing: New Insights from Global Analyses. *Cell*. 2006;126(1):37-47. doi:10.1016/j.cell.2006.06.023
72. Hallegger M, Llorian M, Smith CWJ. Alternative splicing: global insights. *FEBS J*. 2010;277(4):856-866. doi:10.1111/j.1742-4658.2009.07521.x
73. Fagnani M, Barash Y, Ip JY, et al. Functional coordination of alternative splicing in the mammalian central nervous system.

Genome Biol. 2007;8(6):R108. doi:10.1186/gb-2007-8-6-r108
74. Lee SCW, Abdel-Wahab O. Therapeutic targeting of splicing in cancer. *Nat Med*. 2016;22(9):976-986. doi:10.1038/nm.4165
75. Dvinge H, Kim E, Abdel-Wahab O, Bradley RK. RNA splicing factors as oncoproteins and tumour suppressors. *Nat Rev Cancer*. 2016;16(7):413-430. doi:10.1038/nrc.2016.51
76. Kahles A, Lehmann KV, Toussaint NC, et al. Comprehensive Analysis of Alternative Splicing Across Tumors from 8,705 Patients. *Cancer Cell*. 2018;34(2):211-224.e6. doi:10.1016/j.ccell.2018.07.001
77. Seiler M, Peng S, Agrawal AA, et al. Somatic Mutational Landscape of Splicing Factor Genes and Their Functional Consequences across 33 Cancer Types. *Cell Reports*. 2018;23(1):282-296.e4. doi:10.1016/j.celrep.2018.01.088
78. Dvinge H, Bradley RK. Widespread intron retention diversifies most cancer transcriptomes. *Genome Medicine*. 2015;7(1):45. doi:10.1186/s13073-015-0168-9
79. Supek F, Miñana B, Valcárcel J, Gabaldón T, Lehner B. Synonymous Mutations Frequently Act as Driver Mutations in Human Cancers. *Cell*. 2014;156(6):1324-1335. doi:10.1016/j.cell.2014.01.051
80. Danan-Gotthold M, Golan-Gerstl R, Eisenberg E, Meir K, Karni R, Levanon EY. Identification of recurrent regulated alternative splicing events across human solid tumors. *Nucleic Acids Res*. 2015;43(10):5130-5144. doi:10.1093/nar/gkv210
81. Marabti EE, Abdel-Wahab O. Therapeutic Modulation of RNA Splicing in Malignant and Non-Malignant Disease. *Trends in Molecular Medicine*. 2021;27(7):643-659. doi:10.1016/j.molmed.2021.04.005
82. Stanley RF, Abdel-Wahab O. Dysregulation and therapeutic targeting of RNA splicing in cancer. *Nat Cancer*. 2022;3(5):536-546. doi:10.1038/s43018-022-00384-z
83. Chen L, Tovar-Corona JM, Urrutia AO. Increased levels of noisy splicing in cancers, but not for oncogene-derived transcripts. *Hum Mol Genet*. 2011;20(22):4422-4429. doi:10.1093/hmg/ddr370
84. Jung H, Lee D, Lee J, et al. Intron retention is a widespread mechanism of tumor-suppressor inactivation. *Nat Genet*. 2015;47(11):1242-1248. doi:10.1038/ng.3414
85. Cao S, Zhou DC, Oh C, et al. Discovery of driver non-coding splice-site-creating mutations in cancer. *Nat Commun*.

2020;11(1):5573. doi:10.1038/s41467-020-19307-6
86. Yoshida K, Sanada M, Shiraishi Y, et al. Frequent pathway mutations of splicing machinery in myelodysplasia. *Nature*. 2011;478(7367):64-69. doi:10.1038/nature10496
87. Papaemmanuil E, Cazzola M, Boultwood J, et al. Somatic SF3B1 mutation in myelodysplasia with ring sideroblasts. *N Engl J Med*. 2011;365(15):1384-1395. doi:10.1056/NEJMoa1103283
88. Harbour JW, Roberson EDO, Anbunathan H, Onken MD, Worley LA, Bowcock AM. Recurrent mutations at codon 625 of the splicing factor SF3B1 in uveal melanoma. *Nat Genet*. 2013;45(2):133-135. doi:10.1038/ng.2523
89. Martin M, Maßhöfer L, Temming P, et al. Exome sequencing identifies recurrent somatic mutations in EIF1AX and SF3B1 in uveal melanoma with disomy 3. *Nat Genet*. 2013;45(8):933-936. doi:10.1038/ng.2674
90. Suzuki H, Kumar SA, Shuai S, et al. Recurrent noncoding U1 snRNA mutations drive cryptic splicing in SHH medulloblastoma. *Nature*. 2019;574(7780):707-711. doi:10.1038/s41586-019-1650-0
91. Wang L, Lawrence MS, Wan Y, et al. SF3B1 and Other Novel Cancer Genes in Chronic Lymphocytic Leukemia. *New England Journal of Medicine*. 2011;365(26):2497-2506. doi:10.1056/NEJMoa1109016
92. Quesada V, Conde L, Villamor N, et al. Exome sequencing identifies recurrent mutations of the splicing factor SF3B1 gene in chronic lymphocytic leukemia. *Nat Genet*. 2011;44(1):47-52. doi:10.1038/ng.1032
93. Malcovati L, Karimi M, Papaemmanuil E, et al. SF3B1 mutation identifies a distinct subset of myelodysplastic syndrome with ring sideroblasts. *Blood*. 2015;126(2):233-241. doi:10.1182/blood-2015-03-633537
94. Nadeu F, Clot G, Delgado J, et al. Clinical impact of the subclonal architecture and mutational complexity in chronic lymphocytic leukemia. *Leukemia*. 2018;32(3):645-653. doi:10.1038/leu.2017.291
95. Graubert TA, Shen D, Ding L, et al. Recurrent mutations in the U2AF1 splicing factor in myelodysplastic syndromes. *Nat Genet*. 2011;44(1):53-57. doi:10.1038/ng.1031
96. Imielinski M, Berger AH, Hammerman PS, et al. Mapping the hallmarks of lung adenocarcinoma with massively parallel sequencing. *Cell*. 2012;150(6):1107-1120.

doi:10.1016/j.cell.2012.08.029
97. Hou HA, Liu CY, Kuo YY, et al. Splicing factor mutations predict poor prognosis in patients with de novo acute myeloid leukemia. *Oncotarget*. 2016;7(8):9084-9101. doi:10.18632/oncotarget.7000
98. Wang H, Zhang N, Wu X, Zheng X, Ling Y, Gong Y. Prognostic value of U2AF1 mutant in patients with de novo myelodysplastic syndromes: a meta-analysis. *Ann Hematol*. 2019;98(12):2629-2639. doi:10.1007/s00277-019-03843-3
99. Thol F, Kade S, Schlarmann C, et al. Frequency and prognostic impact of mutations in SRSF2, U2AF1, and ZRSR2 in patients with myelodysplastic syndromes. *Blood*. 2012;119(15):3578-3584. doi:10.1182/blood-2011-12-399337
100. Lasho TL, Jimma T, Finke CM, et al. SRSF2 mutations in primary myelofibrosis: significant clustering with IDH mutations and independent association with inferior overall and leukemia-free survival. *Blood*. 2012;120(20):4168-4171. doi:10.1182/blood-2012-05-429696
101. Arbab Jafari P, Ayatollahi H, Sadeghi R, Sheikhi M, Asghari A. Prognostic significance of SRSF2 mutations in myelodysplastic syndromes and chronic myelomonocytic leukemia: a meta-analysis. *Hematology*. 2018;23(10):778-784. doi:10.1080/10245332.2018.1471794
102. Madan V, Kanojia D, Li J, et al. Aberrant splicing of U12-type introns is the hallmark of ZRSR2 mutant myelodysplastic syndrome. *Nat Commun*. 2015;6:6042. doi:10.1038/ncomms7042
103. Shuai S, Suzuki H, Diaz-Navarro A, et al. The U1 spliceosomal RNA is recurrently mutated in multiple cancers. *Nature*. 2019;574(7780):712-716. doi:10.1038/s41586-019-1651-z
104. Bousquets-Muñoz P, Díaz-Navarro A, Nadeu F, et al. PanCancer analysis of somatic mutations in repetitive regions reveals recurrent mutations in snRNA U2. *npj Genom Med*. 2022;7(1):1-12. doi:10.1038/s41525-022-00292-2
105. Hanahan D. Hallmarks of Cancer: New Dimensions. *Cancer Discovery*. 2022;12(1):31-46. doi:10.1158/2159-8290.CD-21-1059
106. Oltean S, Bates DO. Hallmarks of alternative splicing in cancer. *Oncogene*. 2014;33(46):5311-5318. doi:10.1038/onc.2013.533
107. David CJ, Manley JL. Alternative pre-mRNA splicing regulation in cancer: pathways and programs unhinged. *Genes Dev*. 2010;24(21):2343-2364. doi:10.1101/gad.1973010

108. Ladomery M. Aberrant alternative splicing is another hallmark of cancer. *Int J Cell Biol*. 2013;2013:463786. doi:10.1155/2013/463786
109. Urbanski LM, Leclair N, Anczuków O. Alternative-splicing defects in cancer: Splicing regulators and their downstream targets, guiding the way to novel cancer therapeutics. *Wiley Interdiscip Rev RNA*. 2018;9(4):e1476. doi:10.1002/wrna.1476
110. Kozlovski I, Siegfried Z, Amar-Schwartz A, Karni R. The role of RNA alternative splicing in regulating cancer metabolism. *Hum Genet*. 2017;136(9):1113-1127. doi:10.1007/s00439-017-1803-x
111. Di C, Syafrizayanti, Zhang Q, et al. Function, clinical application, and strategies of Pre-mRNA splicing in cancer. *Cell Death Differ*. 2019;26(7):1181-1194. doi:10.1038/s41418-018-0231-3
112. Boise LH, González-García M, Postema CE, et al. bcl-x, a bcl-2-related gene that functions as a dominant regulator of apoptotic cell death. *Cell*. 1993;74(4):597-608. doi:10.1016/0092-8674(93)90508-n
113. Clarke MF, Apel IJ, Benedict MA, et al. A recombinant bcl-x s adenovirus selectively induces apoptosis in cancer cells but not in normal bone marrow cells. *Proc Natl Acad Sci U S A*. 1995;92(24):11024-11028. doi:10.1073/pnas.92.24.11024
114. Minn AJ, Boise LH, Thompson CB. Bcl-x(S) anatagonizes the protective effects of Bcl-x(L). *J Biol Chem*. 1996;271(11):6306-6312. doi:10.1074/jbc.271.11.6306
115. Cheng J, Zhou T, Liu C, et al. Protection from Fas-mediated apoptosis by a soluble form of the Fas molecule. *Science*. 1994;263(5154):1759-1762. doi:10.1126/science.7510905
116. Cascino I, Fiucci G, Papoff G, Ruberti G. Three functional soluble forms of the human apoptosis-inducing Fas molecule are produced by alternative splicing. *J Immunol*. 1995;154(6):2706-2713.
117. Izquierdo JM. Hu antigen R (HuR) functions as an alternative pre-mRNA splicing regulator of Fas apoptosis-promoting receptor on exon definition. *J Biol Chem*. 2008;283(27):19077-19084. doi:10.1074/jbc.M800017200
118. Izquierdo JM, Majós N, Bonnal S, et al. Regulation of Fas alternative splicing by antagonistic effects of TIA-1 and PTB on exon definition. *Mol Cell*. 2005;19(4):475-484. doi:10.1016/j.molcel.2005.06.015

119. Warburg O. On the origin of cancer cells. *Science*. 1956;123(3191):309-314. doi:10.1126/science.123.3191.309
120. Mazurek S, Boschek CB, Hugo F, Eigenbrodt E. Pyruvate kinase type M2 and its role in tumor growth and spreading. *Semin Cancer Biol*. 2005;15(4):300-308. doi:10.1016/j.semcancer.2005.04.009
121. Vander Heiden MG, Cantley LC, Thompson CB. Understanding the Warburg Effect: The Metabolic Requirements of Cell Proliferation. *Science*. 2009;324(5930):1029-1033. doi:10.1126/science.1160809
122. Christofk HR, Vander Heiden MG, Wu N, Asara JM, Cantley LC. Pyruvate kinase M2 is a phosphotyrosine-binding protein. *Nature*. 2008;452(7184):181-186. doi:10.1038/nature06667
123. Christofk HR, Vander Heiden MG, Harris MH, et al. The M2 splice isoform of pyruvate kinase is important for cancer metabolism and tumour growth. *Nature*. 2008;452(7184):230-233. doi:10.1038/nature06734
124. David CJ, Chen M, Assanah M, Canoll P, Manley JL. HnRNP proteins controlled by c-Myc deregulate pyruvate kinase mRNA splicing in cancer. *Nature*. 2010;463(7279):364-368. doi:10.1038/nature08697
125. Clower CV, Chatterjee D, Wang Z, Cantley LC, Vander Heiden MG, Krainer AR. The alternative splicing repressors hnRNP A1/A2 and PTB influence pyruvate kinase isoform expression and cell metabolism. *Proc Natl Acad Sci U S A*. 2010;107(5):1894-1899. doi:10.1073/pnas.0914845107
126. Bates DO, Cui TG, Doughty JM, et al. VEGF165b, an inhibitory splice variant of vascular endothelial growth factor, is down-regulated in renal cell carcinoma. *Cancer Res*. 2002;62(14):4123-4131.
127. Harper SJ, Bates DO. VEGF-A splicing: the key to anti-angiogenic therapeutics? *Nat Rev Cancer*. 2008;8(11):880-887. doi:10.1038/nrc2505
128. Woolard J, Wang WY, Bevan HS, et al. VEGF165b, an inhibitory vascular endothelial growth factor splice variant: mechanism of action, in vivo effect on angiogenesis and endogenous protein expression. *Cancer Res*. 2004;64(21):7822-7835. doi:10.1158/0008-5472.CAN-04-0934
129. Nowak DG, Woolard J, Amin EM, et al. Expression of pro- and anti-angiogenic isoforms of VEGF is differentially regulated by splicing and growth factors. *J Cell Sci*. 2008;121(Pt 20):3487-3495.

doi:10.1242/jcs.016410
130. Betticher DC, Thatcher N, Altermatt HJ, Hoban P, Ryder WD, Heighway J. Alternate splicing produces a novel cyclin D1 transcript. *Oncogene*. 1995;11(5):1005-1011.
131. Lu F, Gladden AB, Diehl JA. An alternatively spliced cyclin D1 isoform, cyclin D1b, is a nuclear oncogene. *Cancer Res*. 2003;63(21):7056-7061.
132. Solomon DA, Wang Y, Fox SR, et al. Cyclin D1 Splice Variants: DIFFERENTIAL EFFECTS ON LOCALIZATION, RB PHOSPHORYLATION, AND CELLULAR TRANSFORMATION*. *Journal of Biological Chemistry*. 2003;278(32):30339-30347. doi:10.1074/jbc.M303969200
133. Comstock CES, Augello MA, Benito RP, et al. Cyclin D1 splice variants: polymorphism, risk, and isoform-specific regulation in prostate cancer. *Clin Cancer Res*. 2009;15(17):5338-5349. doi:10.1158/1078-0432.CCR-08-2865
134. Olshavsky NA, Comstock CES, Schiewer MJ, et al. Identification of ASF/SF2 as a critical, allele-specific effector of the cyclin D1b oncogene. *Cancer Res*. 2010;70(10):3975-3984. doi:10.1158/0008-5472.CAN-09-3468
135. Brown RL, Reinke LM, Damerow MS, et al. CD44 splice isoform switching in human and mouse epithelium is essential for epithelial-mesenchymal transition and breast cancer progression. *J Clin Invest*. 2011;121(3):1064-1074. doi:10.1172/JCI44540
136. Günthert U, Hofmann M, Rudy W, et al. A new variant of glycoprotein CD44 confers metastatic potential to rat carcinoma cells. *Cell*. 1991;65(1):13-24. doi:10.1016/0092-8674(91)90403-l
137. Ponta H, Sherman L, Herrlich PA. CD44: from adhesion molecules to signalling regulators. *Nat Rev Mol Cell Biol*. 2003;4(1):33-45. doi:10.1038/nrm1004
138. Yan G, Fukabori Y, McBride G, Nikolaropolous S, McKeehan WL. Exon switching and activation of stromal and embryonic fibroblast growth factor (FGF)-FGF receptor genes in prostate epithelial cells accompany stromal independence and malignancy. *Mol Cell Biol*. 1993;13(8):4513-4522. doi:10.1128/mcb.13.8.4513-4522.1993
139. Luco RF, Pan Q, Tominaga K, Blencowe BJ, Pereira-Smith OM, Misteli T. Regulation of alternative splicing by histone modifications. *Science*. 2010;327(5968):996-1000. doi:10.1126/science.1184208
140. Warzecha CC, Sato TK, Nabet B, Hogenesch JB, Carstens

RP. ESRP1 and ESRP2 are epithelial cell-type-specific regulators of FGFR2 splicing. *Mol Cell*. 2009;33(5):591-601. doi:10.1016/j.molcel.2009.01.025
141. Yamaguchi F, Saya H, Bruner JM, Morrison RS. Differential expression of two fibroblast growth factor-receptor genes is associated with malignant progression in human astrocytomas. *Proc Natl Acad Sci U S A*. 1994;91(2):484-488. doi:10.1073/pnas.91.2.484
142. Wang F, Kan M, Yan G, Xu J, McKeehan WL. Alternately spliced NH2-terminal immunoglobulin-like Loop I in the ectodomain of the fibroblast growth factor (FGF) receptor 1 lowers affinity for both heparin and FGF-1. *J Biol Chem*. 1995;270(17):10231-10235. doi:10.1074/jbc.270.17.10231
143. Jin W, Bruno IG, Xie TX, Sanger LJ, Cote GJ. Polypyrimidine tract-binding protein down-regulates fibroblast growth factor receptor 1 alpha-exon inclusion. *Cancer Res*. 2003;63(19):6154-6157.
144. Siegfried Z, Karni R. The role of alternative splicing in cancer drug resistance. *Curr Opin Genet Dev*. 2018;48:16-21. doi:10.1016/j.gde.2017.10.001
145. Antonarakis ES, Lu C, Luber B, et al. Clinical Significance of Androgen Receptor Splice Variant-7 mRNA Detection in Circulating Tumor Cells of Men With Metastatic Castration-Resistant Prostate Cancer Treated With First- and Second-Line Abiraterone and Enzalutamide. *J Clin Oncol*. 2017;35(19):2149-2156. doi:10.1200/JCO.2016.70.1961
146. Antonarakis ES, Lu C, Wang H, et al. AR-V7 and resistance to enzalutamide and abiraterone in prostate cancer. *N Engl J Med*. 2014;371(11):1028-1038. doi:10.1056/NEJMoa1315815
147. Sowalsky AG, Figueiredo I, Lis RT, et al. Assessment of Androgen Receptor Splice Variant-7 as a Biomarker of Clinical Response in Castration-Sensitive Prostate Cancer. *Clin Cancer Res*. 2022;28(16):3509-3525. doi:10.1158/1078-0432.CCR-22-0851
148. Li D, Harlan-Williams LM, Kumaraswamy E, Jensen RA. BRCA1—No Matter How You Splice It. *Cancer Research*. 2019;79(9):2091-2098. doi:10.1158/0008-5472.CAN-18-3190
149. Wang Y, Bernhardy AJ, Cruz C, et al. The BRCA1-Δ11q Alternative Splice Isoform Bypasses Germline Mutations and Promotes Therapeutic Resistance to PARP Inhibition and Cisplatin. *Cancer Res*. 2016;76(9):2778-2790. doi:10.1158/0008-5472.CAN-16-0186

150. Sotillo E, Barrett DM, Black KL, et al. Convergence of Acquired Mutations and Alternative Splicing of CD19 Enables Resistance to CART-19 Immunotherapy. *Cancer Discovery*. 2015;5(12):1282-1295. doi:10.1158/2159-8290.CD-15-1020
151. Cortés-López M, Schulz L, Enculescu M, et al. High-throughput mutagenesis identifies mutations and RNA-binding proteins controlling CD19 splicing and CART-19 therapy resistance. *Nat Commun*. 2022;13(1):5570. doi:10.1038/s41467-022-31818-y
152. Lee SCW, North K, Kim E, et al. Synthetic Lethal and Convergent Biological Effects of Cancer-Associated Spliceosomal Gene Mutations. *Cancer Cell*. 2018;34(2):225-241.e8. doi:10.1016/j.ccell.2018.07.003
153. Taylor J, Mi X, North K, et al. Single-cell genomics reveals the genetic and molecular bases for escape from mutational epistasis in myeloid neoplasms. *Blood*. 2020;136(13):1477-1486. doi:10.1182/blood.2020006868
154. Zhou Q, Derti A, Ruddy D, et al. A chemical genetics approach for the functional assessment of novel cancer genes. *Cancer Res*. 2015;75(10):1949-1958. doi:10.1158/0008-5472.CAN-14-2930
155. Lee SCW, Dvinge H, Kim E, et al. Modulation of splicing catalysis for therapeutic targeting of leukemia with mutations in genes encoding spliceosomal proteins. *Nat Med*. 2016;22(6):672-678. doi:10.1038/nm.4097
156. Fei DL, Motowski H, Chatrikhi R, et al. Wild-Type U2AF1 Antagonizes the Splicing Program Characteristic of U2AF1-Mutant Tumors and Is Required for Cell Survival. *PLOS Genetics*. 2016;12(10):e1006384. doi:10.1371/journal.pgen.1006384
157. Bonnal S, Vigevani L, Valcárcel J. The spliceosome as a target of novel antitumour drugs. *Nat Rev Drug Discov*. 2012;11(11):847-859. doi:10.1038/nrd3823
158. Levin AA. Treating Disease at the RNA Level with Oligonucleotides. *N Engl J Med*. 2019;380(1):57-70. doi:10.1056/NEJMra1705346
159. Raal FJ, Santos RD, Blom DJ, et al. Mipomersen, an apolipoprotein B synthesis inhibitor, for lowering of LDL cholesterol concentrations in patients with homozygous familial hypercholesterolaemia: a randomised, double-blind, placebo-controlled trial. *Lancet*. 2010;375(9719):998-1006. doi:10.1016/S0140-6736(10)60284-X

160. Ray KK, Landmesser U, Leiter LA, et al. Inclisiran in Patients at High Cardiovascular Risk with Elevated LDL Cholesterol. *New England Journal of Medicine*. 2017;376(15):1430-1440. doi:10.1056/NEJMoa1615758
161. McDonald CM, Shieh PB, Abdel-Hamid HZ, et al. Open-Label Evaluation of Eteplirsen in Patients with Duchenne Muscular Dystrophy Amenable to Exon 51 Skipping: PROMOVI Trial. *J Neuromuscul Dis*. 2021;8(6):989-1001. doi:10.3233/JND-210643
162. Finkel RS, Mercuri E, Darras BT, et al. Nusinersen versus Sham Control in Infantile-Onset Spinal Muscular Atrophy. *N Engl J Med*. 2017;377(18):1723-1732. doi:10.1056/NEJMoa1702752
163. Moulder SL, Symmans WF, Booser DJ, et al. Phase I/II Study of G3139 (Bcl-2 Antisense Oligonucleotide) in Combination with Doxorubicin and Docetaxel in Breast Cancer. *Clin Cancer Res*. 2008;14(23):7909-7916. doi:10.1158/1078-0432.CCR-08-1104
164. Rudin CM, Salgia R, Wang X, et al. Randomized Phase II Study of Carboplatin and Etoposide With or Without the bcl-2 Antisense Oligonucleotide Oblimersen for Extensive-Stage Small-Cell Lung Cancer: CALGB 30103. *JCO*. 2008;26(6):870-876. doi:10.1200/JCO.2007.14.3461
165. Rudin CM, Otterson GA, Mauer AM, et al. A pilot trial of G3139, a bcl-2 antisense oligonucleotide,and paclitaxel in patients with chemorefractory small-cell lung cancer. *Annals of Oncology*. 2002;13(4):539-545. doi:10.1093/annonc/mdf124
166. Walker AR, Marcucci G, Yin J, et al. Phase 3 randomized trial of chemotherapy with or without oblimersen in older AML patients: CALGB 10201 (Alliance). *Blood Adv*. 2021;5(13):2775-2787. doi:10.1182/bloodadvances.2021004233
167. Cunningham CC, Holmlund JT, Geary RS, et al. A Phase I trial of H-ras antisense oligonucleotide ISIS 2503 administered as a continuous intravenous infusion in patients with advanced carcinoma. *Cancer*. 2001;92(5):1265-1271. doi:10.1002/1097-0142(20010901)92:5<1265::aid-cncr1447>3.0.co;2-5
168. Adjei AA, Dy GK, Erlichman C, et al. A phase I trial of ISIS 2503, an antisense inhibitor of H-ras, in combination with gemcitabine in patients with advanced cancer. *Clin Cancer Res*. 2003;9(1):115-123.
169. Reilley MJ, McCoon P, Cook C, et al. STAT3 antisense oligonucleotide AZD9150 in a subset of patients with heavily pretreated lymphoma: results of a phase 1b trial. *J Immunother Cancer*. 2018;6(1):119. doi:10.1186/s40425-018-0436-5

170. Hong D, Kurzrock R, Kim Y, et al. AZD9150, a Next-Generation Antisense Oligonucleotide Inhibitor of STAT3 with Early Evidence of Clinical Activity in Lymphoma and Lung Cancer. *Sci Transl Med*. 2015;7(314):314ra185. doi:10.1126/scitranslmed.aac5272
171. Ohanian M, Tari Ashizawa A, Garcia-Manero G, et al. Liposomal Grb2 antisense oligodeoxynucleotide (BP1001) in patients with refractory or relapsed haematological malignancies: a single-centre, open-label, dose-escalation, phase 1/1b trial. *Lancet Haematol*. 2018;5(4):e136-e146. doi:10.1016/S2352-3026(18)30021-8
172. Kaida D, Motoyoshi H, Tashiro E, et al. Spliceostatin A targets SF3b and inhibits both splicing and nuclear retention of pre-mRNA. *Nat Chem Biol*. 2007;3(9):576-583. doi:10.1038/nchembio.2007.18
173. Makowski K, Vigevani L, Albericio F, Valcárcel J, Álvarez M. Sudemycin K: A Synthetic Antitumor Splicing Inhibitor Variant with Improved Activity and Versatile Chemistry. *ACS Chem Biol*. 2017;12(1):163-173. doi:10.1021/acschembio.6b00562
174. Fan L, Lagisetti C, Edwards CC, Webb TR, Potter PM. Sudemycins, novel small molecule analogues of FR901464, induce alternative gene splicing. *ACS Chem Biol*. 2011;6(6):582-589. doi:10.1021/cb100356k
175. Kotake Y, Sagane K, Owa T, et al. Splicing factor SF3b as a target of the antitumor natural product pladienolide. *Nat Chem Biol*. 2007;3(9):570-575. doi:10.1038/nchembio.2007.16
176. Folco EG, Coil KE, Reed R. The anti-tumor drug E7107 reveals an essential role for SF3b in remodeling U2 snRNP to expose the branch point-binding region. *Genes Dev*. 2011;25(5):440-444. doi:10.1101/gad.2009411
177. Eskens FALM, Ramos FJ, Burger H, et al. Phase I pharmacokinetic and pharmacodynamic study of the first-in-class spliceosome inhibitor E7107 in patients with advanced solid tumors. *Clin Cancer Res*. 2013;19(22):6296-6304. doi:10.1158/1078-0432.CCR-13-0485
178. Hong DS, Kurzrock R, Naing A, et al. A phase I, open-label, single-arm, dose-escalation study of E7107, a precursor messenger ribonucleic acid (pre-mRNA) splicesome inhibitor administered intravenously on days 1 and 8 every 21 days to patients with solid tumors. *Invest New Drugs*. 2014;32(3):436-444. doi:10.1007/s10637-013-0046-5

179. Seiler M, Yoshimi A, Darman R, et al. H3B-8800, an orally available small-molecule splicing modulator, induces lethality in spliceosome-mutant cancers. *Nat Med*. 2018;24(4):497-504. doi:10.1038/nm.4493
180. Steensma DP, Wermke M, Klimek VM, et al. Phase I First-in-Human Dose Escalation Study of the oral SF3B1 modulator H3B-8800 in myeloid neoplasms. *Leukemia*. 2021;35(12):3542-3550. doi:10.1038/s41375-021-01328-9
181. Hasegawa M, Miura T, Kuzuya K, et al. Identification of SAP155 as the target of GEX1A (Herboxidiene), an antitumor natural product. *ACS Chem Biol*. 2011;6(3):229-233. doi:10.1021/cb100248e
182. Ghosh AK, Allu SR, Reddy GC, Lopez AG, Mendez P, Jurica MS. Design and synthesis of herboxidiene derivatives that potently inhibit in vitro splicing. *Org Biomol Chem*. 2021;19(6):1365-1377. doi:10.1039/D0OB02532A
183. Jagtap PKA, Kubelka T, Soni K, et al. Identification of phenothiazine derivatives as UHM-binding inhibitors of early spliceosome assembly. *Nat Commun*. 2020;11(1):5621. doi:10.1038/s41467-020-19514-1
184. Chatrikhi R, Feeney CF, Pulvino MJ, et al. A synthetic small molecule stalls pre-mRNA splicing by promoting an early-stage U2AF2-RNA complex. *Cell Chem Biol*. 2021;28(8):1145-1157.e6. doi:10.1016/j.chembiol.2021.02.007
185. Fong JY, Pignata L, Goy PA, et al. Therapeutic Targeting of RNA Splicing Catalysis through Inhibition of Protein Arginine Methylation. *Cancer Cell*. 2019;36(2):194-209.e9. doi:10.1016/j.ccell.2019.07.003
186. Radzisheuskaya A, Shliaha PV, Grinev V, et al. PRMT5 methylome profiling uncovers a direct link to splicing regulation in acute myeloid leukemia. *Nat Struct Mol Biol*. 2019;26(11):999-1012. doi:10.1038/s41594-019-0313-z
187. Ting TC, Goralski M, Klein K, et al. Aryl Sulfonamides Degrade RBM39 and RBM23 by Recruitment to CRL4-DCAF15. *Cell Rep*. 2019;29(6):1499-1510.e6. doi:10.1016/j.celrep.2019.09.079
188. Han T, Goralski M, Gaskill N, et al. Anticancer sulfonamides target splicing by inducing RBM39 degradation via recruitment to DCAF15. *Science*. 2017;356(6336):eaal3755. doi:10.1126/science.aal3755
189. Assi R, Kantarjian HM, Kadia TM, et al. Final results of a

phase 2, open-label study of indisulam, idarubicin, and cytarabine in patients with relapsed or refractory acute myeloid leukemia and high-risk myelodysplastic syndrome. *Cancer*. 2018;124(13):2758-2765. doi:10.1002/cncr.31398
190. Frankiw L, Baltimore D, Li G. Alternative mRNA splicing in cancer immunotherapy. *Nat Rev Immunol*. 2019;19(11):675-687. doi:10.1038/s41577-019-0195-7
191. Lu SX, Neef ED, Thomas JD, et al. Pharmacologic modulation of RNA splicing enhances anti-tumor immunity. *Cell*. 2021;184(15):4032-4047.e31. doi:10.1016/j.cell.2021.05.038
192. Laumont CM, Vincent K, Hesnard L, et al. Noncoding regions are the main source of targetable tumor-specific antigens. *Sci Transl Med*. 2018;10(470):eaau5516. doi:10.1126/scitranslmed.aau5516
193. Jayasinghe RG, Cao S, Gao Q, et al. Systematic Analysis of Splice-Site-Creating Mutations in Cancer. *Cell Rep*. 2018;23(1):270-281.e3. doi:10.1016/j.celrep.2018.03.052
194. Smart AC, Margolis CA, Pimentel H, et al. Intron retention is a source of neoepitopes in cancer. *Nat Biotechnol*. 2018;36(11):1056-1058. doi:10.1038/nbt.4239
195. Sha D, Jin Z, Budczies J, Kluck K, Stenzinger A, Sinicrope FA. Tumor Mutational Burden as a Predictive Biomarker in Solid Tumors. *Cancer Discov*. 2020;10(12):1808-1825. doi:10.1158/2159-8290.CD-20-0522
196. Yarchoan M, Hopkins A, Jaffee EM. Tumor Mutational Burden and Response Rate to PD-1 Inhibition. *N Engl J Med*. 2017;377(25):2500-2501. doi:10.1056/NEJMc1713444
197. Schumacher TN, Schreiber RD. Neoantigens in cancer immunotherapy. *Science*. 2015;348(6230):69-74. doi:10.1126/science.aaa4971
198. Le DT, Durham JN, Smith KN, et al. Mismatch repair deficiency predicts response of solid tumors to PD-1 blockade. *Science*. 2017;357(6349):409-413. doi:10.1126/science.aan6733
199. Cercek A, Lumish M, Sinopoli J, et al. PD-1 Blockade in Mismatch Repair–Deficient, Locally Advanced Rectal Cancer. *N Engl J Med*. 2022;386(25):2363-2376. doi:10.1056/NEJMoa2201445
200. André T, Shiu KK, Kim TW, et al. Pembrolizumab in Microsatellite-Instability–High Advanced Colorectal Cancer. *New England Journal of Medicine*. 2020;383(23):2207-2218. doi:10.1056/NEJMoa2017699

201. Siegel RL, Miller KD, Fuchs HE, Jemal A. Cancer statistics, 2022. *CA Cancer J Clin*. 2022;72(1):7-33. doi:10.3322/caac.21708
202. Gandini S, Sera F, Cattaruzza MS, et al. Meta-analysis of risk factors for cutaneous melanoma: I. Common and atypical naevi. *Eur J Cancer*. 2005;41(1):28-44. doi:10.1016/j.ejca.2004.10.015
203. Boniol M, Autier P, Boyle P, Gandini S. Cutaneous melanoma attributable to sunbed use: systematic review and meta-analysis. *BMJ*. 2012;345:e4757. doi:10.1136/bmj.e4757
204. Schadendorf D, Fisher DE, Garbe C, et al. Melanoma. *Nat Rev Dis Primers*. 2015;1(1):1-20. doi:10.1038/nrdp.2015.3
205. Arnold M, Singh D, Laversanne M, et al. Global Burden of Cutaneous Melanoma in 2020 and Projections to 2040. *JAMA Dermatology*. 2022;158(5):495-503. doi:10.1001/jamadermatol.2022.0160
206. Gershenwald JE, Scolyer RA, Hess KR, et al. Melanoma staging: Evidence-based changes in the American Joint Committee on Cancer eighth edition cancer staging manual. *CA Cancer J Clin*. 2017;67(6):472-492. doi:10.3322/caac.21409
207. Grob JJ, Schadendorf D, Lorigan P, et al. Eighth American Joint Committee on Cancer (AJCC) melanoma classification: Let us reconsider stage III. *Eur J Cancer*. 2018;91:168-170. doi:10.1016/j.ejca.2017.11.023
208. Miller AJ, Mihm MC. Melanoma. *N Engl J Med*. 2006;355(1):51-65. doi:10.1056/NEJMra052166
209. Shain AH, Yeh I, Kovalyshyn I, et al. The Genetic Evolution of Melanoma from Precursor Lesions. *N Engl J Med*. 2015;373(20):1926-1936. doi:10.1056/NEJMoa1502583
210. Albino AP, Nanus DM, Mentle IR, et al. Analysis of ras oncogenes in malignant melanoma and precursor lesions: correlation of point mutations with differentiation phenotype. *Oncogene*. 1989;4(11):1363-1374.
211. Davies H, Bignell GR, Cox C, et al. Mutations of the BRAF gene in human cancer. *Nature*. 2002;417(6892):949-954. doi:10.1038/nature00766
212. Omholt K, Platz A, Kanter L, Ringborg U, Hansson J. NRAS and BRAF mutations arise early during melanoma pathogenesis and are preserved throughout tumor progression. *Clin Cancer Res*. 2003;9(17):6483-6488.
213. Pollock PM, Harper UL, Hansen KS, et al. High frequency of BRAF mutations in nevi. *Nat Genet*. 2003;33(1):19-20.

doi:10.1038/ng1054
214. Michaloglou C, Vredeveld LCW, Soengas MS, et al. BRAFE600-associated senescence-like cell cycle arrest of human naevi. *Nature*. 2005;436(7051):720-724. doi:10.1038/nature03890
215. Dankort D, Curley DP, Cartlidge RA, et al. Braf(V600E) cooperates with Pten loss to induce metastatic melanoma. *Nat Genet*. 2009;41(5):544-552. doi:10.1038/ng.356
216. Hodis E, Watson IR, Kryukov GV, et al. A landscape of driver mutations in melanoma. *Cell*. 2012;150(2):251-263. doi:10.1016/j.cell.2012.06.024
217. Nikolaev SI, Rimoldi D, Iseli C, et al. Exome sequencing identifies recurrent somatic MAP2K1 and MAP2K2 mutations in melanoma. *Nat Genet*. 2011;44(2):133-139. doi:10.1038/ng.1026
218. Stark MS, Woods SL, Gartside MG, et al. Frequent somatic mutations in MAP3K5 and MAP3K9 in metastatic melanoma identified by exome sequencing. *Nat Genet*. 2011;44(2):165-169. doi:10.1038/ng.1041
219. Berger MF, Hodis E, Heffernan TP, et al. Melanoma genome sequencing reveals frequent PREX2 mutations. *Nature*. 2012;485(7399):502-506. doi:10.1038/nature11071
220. Kamb A, Shattuck-Eidens D, Eeles R, et al. Analysis of the p16 gene (CDKN2) as a candidate for the chromosome 9p melanoma susceptibility locus. *Nat Genet*. 1994;8(1):23-26. doi:10.1038/ng0994-22
221. Hussussian CJ, Struewing JP, Goldstein AM, et al. Germline p16 mutations in familial melanoma. *Nat Genet*. 1994;8(1):15-21. doi:10.1038/ng0994-15
222. Sauter ER, Yeo UC, von Stemm A, et al. Cyclin D1 is a candidate oncogene in cutaneous melanoma. *Cancer Res*. 2002;62(11):3200-3206.
223. Huang FW, Hodis E, Xu MJ, Kryukov GV, Chin L, Garraway LA. Highly recurrent TERT promoter mutations in human melanoma. *Science*. 2013;339(6122):957-959. doi:10.1126/science.1229259
224. Horn S, Figl A, Rachakonda PS, et al. TERT promoter mutations in familial and sporadic melanoma. *Science*. 2013;339(6122):959-961. doi:10.1126/science.1230062
225. Akbani R, Akdemir KC, Aksoy BA, et al. Genomic Classification of Cutaneous Melanoma. *Cell*. 2015;161(7):1681-1696. doi:10.1016/j.cell.2015.05.044
226. Hayward NK, Wilmott JS, Waddell N, et al. Whole-genome

landscapes of major melanoma subtypes. *Nature*. 2017;545(7653):175-180. doi:10.1038/nature22071
227. Michielin O, Akkooi ACJ van, Ascierto PA, Dummer R, Keilholz U. Cutaneous melanoma: ESMO Clinical Practice Guidelines for diagnosis, treatment and follow-up †. *Annals of Oncology*. 2019;30(12):1884-1901. doi:10.1093/annonc/mdz411
228. Curti BD, Faries MB. Recent Advances in the Treatment of Melanoma. *New England Journal of Medicine*. 2021;384(23):2229-2240. doi:10.1056/NEJMra2034861
229. Eggermont AMM, Hamid O, Long GV, Luke JJ. Optimal systemic therapy for high-risk resectable melanoma. *Nat Rev Clin Oncol*. 2022;19(7):431-439. doi:10.1038/s41571-022-00630-4
230. Eigentler TK, Caroli UM, Radny P, Garbe C. Palliative therapy of disseminated malignant melanoma: a systematic review of 41 randomised clinical trials. *Lancet Oncol*. 2003;4(12):748-759. doi:10.1016/s1470-2045(03)01280-4
231. Ugurel S, Röhmel J, Ascierto PA, et al. Survival of patients with advanced metastatic melanoma: The impact of novel therapies. *European Journal of Cancer*. 2016;53:125-134. doi:10.1016/j.ejca.2015.09.013
232. Ugurel S, Röhmel J, Ascierto PA, et al. Survival of patients with advanced metastatic melanoma: The impact of MAP kinase pathway inhibition and immune checkpoint inhibition - Update 2019. *Eur J Cancer*. 2020;130:126-138. doi:10.1016/j.ejca.2020.02.021
233. Hodi FS, O'Day SJ, McDermott DF, et al. Improved survival with ipilimumab in patients with metastatic melanoma. *N Engl J Med*. 2010;363(8):711-723. doi:10.1056/NEJMoa1003466
234. Robert C, Thomas L, Bondarenko I, et al. Ipilimumab plus dacarbazine for previously untreated metastatic melanoma. *N Engl J Med*. 2011;364(26):2517-2526. doi:10.1056/NEJMoa1104621
235. Tang J, Yu JX, Hubbard-Lucey VM, Neftelinov ST, Hodge JP, Lin Y. The clinical trial landscape for PD1/PDL1 immune checkpoint inhibitors. *Nature Reviews Drug Discovery*. 2018;17(12):854-855. doi:10.1038/nrd.2018.210
236. Xin Yu J, Hubbard-Lucey VM, Tang J. Immuno-oncology drug development goes global. *Nature Reviews Drug Discovery*. 2019;18(12):899-900. doi:10.1038/d41573-019-00167-9
237. Patsoukis N, Wang Q, Strauss L, Boussiotis VA. Revisiting the PD-1 pathway. *Science Advances*. 2020;6(38):eabd2712. doi:10.1126/sciadv.abd2712

238. Upadhaya S, Neftelinov ST, Hodge J, Campbell J. Challenges and opportunities in the PD1/PDL1 inhibitor clinical trial landscape. *Nature Reviews Drug Discovery*. 2022;21(7):482-483. doi:10.1038/d41573-022-00030-4
239. Robert C, Long GV, Brady B, et al. Nivolumab in previously untreated melanoma without BRAF mutation. *N Engl J Med*. 2015;372(4):320-330. doi:10.1056/NEJMoa1412082
240. Weber JS, D'Angelo SP, Minor D, et al. Nivolumab versus chemotherapy in patients with advanced melanoma who progressed after anti-CTLA-4 treatment (CheckMate 037): a randomised, controlled, open-label, phase 3 trial. *Lancet Oncol*. 2015;16(4):375-384. doi:10.1016/S1470-2045(15)70076-8
241. Larkin J, Minor D, D'Angelo S, et al. Overall Survival in Patients With Advanced Melanoma Who Received Nivolumab Versus Investigator's Choice Chemotherapy in CheckMate 037: A Randomized, Controlled, Open-Label Phase III Trial. *J Clin Oncol*. 2018;36(4):383-390. doi:10.1200/JCO.2016.71.8023
242. Robert C, Schachter J, Long GV, et al. Pembrolizumab versus Ipilimumab in Advanced Melanoma. *N Engl J Med*. 2015;372(26):2521-2532. doi:10.1056/NEJMoa1503093
243. Hamid O, Puzanov I, Dummer R, et al. Final analysis of a randomised trial comparing pembrolizumab versus investigator-choice chemotherapy for ipilimumab-refractory advanced melanoma. *Eur J Cancer*. 2017;86:37-45. doi:10.1016/j.ejca.2017.07.022
244. Schachter J, Ribas A, Long GV, et al. Pembrolizumab versus ipilimumab for advanced melanoma: final overall survival results of a multicentre, randomised, open-label phase 3 study (KEYNOTE-006). *Lancet*. 2017;390(10105):1853-1862. doi:10.1016/S0140-6736(17)31601-X
245. Patel SA, Minn AJ. Combination Cancer Therapy with Immune Checkpoint Blockade: Mechanisms and Strategies. *Immunity*. 2018;48(3):417-433. doi:10.1016/j.immuni.2018.03.007
246. Zappasodi R, Merghoub T, Wolchok JD. Emerging Concepts for Immune Checkpoint Blockade-Based Combination Therapies. *Cancer Cell*. 2018;33(4):581-598. doi:10.1016/j.ccell.2018.03.005
247. Larkin J, Chiarion-Sileni V, Gonzalez R, et al. Combined Nivolumab and Ipilimumab or Monotherapy in Untreated Melanoma. *N Engl J Med*. 2015;373(1):23-34. doi:10.1056/NEJMoa1504030

248. Wolchok JD, Chiarion-Sileni V, Gonzalez R, et al. Overall Survival with Combined Nivolumab and Ipilimumab in Advanced Melanoma. *N Engl J Med*. 2017;377(14):1345-1356. doi:10.1056/NEJMoa1709684
249. Tawbi HA, Schadendorf D, Lipson EJ, et al. Relatlimab and Nivolumab versus Nivolumab in Untreated Advanced Melanoma. *N Engl J Med*. 2022;386(1):24-34. doi:10.1056/NEJMoa2109970
250. Ascierto PA, Ferrucci PF, Fisher R, et al. Dabrafenib, trametinib and pembrolizumab or placebo in BRAF-mutant melanoma. *Nat Med*. 2019;25(6):941-946. doi:10.1038/s41591-019-0448-9
251. Ribas A, Lawrence D, Atkinson V, et al. Combined BRAF and MEK inhibition with PD-1 blockade immunotherapy in BRAF-mutant melanoma. *Nat Med*. 2019;25(6):936-940. doi:10.1038/s41591-019-0476-5
252. Gutzmer R, Stroyakovskiy D, Gogas H, et al. Atezolizumab, vemurafenib, and cobimetinib as first-line treatment for unresectable advanced BRAFV600 mutation-positive melanoma (IMspire150): primary analysis of the randomised, double-blind, placebo-controlled, phase 3 trial. *Lancet*. 2020;395(10240):1835-1844. doi:10.1016/S0140-6736(20)30934-X
253. Dummer R, Lebbé C, Atkinson V, et al. Combined PD-1, BRAF and MEK inhibition in advanced BRAF-mutant melanoma: safety run-in and biomarker cohorts of COMBI-i. *Nat Med*. 2020;26(10):1557-1563. doi:10.1038/s41591-020-1082-2
254. Arance A, de la Cruz-Merino L, Petrella TM, et al. Phase II LEAP-004 Study of Lenvatinib Plus Pembrolizumab for Melanoma With Confirmed Progression on a Programmed Cell Death Protein-1 or Programmed Death Ligand 1 Inhibitor Given as Monotherapy or in Combination. *JCO*. Published online July 22, 2022:JCO.22.00221. doi:10.1200/JCO.22.00221
255. Chapman PB, Hauschild A, Robert C, et al. Improved survival with vemurafenib in melanoma with BRAF V600E mutation. *N Engl J Med*. 2011;364(26):2507-2516. doi:10.1056/NEJMoa1103782
256. Hauschild A, Grob JJ, Demidov LV, et al. Dabrafenib in BRAF-mutated metastatic melanoma: a multicentre, open-label, phase 3 randomised controlled trial. *The Lancet*. 2012;380(9839):358-365. doi:10.1016/S0140-6736(12)60868-X
257. Larkin J, Ascierto PA, Dréno B, et al. Combined vemurafenib and cobimetinib in BRAF-mutated melanoma. *N Engl*

J Med. 2014;371(20):1867-1876. doi:10.1056/NEJMoa1408868
258. Ascierto PA, McArthur GA, Dréno B, et al. Cobimetinib combined with vemurafenib in advanced BRAF(V600)-mutant melanoma (coBRIM): updated efficacy results from a randomised, double-blind, phase 3 trial. *Lancet Oncol*. 2016;17(9):1248-1260. doi:10.1016/S1470-2045(16)30122-X
259. Long GV, Stroyakovskiy D, Gogas H, et al. Combined BRAF and MEK inhibition versus BRAF inhibition alone in melanoma. *N Engl J Med*. 2014;371(20):1877-1888. doi:10.1056/NEJMoa1406037
260. Robert C, Grob JJ, Stroyakovskiy D, et al. Five-Year Outcomes with Dabrafenib plus Trametinib in Metastatic Melanoma. *N Engl J Med*. 2019;381(7):626-636. doi:10.1056/NEJMoa1904059
261. Dummer R, Ascierto PA, Gogas HJ, et al. Encorafenib plus binimetinib versus vemurafenib or encorafenib in patients with BRAF-mutant melanoma (COLUMBUS): a multicentre, open-label, randomised phase 3 trial. *The Lancet Oncology*. 2018;19(5):603-615. doi:10.1016/S1470-2045(18)30142-6
262. Dummer R, Flaherty K, Robert C, et al. Five-year overall survival (OS) in COLUMBUS: A randomized phase 3 trial of encorafenib plus binimetinib versus vemurafenib or encorafenib in patients (pts) with BRAF V600-mutant melanoma. *JCO*. 2021;39(15_suppl):9507-9507. doi:10.1200/JCO.2021.39.15_suppl.9507
263. Dummer R, Hauschild A, Santinami M, et al. Five-Year Analysis of Adjuvant Dabrafenib plus Trametinib in Stage III Melanoma. *New England Journal of Medicine*. 2020;383(12):1139-1148. doi:10.1056/NEJMoa2005493
264. Ascierto PA, Del Vecchio M, Mandalá M, et al. Adjuvant nivolumab versus ipilimumab in resected stage IIIB-C and stage IV melanoma (CheckMate 238): 4-year results from a multicentre, double-blind, randomised, controlled, phase 3 trial. *Lancet Oncol*. 2020;21(11):1465-1477. doi:10.1016/S1470-2045(20)30494-0
265. Eggermont AMM, Blank CU, Mandalà M, et al. Adjuvant pembrolizumab versus placebo in resected stage III melanoma (EORTC 1325-MG/KEYNOTE-054): distant metastasis-free survival results from a double-blind, randomised, controlled, phase 3 trial. *Lancet Oncol*. 2021;22(5):643-654. doi:10.1016/S1470-2045(21)00065-6
266. Luke JJ, Rutkowski P, Queirolo P, et al. Pembrolizumab

versus placebo as adjuvant therapy in completely resected stage IIB or IIC melanoma (KEYNOTE-716): a randomised, double-blind, phase 3 trial. *The Lancet*. 2022;399(10336):1718-1729. doi:10.1016/S0140-6736(22)00562-1
267. Blank CU, Rozeman EA, Fanchi LF, et al. Neoadjuvant versus adjuvant ipilimumab plus nivolumab in macroscopic stage III melanoma. *Nat Med*. 2018;24(11):1655-1661. doi:10.1038/s41591-018-0198-0
268. Long GV, Saw RPM, Lo S, et al. Neoadjuvant dabrafenib combined with trametinib for resectable, stage IIIB-C, BRAFV600 mutation-positive melanoma (NeoCombi): a single-arm, open-label, single-centre, phase 2 trial. *Lancet Oncol*. 2019;20(7):961-971. doi:10.1016/S1470-2045(19)30331-6
269. Menzies AM, Amaria RN, Rozeman EA, et al. Pathological response and survival with neoadjuvant therapy in melanoma: a pooled analysis from the International Neoadjuvant Melanoma Consortium (INMC). *Nat Med*. 2021;27(2):301-309. doi:10.1038/s41591-020-01188-3
270. Rozeman EA, Hoefsmit EP, Reijers ILM, et al. Survival and biomarker analyses from the OpACIN-neo and OpACIN neoadjuvant immunotherapy trials in stage III melanoma. *Nat Med*. 2021;27(2):256-263. doi:10.1038/s41591-020-01211-7
271. Amaria RN, Postow M, Burton EM, et al. Neoadjuvant relatlimab and nivolumab in resectable melanoma. *Nature*. Published online October 26, 2022:1-6. doi:10.1038/s41586-022-05368-8
272. McArthur GA, Chapman PB, Robert C, et al. Safety and efficacy of vemurafenib in BRAF(V600E) and BRAF(V600K) mutation-positive melanoma (BRIM-3): extended follow-up of a phase 3, randomised, open-label study. *Lancet Oncol*. 2014;15(3):323-332. doi:10.1016/S1470-2045(14)70012-9
273. Chapman PB, Robert C, Larkin J, et al. Vemurafenib in patients with BRAFV600 mutation-positive metastatic melanoma: final overall survival results of the randomized BRIM-3 study. *Annals of Oncology*. 2017;28(10):2581-2587. doi:10.1093/annonc/mdx339
274. Dreno B, Ascierto PA, McArthur GA, et al. Efficacy and safety of cobimetinib (C) combined with vemurafenib (V) in patients (pts) with BRAFV600 mutation–positive metastatic melanoma: analysis from the 4-year extended follow-up of the phase 3 coBRIM study. *JCO*. 2018;36(15_suppl):9522-9522.

doi:10.1200/JCO.2018.36.15_suppl.9522
275. Ascierto PA, Dréno B, Larkin J, et al. 5-Year Outcomes with Cobimetinib plus Vemurafenib in *BRAF* V600 Mutation–Positive Advanced Melanoma: Extended Follow-up of the coBRIM Study. *Clinical Cancer Research*. 2021;27(19):5225-5235. doi:10.1158/1078-0432.CCR-21-0809
276. Chapman PB, Ascierto PA, Schadendorf D, et al. Updated 5-y landmark analyses of phase 2 (BREAK-2) and phase 3 (BREAK-3) studies evaluating dabrafenib monotherapy in patients with BRAF V600–mutant melanoma. *JCO*. 2017;35(15_suppl):9526-9526. doi:10.1200/JCO.2017.35.15_suppl.9526
277. Hauschild A. Long-term outcomes in patients with BRAF V600-mutant metastatic melanoma receiving dabrafenib monotherapy: Analysis from phase 2 and 3 clinical trials. *European Journal of Cancer*. Published online 2020:7.
278. Robert C, Flaherty K, Nathan P, et al. Five-year outcomes from a phase 3 METRIC study in patients with BRAF V600 E/K–mutant advanced or metastatic melanoma. *European Journal of Cancer*. 2019;109:61-69. doi:10.1016/j.ejca.2018.12.015
279. Robert C, Karaszewska B, Schachter J, et al. Improved Overall Survival in Melanoma with Combined Dabrafenib and Trametinib. *New England Journal of Medicine*. 2015;372(1):30-39. doi:10.1056/NEJMoa1412690
280. Robert C, Karaszewska B, Schachter J, et al. Three-year estimate of overall survival in COMBI-v, a randomized phase 3 study evaluating first-line dabrafenib (D) + trametinib (T) in patients (pts) with unresectable or metastatic BRAF V600E/K–mutant cutaneous melanoma. *Annals of Oncology*. 2016;27:vi575. doi:10.1093/annonc/mdw435.37
281. Long GV, Flaherty KT, Stroyakovskiy D, et al. Dabrafenib plus trametinib versus dabrafenib monotherapy in patients with metastatic BRAF V600E/K-mutant melanoma: long-term survival and safety analysis of a phase 3 study. *Annals of Oncology*. 2017;28(7):1631-1639. doi:10.1093/annonc/mdx176
282. Ascierto PA, Dummer R, Gogas HJ, et al. Update on tolerability and overall survival in COLUMBUS: landmark analysis of a randomised phase 3 trial of encorafenib plus binimetinib vs vemurafenib or encorafenib in patients with BRAF V600-mutant melanoma. *Eur J Cancer*. 2020;126:33-44. doi:10.1016/j.ejca.2019.11.016
283. Dummer R, Flaherty K, Robert C, et al. Five-year overall

survival (OS) in COLUMBUS: A randomized phase 3 trial of encorafenib plus binimetinib versus vemurafenib or encorafenib in patients (pts) with BRAF V600-mutant melanoma. *JCO*. 2021;39(15_suppl):9507-9507. doi:10.1200/JCO.2021.39.15_suppl.9507
284. Dummer R, Long GV, Robert C, et al. Randomized Phase III Trial Evaluating Spartalizumab Plus Dabrafenib and Trametinib for BRAF V600–Mutant Unresectable or Metastatic Melanoma. *JCO*. 2022;40(13):1428-1438. doi:10.1200/JCO.21.01601
285. McArthur GA, Gutzmer R, Stroyakovskiy D, et al. Overall survival (OS) with first-line atezolizumab (A) or placebo (P) in combination with vemurafenib (V) and cobimetinib (C) in BRAFV600 mutation-positive advanced melanoma: Second interim OS analysis of the phase 3 IMspire150 study. *JCO*. 2022;40(16_suppl):9547-9547. doi:10.1200/JCO.2022.40.16_suppl.9547
286. Ascierto PA, Ferrucci PF, Stephens R, et al. KEYNOTE-022 Part 3: Phase II randomized study of 1L dabrafenib (D) and trametinib (T) plus pembrolizumab (Pembro) or placebo (PBO) for BRAF-mutant advanced melanoma. *Annals of Oncology*. 2018;29:viii442. doi:10.1093/annonc/mdy289
287. Ferrucci PF, Di Giacomo AM, Del Vecchio M, et al. KEYNOTE-022 part 3: a randomized, double-blind, phase 2 study of pembrolizumab, dabrafenib, and trametinib in BRAF-mutant melanoma. *J Immunother Cancer*. 2020;8(2):e001806. doi:10.1136/jitc-2020-001806
288. Rapp UR, Goldsborough MD, Mark GE, et al. Structure and biological activity of v-raf, a unique oncogene transduced by a retrovirus. *Proc Natl Acad Sci U S A*. 1983;80(14):4218-4222. doi:10.1073/pnas.80.14.4218
289. PCAWG Drivers and Functional Interpretation Working Group, PCAWG Structural Variation Working Group, PCAWG Consortium, et al. Analyses of non-coding somatic drivers in 2,658 cancer whole genomes. *Nature*. 2020;578(7793):102-111. doi:10.1038/s41586-020-1965-x
290. Zehir A, Benayed R, Shah RH, et al. Mutational landscape of metastatic cancer revealed from prospective clinical sequencing of 10,000 patients. *Nat Med*. 2017;23(6):703-713. doi:10.1038/nm.4333
291. Cerami E, Gao J, Dogrusoz U, et al. The cBio cancer genomics portal: an open platform for exploring multidimensional

cancer genomics data. *Cancer Discov*. 2012;2(5):401-404. doi:10.1158/2159-8290.CD-12-0095
292. Gao J, Aksoy BA, Dogrusoz U, et al. Integrative analysis of complex cancer genomics and clinical profiles using the cBioPortal. *Sci Signal*. 2013;6(269):pl1. doi:10.1126/scisignal.2004088
293. Campbell PJ, Getz G, Korbel JO, et al. Pan-cancer analysis of whole genomes. *Nature*. 2020;578(7793):82-93. doi:10.1038/s41586-020-1969-6
294. Garnett MJ, Marais R. Guilty as charged: B-RAF is a human oncogene. *Cancer Cell*. 2004;6(4):313-319. doi:10.1016/j.ccr.2004.09.022
295. Wellbrock C, Karasarides M, Marais R. The RAF proteins take centre stage. *Nat Rev Mol Cell Biol*. 2004;5(11):875-885. doi:10.1038/nrm1498
296. Holderfield M, Deuker MM, McCormick F, McMahon M. Targeting RAF kinases for cancer therapy: BRAF-mutated melanoma and beyond. *Nat Rev Cancer*. 2014;14(7):455-467. doi:10.1038/nrc3760
297. Lavoie H, Therrien M. Regulation of RAF protein kinases in ERK signalling. *Nat Rev Mol Cell Biol*. 2015;16(5):281-298. doi:10.1038/nrm3979
298. Dankner M, Rose AAN, Rajkumar S, Siegel PM, Watson IR. Classifying BRAF alterations in cancer: new rational therapeutic strategies for actionable mutations. *Oncogene*. 2018;37(24):3183-3199. doi:10.1038/s41388-018-0171-x
299. Śmiech M, Leszczyński P, Kono H, Wardell C, Taniguchi H. Emerging BRAF Mutations in Cancer Progression and Their Possible Effects on Transcriptional Networks. *Genes (Basel)*. 2020;11(11):1342. doi:10.3390/genes11111342
300. Park E, Rawson S, Li K, et al. Architecture of autoinhibited and active BRAF–MEK1–14-3-3 complexes. *Nature*. 2019;575(7783):545-550. doi:10.1038/s41586-019-1660-y
301. Yao Z, Torres NM, Tao A, et al. BRAF Mutants Evade ERK-Dependent Feedback by Different Mechanisms that Determine Their Sensitivity to Pharmacologic Inhibition. *Cancer Cell*. 2015;28(3):370-383. doi:10.1016/j.ccell.2015.08.001
302. Yao Z, Yaeger R, Rodrik-Outmezguine VS, et al. Tumours with class 3 BRAF mutants are sensitive to the inhibition of activated RAS. *Nature*. 2017;548(7666):234-238. doi:10.1038/nature23291
303. Hanrahan AJ, Solit DB. BRAF Mutations: The Discovery of

Allele- and Lineage-Specific Differences. *Cancer Res*. 2022;82(1):12-14. doi:10.1158/0008-5472.CAN-21-3377
304. Brose MS, Volpe P, Feldman M, et al. BRAF and RAS mutations in human lung cancer and melanoma. *Cancer Res*. 2002;62(23):6997-7000.
305. Cohn AL, Day BM, Abhyankar S, McKenna E, Riehl T, Puzanov I. BRAFV600 mutations in solid tumors, other than metastatic melanoma and papillary thyroid cancer, or multiple myeloma: a screening study. *Onco Targets Ther*. 2017;10:965-971. doi:10.2147/OTT.S120440
306. Eblen ST. Extracellular-Regulated Kinases: Signaling From Ras to ERK Substrates to Control Biological Outcomes. *Adv Cancer Res*. 2018;138:99-142. doi:10.1016/bs.acr.2018.02.004
307. Lemmon MA, Schlessinger J. Cell signaling by receptor tyrosine kinases. *Cell*. 2010;141(7):1117-1134. doi:10.1016/j.cell.2010.06.011
308. Jaumot M, Hancock JF. Protein phosphatases 1 and 2A promote Raf-1 activation by regulating 14-3-3 interactions. *Oncogene*. 2001;20(30):3949-3958. doi:10.1038/sj.onc.1204526
309. Dhillon AS, Meikle S, Yazici Z, Eulitz M, Kolch W. Regulation of Raf-1 activation and signalling by dephosphorylation. *EMBO J*. 2002;21(1-2):64-71. doi:10.1093/emboj/21.1.64
310. Chong H, Vikis HG, Guan KL. Mechanisms of regulating the Raf kinase family. *Cell Signal*. 2003;15(5):463-469. doi:10.1016/s0898-6568(02)00139-0
311. Haling JR, Sudhamsu J, Yen I, et al. Structure of the BRAF-MEK complex reveals a kinase activity independent role for BRAF in MAPK signaling. *Cancer Cell*. 2014;26(3):402-413. doi:10.1016/j.ccr.2014.07.007
312. Diedrich B, Rigbolt KT, Röring M, et al. Discrete cytosolic macromolecular BRAF complexes exhibit distinct activities and composition. *EMBO J*. 2017;36(5):646-663. doi:10.15252/embj.201694732
313. Thevakumaran N, Lavoie H, Critton DA, et al. Crystal structure of a BRAF kinase domain monomer explains basis for allosteric regulation. *Nat Struct Mol Biol*. 2015;22(1):37-43. doi:10.1038/nsmb.2924
314. Rajakulendran T, Sahmi M, Lefrançois M, Sicheri F, Therrien M. A dimerization-dependent mechanism drives RAF catalytic activation. *Nature*. 2009;461(7263):542-545. doi:10.1038/nature08314

315. Wan PTC, Garnett MJ, Roe SM, et al. Mechanism of activation of the RAF-ERK signaling pathway by oncogenic mutations of B-RAF. *Cell*. 2004;116(6):855-867. doi:10.1016/s0092-8674(04)00215-6
316. Hingorani SR, Jacobetz MA, Robertson GP, Herlyn M, Tuveson DA. Suppression of BRAF(V599E) in human melanoma abrogates transformation. *Cancer Res*. 2003;63(17):5198-5202.
317. Karasarides M, Chiloeches A, Hayward R, et al. B-RAF is a therapeutic target in melanoma. *Oncogene*. 2004;23(37):6292-6298. doi:10.1038/sj.onc.1207785
318. Hoeflich KP, Gray DC, Eby MT, et al. Oncogenic BRAF is required for tumor growth and maintenance in melanoma models. *Cancer Res*. 2006;66(2):999-1006. doi:10.1158/0008-5472.CAN-05-2720
319. Eisen T, Ahmad T, Flaherty KT, et al. Sorafenib in advanced melanoma: a Phase II randomised discontinuation trial analysis. *Br J Cancer*. 2006;95(5):581-586. doi:10.1038/sj.bjc.6603291
320. Kefford R, Arkenau H, Brown MP, et al. Phase I/II study of GSK2118436, a selective inhibitor of oncogenic mutant BRAF kinase, in patients with metastatic melanoma and other solid tumors. *JCO*. 2010;28(15_suppl):8503-8503. doi:10.1200/jco.2010.28.15_suppl.8503
321. Flaherty KT, Puzanov I, Kim KB, et al. Inhibition of mutated, activated BRAF in metastatic melanoma. *N Engl J Med*. 2010;363(9):809-819. doi:10.1056/NEJMoa1002011
322. Heidorn SJ, Milagre C, Whittaker S, et al. Kinase-dead BRAF and oncogenic RAS cooperate to drive tumor progression through CRAF. *Cell*. 2010;140(2):209-221. doi:10.1016/j.cell.2009.12.040
323. Hatzivassiliou G, Song K, Yen I, et al. RAF inhibitors prime wild-type RAF to activate the MAPK pathway and enhance growth. *Nature*. 2010;464(7287):431-435. doi:10.1038/nature08833
324. Poulikakos PI, Zhang C, Bollag G, Shokat KM, Rosen N. RAF inhibitors transactivate RAF dimers and ERK signalling in cells with wild-type BRAF. *Nature*. 2010;464(7287):427-430. doi:10.1038/nature08902
325. Gibney GT, Messina JL, Fedorenko IV, Sondak VK, Smalley KSM. Paradoxical oncogenesis—the long-term effects of BRAF inhibition in melanoma. *Nat Rev Clin Oncol*. 2013;10(7):390-399. doi:10.1038/nrclinonc.2013.83
326. Karoulia Z, Wu Y, Ahmed TA, et al. An Integrated Model

of RAF Inhibitor Action Predicts Inhibitor Activity against Oncogenic BRAF Signaling. *Cancer Cell*. 2016;30(3):485-498. doi:10.1016/j.ccell.2016.06.024
327. Planchard D, Besse B, Groen HJM, et al. Phase 2 Study of Dabrafenib Plus Trametinib in Patients With BRAF V600E-Mutant Metastatic NSCLC: Updated 5-Year Survival Rates and Genomic Analysis. *Journal of Thoracic Oncology*. 2022;17(1):103-115. doi:10.1016/j.jtho.2021.08.011
328. Subbiah V, Kreitman RJ, Wainberg ZA, et al. Dabrafenib and Trametinib Treatment in Patients With Locally Advanced or Metastatic BRAF V600-Mutant Anaplastic Thyroid Cancer. *J Clin Oncol*. 2018;36(1):7-13. doi:10.1200/JCO.2017.73.6785
329. Tabernero J, Grothey A, Van Cutsem E, et al. Encorafenib Plus Cetuximab as a New Standard of Care for Previously Treated BRAF V600E-Mutant Metastatic Colorectal Cancer: Updated Survival Results and Subgroup Analyses from the BEACON Study. *J Clin Oncol*. 2021;39(4):273-284. doi:10.1200/JCO.20.02088
330. Poulikakos PI, Sullivan RJ, Yaeger R. Molecular Pathways and Mechanisms of BRAF in Cancer Therapy. *Clinical Cancer Research*. 2022;28(21):4618-4628. doi:10.1158/1078-0432.CCR-21-2138
331. Amaral T, Sinnberg T, Meier F, et al. The mitogen-activated protein kinase pathway in melanoma part I – Activation and primary resistance mechanisms to BRAF inhibition. *European Journal of Cancer*. 2017;73:85-92. doi:10.1016/j.ejca.2016.12.010
332. Amaral T, Sinnberg T, Meier F, et al. MAPK pathway in melanoma part II—secondary and adaptive resistance mechanisms to BRAF inhibition. *European Journal of Cancer*. 2017;73:93-101. doi:10.1016/j.ejca.2016.12.012
333. Hugo W, Shi H, Sun L, et al. Non-genomic and Immune Evolution of Melanoma Acquiring MAPKi Resistance. *Cell*. 2015;162(6):1271-1285. doi:10.1016/j.cell.2015.07.061
334. Nazarian R, Shi H, Wang Q, et al. Melanomas acquire resistance to B-RAF(V600E) inhibition by RTK or N-RAS upregulation. *Nature*. 2010;468(7326):973-977. doi:10.1038/nature09626
335. Straussman R, Morikawa T, Shee K, et al. Tumour micro-environment elicits innate resistance to RAF inhibitors through HGF secretion. *Nature*. 2012;487(7408):500-504. doi:10.1038/nature11183
336. Wagle N, Emery C, Berger MF, et al. Dissecting therapeutic

resistance to RAF inhibition in melanoma by tumor genomic profiling. *J Clin Oncol*. 2011;29(22):3085-3096. doi:10.1200/JCO.2010.33.2312
337. Trunzer K, Pavlick AC, Schuchter L, et al. Pharmacodynamic effects and mechanisms of resistance to vemurafenib in patients with metastatic melanoma. *J Clin Oncol*. 2013;31(14):1767-1774. doi:10.1200/JCO.2012.44.7888
338. Villanueva J, Infante JR, Krepler C, et al. Concurrent MEK2 Mutation and BRAF Amplification Confer Resistance to BRAF and MEK Inhibitors in Melanoma. *Cell Reports*. 2013;4(6):1090-1099. doi:10.1016/j.celrep.2013.08.023
339. Shi H, Moriceau G, Kong X, et al. Melanoma whole-exome sequencing identifies (V600E)B-RAF amplification-mediated acquired B-RAF inhibitor resistance. *Nat Commun*. 2012;3:724. doi:10.1038/ncomms1727
340. Poulikakos PI, Persaud Y, Janakiraman M, et al. RAF inhibitor resistance is mediated by dimerization of aberrantly spliced BRAF(V600E). *Nature*. 2011;480(7377):387-390. doi:10.1038/nature10662
341. Montagut C, Sharma SV, Shioda T, et al. Elevated CRAF as a potential mechanism of acquired resistance to BRAF inhibition in melanoma. *Cancer Res*. 2008;68(12):4853-4861. doi:10.1158/0008-5472.CAN-07-6787
342. Shao Y, Aplin AE. Akt3-mediated resistance to apoptosis in B-RAF-targeted melanoma cells. *Cancer Res*. 2010;70(16):6670-6681. doi:10.1158/0008-5472.CAN-09-4471
343. Paraiso KHT, Xiang Y, Rebecca VW, et al. PTEN loss confers BRAF inhibitor resistance to melanoma cells through the suppression of BIM expression. *Cancer Res*. 2011;71(7):2750-2760. doi:10.1158/0008-5472.CAN-10-2954
344. Smalley KSM, Lioni M, Dalla Palma M, et al. Increased cyclin D1 expression can mediate BRAF inhibitor resistance in BRAF V600E-mutated melanomas. *Mol Cancer Ther*. 2008;7(9):2876-2883. doi:10.1158/1535-7163.MCT-08-0431
345. Nathanson KL, Martin AM, Wubbenhorst B, et al. Tumor genetic analyses of patients with metastatic melanoma treated with the BRAF inhibitor dabrafenib (GSK2118436). *Clin Cancer Res*. 2013;19(17):4868-4878. doi:10.1158/1078-0432.CCR-13-0827
346. Gowrishankar K, Snoyman S, Pupo GM, Becker TM, Kefford RF, Rizos H. Acquired resistance to BRAF inhibition can confer cross-resistance to combined BRAF/MEK inhibition. *J*

Invest Dermatol. 2012;132(7):1850-1859. doi:10.1038/jid.2012.63
347. Shi H, Hugo W, Kong X, et al. Acquired Resistance and Clonal Evolution in Melanoma during BRAF Inhibitor Therapy. *Cancer Discovery*. 2014;4(1):80-93. doi:10.1158/2159-8290.CD-13-0642
348. Basile KJ, Abel EV, Dadpey N, Hartsough EJ, Fortina P, Aplin AE. *In Vivo* MAPK Reporting Reveals the Heterogeneity in Tumoral Selection of Resistance to RAF Inhibitors. *Cancer Research*. 2013;73(23):7101-7110. doi:10.1158/0008-5472.CAN-13-1628
349. Carlino MS, Todd JR, Gowrishankar K, et al. Differential activity of MEK and ERK inhibitors in BRAF inhibitor resistant melanoma. *Mol Oncol*. 2014;8(3):544-554. doi:10.1016/j.molonc.2014.01.003
350. Kemper K, Krijgsman O, Kong X, et al. BRAF(V600E) Kinase Domain Duplication Identified in Therapy-Refractory Melanoma Patient-Derived Xenografts. *Cell Rep*. 2016;16(1):263-277. doi:10.1016/j.celrep.2016.05.064
351. Rizos H, Menzies AM, Pupo GM, et al. BRAF Inhibitor Resistance Mechanisms in Metastatic Melanoma: Spectrum and Clinical Impact. *Clinical Cancer Research*. 2014;20(7):1965-1977. doi:10.1158/1078-0432.CCR-13-3122
352. Carlino MS, Gowrishankar K, Saunders CAB, et al. Antiproliferative Effects of Continued Mitogen-Activated Protein Kinase Pathway Inhibition following Acquired Resistance to BRAF and/or MEK Inhibition in Melanoma. *Molecular Cancer Therapeutics*. 2013;12(7):1332-1342. doi:10.1158/1535-7163.MCT-13-0011
353. Wagle N, Van Allen EM, Treacy DJ, et al. MAP Kinase Pathway Alterations in *BRAF* -Mutant Melanoma Patients with Acquired Resistance to Combined RAF/MEK Inhibition. *Cancer Discovery*. 2014;4(1):61-68. doi:10.1158/2159-8290.CD-13-0631
354. Van Allen EM, Wagle N, Sucker A, et al. The Genetic Landscape of Clinical Resistance to RAF Inhibition in Metastatic Melanoma. *Cancer Discovery*. 2014;4(1):94-109. doi:10.1158/2159-8290.CD-13-0617
355. Johnson DB, Menzies AM, Zimmer L, et al. Acquired BRAF inhibitor resistance: A multicenter meta-analysis of the spectrum and frequencies, clinical behaviour, and phenotypic associations of resistance mechanisms. *European Journal of Cancer*. 2015;51(18):2792-2799. doi:10.1016/j.ejca.2015.08.022

356. Long GV, Fung C, Menzies AM, et al. Increased MAPK reactivation in early resistance to dabrafenib/trametinib combination therapy of BRAF-mutant metastatic melanoma. *Nat Commun*. 2014;5(1):5694. doi:10.1038/ncomms6694
357. Clark ME, Rizos H, Pereira MR, et al. Detection of *BRAF* splicing variants in plasma-derived cell-free nucleic acids and extracellular vesicles of melanoma patients failing targeted therapy therapies. *Oncotarget*. 2020;11(44):4016-4027. doi:10.18632/oncotarget.27790
358. Salton M, Kasprzak WK, Voss T, Shapiro BA, Poulikakos PI, Misteli T. Inhibition of vemurafenib-resistant melanoma by interference with pre-mRNA splicing. *Nat Commun*. 2015;6(1):7103. doi:10.1038/ncomms8103
359. Pupo GM, Boyd SC, Fung C, et al. Clinical significance of intronic variants in BRAF inhibitor resistant melanomas with altered BRAF transcript splicing. *Biomark Res*. 2017;5(1):17. doi:10.1186/s40364-017-0098-3
360. Ahronian LG, Sennott EM, Van Allen EM, et al. Clinical Acquired Resistance to RAF Inhibitor Combinations in BRAF-Mutant Colorectal Cancer through MAPK Pathway Alterations. *Cancer Discovery*. 2015;5(4):358-367. doi:10.1158/2159-8290.CD-14-1518
361. Ortiz-Cuaran S, Mezquita L, Swalduz A, et al. MA21.07 Circulating Tumor DNA Analysis Depicts Potential Mechanisms of Resistance to BRAF-Targeted Therapies in BRAF+ Non-Small Cell Lung Cancer. *Journal of Thoracic Oncology*. 2019;14(10, Supplement):S337. doi:10.1016/j.jtho.2019.08.678
362. Facchinetti F, Lacroix L, Mezquita L, et al. Molecular mechanisms of resistance to BRAF and MEK inhibitors in BRAFV600E non–small cell lung cancer. *European Journal of Cancer*. 2020;132:211-223. doi:10.1016/j.ejca.2020.03.025
363. Lin L, Asthana S, Chan E, et al. Mapping the molecular determinants of BRAF oncogene dependence in human lung cancer. *Proceedings of the National Academy of Sciences*. 2014;111(7):E748-E757. doi:10.1073/pnas.1320956111
364. Jones DTW, Kocialkowski S, Liu L, et al. Tandem duplication producing a novel oncogenic BRAF fusion gene defines the majority of pilocytic astrocytomas. *Cancer Res*. 2008;68(21):8673-8677. doi:10.1158/0008-5472.CAN-08-2097
365. Ross JS, Wang K, Chmielecki J, et al. The distribution of BRAF gene fusions in solid tumors and response to targeted

therapy. *Int J Cancer*. 2016;138(4):881-890. doi:10.1002/ijc.29825
366. Botton T, Yeh I, Nelson T, et al. Recurrent BRAF kinase fusions in melanocytic tumors offer an opportunity for targeted therapy. *Pigment Cell Melanoma Res*. 2013;26(6):845-851. doi:10.1111/pcmr.12148
367. Lu H, Villafane N, Dogruluk T, et al. Engineering and Functional Characterization of Fusion Genes Identifies Novel Oncogenic Drivers of Cancer. *Cancer Res*. 2017;77(13):3502-3512. doi:10.1158/0008-5472.CAN-16-2745
368. Botton T, Talevich E, Mishra VK, et al. Genetic Heterogeneity of BRAF Fusion Kinases in Melanoma Affects Drug Responses. *Cell Reports*. 2019;29(3):573-588.e7. doi:10.1016/j.celrep.2019.09.009
369. Hutchinson KE, Lipson D, Stephens PJ, et al. BRAF fusions define a distinct molecular subset of melanomas with potential sensitivity to MEK inhibition. *Clin Cancer Res*. 2013;19(24):6696-6702. doi:10.1158/1078-0432.CCR-13-1746
370. Kulkarni A, Al-Hraishawi H, Simhadri S, et al. BRAF Fusion as a Novel Mechanism of Acquired Resistance to Vemurafenib in BRAFV600E Mutant Melanoma. *Clinical Cancer Research*. 2017;23(18):5631-5638. doi:10.1158/1078-0432.CCR-16-0758
371. Klempner SJ, Bordoni R, Gowen K, et al. Identification of *BRAF* Kinase Domain Duplications Across Multiple Tumor Types and Response to RAF Inhibitor Therapy. *JAMA Oncol*. 2016;2(2):272. doi:10.1001/jamaoncol.2015.4437
372. Johnson DB, Childress MA, Chalmers ZR, et al. BRAF internal deletions and resistance to BRAF/MEK inhibitor therapy. *Pigment Cell & Melanoma Research*. 2018;31(3):432-436. doi:10.1111/pcmr.12674
373. Yaeger R, Yao Z, Hyman DM, et al. Mechanisms of Acquired Resistance to BRAF V600E Inhibition in Colon Cancers Converge on RAF Dimerization and Are Sensitive to Its Inhibition. *Cancer Research*. 2017;77(23):6513-6523. doi:10.1158/0008-5472.CAN-17-0768
374. Tung JK, Neishaboori N, Haraldsdottir S, Suarez CJ. An amino-terminal BRAF deletion accounting for acquired resistance to RAF/EGFR inhibition in colorectal cancer. *Cold Spring Harb Mol Case Stud*. 2020;6(4):a005140. doi:10.1101/mcs.a005140
375. Sheikine Y, Pavlick D, Klempner SJ, et al. BRAF in Lung Cancers: Analysis of Patient Cases Reveals Recurrent BRAF

Mutations, Fusions, Kinase Duplications, and Concurrent Alterations. *JCO Precision Oncology*. 2018;(2):1-15. doi:10.1200/PO.17.00172
376. Foster SA, Whalen DM, Özen A, et al. Activation Mechanism of Oncogenic Deletion Mutations in BRAF, EGFR, and HER2. *Cancer Cell*. 2016;29(4):477-493. doi:10.1016/j.ccell.2016.02.010
377. Chen SH, Zhang Y, Van Horn RD, et al. Oncogenic *BRAF* Deletions That Function as Homodimers and Are Sensitive to Inhibition by RAF Dimer Inhibitor LY3009120. *Cancer Discovery*. 2016;6(3):300-315. doi:10.1158/2159-8290.CD-15-0896
378. Tapial J, Ha KCH, Sterne-Weiler T, et al. An atlas of alternative splicing profiles and functional associations reveals new regulatory programs and genes that simultaneously express multiple major isoforms. *Genome Res*. 2017;27(10):1759-1768. doi:10.1101/gr.220962.117
379. Song C, Piva M, Sun L, et al. Recurrent Tumor Cell-Intrinsic and -Extrinsic Alterations during MAPKi-Induced Melanoma Regression and Early Adaptation. *Cancer Discov*. 2017;7(11):1248-1265. doi:10.1158/2159-8290.CD-17-0401
380. Kunz M, Löffler-Wirth H, Dannemann M, et al. RNA-seq analysis identifies different transcriptomic types and developmental trajectories of primary melanomas. *Oncogene*. 2018;37(47):6136-6151. doi:10.1038/s41388-018-0385-y
381. Tsoi J, Robert L, Paraiso K, et al. Multi-stage Differentiation Defines Melanoma Subtypes with Differential Vulnerability to Drug-Induced Iron-Dependent Oxidative Stress. *Cancer Cell*. 2018;33(5):890-904.e5. doi:10.1016/j.ccell.2018.03.017
382. Bairoch A. The Cellosaurus, a Cell-Line Knowledge Resource. *J Biomol Tech*. 2018;29(2):25-38. doi:10.7171/jbt.18-2902-002
383. Tate JG, Bamford S, Jubb HC, et al. COSMIC: the Catalogue Of Somatic Mutations In Cancer. *Nucleic Acids Research*. 2019;47(D1):D941-D947. doi:10.1093/nar/gky1015
384. Villanueva J, Vultur A, Lee JT, et al. Acquired resistance to BRAF inhibitors mediated by a RAF kinase switch in melanoma can be overcome by cotargeting MEK and IGF-1R/PI3K. *Cancer Cell*. 2010;18(6):683-695. doi:10.1016/j.ccr.2010.11.023
385. Garrison E, Marth G. Haplotype-based variant detection from short-read sequencing. Published online July 20, 2012. Accessed November 21, 2022. http://arxiv.org/abs/1207.3907

386. Cingolani P, Platts A, Wang LL, et al. A program for annotating and predicting the effects of single nucleotide polymorphisms, SnpEff: SNPs in the genome of Drosophila melanogaster strain w ^{1118} ; iso-2; iso-3. *Fly*. 2012;6(2):80-92. doi:10.4161/fly.19695
387. Mayakonda A, Lin DC, Assenov Y, Plass C, Koeffler HP. Maftools: efficient and comprehensive analysis of somatic variants in cancer. *Genome Res*. 2018;28(11):1747-1756. doi:10.1101/gr.239244.118
388. Pupo GM, Boyd SC, Fung C, et al. Clinical significance of intronic variants in BRAF inhibitor resistant melanomas with altered BRAF transcript splicing. *Biomark Res*. 2017;5:17. doi:10.1186/s40364-017-0098-3
389. Poulikakos PI, Persaud Y, Janakiraman M, et al. RAF inhibitor resistance is mediated by dimerization of aberrantly spliced BRAF(V600E). *Nature*. 2011;480(7377):387-390. doi:10.1038/nature10662
390. McLaren W, Gil L, Hunt SE, et al. The Ensembl Variant Effect Predictor. *Genome Biology*. 2016;17(1):122. doi:10.1186/s13059-016-0974-4
391. Cvitkovic I, Jurica MS. Spliceosome database: a tool for tracking components of the spliceosome. *Nucleic Acids Res*. 2013;41(Database issue):D132-141. doi:10.1093/nar/gks999
392. Wang T, Wei JJ, Sabatini DM, Lander ES. Genetic screens in human cells using the CRISPR-Cas9 system. *Science*. 2014;343(6166):80-84. doi:10.1126/science.1246981
393. Shalem O, Sanjana NE, Hartenian E, et al. Genome-scale CRISPR-Cas9 knockout screening in human cells. *Science*. 2014;343(6166):84-87. doi:10.1126/science.1247005
394. Hart T, Chandrashekhar M, Aregger M, et al. High-Resolution CRISPR Screens Reveal Fitness Genes and Genotype-Specific Cancer Liabilities. *Cell*. 2015;163(6):1515-1526. doi:10.1016/j.cell.2015.11.015
395. Shalem O, Sanjana NE, Zhang F. High-throughput functional genomics using CRISPR–Cas9. *Nat Rev Genet*. 2015;16(5):299-311. doi:10.1038/nrg3899
396. Cao J, Wei J, Yang P, et al. Genome-scale CRISPR-Cas9 knockout screening in gastrointestinal stromal tumor with Imatinib resistance. *Mol Cancer*. 2018;17(1):121. doi:10.1186/s12943-018-0865-2
397. Zimmermann M, Murina O, Reijns MAM, et al. CRISPR

screens identify genomic ribonucleotides as a source of PARP-trapping lesions. *Nature*. 2018;559(7713):285-289. doi:10.1038/s41586-018-0291-z
398. Wei L, Lee D, Law CT, et al. Genome-wide CRISPR/Cas9 library screening identified PHGDH as a critical driver for Sorafenib resistance in HCC. *Nat Commun*. 2019;10(1):4681. doi:10.1038/s41467-019-12606-7
399. Wang E, Lu SX, Pastore A, et al. Targeting an RNA-Binding Protein Network in Acute Myeloid Leukemia. *Cancer Cell*. 2019;35(3):369-384.e7. doi:10.1016/j.ccell.2019.01.010
400. Li Z, Wang B, Gu S, et al. CRISPR Screens Identify Essential Cell Growth Mediators in BRAF Inhibitor-resistant Melanoma. *Genomics, Proteomics & Bioinformatics*. 2020;18(1):26-40. doi:10.1016/j.gpb.2020.02.002
401. Christodoulou E, Rashid M, Pacini C, et al. Analysis of CRISPR-Cas9 screens identifies genetic dependencies in melanoma. *Pigment Cell & Melanoma Research*. 2021;34(1):122-131. doi:10.1111/pcmr.12919
402. Gautron A, Bachelot L, Aubry M, et al. CRISPR screens identify tumor-promoting genes conferring melanoma cell plasticity and resistance. *EMBO Molecular Medicine*. 2021;13(5):e13466. doi:10.15252/emmm.202013466
403. van der Weyden L, Harle V, Turner G, et al. CRISPR activation screen in mice identifies novel membrane proteins enhancing pulmonary metastatic colonisation. *Commun Biol*. 2021;4(1):1-12. doi:10.1038/s42003-021-01912-w
404. Li W, Xu H, Xiao T, et al. MAGeCK enables robust identification of essential genes from genome-scale CRISPR/Cas9 knockout screens. Published online 2014:12.
405. Hart T, Moffat J. BAGEL: a computational framework for identifying essential genes from pooled library screens. *BMC Bioinformatics*. 2016;17(1):164. doi:10.1186/s12859-016-1015-8
406. Mi H, Muruganujan A, Casagrande JT, Thomas PD. Large-scale gene function analysis with the PANTHER classification system. *Nat Protoc*. 2013;8(8):1551-1566. doi:10.1038/nprot.2013.092
407. Thomas PD, Ebert D, Muruganujan A, Mushayahama T, Albou LP, Mi H. PANTHER: Making genome-scale phylogenetics accessible to all. *Protein Sci*. 2022;31(1):8-22. doi:10.1002/pro.4218
408. Vasan N, Baselga J, Hyman DM. A view on drug resistance

in cancer. *Nature*. 2019;575(7782):299-309. doi:10.1038/s41586-019-1730-1
409. Tyner JW, Haderk F, Kumaraswamy A, et al. Understanding Drug Sensitivity and Tackling Resistance in Cancer. *Cancer Research*. 2022;82(8):1448-1460. doi:10.1158/0008-5472.CAN-21-3695
410. Yao Z, Gao Y, Su W, et al. RAF inhibitor PLX8394 selectively disrupts BRAF-dimers and RAS-independent BRAF mutant-driven signaling. *Nat Med*. 2019;25(2):284-291. doi:10.1038/s41591-018-0274-5
411. Baitei EY, Zou M, Al-Mohanna F, et al. Aberrant BRAF splicing as an alternative mechanism for oncogenic B-Raf activation in thyroid carcinoma. *The Journal of Pathology*. 2009;217(5):707-715. doi:10.1002/path.2496
412. Kim HS, Jung M, Kang HN, et al. Oncogenic BRAF fusions in mucosal melanomas activate the MAPK pathway and are sensitive to MEK/PI3K inhibition or MEK/CDK4/6 inhibition. *Oncogene*. 2017;36(23):3334-3345. doi:10.1038/onc.2016.486
413. Turner JA, Bemis JGT, Bagby SM, et al. BRAF fusions identified in melanomas have variable treatment responses and phenotypes. *Oncogene*. 2019;38(8):1296-1308. doi:10.1038/s41388-018-0514-7
414. Sanlorenzo M, Vujic I, Esteve-Puig R, et al. The lincRNA MIRAT binds to IQGAP1 and modulates the MAPK pathway in NRAS mutant melanoma. *Sci Rep*. 2018;8(1):10902. doi:10.1038/s41598-018-27643-3
415. Müller J, Krijgsman O, Tsoi J, et al. Low MITF/AXL ratio predicts early resistance to multiple targeted drugs in melanoma. *Nat Commun*. 2014;5:5712. doi:10.1038/ncomms6712
416. Paudel BB, Lewis JE, Hardeman KN, et al. An Integrative Gene Expression and Mathematical Flux Balance Analysis Identifies Targetable Redox Vulnerabilities in Melanoma Cells. *Cancer Res*. 2020;80(20):4565-4577. doi:10.1158/0008-5472.CAN-19-3588
417. Babraham Bioinformatics - FastQC A Quality Control tool for High Throughput Sequence Data. Accessed December 4, 2022. https://www.bioinformatics.babraham.ac.uk/projects/fastqc/
418. Hadley Wickham. *Ggplot2: Elegant Graphics for Data Analysis*. Springer-Verlag New York; 2016. https://ggplot2.tidyverse.org
419. Robinson JT, Thorvaldsdóttir H, Winckler W, et al.

Integrative genomics viewer. *Nat Biotechnol*. 2011;29(1):24-26. doi:10.1038/nbt.1754
420. Sakamoto H, Inoue K, Higuchi I, Ono Y, Shimura Y. Control of Drosophila Sex-lethal pre-mRNA splicing by its own female-specific product. *Nucleic Acids Res*. 1992;20(21):5533-5540.
421. Li H, Durbin R. Fast and accurate short read alignment with Burrows-Wheeler transform. *Bioinformatics*. 2009;25(14):1754-1760. doi:10.1093/bioinformatics/btp324
422. Danecek P, Bonfield JK, Liddle J, et al. Twelve years of SAMtools and BCFtools. *GigaScience*. 2021;10(2):giab008. doi:10.1093/gigascience/giab008
423. Ou J, Zhu LJ. trackViewer: a Bioconductor package for interactive and integrative visualization of multi-omics data. *Nat Methods*. 2019;16(6):453-454. doi:10.1038/s41592-019-0430-y
424. Hart T, Tong AHY, Chan K, et al. Evaluation and Design of Genome-Wide CRISPR/SpCas9 Knockout Screens. *G3 (Bethesda)*. 2017;7(8):2719-2727. doi:10.1534/g3.117.041277
425. Chan K, Tong AHY, Brown KR, Mero P, Moffat J. Pooled CRISPR-Based Genetic Screens in Mammalian Cells. *JoVE*. 2019;(151):59780. doi:10.3791/59780
426. Martin M. Cutadapt removes adapter sequences from high-throughput sequencing reads. *EMBnet.journal*. 2011;17(1):10-12. doi:10.14806/ej.17.1.200
427. Wang B, Wang M, Zhang W, et al. Integrative analysis of pooled CRISPR genetic screens using MAGeCKFlute. *Nat Protoc*. 2019;14(3):756-780. doi:10.1038/s41596-018-0113-7
428. Hart T, Brown KR, Sircoulomb F, Rottapel R, Moffat J. Measuring error rates in genomic perturbation screens: gold standards for human functional genomics. *Mol Syst Biol*. 2014;10(7):733. doi:10.15252/msb.20145216
429. Langmead B, Trapnell C, Pop M, Salzberg SL. Ultrafast and memory-efficient alignment of short DNA sequences to the human genome. *Genome Biology*. 2009;10(3):R25. doi:10.1186/gb-2009-10-3-r25

Appendix

Supplementary Tables

Supplementary tables can be found in the provided link.

Table S1. List of genome-wide mutated genes in SKMEL293 and C3 BRAF3-9. Relative to Figure 25.

Table S2. List of genes encoding spliceosome-related proteins and RBPs involved in splicing. Relative to Figure 26

Table S3. Gene summary files of CRISPR screens data of SKMEL293 and C3 BRAF3-9 at day +8 (MAGeCK RRA). Test and ranks of genes calculated with MAGeCK RRA.

Table S4. Gene summary files of CRISPR screens data of SKMEL293, "bulk" C3, and C3 BRAF3-9 (MAGeCK MLE). Test and ranks of genes calculated with MAGeCK MLE.

Table S5. Gene list and Bayes Factors calculated with BAGEL in SKMEL293 and C3 BRAF3-9 (d+8) screen

Dedication and acknowledgements

Gracias a Ana y a Juan por brindarme esta oportunidad única, la confianza depositada en mí, la libertad y las enseñanzas a lo largo de este camino, que ha sido de todo, menos fácil.

Gracias al Valcárcel lab por acogerme y hacerme sentirme en casa desde el principio. Especialmente a Sophie y a Anna por enseñarme los secretos del trabajo en el laboratorio y de la biología molecular; a Estefi y a Simon por ayudarme con la bioinformática; a Gosia, Claudia, Suzanne, Belén, Jonàs… por el tiempo compartido. Gracias a Pablo por su implicación en el proyecto y su disponibilidad en todo momento.

Gracias a los miembros del TAC y a todos aquellos miembros del CRG que me ofrecieron soporte cuando lo necesité.

Gracias a mis compañeros en el Hospital y a los pacientes, por ayudarme a mantener siempre con un pie en la clínica.

Gracias a Ibon por su incondicionalidad.

Gracias a mis padres: en lo que me he convertido, sin duda, es gracias a ellos.